Integrated Systems Analyses of Using Geologically Stored CO_2 and Sedimentary Basin Geothermal Resources to Produce and Store Energy

Dissertation

Presented in Partial Fulfillment of the Requirements for the Degree Doctor of Philosophy in the Graduate School of The Ohio State University

By

Jonathan Davis Ogland-Hand, M.S.

Graduate Program in Environmental Science

The Ohio State University

2019

Dissertation Committee

Jeffrey M. Bielicki, Adviser

Ramteen Sioshansi

Gil Bohrer

Brent Sohngen

Abstract

Reducing carbon dioxide (CO_2) emissions is one of the most pressing issues facing the electricity system. Towards this end, prior work investigated generating electricity with geologically stored CO_2 by using it to extract heat from sedimentary basins geothermal resources. This dissertation expands on this idea by developing and valuing approaches for CO_2-based energy storage.

In the first chapter, we investigate the value that three bulk energy storage (BES) approaches have for reducing system-wide CO_2 emissions and water requirements: CO_2-Bulk Energy Storage (CO_2-BES), which is a CO_2-based energy storage approach that uses a concentric-ring, pressure based (CRP-BES) design, Pumped Hydro Energy Storage (PHES), and Compressed Air Energy Storage (CAES). Our results suggest that BES could decrease system-wide CO_2 emissions by increasing the utilization of wind, but it can also alter the dispatch order of regional electricity systems in other ways (e.g., increase in the utilization of natural gas power capacity and of coal power capacity, decrease in the utilization of nuclear power capacity). While some changes provide negative value (e.g., decrease in nuclear increased CO_2 emission), the system-wide values can be greater than operating cost of BES.

In the second and third chapters, we investigate two mechanisms for using CO_2 for energy storage: storage of (1) pressure and (2) heat. For pressure storage, we investigated the efficacy of the CO_2-BES system using the CRP-BES design over cycles of varying durations. We found that CO_2-BES could time-shift up to a couple weeks of electricity, but the system cannot frequently dispatch electricity for longer durations than was stored. Also, the cycle duration does not substantially affect the power storage capacity and power output capacity if the total time spent charging, discharging, or idling is equal over a multi-year

period. For thermal energy storage, we investigated the efficacy of using pre-heated CO_2 and pre-heated brine as the media for thermal energy storage in the subsurface. We found that it is likely that the thermophysical characteristics of brine render it advantageous over CO_2 for this purpose.

In the fourth chapter, we determine the potential that the CO_2-BES system using the CRP-BES design has to increasing the profit-maximizing high voltage direct current (HVDC) transmission capacity that connects a wind farm in Eastern Wyoming to Los Angeles, California. Our results suggest that the optimal dispatch of the CO_2-BES system in this application includes operating as both a geothermal power plant and an energy storage facility and that the system can increase the profit-maximizing HVDC transmission capacity.

With these findings, we conclude that using geologically stored CO_2 and geothermal resources for energy storage can provide value to the electricity system in multiple ways in part because these systems have unique operational capabilities compared to conventional energy storage approaches (e.g., PHES, CAES). Potential future works include optimizing the CRP-BES design for a specific application, developing a CO_2-seasonal energy storage approach, and expanding the model boundaries to include the source of CO_2.

Dedication

I once had a conversation with an artist who asked me about my research. After I told her about it, she said something around the lines of "wow, it sounds like you are actually doing something useful." I replied by saying that I hoped some aspect of my research provides use to the larger effort of addressing climate change, but that in my opinion, no technology or study will be useful unless people already have a desire to act. And in this sense, a case could be made that art is perhaps more useful than science and engineering because it has the power to inspire people.

This dissertation is dedicated to artists, especially those whose creations make others appreciate the value of the natural world. Thank you

The Real Poem by Mary Oliver

I rose this morning early as usual, and went to my desk.
But it's Spring,

and the thrush is in the woods,
somewhere in the twirled branches, and he is singing.

And so, now, I am standing by the open door,
And now I am stepping down into the grass.

I am touching a few leaves.
I am noticing the way the yellow butterflies
move together, in a twinkling cloud, over the field.

And I am thinking: maybe just looking and listening
is the real work.

Maybe the world, without us,
is the real poem.

Acknowledgements

First, I would of course like to thank Jeff Bielicki for being my advisor over past five years of my life. You taught me a lot, opened doors for me that I did not even know existed, and also brought in the grant funding that has financially supported me on this journey. Thank you!

I also like to thank all the other OSU Professors that were part of my graduate school career, including my committee members. First, Ramteen Sioshansi for your guidance, mentorship, and enjoyable conversations over the lunches we shared. If given the opportunity, there is not a lot that I would change about my time at OSU, but I do wish I could have worked with you more. Second, Gil Bohrer for always supporting me and students in general and especially for attending almost every ESGP happy hour. Last but not least, Brent Sohngen - I always appreciated your directness, sincerity, and humor. I would also like to thank Alan Randall, Gaj Sivandran, Elena Erwin, Saytha Gopalakrishnan, Elizabeth and Eric Toman, and Marc Posner for either teaching an awesome class or a valuable lesson through research.

I would also like to thank the larger CPG group: Martin Saar, Nagasree Garapati, Mark Fleming, and Jimmy Randolph for the advice and conversation during our online group meetings and all the edits and comments on our publications. Especially huge thanks to Ben Adams for the support and jokes throughout the years and also for guiding me through constructing a well model, power cycle models, and cost model - I owe you a lot of beers.

I also want to thank all the ESRL-mates that I have had the joy of meeting and working with: Julie Lagenfeld, Iti Patel, Glenn Sutula, Paige Hagley, Kelsey Hunter, Amlan Rath, Chante Vines, Yaoping Wang, Marcos Miranda, Soomin Chun, and Stephen Maldonado. Also all of my other OSU friends including but not limited to Billy Fagan, Eric Loria, Camilo Rey Sanchez, Steve Tuozzolo, Nall Moonilall, Haley Kujawa, Sarah Haines, Anjelica Moreno, Demie Huffman, Matt Young, and Sami McCabe. Thank you for the community and friendship!

I would also like to thank my Valpo roots - Robert Palumbo, Luke Venstrom, Scott Duncan, and the Sigma Phi Epsilon chapter down at 705 Mound Street - for providing me with an incredibly strong foundation that I am still appreciating more and more each day.

Thanks to Meredith Irvin, whom I dated for almost all of my time at OSU. Many of my fondest grad school memories include her in some way and it is also likely that I would not have finished this doctorate if I had we not been dating. Thanks Mer.

Tremendous thanks to Michael Hagenberger for his friendship, guidance, and support through all the ups and downs over the past five years. You the man Mike.

Special thanks to my all my non-blood related family members starting with my brother Jamo Karsten and also the Karsten-DeJonge family. Thanks for always being there and go Bucks!! Also my real LAP bros Mickey Delcambre, Matt West, and Noah Neuenfeldt for your friendship and thought-provoking discussions. You dudes are the best.

Last but certainly not least I would like to thank my parents and my sister. Having you all in my corner is my life's greatest blessing. I cannot thank you enough.

There are so many more that I would like to thank too, but the list is too long. To everyone listed above and all the others that should be listed – thank you so much. This dissertation would not have happened without you.

Vita

May 2010…………………………..….. East Grand Rapids High School

May 2014……………….………... B.S. in Mechanical Engineering, Valparaiso University

August 2017 ……………………….. M.S. in Environmental Science, The Ohio State University

May 2019…………………………... Ph.D. in Environmental Science, The Ohio State University

Publications

Ogland-Hand, J., Bielicki, J., Wang, Y., Adams, B., Buscheck, T., Saar, M. (2019) "The Value of Bulk Energy Storage for Reducing CO_2 Emissions and Water Requirements from Regional Electricity Systems." *Energy Conversion and Management,* 181, 674-685.

Fields of Study

Major Field: Environmental Science

Table of Contents

List of Tables

List of Figures

Chapter 1: Introduction

1.1. Introduction

Greenhouse gases (GHGs) raise the temperature of the atmosphere by absorbing the reradiated infrared radiation from the Earth. This phenomenon is called the greenhouse effect and it is essential for life, but human activities are substantially increasing the atmospheric concentration of GHGs, which is driving climate change [1]. As of 2018, long-term changes to the climate system (e.g., sea-level rise) have caused negative impacts to biodiversity and ecosystems (e.g., species loss and extinction), and ultimately pose risks to human health and economic growth [2]. To limit this damage, GHGs emissions must be reduced.

Carbon dioxide (CO_2) contributed 81% of all GHG emissions in the United States in 2016, with methane (10%), nitrous oxide (6%), and fluorinated gases (3%) contributing the remainder [3]. CO_2 is the largest portion of total GHG emissions in the United States in part because the economy relies on many technologies and processes that burn fossil fuels and thus emit CO_2 [4]. In addition to the increased quantity of CO_2 emitted compared to other GHGs, the residence time of CO_2 is much longer (i.e., hundreds of years long) than methane (i.e., ~10 years), the next most emitted GHG. As a result, many climate change mitigation efforts focus specifically on reducing CO_2 emissions.

The electricity sector is one of the largest sources of CO_2 emissions in the United States. For example, in 2016, the electricity sector emitted 34% of all CO_2 emissions in the United States, and transportation (34%), industrial processes (15%), residential and commercial processes (10%), and other processes like land-use change (6%) were responsible for the remainder [5]. Despite this high CO_2 emission intensity, least-cost climate change mitigation pathways rely on the electricity system reaching near zero CO_2 emissions by 2050 and then achieving negative CO_2 emissions afterwards, all while the overall demand for electricity increases from the electrification of substantial portions of the transportation, heating, and industrial sectors [6,7]. As a consequence, rapidly reducing CO_2 emissions from the electricity system is one of the most pressing challenges to addressing climate change.

Variable renewable energy technologies (i.e., wind turbines, solar photovoltaics) can generate electricity without emitting CO_2, but relying on these technologies to meet most or all of the electricity demand is expensive in part because wind and sunlight may not be available when electricity is demanded [8]. As a result, energy storage technologies are needed that can time-shift electricity generation from when it is generated to when it is demanded [9]. Although an electricity system comprised entirely of conventional approaches to energy storage (e.g., batteries, pumped-hydro energy storage) and variable renewable energy technologies could theoretically meet demand [10], that electricity system could only eliminate CO_2 emissions, it could not achieve negative CO_2 emissions. As a consequence, in addition to variable renewable energy technologies and energy storage, other resources and processes will also be required to meet climate change mitigation goals.

One such process is geologic CO_2 storage, which is part of the CO_2 capture and storage (CCS) process. During CCS, CO_2 emissions are captured from large point sources (e.g., coal-fired power plant, cement manufacturer) and injected into deep saline aquifers [11,12]. Negative CO_2 emissions can be obtained by coupling CCS with bio-energy power production [13,14]. In bio-energy CO_2 capture and storage (BECCS) processes, electricity is generated using heat obtained from burning biomass feedstocks (e.g., corn stover, grass crops, woody plants) that reduced the atmospheric concentration of CO_2 via photosynthesis during growth. The CO_2 emissions from burning the feedstocks are captured and isolated from the atmosphere by storing them in the subsurface. In this way, geologic CO_2 storage is required to achieve negative CO_2 emissions.

Geothermal energy is another renewable energy resource that can be used to generate electricity without emitting CO_2. During geothermal power production, heat from the subsurface is extracted to the surface and used to generate electricity. Unlike variable renewable energy resources, geothermal heat is constant and as such geothermal power plants can generate electricity on demand. Due to this dispatchability, geothermal power plants are included in least cost electricity systems that reduce CO_2 emissions even though these power plants have higher costs than other low-carbon generation technologies, namely variable renewable energy technologies [15].

Emerging approaches to geothermal power production seek to extract geothermal heat using geologically stored CO_2 [16–19]. In this CO_2 capture, *utilization,* and storage process (CCUS), a portion of the CO_2 that is stored in the subsurface is intentionally produced to the surface and the pressure and heat energy in the fluid is used to generate electricity before re-injecting the CO_2 back underground.

The research presented in this dissertation builds on this concept by using geologically stored CO_2 to extract geothermal heat in a way that provides energy storage services that address challenges of integrating and utilizing variable renewable energy technologies. This introduction chapter presents a more in depth background on geothermal energy and the use of geologically stored CO_2 as a heat extraction fluid to provide context for CO_2-based energy storage (Section 1.2), before discussing the knowledge gaps that the subsequent chapters of the dissertation address (Section 1.3).

1.2. Combining Geothermal Energy and Geologic CO_2 Storage: Context for CO_2-Based Energy Storage

Geothermal energy is the thermal energy that is contained in the crust of the earth [20]. Approximately 60% of this thermal energy arises from the radioactive decay of elemental isotopes (i.e., potassium, uranium, thorium) and the remaining 40% this thermal energy is conducted and/or convected from the core of the earth outward toward the surface of the earth [21–23]. In the subsurface, this energy is distributed between the host rock and brine contained in the pores, faults, and fractures within that rock [20,21].

To use this thermal energy to generate electricity, the heat (high temperature source) is extracted to the surface and exchanged with the atmosphere or cooling water (low temperature sink) in a geothermal power plant [24,25]. In 2011, the Intergovernmental Panel on Climate Change estimated the global technical potential to generate electricity from geothermal resources between 117.5 EJ/yr and 1,108.6 EJ/yr [26]. For reference, approximately 565 EJ of primary energy was consumed globally in 2013 [27].

In addition to heat that can be extracted, geothermal resources also require fluids to extract that heat, and permeability through which those fluids can flow through the subsurface. To date, brine has been the primary heat extraction fluid because it often exists in the geologic formations that have conventionally been used for geothermal power production. But emerging approaches seek to instead use CO_2 as the heat extraction fluid due to (a) some advantageous thermophysical properties and (b) the potential to sequester CO_2 from the atmosphere and produce electricity with negative CO_2 emissions. In this section, the state of understanding of the types of geologic formations that can be geothermal resources (Section 1.2.1), and the potential benefits of using CO_2 as the heat extraction (Section 1.2.2) are discussed to provide the context to using geologically stored CO_2 to extract geothermal heat in a way that time-shifts electricity generation.

1.2.1. Geologic Formations that Can Be Geothermal Resources

There are three primary geologic formations that could be used as geothermal resource for electricity production: naturally faulted and fractured formations (Section 1.2.1.1), hot dry rock (Section 1.2.1.2), and sedimentary basins (Section 1.2.1.3). Table 1 lists the conventionally accepted taxonomy for depths and temperatures across of all three of these geologic formations.

Table 1: Typical Grades of Geothermal Resource Depth and Temperature [28,29].

Resource Depth (D)			**Resource Temperature (T)**		
Shallow	Mid-Range	Deep	Low	Intermediate	High
1 km ≤ D ≤ 3 km	3 km ≤ D ≤ 6 km	6 km ≤ D ≤ 10 km	T < 100°C	100°C ≤ T ≤ 180°C	T > 180°C

1.2.1.1. Naturally Faulted and Fractured Formations

Naturally fractured and faulted formations that contain fluids at sufficient temperatures (over 150°C) have typically been the resource that has provided geothermal heat for electricity production [30,31]. These resources are typically located 1 – 4 km deep [21] and are often associated with volcanic activity or found by plate tectonic boundaries [26]. Geofluid/brine is present in a surface manifestation (e.g., a hot spring), or it can be extracted from naturally faulted and fractured formations through a well. The fluid in these formations is recharged with rain or groundwater that enters the resource through a surficial recharge area (e.g., a fault) [32]. Artificial recharge injection wells may be used to maintain or replenish resources if these resources are not sufficiently connected to a surficial recharge area [33].

To date, geothermal energy development has been economically feasible where geological and hydrological conditions favor the formation of hydrothermal systems: naturally faulted and fractured formations that contain water/brine at locations that have high geothermal temperature gradients. These conditions are likely to be found in volcanic and tectonic areas because they tend to have highly permeability faults and fractures that allows brine to circulate to depths of a few kilometers in the subsurface, where it heats up and can ascend due to buoyancy [34]. In the United States, these formations with sufficient heat exist in the western third of the country, and have an identified potential of 9,057 MWe of an estimated possible 30,033 MWe [21,35].

1.2.1.2. Impervious/Low Permeability and Low Porosity Formations: Hot Dry Rock

Naturally faulted and fractured formations with sufficient temperature are limited geographically and many of the known and economically-viable opportunities to use the geothermal heat in these resources have already been developed [20]. Estimates of geothermal resources have tended to focus on high-grade, naturally faulted and fractured systems with in situ brine [26]. But these “hydrothermal” systems are limited in number and in location and are thus unlikely to provide the basis for major long-term expansion of geothermal energy. This perception has led to undervaluing the long-term potential of geothermal energy by missing an opportunity to develop technologies to mine heat from large volumes of accessible hot rock [36].

Another potential resource does not have the natural pathways, but has an enormous potential to provide usable heat: Hot Dry Rock (HDR). HDR resources are comprised of mostly granite [37], and lack sufficient porosity and permeability for fluids to be present and flow, and/or an adequate reservoir to recharge these fluids [20]. HDR resources are common up to 10 km deep throughout the world [36,38].

Enhanced Geothermal Systems (EGS) in HDR resources could expand geothermal electricity production to many parts of the world [36]. An EGS facility could theoretically be implemented anywhere the subsurface is hot enough (150-300 ^{o}C) that it can to be used to generate electricity [20,21,28], which is typically between 3 and 10 km deep [36]. With EGS, the otherwise unobtainable heat resource in HDR can be accessed by engineering, or "enhancing," the reservoir [21,26,28]. Fluids are injected under high-pressure through a well to create fractures in the HDR. A heat extraction fluid is pumped through these fractures, is heated by the surrounding rock, and is then extracted to the surface by a production well in a closed loop process [20,32]. In the United States alone, estimates suggest that over 200,000 EJ of primary energy could be extracted with EGS and 100 GW_e or more of cost competitive generating capacity could be established by 2060 [21,23,26,36]. For the EGS approach to realize this potential from a technical perspective, technological advances must: (1) double to quadruple production rates, and (2) achieve sustained production of fluids with sufficient thermal lifetime (3) over a range of geologic conditions [39].

1.2.1.3. Porous and Permeable Formations: Sedimentary Basins

EGS involves engineered stimulation of the HDR and thus may encounter real or perceived risks that could impede its deployment (e.g., induced seismicity) [40]. In contrast, sedimentary basin (or stratigraphic) reservoirs are naturally porous and permeable and thus do not require such stimulation [16]. Sedimentary basins are regions in the crust of the earth where sediment has accumulated for long geologic time periods and are ubiquitous throughout the world [41,42]. For example, these basins underlie approximately half of North America [43,44]. Naturally porous and permeable sedimentary basin resources tend to be shallower (1-5 km) and cooler (90-300°C) than HDR resources. These cooler temperatures are the primary reason why sedimentary basins are currently underexplored for geothermal energy development, but they are much larger than EGS resources, and have much higher permeabilities than naturally faulted/fractured resources and HDR resources.

1.2.2. Using Geologically Stored CO_2 as a Heat Extraction Fluid

Using CO_2 as a heat extraction fluid was first proposed for EGS in HDR [45]. Since then, numerous studies have investigated using CO_2 in HDR and sedimentary basin formations and have found that CO_2 extracts heat more effectively than brine in both HDR and sedimentary basin resources [18,46]. In general, the amount of heat that can be extracted by a fluid depends on the specific heat of the fluid and the mobility (ratio of density to kinematic viscosity) of the fluid [16]. Although CO_2 has roughly half the specific heat of water, CO_2 has a much higher mobility in part because it is supercritical below 800m and thus has the density of a liquid but the viscosity of a gas. The low viscosity of CO_2 permits large mass flow rates in the subsurface [47]. As a result, CO_2 can extract up to four times as much heat as water/brine, depending on the combination of depth and temperature [16,45,48].

Using CO_2 to extract heat from sedimentary basins was first proposed as a way to improve the economic viability of CCS [16]. These porous and permeable saline aquifers can hold large amounts of CO_2 [49] that could be used to extract the heat in the aquifer, which is typically low- to medium-grade [50]. Hot CO_2 would be extracted through a production well where the heat would be converted into electricity in a geothermal power plant [16,18]. As a consequence, using sequestered CO_2 as the heat extraction fluid in sedimentary basins could expand the geothermal resource base by using resources that are cooler than HDR and would otherwise not be used to produce electricity.

An additional benefit to using CO_2 is that the density of CO_2 is more sensitive to changes in temperature and pressure than is brine. As a result, CO_2 is buoyant in sedimentary basins because it is less dense than the native brine. This buoyancy encourages the CO_2 to rise up a production well without the need for a costly pump. Further, the CO_2 is much denser at the injection well, after being cooled in the geothermal power plant, than at the production well, and these density differences can automatically generate flow through the system due to a self-convecting thermosiphon that forms [51]. This thermosiphon can be beneficial because it can reduce the parasitic pumping requirements that are necessary to circulate the heat extraction fluid [17].

1.3. Scope of Dissertation

Multi-fluid geo-energy systems that use both CO_2 and brine to extract heat from sedimentary basin geothermal resources have also been proposed [52–54]. These systems use two geothermal power plants to generate electricity (i.e., a CO_2-based power plant, and a brine-based power plant) and a concentric-ring well pattern is used in the subsurface to separate these two fluids from one another: CO_2 is injected into an inner ring of wells while in-situ brine is produced to the surface and then re-injected into rings of wells that surround CO_2. This concentric ring well pattern controls both the migration of the CO_2 plume and the overpressure (i.e., the pressure above hydrostatic) in the subsurface. As such, in these systems, geologically stored CO_2 is used for both pressure support and to extract geothermal heat.

A multi-fluid geo-energy system can operate a geothermal power plant to provide continuous power by constantly (a) producing geothermally heated CO_2 and brine to the surface, (b) using the heat and pressure energy in these fluids to generate electricity in the two geothermal power plants, and (c) re-injecting these fluids back into the subsurface. Additionally, it is also possible to use the system to time-shift electricity production [54]. During this mode of operation, electricity is produced by using the energy in the fluids to generate electricity in their respective power plants, but the produced brine is stored in holding ponds at the surface instead of being immediately re-injected into the outer rings. Electricity can be then later be used (stored) by powering pumps to re-inject the brine from the holding pond along with new CO_2 into the sedimentary basin. In this way, multi-fluid geo-energy systems can store electricity in the form of pressure in the subsurface.

The work presented in this dissertation builds on this idea by on developing and valuing CO_2-based approaches for energy storage by integrating both process-level and systems-level models. More specifically, this dissertation (1) deepens the understanding the physical and economic performance of this concentric-ring, pressure-based system design (referred to as CO_2-Bulk Energy Storage (CO_2-BES) or concentric-ring, pressure-based bulk energy storage (CRP-BES)), (2) values the potential that it has to multiple electricity system applications, and (3) compares and contrasts the use of CO_2 vs brine as a medium for subsurface thermal energy storage. In this section, context for each subsequent chapter is provided and the knowledge gaps that were addressed are discussed.

1.3.1. Chapter Two: The Value of Bulk Energy Storage for Reducing CO_2 Emissions and Water Requirements from Regional Electricity Systems

Conventional electricity systems supply demand using flexible (e.g., natural gas) and inflexible (e.g., coal, nuclear) power plants [9]. Inflexible power plants were designed to meet the portion of demand that is constant, and as such require hours to adjust their output in response to a change in demand [55]. Because inflexible power plants cannot quickly adjust electricity production, electricity generated by wind and solar energy technologies may be curtailed if there is not enough demand (e.g., on a sunny, cool afternoon). As a result, one application for energy storage is storing electricity generated from renewable energy sources during hours of excess supply and dispatching that stored electricity when demanded. System-wide CO_2

emissions are reduced if this time-shifting reduces the amount of electricity that conventional power plants need to generate. Further, because conventional power plants also require water for cooling, this time-shifting can also reduce system-wide water requirements.

In this chapter, a mixed-integer linear optimization model was built and used to monetize the value of three different energy storage technologies for reducing operational CO_2 emissions and water requirements: Pumped Hydro Energy Storage (PHES), Compressed Air Energy Storage (CAES), and CO_2-BES. Prior to this study, the value of these services had not been monetized or compared across different approaches to energy storage.

This study also depended the understanding of the physical performance of CO_2-BES system. Prior to this study, the performance of a CO_2-BES facility was approximated by multiplying (a) data from subsurface fluid flow simulations where CO_2 and brine were continuously produced and re-injected (i.e., operating as a geothermal power plant, not as an energy storage facility) at the flowrate that was generated by the pressure in the subsurface (i.e., artesian flowrates, no pumping), by (b) estimated power generation coefficients for each geothermal power plant [54]. In this study, the continuous artesian flowrate reservoir results were still used, but models of the production and injection wells and of the two geothermal power cycles were built and used to estimate the power output and storage capacities instead of relying on estimated power generation coefficients.

1.3.2. Chapter Three: Potential Mechanisms for Using Geologically Stored CO_2 for Energy Storage

In addition to hourly fluctuations, the availability of wind and sunlight also varies on seasonal timescales. As a result, there may be a need for seasonal energy storage approaches that can time-shift electricity generation from summer to winter, for example [10,56–61]. Despite this need, there are few if any approaches to energy storage that are currently capable of time-shifting electricity for weeks to months at a time.

This study continued to deepen the understanding of the physical capabilities of the CO_2-BES system by (1) introducing a fully integrated model of the CO_2-BES facility that does not rely on previously published artesian reservoir simulation results and (2) using the integrated model to investigate the maximum duration over which a CO_2-BES facility could time-shift electricity generation by specifying different energy storage operational cycles (i.e., time-shifted fluid injection and production) within the reservoir simulator.

Further, this study also presents an initial comparison of using pre-heated CO_2 vs pre-heated brine for underground thermal energy storage. Storing energy in the subsurface as pressure (i.e., the CO_2-BES process) may limit the length of time that energy can be stored or discharged if the increase in overpressure exceeds the caprock fracture pressure. Alternatively, thermal energy could be stored by pre-heating fluids prior to injection. For example, during seasons when energy needs to be stored, thermal energy from a nuclear powerplant could be transferred to a fluid, instead of being used to generate electricity, and the heated fluid could be stored underground [62,63]. In this process, the subsurface would thermally insulate the fluid and the heated fluid could be later produced to the surface and used to generate electricity. As an initial investigation into this process, this study compared using pre-heated CO_2 vs brine on four metrics: (1) the power required to compress and inject the fluids into the subsurface, (2) the effect that the injection of fluids that have been pre-heated to various extents on the downhole temperature of the reservoir, (3) the total amount of energy that is stored and available for dispatch in the subsurface; and (4) the thermal energy storage efficiency.

1.3.3. Chapter Four: Operational Characteristics of a Geologic CO_2 Storage Bulk Energy Storage Technology

Unlike conventional energy storage approaches (i.e., PHES, CAES), the length of time that the CO_2-BES facility dispatches electricity is not constrained by the amount of energy that was previously stored. For example, at any given time, there is flexibility for a CO_2-BES operator to dispatch electricity at capacity for 1 hour, or over 12 hours, because the system relies on the overpressure in the subsurface and the geothermal heat for power production. But over the lifetime of the facility, these operational decisions could affect how the facility operates if the charge and discharge duration substantially changes the overpressure or the rate at which geothermal heat is extracted. In this conference paper, the integrated model of the CO_2-BES system is used to investigate the potential that charging and discharging cycles of differing lengths may have on the power storage capacity and power output capacity of the CO_2-BES facility.

1.3.4. Chapter Five: The Value of CO_2-Bulk Energy Storage with Wind in Transmission Constrained Electric Power Systems

Another challenge to variable renewable energy integration is that wind and solar energy resources may not be located in the same area that electricity is demanded. For example, much of the high quality wind resource in the United States is far away from major load centers [64]. High voltage direct current (HVDC) transmission lines are used to transmit electricity over long distances, but HVDC infrastructure is expensive, and sizing the capacity of the HVDC lines is difficult given the fluctuations in the amount of electricity that is produced by the variable renewable solar and wind resources. For example, electricity generated by a wind farm may be curtailed if the generation exceeds the HVDC transmission capacity, but increasing the capacity is costly. As a result, one application for energy storage is in transmission constrained electricity systems: excess electricity can be stored instead of curtailed, and then dispatched later when the output from the wind farm is less than capacity of the HVDC transmission.

In this chapter, the value of a CO_2-BES to increasing the profit-maximizing HVDC transmission line is investigated by using (1) the integrated process-level model of the CO_2-BES facility, (2) a cost-model of the CO_2-BES facility that was developed for this study to estimate the capital cost and additional operating cost of the facility, and (3) a mixed-integer linear optimization model that was developed for this study to simulate a CO_2-BES facility operating with a wind farm in Eastern Wyoming to sell electricity to Los Angeles, CA via a 960 mile HVDC transmission line. Prior to this chapter, the cost of a CO_2-BES facility was poorly understood and the optimal dispatch of CO_2-BES when coupled with a variable renewable energy technology to sell electricity to a distant load center had not been studied. Further, although there are many applications for energy storage, there are currently little to no market rules in the United States that enable these technologies to be used within the electricity system [65,66]. As a consequence, one of the largest markets for energy storage is applications with transmission infrastructure, in part because of the discrepancy between where electricity is demanded and where variable renewable energy resources are located [67]. As a result, this chapter is also the first to determine the profitability of a CO_2-BES facility when being used in one of the most valuable applications for energy storage.

1.3.5. Chapter Six: Conclusion

This dissertation concludes by presenting holistic conclusions that can be made by looking across each chapter and then discussing related knowledge gaps that could be addressed with future research.

Chapter 2. The Value of Bulk Energy Storage for Reducing CO_2 Emissions and Water Requirements from Regional Electricity Systems

2.1 Introduction

Human-induced climate change is driven by the accumulation of greenhouse gases (GHGs) in the atmosphere [68]. Carbon dioxide (CO_2) is a particularly worrisome GHG in part because modern energy systems and industry infrastructure (e.g., cement manufacturing, oil refining) rely on processes that emit CO_2 [4]. In 2016, fossil-fueled thermoelectric power capacity generated ~65% of electricity in the United States and emitted ~35% of the 1.8×10^3 million metric tonnes of CO_2 ($MtCO_2$) from the energy industry [69]. These power plants also require water for cooling and withdrew 30 trillion gallons in 2015 [70], even having reached ~40% of total annual freshwater withdrawals [71]. Water demand exceeds supply in ~10% of the watersheds in the United States [72], and water stress such as this is expected to worsen as climate change amplifies precipitation variability [68] and populations grow [73].

The challenges of reducing CO_2 emissions and water requirements can be addressed in part by increasing the deployment and utilization of wind and solar energy technologies now [74] and with further climate warming [75]. But wind and sunlight are variable and there may be times when wind- or and solar-generated electricity must be curtailed because (a) the total generation exceeds demand, or (b) other electricity capacity cannot ramp to accommodate the fluctuations. Energy storage technologies can time-shift excess electricity when it is generated and dispatch it when it is needed [9], substitute coal-fired power plants with variable renewable energy technologies [76], and address large fluctuations in electricity generation from those technologies [77]. In particular, bulk energy storage (BES) technologies have high capacities (≥100 MW) and discharge times on the order of hours, and can thus be used for large-scale applications [78].

Pumped Hydroelectric Energy Storage (PHES) is the dominant BES approach, and works by using energy to pump water to a higher elevation and later letting that stored water flow downhill through a turbine to generate electricity and into a lower reservoir [79]. There were over 129 gigawatts (GW) of PHES capacity in 2014, which comprised 99% of the BES capacity worldwide [80]. The other industrial-scale BES technology is Compressed Air Energy Storage (CAES), which typically uses electricity to store compressed air underground [81] and later dispatches electricity by injecting a fuel (e.g., natural gas), burning that fuel, and expanding the combustion products through a turbine [82]. Recently, CO_2 Bulk Energy Storage (CO_2-BES), which is based on CO_2 Plume Geothermal technology [16,83], has been proposed. In the CO_2-BES design that we consider here [54], energy is stored by pressurizing and injecting CO_2 and produced brine into deep (>800 m) porous and permeable aquifers with a sufficient geothermal heat flux [18]. Electricity is later generated by producing some of the brine and CO_2 to the surface, with the benefit of a self-convecting thermosiphon [17], and flowing these heated fluids through geothermal power plants [18].

The dispatch of any of these BES technologies in the United States would be orchestrated by Independent System Operators (ISOs) and Regional Transmission Operators (RTOs). Collectively, these entities manage the dispatch of ~60% of the electricity that is generated in the United States to ensure that supply meets demand [84]. To do so, electricity generating units (EGUs) submit for day-ahead markets hourly price-quantity bids that are based on their operating costs [85]. These bids establish the dispatch order, where facilities with cheaper bids are dispatched before those with costlier bids [86]. In some regions, ISOs and RTOs also compensate facilities for providing ancillary grid services, such as frequency regulation and spinning reserves [85].

Implementing BES in a regional electricity system can alter the dispatch order, with concomitant changes in system-wide CO_2 emissions due to the re-prioritization of power plants that emit CO_2 (e.g., coal, natural gas), and their possible displacement with increased utilization of renewable energy capacity. Prior studies have found that the implementation of bulk energy storage increases CO_2 emissions in regional electricity systems [87,88], unless there is very high penetration of wind energy technologies [89], but consideration of fuller effects on the dispatch curve is nascent [90]. Further, studies of the effects of dispatching BES have not investigated the water requirements of the energy technologies that could be dispatched, despite the importance of the energy-water nexus in understanding the environmental implications of energy systems [91]. Since the power plants that emit CO_2 are a subset of the thermoelectric power plants that require water for cooling (e.g., nuclear), changes in the dispatch order due to the implementation of BES could also affect system-wide water requirements.

Full consideration of the distribution of energy technologies in regional energy systems [92,93] the ways in which the use of BES can alter the dispatch order, and the temporal characteristics of electricity can uncover how the use of BES can result in an increase in electricity generation from energy technologies that emit less CO_2 or require less water than those that would otherwise be dispatched. As such, this investigation is novel in a few ways. First, we consider the characteristics for dispatch of each individual EGU in a regional energy system. Second, while some studies have investigated how individual BES technologies may affect CO_2 emissions [94,95], or be dispatched under different CO_2 emissions limits [93,96,97], studies that compare BES technologies in the same regional electricity system are lacking. Third, CO_2-BES has been recently proposed and, unlike PHES and CAES, its dispatchability and effects in regional electricity systems has yet to be investigated. Fourth, we are not aware of prior studies that have monetized the value that BES may have for reducing operational CO_2 emissions in regional electricity systems. Fifth, to our knowledge, changes in water requirements due to BES have not yet been investigated, let alone monetized.

This paper is organized as follows: Section 2 presents the methods to determine the dispatch curve and to value the changes in system-wide CO_2 emissions and water requirements, the critical parameters for environmental variables and operating characteristics of individual energy technologies, and the case study on the Electric Reliable Council of Texas (U.S.A.). Section 3 contains the results—including sensitivity analyses of the effects of critical parameters—of changes in the dispatch order, the resulting changes in

CO_2 emissions and in water requirements, and the value of these changes. Section 4 contains a discussion and conclusions, which include implications for the development of market rules for ISOs and RTOs that incorporate how BES can help to enhance the stability of the grid and also compensate facilities for their contribution to the environment.

2.2 Methods

As shown in Figure 1, we developed and implemented a framework that includes a mixed integer linear program (MILP) to optimize how BES may be dispatched in the regional electricity system (Section 2.2.1). We incorporated the performance characteristics of PHES, CAES, and CO_2-BES, as well as facility-level data on heat rates (and thus CO_2 intensities) and water intensities from the electricity system in the Electricity Reliability Council of Texas (ERCOT) region (Section 2.2.2). To incorporate uncertainty, we implemented sensitivity analyses using (a) a Monte Carlo Analysis for the price of natural gas, the price of coal, the operating cost for wind power, and the operating cost for nuclear power (Section 2.2.3.2); and (b) various discrete values for CO_2 prices, water prices, and renewable energy generation scenarios (Section 2.2.3.1).

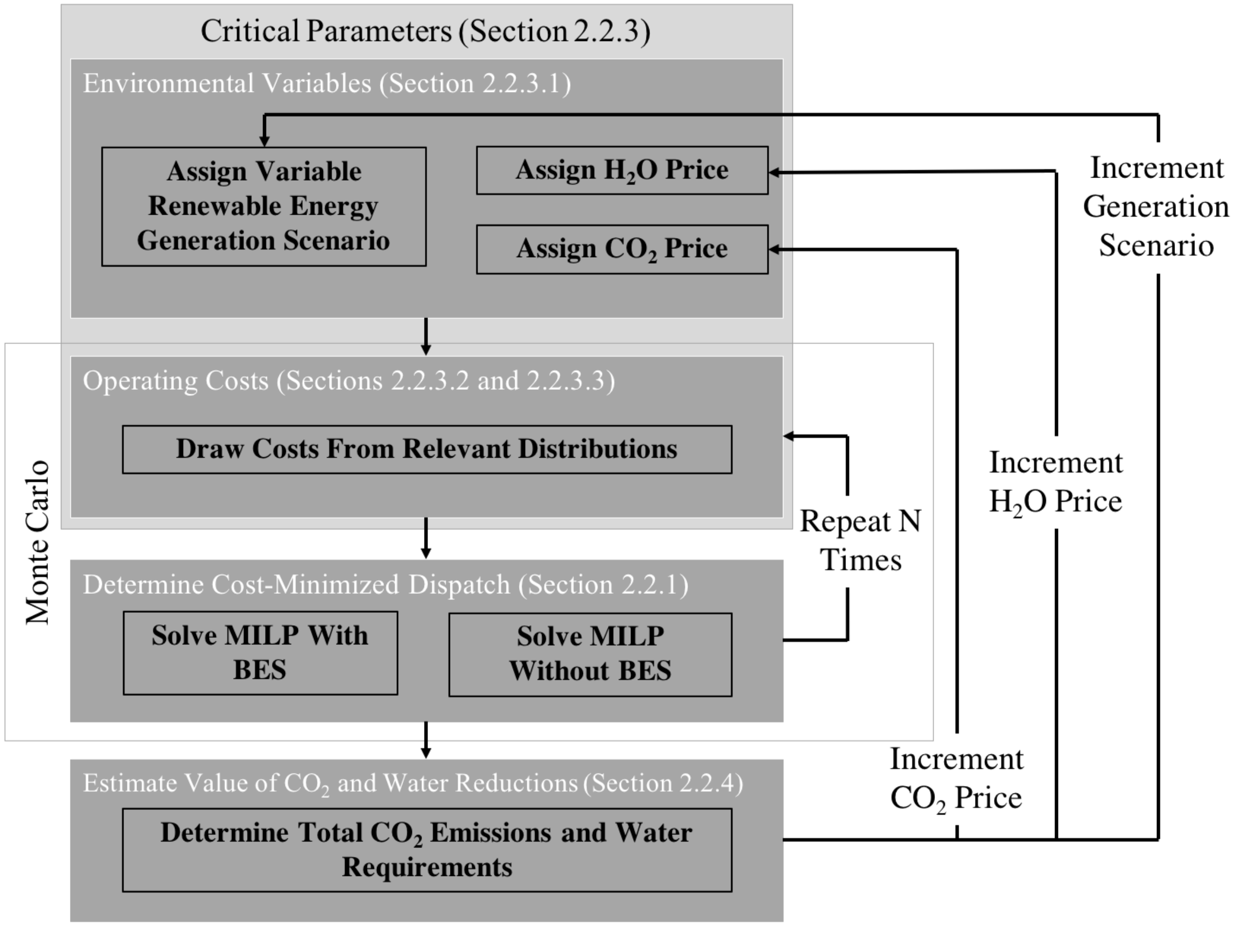

Figure 1: Framework for Estimating the Value of BES to Reducing System-Wide CO_2 Emissions and Water Requirements.

2.2.1 Mixed-Integer Linear Program

Here we provide a brief description of the MILP, which determines the least-cost dispatch of electricity-generating facilities to meet demand, as a function of the operating costs of the facilities ($O_{(.)}$), the CO_2 price (P_{CO_2}), and the water price (P_{H_2O}),

$$\sum_{t=0}^{T}\left\{\frac{1+\eta}{\eta}Q_{B,t}O_B+Q_{B,t}\left(\alpha_B P_{CO_2}+\beta_B P_{H_2O}\right)+Q_{r,t}O_r+\sum_i\left[Q_{i,t}O_i\right]+\sum_j\left[Q_{j,t}O_j\right]+\sum_k\left[Q_{k,t}O_k\right]\right\} \quad (1)$$

where $Q_{(.)}$ is the quantity of electricity that is generated by bulk energy storage (B), variable renewable energy (r), nuclear (i), coal (j), and natural gas (k) energy technologies; $O_{(.)}$ refers to the operating costs for those energy technologies. For BES, η is the round-trip efficiency (ratio of the energy that is dispatched to the energy that is stored), α is the CO_2 emissions intensity (tCO_2/megawatt-hour (MWh)), and β is the water requirement intensity (gal/MWh). The full specification is included in Section 1 of Appendix A.

We represented variable renewable energy as a separate, aggregate component because wind and solar energy technologies do not emit CO_2 or require water when they are operated. The BES technology was also included as one aggregate component because we were interested in the level at which it would be dispatched (i.e., MWh). For the individual dispatchable units, we represented the coal and natural gas energy technologies at the EGU level to capture differences in CO_2 emissions intensities, water requirement intensities, and operating costs. We represented the nuclear energy technologies at the power plant level because their water requirements are at the plant level. Overall, the CO_2 emissions intensities and water requirement intensities of these energy technologies are incorporated into the operating cost equations, as detailed in Section 1 of Appendix A. The MILP also incorporates a few other common assumptions:

1. Perfect foresight of demand and of the availability of variable renewable energy resources [98,99];
2. The dispatch order is based on operating costs [86]; and
3. Since we modeled one day at a time, there is an implicit assumption that the energy that is stored by BES is worthless if it has not been fully discharged by the end of the day.

2.2.2 Case Study: Electricity Reliability Council of Texas

We used data on the electricity-generating facilities, electricity demand, and electricity that was generated by wind in the ERCOT region. There are four principle reasons why we selected ERCOT:

1. ERCOT is an ISO that manages the electricity market for over 75% of the area of Texas, as shown in Figure 2, which represents 90% of the electricity load in Texas [100,101].
2. The electricity system in the ERCOT region is almost completely isolated from the Eastern and Western Interconnections and the Mexican Power Grid. Only ~10% of the electricity demand within the ERCOT region is supplied by imports [102].

3. Texas has adequate wind and solar resources that could be used to generate electricity [103] as well as sedimentary basin resources that could be used for subsurface energy storage. Sedimentary basin resources are relatively ubiquitous [41,42,104], and underlie approximately half of North America [44,49]. As a result, it is likely that a region with a footprint comparable to ERCOT may have similar combinations of resources.
4. Texas has the largest installed capacity of wind turbines in the United States: 20,321 MW as of 2016 [105].

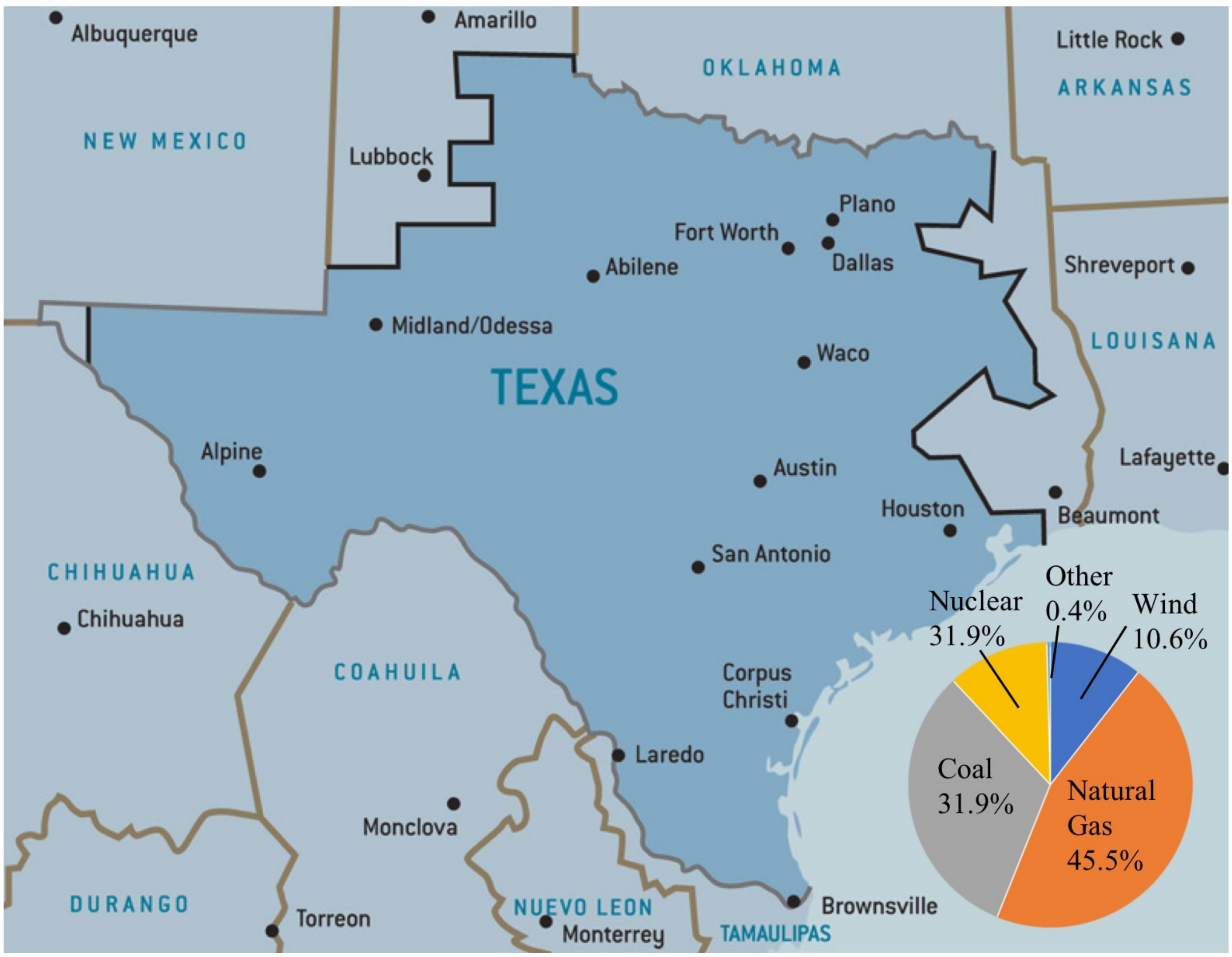

Figure 2: Extent of the Electricity Reliability Council of Texas (ERCOT) Region [106]**.** The approximate percentages of generation by capacity are from 2014 [107].

We obtained data on electricity generation and fuel type for each EGU at fifteen-minute intervals from the ERCOT 60-Day Security Constrained Economic Dispatch Disclosure Reports [107]. From these data, we included in our analysis wind, natural gas, coal, and nuclear because, as shown in Figure 2, these resources accounted for 99.6% of the electricity that was generated in ERCOT in 2014. We obtained the monthly heat rate, capacity, and water withdrawal data for the nineteen coal EGUs and 59 natural gas EGUs from the U.S. Energy Information Administration (EIA) [70,108]. We used yearly averages of the heat rate, capacity, and water withdrawals for each of these EGUs. We gap-filled the three missing heat rates for natural gas EGUs and twelve of the fourteen missing water withdrawal rates for natural gas EGUs by using the averages of the other EGUs with the same prime mover (e.g., steam) and type of cooling system (e.g., once-through). The two other water withdrawal rates had unique combinations of prime movers and cooling systems, and we used the appropriate median values from a recent review article [109]. For the two nuclear power plants, we obtained water withdrawal rates from the EIA data and the plant capacities from the Nuclear Resource Council [110]. We also acquired hourly data on the electricity load and the amount of electricity that was generated by wind turbines in 2014 [111]. (Section 2 of Appendix A includes more details on the data.)

2.2.3 Critical Parameters and Data

2.2.3.1 Environmental Variables – Net Load, Renewable Energy Generation, CO_2 Price, and Water Price

In 2014, wind turbines generated 11% of the electricity that was supplied in the region [107]. We investigated three renewable energy generation scenarios that are multiples of that amount: 11% (baseline), 22% (medium), and 44% (high). The "net load" is the electricity load less the amount of electricity that is generated by variable renewable energy technologies. As such, the net load is the amount of electricity that must be generated from the coal, natural gas, and nuclear facilities, and thus indicates how much of the dispatch order must be used.

We varied the CO_2 price from \$0/tCO_2 (baseline) to \$100/tCO_2, in increments of \$20/tCO_2. This range is consistent with prior studies that investigated BES and renewable energy technologies [112], and encompasses current and potential CO_2 prices and CO_2 capture costs [113–115].

Water lease rates for electricity generation in Texas have been about \$0.0003/gal (\$100/acre-ft) [116], but the social cost of water is higher than typical market transactions and increased water stress may lead to higher water prices [117]. As such, we investigated three water prices: \$0.0003/gal (historical baseline), \$0.001/gal (medium), and \$0.01/gal (high).

2.2.3.2 Power Plant, Electricity Generating Unit, and Wind Component

The operating costs for the coal and natural gas EGUs depend on their heat rates and the cost of the fuel, as well as the price of CO_2 and the price of water (because they emit CO_2 and require water for cooling). The operating costs for nuclear power plants similarly depend on the price of water, but they do not depend on the price of CO_2 because these plants do not emit CO_2. Table 2 shows the other components of operating costs (Eqs. 17- 20 in Appendix A). The ranges are the endpoints of the distributions that we sampled in the Monte Carlo analysis approach to the sensitivity analysis (Section 2.2.5).

Table 2: Components of the Operating Costs for Select Energy Generation Technologies. The non-fuel related costs are the total operating costs for nuclear power plants and the wind component, and the fixed operating costs for the coal and natural gas EGUs.

	Non-Fuel Related Costs (\$/MWh)	Fuel Price (\$/MMBtu)	CO_2 Emissions Rate (tCO_2/MMBtu)
Nuclear Power Plants	[1.46, 16.16] [a]	N/A	N/A
Coal EGUs	2.97 [b]	[1.25, 1.64] [c]	0.0977 [e]
Natural Gas EGUs	0.67 [b]	[1.85, 11.80] [d]	0.0531 [e]
Wind Component	[3.42, 13.42] [a]	N/A	N/A

[a]The maximum and minimum sum of the variable and fixed operating costs from 2009 to 2016 [118], [119], [120], [121], [122], [123], [124], [125]; [b]Average fixed cost from 2009 to 2012 [118], [119], [120], [121]; [c]The quarterly price range in Texas for electricity production from Quarter 1 2008 to Quarter 2, 2016 [126]; [d]The monthly price range in Texas for electricity production from January 2002 to October 2016 [127]; [e]CO_2 emissions rate for lignite coal and natural gas, respectively [128].

Table 3 shows the operating characteristics that limit facilities from accommodating fluctuations in electricity generation from variable renewable energy technologies.

Table 3: Characteristics of the Flexibility of Select Energy Technologies

	Minimum Load (% Capacity)	Ramp Rate (%/hour)	Minimum Up Time (hours)	Minimum Down Time (hours)
Gas Turbine	50[a]	500[a]	4[d]	6[d]
Natural Gas Combined Cycle	50[a]	300[a]	4[d]	2[d]
Coal	50[b]	158[c]	2[d]	3[d]
Nuclear	100	0	N/A	N/A

[a][129]; [b][130]; [c]The largest ramp rate [131]; [d]The average down time [132]

2.2.3.3 Bulk Energy Storage Technologies

Neither PHES nor CO_2-BES emit CO_2 when operated, but the operating costs of CAES depend on the price of CO_2 because the technology emits CO_2 when the fuel is burned to generate electricity. We used the heat rate for CAES and the CO_2 intensity of natural gas to account for these emissions. Each of the BES technologies that we considered requires water and thus the respective operating costs depend on the price of water: (a) PHES uses water to store the potential energy in an upper reservoir; (b) CO_2-BES uses water in the cooling and condensing towers; and (c) CAES uses water for cooling when compressing the air.

We used the round-trip efficiency instead of an energy ratio, which is sometimes used in situations when the round-trip efficiency can be greater than one (e.g., due to the energy input from natural gas with CAES [133], geothermal heat extraction with CO_2-BES [54]) because the MILP is a systems-level model that does not consider the process level details of how BES operates. As such, for the round-trip efficiency of CAES, we used the inverse of the largest energy ratio (0.8) in a recent review [97] because a larger energy ratio corresponds to a smaller round-trip efficiency.

We estimated the round-trip efficiency and water requirement intensity of CO_2-BES by coupling prior reservoir simulations [54] to well and power cycle models based on our prior work [18]. These models represent (1) the injection and production wells, (2) the direct CO_2 power cycle, and (3) the indirect brine power cycle. We used prior, published results in which 240 kg/s of CO_2 was injected into a 3 km deep reservoir and brined was re-injected to maintain 10 MPa reservoir overpressure. This scenario had the highest operating cost and will lead to the least dispatch of CO_2-BES, all else constant. We estimated the round-trip efficiency by dividing the power that would be generated from the CO_2-BES facility by the power that would be consumed during the charging phase. The water intensity was calculated by assuming that the heat that is rejected by the cooling and condensing towers is used to vaporize water. (Section 3.5 of Appendix A contains more details.)

Table 4. Characteristics and Parameters of the Three Bulk Energy Storage (BES) Technologies

	Operating Cost ($/MWh)	**Round-Trip Efficiency**	**CO_2 Emissions Rate (tCO_2/MWh)**	**Water Intensity (gal/MWh)[g]**
CO_2-BES	35.97[a]	1.64	0.000	6,800
PHES	9[b]	0.75[d]	0.000	440,000[e]
CAES	3[c] + 4.43[d]*P_{ng}	1.25[d]	0.235	200[f]

[a]The largest operating cost of CO_2-BES [54]; [b]The largest operating cost of PHES [134], [135]; [c][136]; [d]Inverse of the energy ratio [97]; [e][137]; [f][138];[g]does not include evaporation.

2.2.4 Valuation of Reductions in System-Wide CO_2 Emissions and Water Requirements

We defined the value that BES has to reducing system-wide CO_2 emissions (V_{CO_2}) or system-wide water requirements (V_{H_2O}) as the product of the price on the environmental variable and difference in the quantity of the environmental variable between parallel cases (where we solved the MILP with BES available to be dispatched and where it was not available to be dispatched), divided by the amount of electricity that is dispatched from BES:

$$V_{CO_2}=\frac{\left(T_{CO_2\,\text{without BES}}-T_{CO_2\,\text{with BES}}\right)*P_{CO_2}}{\Sigma_t\,[Q_{B,t}]} \tag{2}$$

$$V_{water}=\frac{\left(T_{H_2O\,\text{without BES}}-T_{H_2O\,\text{with BES}}\right)*P_{H_2O}}{\Sigma_t\,[Q_{B,t}]} \tag{3}$$

where T_{CO_2} is the system-wide CO_2 emissions and T_{H_2O} is the system-wide water requirements:

$$T_{CO_2}=\sum_{t=0}^{T}\left(\Sigma_j\,[Q_{j,t}*H_j*R_{coal}]+\Sigma_k\,[Q_{k,t}*H_k*R_{ng}]+Q_{B,t}*\alpha\right) \tag{4}$$

$$T_{H_2O}=\sum_{t=0}^{T}\left(\Sigma_i\,[Q_{i,t}*\beta_i]+\Sigma_j\,[Q_{j,t}*\beta_j]+\Sigma_k\,[Q_{k,t}*\beta_k]+Q_{B,t}*\beta_B\right) \tag{5}$$

and $H_{(\cdot)}$ is the heat rate for the EGU and $R_{(\cdot)}$ is the CO_2 emissions rate for the fossil fuel.

2.2.5 Implementation of the General Framework for the ERCOT Case Study

Since each combination of critical parameters could yield a different dispatch curve, and many days will have similar characteristics of net load, as in prior work we conducted a bounding analysis to select particular days to investigate in detail [8]. We solved the MILP for the net load on each day in 2014 with every combination of (1) the endpoints of the ranges of values for each parameter that determine operating costs (Table 2); (2) the baseline and high CO_2 prices ($0/t$CO_2$, $100/t$CO_2$); (3) low and high water prices ($0/gal, $0.10/gal); (4) the high wind energy generation scenario (44%); and the (5) round-trip efficiency, water intensity, CO_2 emissions rate, and operating cost of CO_2-BES. These parameters represent extreme values and thus provide more heterogeneity in the results. From these results, we selected twelve days that best match the means and standard deviations for the reductions in system-wide CO_2 emissions and in water requirements as well as the values of these reductions. (Section 4 of Appendix A contains more details on the bounding analysis.)

For each day that we selected from the bounding analysis, we then implemented the framework in Figure 1 separately for each of the three BES technologies that we investigated. For each combination of the environmental variables, the Monte Carlo sensitivity analysis drew two hundred samples from the distributions of the determinants of operating costs in Table 2. For the non-fuel operating costs of nuclear and wind energy technologies, we implemented a triangular distribution, as in prior studies [139,140], with the peak at the midpoint of the minimum and maximum values of the range. For the coal and natural gas prices we sampled from the actual distribution of these prices in Texas (see Section 5 in Appendix A).

2.3 Results

The dispatch of BES changed the system-wide CO_2 emissions or water requirements when it altered the dispatch order – and thus the order in which facilities with different CO_2 intensities and water intensities were dispatched. We first present the effect that the critical parameters had on the dispatch order and the dispatch of BES (Section 2.3.1). We then present the effects of BES dispatch on system-wide CO_2 emissions and water requirements (Section 2.3.2), and follow with the value of these changes (Section 2.3.3).

2.3.1 Sensitivity Analysis: Effects of Critical Parameters on the Dispatch of Bulk Energy Storage

2.3.1.1 Environmental Variables: CO_2 Price, Water Price, and Wind Generation Scenario

Bulk energy storage was dispatched more often when the CO_2 price or the water price was high, because it was competitive on cost, but less often when the net load was low, because less expensive EGUs can meet demand – even with a high CO_2 price or a high water price. It is thus likely that BES would be dispatched less often with higher levels of wind-generated electricity, but in our results there were two situations where this did not occur: (1) when BES stored the excess electricity on windy days in the high wind generation scenario with little demand (i.e., the net load could be negative) and dispatched it later; and (2) when the there was little wind-generated electricity during hours with high demand and BES stored electricity *before* high demand, when the net load decreased more than it did *during* times of high demand, when BES then dispatched electricity. As a result, the time-shifted electricity displaced the costlier EGUs that would have been dispatched during high demand.

2.3.1.2 Uncertain Parameters: Operating Costs of Wind and Nuclear Energy Technologies, and Prices of Fossil Fuels

The operating costs tended to have a larger effect on the dispatch order when the CO_2 price or the water price was low, because the dispatch order was relatively fixed. For example, when the water price and the natural gas price were low, natural gas EGUs with high water intensities were lower on the dispatch curve. If the natural gas price was high, these natural gas EGUs would be dispatched more often, and BES would be dispatched less often. But if the water price was high, these natural gas EGUs would be higher on the dispatch curve than BES and BES would be dispatched more often.

2.3.2 Changes to the Dispatch Order and System-Wide CO_2 Emissions and Water Requirements due to the Dispatch of BES

Table 5 shows how the dispatch order changed when a non-trivial amount of BES was dispatched (i.e., > 1 MWh). Because it has the lowest water intensity, a high round-trip efficiency, and a low operating cost, CAES was dispatched most often—especially at low CO_2 prices and low natural gas prices. Since CO_2-BES has the highest round-trip efficiency and the operating costs for PHES has a high water intensity that increases marginal costs when water is priced, CO_2-BES was dispatched more often than PHES.

Table 5: Frequency of Changes to the Dispatch Order due to the Dispatch of BES in the Sensitivity Analysis. The table summarizes the results of all 129,600 combinations of parameters for each BES technology.

	BES Technology		
	CO_2-BES	**CAES**	**PHES**
Total Dispatch Greater than 1 MWh	**79.4%**	**84.9%**	**20.7%**
1. Increased Utilization of Natural Gas Capacity	43.3%	46.3%	6.8%
2. Increased Utilization of Coal Capacity	20.7%	21.2%	12.7%
3. Increased Utilization of Wind Capacity	10.3%	12.3%	3.1%
4. Decreased Utilization of Nuclear Capacity	5.7%	6.4%	0.3%
Subtotal (1 – 4)*	80.0%	86.3%	22.9%
Total Dispatch Less than 1 MWh	**20.6%**	**15.1%**	**79.3%**

* The subtotal is slightly greater than the total because the first three ways that BES changes the dispatch order are not entirely mutually exclusive. To reduce double-counting, results with a decrease in the utilization of nuclear power capacity are not included in the results of the other three changes to the dispatch order.

As shown in Table 5, there were four different changes to the dispatch curve due to the dispatch of BES: (1) an increase in the utilization of natural gas capacity; (2) an increase in the utilization of coal capacity; (3) an increase the utilization of wind capacity; or (4) a decrease in the utilization of nuclear power capacity. The utilization of natural gas capacity increased most often in part because natural gas EGUs are flexible and have roughly half the CO_2 emissions of coal EGUs.

Overall, the changes in system-wide CO_2 emissions and in system-wide water requirements for one of the four changes to the dispatch order depend on (a) the dispatch order, (b) the CO_2 price, (c) the water price, (d) the net electricity load, and (e) the BES technology. Given the nuances of how each of these factors influences the results, we present general summaries here. Table 6 provides a summary of the changes in the system-wide CO_2 emissions and in the system wide water requirements, and Figure 3 shows these results as products of the CO_2 prices and of the water prices that we varied. Section 6.2 of Appendix A contains more details, which includes Figure 36 that separates the results that are presented in Figure 3 individually for each BES technology.

Table 6: Distribution of Reductions in System-Wide CO_2 Emissions and Water Requirements as a Result of the Sensitivity Analysis: median [25th percentile; 75th percentile]. Negative numbers indicate increases. Box and whisker plots are provided in section 6.1 of the Appendix A.

			Decrease in System-Wide CO_2 Emissions [tCO_2]	Decrease in System-Wide Water Requirements [Mgal]
Effect of BES on the Dispatch of Other Energy Technologies	Increase Natural Gas	CO_2-BES	3,524 [773; 10,153]	203 [23; 606]
		CAES	1,197 [118; 4,286]	267 [33; 819]
		PHES	1,121 [91; 5,159]	38 [-9.9; 1,836]
	Increase Coal	CO_2-BES	8.9 [-269; 1,781]	37 [-0.2; 12,597]
		CAES	-494 [-5,170; -25]	105 [1.5; 7,762]
		PHES	429 [-118; 8,759]	1,029 [3.7; 14,549]
	Increase Wind	CO_2-BES	1,125 [211; 6,643]	-1.0 [-12.6; 7.2]
		CAES	1,157 [219; 5,458]	11.5 [0.9; 57.3]
		PHES	60.4 [-2.8; 80.4]	-3.9 [-9.2; 0.1]
	Decrease Nuclear	CO_2-BES	-23,897 [-11,350; -38,882]	3,026 [1,984; 16,028]
		CAES	-40,283 [-55,210; -35,019]	3,029 [2,432, 16,785]
		PHES	-45,335 [-44,221; -46,749]	557 [548; 563]

As Table 4 shows, CAES and PHES have similar operating costs, which are much less than those for CO_2-BES. As such, holding everything else constant, CAES and PHES were dispatched higher in the dispatch order than CO_2-BES. But, as also shown in Table 4, CAES has a positive, non-zero CO_2 emissions intensity (unlike CO_2-BES and PHES), and thus system-wide CO_2 emissions increased with CAES unless the changes in the dispatch order resulted in less CO_2 emissions elsewhere in the system – as was the case when the dispatch of CAES resulted in an increase in the utilization of wind capacity (no CO_2 emissions intensity) or an increase in the utilization of natural gas capacity (smaller CO_2 emissions intensity than coal). System-wide CO_2 emissions increased when the utilization of coal capacity increased (because of the high CO_2 intensity of coal), and when the utilization of nuclear power capacity decreased (because nuclear power plants do not emit CO_2). If there was a price on CO_2 emissions, holding everything else constant, CAES was lower in the dispatch order than PHES (because of their similar operating costs and the non-zero CO_2 emissions from CAES) and natural gas and coal-fired power plants were also lower in the dispatch order than they would be without a CO_2 price. Economic dispatch with non-zero CO_2 prices thus favored energy technologies with few, if any, CO_2 emissions, and the enabling of their dispatch by the use of BES.

The varying degrees of water intensity across the BES technologies that we investigated, as well as across the energy technologies in the ERCOT system, rendered the results of the effects on system-wide water requirements to be more nuanced. In general, holding everything else constant, a price on water substantially decreased the dispatch of PHES because the high-water intensity (as shown in Table 4) caused it to move far down the dispatch curve. As such, PHES was not deployed as often as the other BES technologies. Prices for water also favored the dispatch of electricity from wind and discouraged the dispatch of nuclear power, as well as favored the use of BES to enable those outcomes.

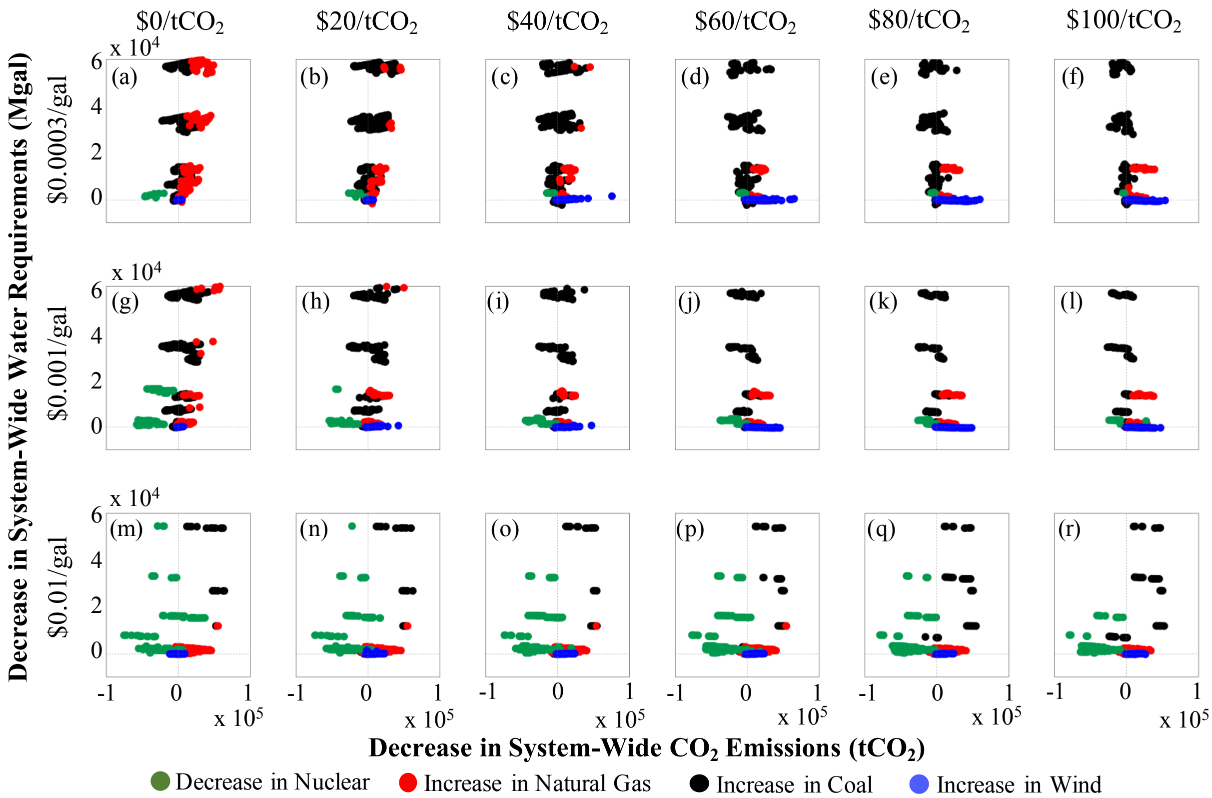

Figure 3: Effect of how BES Dispatch Changed the Dispatch Order. Markers to the right of the vertical line indicate a decrease in system-wide CO_2 emissions. Markers above the horizontal line indicate a decrease in system-wide water requirements.

Across the changes to the dispatch order, the dispatch of CO_2-BES tended to reduce CO_2 emissions more than the dispatch of CAES, in part because CAES emits CO_2. In turn, the dispatch of CAES generally reduced water requirements more than the dispatch of CO_2-BES because CO_2-BES requires more water. The effect of PHES dispatch on system-wide CO_2 emissions and water requirements differed from the effects of the other two BES technologies because of the substantial costs that are incurred when the high water intensity for the technology is multiplied by the water price.

In general, according to the four ways in which the dispatch of BES changed the dispatch order:

1. System-wide CO_2 emissions and system-wide water requirements usually decreased when the utilization of natural gas capacity due to BES increased – which occurred for all CO_2 prices and water prices that we modeled. The effect was greatest when the water price was low, where increased utilization of natural gas power plants can lead to substantial reductions in water requirements, especially at low CO_2 prices, but the magnitude of the reduction in CO_2 emissions was relatively insensitive to the CO_2 price.
2. Increasing the utilization of coal power capacity substantially reduced system-wide water requirements, but the effect on system-wide CO_2 emissions was mixed. System-wide CO_2 emissions decreased when water prices were high, but at low and medium water prices, system-wide CO_2 emissions increased about as often, and about as much, as they decreased—except at high CO_2 prices where the CO_2 emissions increased more often than they decreased. The increase in the utilization of coal power capacity also occurred over all of the CO_2 prices and water prices that we modeled, but it was more frequent at low water prices.
3. System-wide CO_2 emissions usually decreased when the utilization of wind power capacity increased, and the magnitude of these reductions tended to increase at higher CO_2 prices. But there was little effect on system-wide water requirements, regardless of the water price or the CO_2 price.
4. System-wide water requirements tended to decrease when the utilization of nuclear power capacity decreased, but system-wide CO_2 emissions tended to increase. The variability of the decrease in system-wide water requirements decreased as the CO_2 price increased. In fact, at high water prices, there were many situations where CO_2 emissions decreased with low CO_2 prices, but not at high CO_2 prices. The decrease in the utilization of nuclear power capacity was slightly sensitive to the CO_2 price, but it occurred more often at medium and at high water prices.

2.3.3 The Value of Reductions in System-Wide CO_2 Emissions and System-Wide Water Requirements

There are two counteracting effects in the estimated values for reducing system-wide CO_2 emissions or water requirements. First, the value will increase with CO_2 or water price, holding everything else constant. Second, the dispatch order increasingly internalizes the CO_2 intensity and water intensity at higher prices for CO_2 or for water, because the combinations result in larger costs. As a result, facilities with low CO_2 or water intensities will be dispatched before those with high CO_2 or water intensities and there will be less opportunity for reductions in system-wide CO_2 emissions or water requirements.

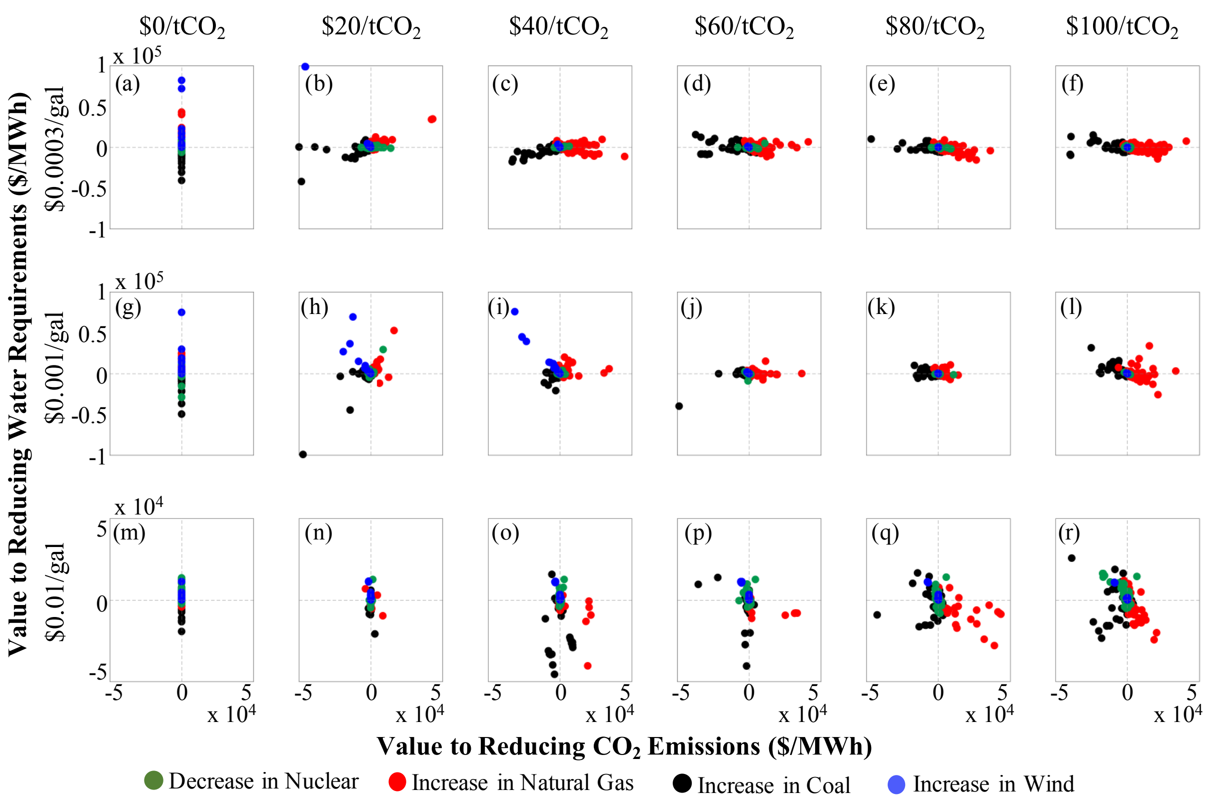

Figure 4: Estimated Values of Reducing the Environmental Requirements in the ERCOT Regional Electricity System. Markers to the right of the vertical axis indicate that BES provided a positive value

for reducing CO_2 emissions (from Eq. 2). Markers above the horizontal axis indicate that BES provided a positive value for reducing water requirements (from Eq. 3).

There were a few ways in which BES provided positive value for reducing water requirements without considering CO_2 emissions (i.e., when there was no CO_2 price, first column in Figure 4): (a) when the utilization of wind capacity increased, which only occurred in the high wind scenario (see Figure 37 – Figure 39 in Appendix A); (b) when the utilization of nuclear power capacity decreased, which was more prevalent in the high wind generation scenario; and (c) when the utilization of natural gas capacity increased, which was more prevalent for the low wind generation scenario. The increase in the utilization of coal capacity was also more prevalent in the low wind generation scenario, but that outcome always yielded a negative value because of the increase in system-wide water requirements.

There was also a negative value to reducing system-wide water requirements in some situations when BES dispatch resulted in increased utilization of natural gas capacity. This outcome occurred when the CO_2 price was at least \$40/tCO_2 and the water price was high, and was more frequent in the high wind-generation scenario. But the primary environmental benefit from the increased utilization of natural gas capacity was to provide a positive value for reducing CO_2 system-wide emissions, which occurred in almost every situation across all of the combinations of environmental parameters and was more common in the low and medium wind generation scenarios.

In contrast, the value to reducing system-wide CO_2 emissions was usually negative when there was an increase in the utilization of coal power capacity—which tended to occur more often for the baseline water price, as well as in the high wind generation scenario. The increase in the utilization of coal power capacity also had mostly negative values for reducing water requirements, but the range of these values tended to be smaller than the range of the values for reducing system-wide CO_2 emissions.

For the most part, when the utilization of nuclear power capacity decreased under non-zero CO_2 prices, there was little if any value to reducing system-wide CO_2 emissions or system-wide water requirements. When there was value, it was usually negative for reducing system-wide CO_2 emissions and it was usually positive for reducing system-wide water requirements.

At high water prices, the increase in the utilization of wind capacity primarily had a positive value for reducing system-wide water requirements, but also had a negative value for reducing CO_2 emissions at the high CO_2 price. At the low water price, there were mixed values for reducing CO_2 emissions, with roughly equal numbers of situations where the value was positive and the value was negative.

The effects of each BES technology on value of changes in system-wide CO_2 emissions and water requirements can be verified by inspection of Figure 40 in the Appendix A, which separates the results that are presented in Figure 4 individually for each BES technology.

2.3.4 Environmental Return on Bulk Energy Storage

We constructed the *Environmental Return on BES* (ERBES) by dividing the median reduction in system-wide CO_2 emissions (or system-wide water requirements) by the operating costs of the BES technology. We used the median value to accommodate the range of cost and operational characteristics within the critical parameters, and thus provide a metric that represents an expected benefit-cost ratio: if the ERBES is greater than one, the BES technology provides a value to the regional electricity system that is greater than the cost of delivering that service.

Table 7: Environmental Return on Bulk Energy Storage (ERBES). The results for the variations in CO_2 price use the low water price ($0.0003/gal). The results for variations in the water price use the $0/t$CO_2$ CO_2 price. The operating cost of CAES used a natural gas price of $4.87/MMBtu, which is the average price of the natural gas between 2002 and 2016.

		Effect of BES Dispatch on Other Energy Technologies											
		Increase Natural Gas			Increase Coal			Increase Wind			Decrease Nuclear		
		CO_2-BES	**CAES**	**PHES**	**CO_2-BES**	**CAES**	**PHES**	**CO_2-BES**	**CAES**	**PHES**	**CO_2-BES**	**CAES**	**PHES**
CO_2 Price ($/t$CO_2$)	**20**	1.3	0.9	0.6	0.0	-0.2	0.0	0.4	0.3	1.0	-608.6	-47.8	-421.6
	40	1.3	0.7	0.6	0.0	-0.3	0.0	0.7	0.5	0.5	-41.1	-2.5	N/A
	60	1.8	0.8	0.9	-0.1	-0.4	0.0	1.0	0.5	1.0	-0.9	-0.6	N/A
	80	1.5	0.8	1.1	0.0	-0.4	0.0	1.0	0.5	1.0	-0.3	-0.5	N/A
	100	1.7	0.8	1.9	0.0	-0.5	0.0	1.1	0.4	0.9	-0.4	-0.4	N/A
Water Price	**0.0003**	1.9	2.3	0.4	-0.3	0.2	0.3	0.0	0.1	-0.9	1,173	113	336
	0.001	2.3	1.7	0.5	0.4	0.9	1.0	-0.1	0.4	-1.0	5.1	4.7	168
	0.01	2.5	9.9	0.3	1.6	2.8	0.3	2.4	1.8	0.0	11	39	2.6

In the results in Table 7, implementing CO_2-BES in the regional electricity system most often resulted in the expectation that it would cost-effectively produce environmental benefits in the system. The ERBES was always at least one when the utilization of natural gas increased, but it was at least one only when (a) the utilization of coal capacity increased under the high water price; (b) the utilization of wind capacity increased under a high water price or for CO_2 prices that are at least $60/t$CO_2$; and (c) when the utilization of nuclear power decreased for all of the water prices that we investigated. In fact, all of the BES technologies had an ERBES above one when the utilization of nuclear power capacity decreased under all of the water prices, but in none of the CO_2 prices that we investigated.

For CAES, the BES technology is likely to cost-effectively reduce system-wide water requirements if there is no CO_2 price and (a) there is an increase in utilization of natural gas power capacity or (b) of nuclear power capacity, or if, under a high water price, it leads to an increase in the utilization of (c) coal power capacity or (d) wind power capacity.

The water intensity of PHES rendered the BES technology least effective at cost-effectively providing positive environmental outcomes in the system. That is, PHES only had more benefits for system-wide water requirements than costs when the utilization of nuclear power capacity decreased (as do the other BES technologies). The only other combinations when PHES provided an ERBES greater than one where when the utilization of natural gas increased for CO_2 prices of \$80/tCO_2 or \$100/tCO_2, where the utilization of wind capacity increased for CO_2 prices of \$20/tCO_2, \$60/tCO_2, and \$80/tCO_2, and where the utilization of coal capacity increased for a water price of \$0.001/gal.

2.4 Discussion and Conclusions

Reducing CO_2 emissions and water requirements in regional electricity systems can decrease stress on the environment, and thus the economies and societies that rely upon it. Implementing bulk energy storage (BES) approaches can help to realize these goals; this work contributes to a nascent body of literature that investigates the impact of BES on system-wide CO_2 emissions [96], [97], [90], and to our knowledge is the first to directly investigate the role that BES may have in reducing system-wide water requirements.

Dispatching BES can cost-effectively enable the supply of electricity to match demand and prioritize dispatch from facilities with lower CO_2 and water intensities. Here, we investigated the value that three BES technologies—Pumped Hydroelectric Energy Storage (PHES), Compressed Air Energy Storage (CAES), and CO_2-Bulk Energy Storage (CO_2-BES)—could provide to reducing the system-wide CO_2 emissions and water requirements in a regional electricity system. While our case study was on the Electricity Reliability Council of Texas (ERCOT) region, our results permit several generalizable conclusions:

1. *The implementation of BES can change the dispatch order for regional electricity systems in multiple ways, not just by enabling an increase in the utilization of variable renewable energy*

capacity (e.g., wind). Our dispatch model minimized the total operating costs of supplying electricity demand. We included the operational details, CO_2 and water intensities for each dispatchable unit, realistic constraints, and sensitivity analyses on operating costs and prices for emitting CO_2 and requiring water. BES can be used to avoid the curtailment of variable electricity generation from wind, and we observed the expected increase in the utilization of wind energy capacity. But we also identified three other ways in which BES can change the dispatch order: (1) increase the utilization of natural gas power capacity, (2) increase the utilization of coal power capacity, and (3) decrease the utilization of nuclear power capacity.

2. *The dispatch of BES can result in changes to system-wide CO_2 emissions and water requirements, but does not necessarily reduce them.* We identified four factors that determine how system-wide CO_2 emissions or water requirements change as a result of the dispatch of BES: (1) the dispatch order; (2) the CO_2 price and the water price; (3) the net electricity load (demand less generation by variable renewable energy technologies); and (4) the BES technology. In general, (a) increasing the utilization of natural gas capacity or of wind capacity is very likely to decrease system-wide CO_2 emissions; and (b) increasing the utilization of natural gas capacity is likely to decrease system-wide water requirements, especially at low prices for CO_2 and water, and do so more than when the utilization of wind capacity increases. In contrast, (c) decreasing the utilization of nuclear power capacity almost certainly increases system-wide CO_2 emissions while decreasing system-wide water requirements. When the utilization of coal power capacity increases, however, the effects on system-wide CO_2 emissions and water requirements are more nuanced and sensitive to the four factors listed above.

3. *Individual BES facilities can reap large positive values by reducing system-wide CO_2 emissions and water requirements and this value can be greater than the cost of operating BES.* The circumstances in which dispatching BES results in the greatest reduction in system-wide CO_2 emissions or water requirements may not be the same as when the greatest value of those reductions

are realized. For many combinations of CO_2 price and water price, increasing the utilization of wind energy capacity could decrease CO_2 emissions more than increasing the utilization of natural gas capacity. But, the value of those decreases when the utilization of natural gas capacity increases is likely to be higher than the value when the utilization of wind capacity increases. In general, the reductions in system-wide CO_2 emissions and water requirements had greater value when electricity from a non-renewable source was time-shifted.

The Environmental Return on Bulk Energy Storage (ERBES) metric suggests that there are many combinations where the costs of operating BES are less than the value it provides to the system. As such, if a market existed to compensate BES facilities for reducing CO_2 emissions or water requirements, it is likely that a BES facility could operate profitably on its contribution to the environmental performance of the system in which it operates.

This work adds to the growing body of literature that suggests the importance of jointly considering CO_2 emissions and water requirements when making policy [75,141]. Other considerations may include the net impact on sectors within the economy. In which case, BES will likely benefit the fossil energy and renewable energy sectors at the expense of the nuclear industry, because the utilization of nuclear power capacity can decrease with the implementation of BES.

In this work, BES technologies incurred costs for emitting CO_2 and requiring water, but were not compensated by the direct reductions of these environmental variables that may be inherent in a BES technology. That is, our approach considered the CO_2 emissions for CAES and the water requirements for PHES, but it did not consider the geologic storage of 20,736 tCO_2/d for the CO_2-BES design that we used to parameterize the optimization model. If this mitigation of CO_2 emissions were considered, there would be fewer system-wide CO_2 emissions and the CO_2-BES facility would be lower in the dispatch order because the revenue from storing CO_2 would reduce its operating costs.

In addition to modeling the direct reductions in CO_2 emissions in CO_2-BES dispatch, future work could also relax some assumptions in our approach. For example, including start-up or shut-down costs would make the electricity system less flexible because there would be cost incentives to minimize the number of start-ups and shut-downs of coal and natural-gas EGUs. As a result, it is likely that BES dispatch would increase because it would be a less costly alternative than starting up or shutting down an EGU. In this way, including start-up and shut-down costs could increase the value of BES for reducing CO_2 emissions or water requirements if the decrease in system-wide CO_2 emissions or water requirements are greater than the increase in electricity dispatched by BES. Either way, it is unlikely that including start-up and shut-down costs would change the outcome of BES dispatch (e.g., increased utilization of natural gas dispatch). In this sense, the values that we estimated may change slightly, but the specific changes to the dispatch order will not because they are determined mostly by the net load. Further, if start up and shut down costs were incorporated, BES would still enable reductions in CO_2 emissions and water requirements elsewhere in the system at current levels of deployment of variable renewable energy generation capacity.

Since BES facilities are compensated for providing ancillary grid services [85], similar incentives could be enacted to compensate BES for reducing CO_2 emissions and water requirements—not just for the direct revenue they may get from ancillary services, price arbitrage, or, in the case of CO_2-BES, the direct reductions in CO_2 emissions. Such policy would focus on the system-wide implications and enable larger reductions, rather than the narrower facility-specific operating details that would otherwise be encouraged. ISOs and RTOs already solicit day-ahead bids for dispatch scheduling, and day-ahead or 8-hr wind or solar forecasts could be used with the anticipated demand to estimate the expected net load. With the knowledge of how the dispatch of a BES facility changes the dispatch order within a net load of those characteristics, the ISO or RTO could dispatch BES facilities to increase desirable environmental outcomes. In this manner, BES facilities could earn revenue for contributing to the environmental sustainability of the grid.

Chapter 3. Potential Mechanisms for Using Geologically Stored CO_2 for Energy Storage

3.1 Introduction

Modern electricity systems are large sources of carbon dioxide (CO_2) emissions, which, along with other greenhouse gases like methane (CH_4), are substantial contributors to the anthropogenic forcings that are altering the climate [142], due to the dominant reliance on the combustion of fossil fuels as the primary source of energy. In fact, in the United States CO_2 emissions from the electricity sector are greater than from other sectors, like transportation or land-use change [5]. Given the magnitude of CO_2 emissions from the electricity system and the availability of technologies that can supply electricity without emitting CO_2, efforts to substantially reduce CO_2 emissions are more likely to succeed by decarbonizing electricity systems than other sectors with CO_2 emissions [5,143,144]. As a result, stabilizing the atmospheric concentration of CO_2 to reduce anthropogenic climate change will likely require a substantial reduction of CO_2 emissions from electricity systems [7,142,145].

The deployment and utilization of wind turbines and solar photovoltaics are options for decarbonizing electricity systems because they generate electricity without emitting CO_2, but the marginal cost of CO_2 emissions mitigation increases with the amount of electricity that is supplied by these variable renewable energy technologies [8]: (1) capital costs increase in part because high penetrations of energy technologies that generate electricity from variable wind and solar resources require generation capacities that are greater than annual peak demand in order to ensure a sufficient supply of electricity [8,146,147]; and (2) operating costs increase when back-up capacity generates electricity when wind and sunlight are not available [77].

Decarbonizing electricity systems in a least-cost manner will likely require other low carbon technologies, such as dispatchable nuclear power plants that do not emit CO_2, fossil- and biomass-fueled power plants with CO_2 capture and geologic CO_2 storage (CCS), and energy storage to store excess energy when it is not demanded [96,97,148,149].

Much effort has investigated energy storage on daily, hourly, and sub-hourly timescales in order to accommodate the variability of electricity that is generated from wind and solar resources [9,150,151], but there is also a need for seasonal energy storage (SES) to meet demand during seasonal minima in the availability of these resources [10,56]. Such SES approaches could store electricity that is generated from wind turbines in the winter when it is windy, and make that energy available in the summer when there is more electricity demand but less wind [10,93]. Power-to-Gas (P2G) is one approach that effectively stores energy on seasonal timescales, where excess electricity is used to produce hydrogen through electrolysis of water, which can then be converted into synthetic CH_4 and stored in existing natural gas storage systems [152]. While P2G could accommodate seasonal variations in electricity generation from wind and solar resources, the technology uses water and may contribute to climate change if fugitive CH_4 is emitted from natural gas infrastructure [153] or if the CO_2 that is produced from the combustion of CH_4 is emitted to the atmosphere.

Approaches that use CO_2 in the subsurface for energy storage could be particularly useful [54,154], especially if they are based in part on CO_2 Plume Geothermal (CPG) technology [16,19,83]. With CPG, geologically stored CO_2 is emplaced in a deep aquifer within a sedimentary basin geothermal resource, and some of this CO_2 is produced to the surface to extract geothermal heat and convert it to electricity. In this CO_2 capture, *utilization*, and storage (CCUS) approach, dispatchable renewable electricity can be generated while isolating CO_2 from the atmosphere. The subsurface is attractive because the saline aquifers that are targets for geologic CO_2 storage have enormous storage capacities, are relatively ubiquitous [44,49], and thus have sufficient size to hold the large volumes of fluid that are necessary for SES.

There are two primary mechanisms by which energy could be stored in the subsurface: as pressure or as heat. Some of our prior work on subsurface energy storage (i.e., CO_2-Bulk Energy Storage (CO_2-BES)) uses a concentric ring, pressure-based bulk energy storage (CRP-BES) design [54]. With this design, CO_2

is injected during a 3-to-5 year "priming" period, and the reservoir overpressure and the migration of the CO_2 plume are controlled by producing and strategically reinjecting brine in concentric rings of wells. Once primed, a facility using the CO_2-BES facility using the CRP-BES design can generate electricity when needed by producing geothermally-heated CO_2 and brine to the surface, and using the heat in these fluids to generate electricity in a direct CO_2 power cycle and an indirect brine power cycle. The produced CO_2 is re-injected (i.e., a CPG process) and the produced brine is stored in holding ponds at the surface. When the supply of electricity exceeds demand, electricity can be used (stored) by re-injecting brine from the holding pond along with more CO_2 that has been captured.

Another mechanism for storing large amounts of energy in the subsurface could be to use excess heat to pre-heat fluids prior to injection. For example, during seasons when energy needs to be stored, thermal energy from a nuclear powerplant could be transferred to a fluid, instead of being used to generate electricity, and the heated fluid could be stored underground [62,63]. This mechanism of storage would rely on the ability of the subsurface to act as a thermally insulated container to store heat and potentially increase the temperature of the stored fluid due to the geothermal heat flux. The stored (and heated) fluid could later be produced to the surface and the heat used to generate electricity.

Here, we extend our prior work in two ways towards developing SES technology. First, we investigate the efficacy of the CRP-BES design for cycles of energy storage and energy dispatch that each have durations that are longer than a day. We do so by implementing a fully integrated model of the CO_2-BES facility using the CRP-BES design [54]. In our prior work we approximated the operational capabilities of a CO_2-BES facility using the CRP-BES design by combining results from reservoir simulations with continuous produced and re-injection at artisanal flowrates with estimated power generation coefficients for a given power cycle [54]. The new integrated model that we present here simulates the operation of CRP-BES in detail by coupling the subsurface fluid flow simulator with a well model and power cycle model. Second, we investigate thermal energy storage in the same porous and permeable aquifers in sedimentary basin geothermal resources. To do so, we use comparatively simple simulations to understand the advantages and disadvantages of using pre-heated CO_2 and pre-heated brine as the media for storing thermal energy. Specifically, we compared these pre-heated fluids on four metrics: (1) the power required to compress and inject the fluids into the subsurface, (2) the effect injecting pre-heated fluids on the downhole temperature of the reservoir, (3) the total amount of energy that is stored in the subsurface and available for dispatch; and (4) the thermal energy storage efficiency.

3.2 Methods

3.2.1 Integrated Model for Concentric-Ring Pressure-Based Bulk Energy Storage (CRP-BES)

The integrated model of the CO_2-BES facility using the CRP-BES design consists of the Non-isothermal Unsaturated Flow and Transport (NUFT) simulator [155], as well as a well model (Section 3.2.1.1), an indirect brine power cycle model (Section 3.2.1.2), and a direct CO_2 power cycle model (Section 3.2.1.3) that we built from our prior work [18] and implemented in MATLAB using the open-source thermophysical fluid property library CoolProp [156]. We used NUFT to simulate the injection and subsurface flow of CO_2 and brine and used that output data as input data to the well model for the production well. The output of the production well model was then used as the input to the power cycle models. These models and the NUFT simulator were then iterated until the temperature of the fluid exiting the injection well model converged with the injection temperature that was set in NUFT.

Using the integrated model, we simulated a CRP-BES facility operating for fourteen years over five durations of energy storage with an equal duration of energy discharge in the cycle. Specifically, the lengths of each cycle that we investigated are: 2 x 12 hours, 2 x 24 hours, 2 x 3 days, 2 x 1 week, and 2 x 1 month. For example, in the cycle with 2 x 3 days duration, the facility continuously alternates between storing energy (injecting CO_2 and brine) for three days and dispatching electricity (producing CO_2 and brine) for three days over fourteen years (i.e., a single complete cycle lasts 2 x 3 = 6 days). Although the indirect brine power cycle and the direct CO_2 power cycle are independent, both cycles are operated in unison (Table 8).

Table 8: Individual Power Cycle Component Operation While Storing Electricity and Dispatching Electricity.

	Indirect Brine Power Cycle	Direct CO_2 Power Cycle
Storing Electricity	Total Production Flowrate: 0 kg/s Total Injection Flowrate: X* kg/s Re-injection Pump: On Boiler + Preheater: Off Turbine: Off Cooler + Condenser: Off ORC Pump: Off	Total Production Flowrate: 0 kg/s Total Injection Flowrate: Z kg/s New CO_2 Pump: On Re-injection pump: Off Turbine: Off Condenser: Off
Dispatching Electricity	Total Production Flowrate: X kg/s Total Injection Flowrate: 0 kg/s Re-injection Pump: Off Boiler + Preheater: On Turbine: On Cooler + Condenser: On ORC Pump: On	Total Production Flowrate: Y kg/s Total Injection Flowrate: Z + Y kg/s New CO_2 Pump: On Re-injection Pump: On Turbine: On Condenser: On
*After the desired overpressure is reached, this value decreases because a portion of the brine is permanently removed from the system to limit the overpressure.		

Before simulating the operation of a CRP-BES design, the NUFT simulator must be parameterized with data for a sedimentary basin geothermal resource. For this study, we assumed that the facility was using the Minnelusa Aquifer in the Powder River Basin (Eastern Wyoming, USA) because the subsurface characteristics are favorable to the CRP-BES design that we considered here. We set the depth to 2.7 km, the thickness to 120 m, the vertical and horizontal permeability and porosity to 10^{-13} m^2 and 16% respectively, and the geothermal temperature gradient to 42 °C/km [49,157–163].

After parameterizing the NUFT simulator with the characteristics of our case study in the Minnelusa Aquifer, the desirable flowrates for brine and for CO_2 ("X" and "Y" in Table 8) were determined by inspecting results from initial simulations. Higher mass flowrates for the production wells can increase the instantaneous power output of both of the power cycles but will also increase the rate of heat depletion in the geothermal reservoir and thus decrease the total power output capacity over time. The desirable flowrates balance this tension between heat extraction and heat depletion in order to yield a high power capacity that can be sustained over time. To determine the flowrates to use, we simulated the CRP-BES facility in operation as a powerplant (i.e., not shifting the parasitic brine pumping power) with a few flowrates for each fluid. From these initial simulations, we chose a total flowrate of 5,000 kg_{brine}/s and a total flowrate of 1,000 $kgCO_2/s$ when the facility was dispatching electricity. (See Section 1 in Appendix B for more information on these choices of flowrates.) It is possible that the desirable flowrates of the two fluids vary as a function of the durations of storage and discharge cycles, or the site-specific well-pattern, but here we used the same flowrates and spacing of the concentric ring of wells in each of the five scenarios for the durations of the cycles in order to be able to compare the design and operation of the CRP-BES facility.

Prior to becoming operational, the subsurface CRP-BES reservoir is primed with CO_2 to increase the reservoir overpressure (pressure above hydrostatic) and to ensure that the fluid that is produced from the CO_2 production wells is primarily CO_2. For this study, we simulated a three-year priming period in which CO_2 and brine were constantly produced and re-injected at 2,000 $kgCO_2/s$ and 5,000 kg_{brine}/s, respectively. These mass flowrates over the three years achieved the goal of ~90% of the 1,000 kg/s production flowrate being comprised of CO_2. During this period, the produced CO_2 was re-injected and the amount of new CO_2 that was injected decreased from 2,000 $kgCO_2/s$ by the rate that CO_2 was produced. We used the final conditions in the reservoir at the end of the priming period as the initial, time-zero, conditions for each of the five storage and discharge durations.

In each of these five scenarios, we also assumed that new CO_2 is captured from an external source, and that this amount is constantly injected ("Z" in Table 8) at a rate of 120 $kgCO_2/s$ (3.78 Mt/yr), regardless when energy was stored or dispatched. This constant CO_2 injection increased the overpressure in the reservoir and we reduced the amount of brine that was re-injected during storage periods to limit the overpressure to 10 MPa [54].

The NUFT simulator generates results at smaller timesteps than are practical to model with the power cycle models and well model. As a result, we sampled the data from the NUFT output every two years of simulated time, by selecting representative data points from the middle of a charge or discharge duration within each year. For example, in the 1-month storage and discharge cycle scenario, we used data from month 24.5 to represent dispatching electricity at two years and data from month 25.5 to represent storing energy at two years (Figure 5). This sampling procedure provided representative "snapshots" of the power output capacity and power storage capacity over a multi-year period that could be compared across all of the scenarios that we simulated.

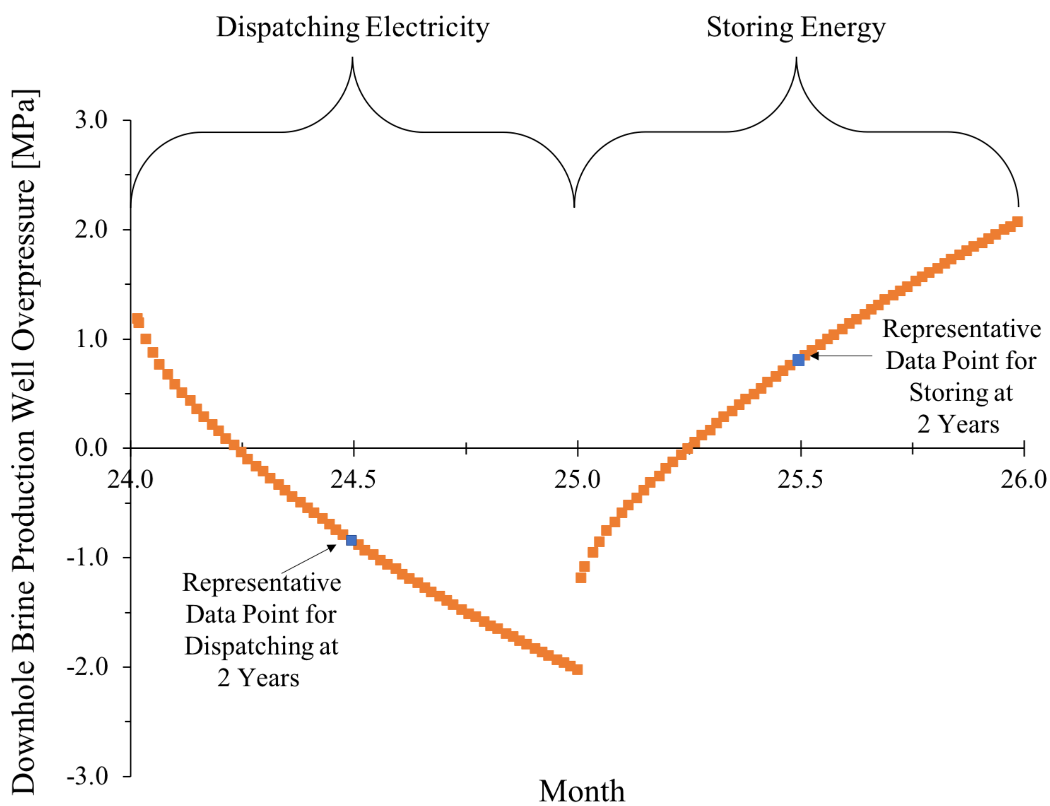

Figure 5: Example of how the Data Points (blue) were Sampled from the Data that was Generated by the Reservoir Simulator (orange). This example contains the results for the 2 x 1 Month cycle duration scenario.

3.2.1.1 Well Model

Consistent with our prior work [18], we numerically estimated the pressure and temperature of the CO_2 and brine throughout the injection and production wells using 100m long axial elements. As shown in Equations 6 to 9, the fluid state in each element (*i+1*) was determined using the first law of thermodynamics, patched Bernoulli, the conservation of mass equations, and the fluid state from the previous element (*i*),

$$h_i + gz_i = h_{i+1} + gz_{i+1} \tag{6}$$

$$P_i + \frac{\rho_i V_i^2}{2} + \rho_i g z_i = P_{i+1} + \frac{\rho_{i+1} V_{i+1}^2}{2} + \rho_{i+1} g z_{i+1} - \Delta P_{loss} \tag{7}$$

$$\Delta P_{loss} = f * \frac{L}{D^5} * \frac{8\dot{m}^2}{\rho\pi^2} \quad (8)$$

$$\dot{m} = \rho_i A V_i = \rho_{i+1} A V_{i+1} \quad (9)$$

where h is the enthalpy of the fluid, g is the gravitational acceleration of Earth, z is depth, P is fluid pressure, ρ is fluid density, V is fluid velocity, f is the friction factor, L is the length of the axial element of the well, D is the diameter of the well, $\dot{m}$ is the mass flowrate of the fluid, and A is the cross-sectional area of the well. We assumed that the friction factor was 0.02 and the well diameter was 0.41m.

3.2.1.2 Indirect Brine Power Cycle Model

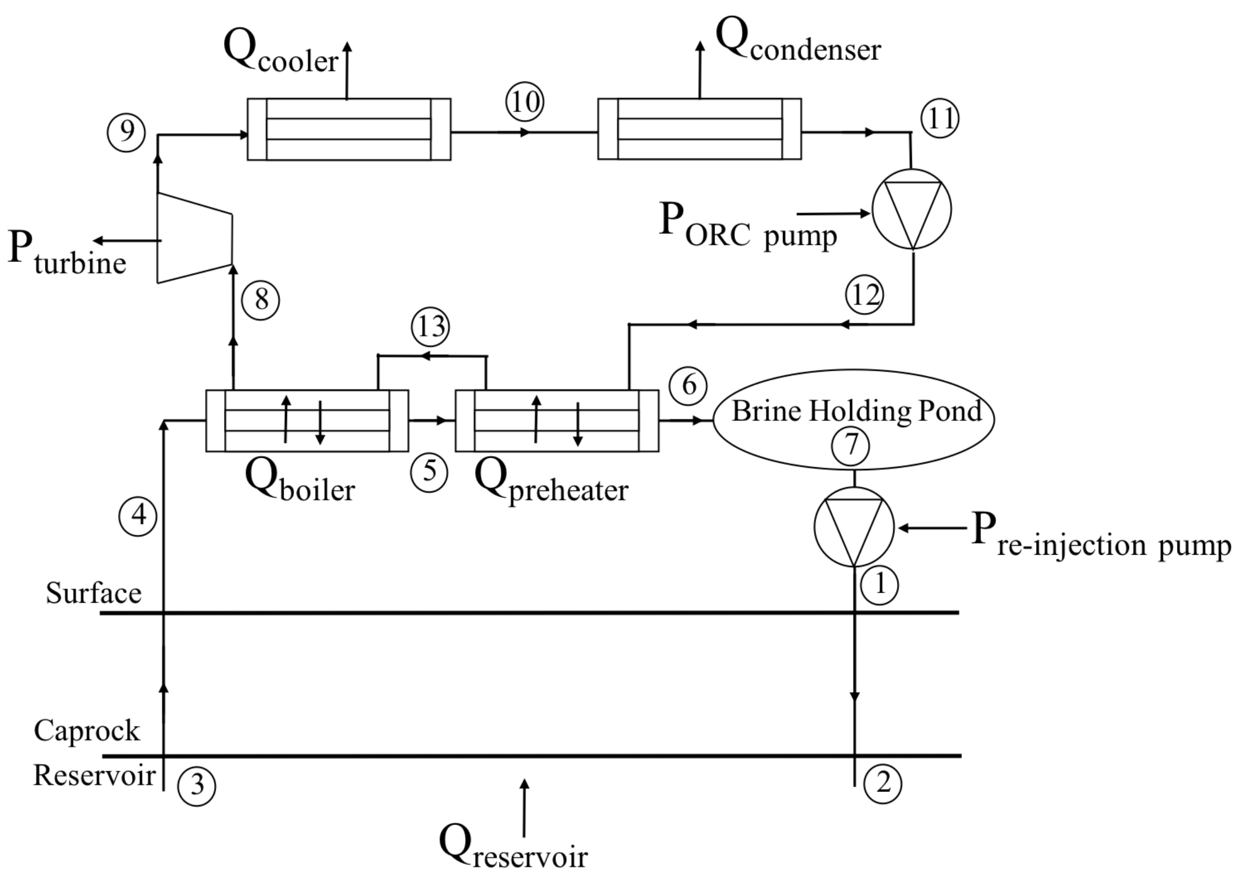

Figure 6: Indirect Brine Power Cycle. In this binary power cycle, brine is used to extract geothermal heat from the geothermal reservoir and heat is transferred to a secondary working fluid to generate electricity.

We simulated the dispatch of electricity with the indirect brine power cycle by producing in-situ brine from the subsurface (states 3 to 4 in Figure 6). Heat is isobarically transferred from the brine to the secondary organic working fluid, which we assumed was R245fa (states 4 to 6), the brine is throttled to atmospheric pressure, and then the brine is held at the surface (state 7). We assumed that the fluid properties of the brine remain constant in the holding pond. Within the secondary cycle, the heated R245fa is expanded through a turbine with an isentropic efficiency of 80% (states 8 to 9), cooled at constant pressure to a saturated vapor at a temperature of 7^{o}C above ambient (states 9 to 10), condensed at constant pressure and temperature to a saturated liquid (states 10 to 11), and pumped by a secondary Organic Rankine Cycle (ORC) pump with an isentropic efficiency of 90% (states 11 to 12). The parasitic loss fractions that were used to estimate the parasitic power cooling and condensing fan requirements were calculated using the regression equations provided in our prior work and assuming an ambient temperature of 15^{o}C [18].

Energy can be stored with the indirect brine cycle by re-injecting the brine from the holding pond into the sedimentary basin geothermal reservoir (states 7 to 2). We assumed that the brine re-injection pump has an isentropic efficiency of 91%. Once the desired reservoir overpressure of 10 MPa was reached, a portion of the produced brine in the holding pond was not re-injected when the facility was storing energy to limit the overpressure to 10 MPa.

We modelled 21 brine production wells and 21 brine injection wells to maintain the per well flowrate under 240 kg_{brine}/s [54].

3.2.1.3 Direct CO_2 Power Cycle Model

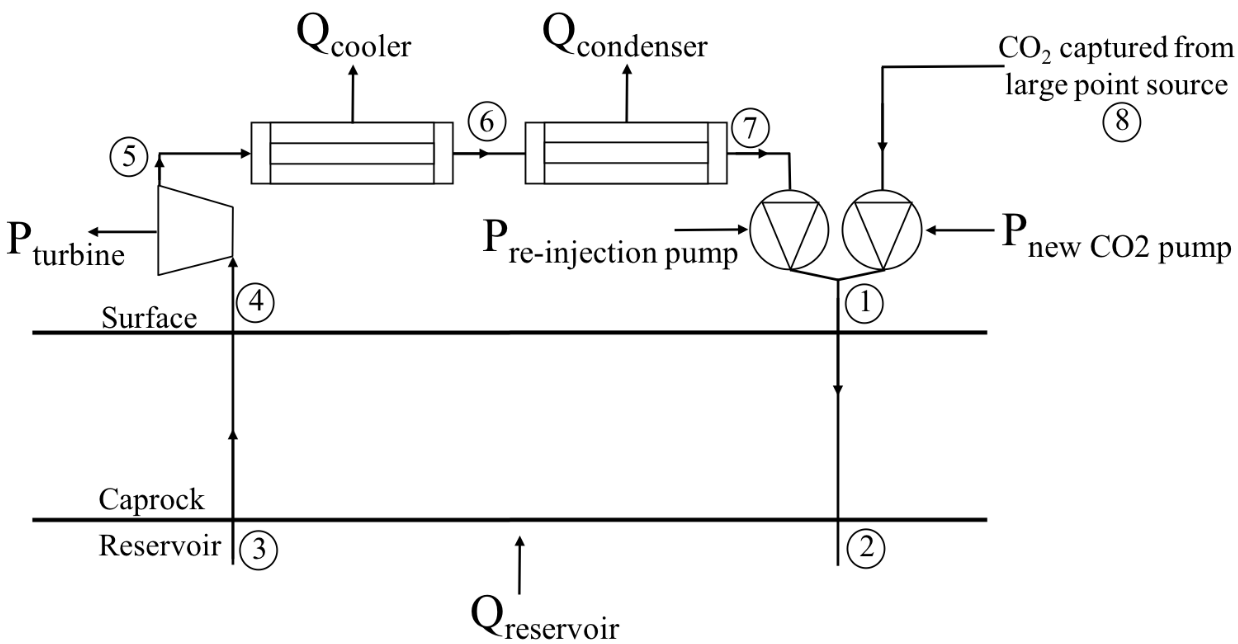

Figure 7: Direct CO_2 Power Cycle. CO_2 is used to extract heat from, and store pressure in, the geothermal reservoir. The energy in the CO_2 that is produced from the reservoir is directly used to generate electricity.

We simulated the discharge of electricity with the direct CO_2 power cycle by producing CO_2 from the reservoir to the surface (states 3 to 4 in Figure 7), and expanding the hot, geothermally heated, CO_2 through a two-phase turbine with isentropic efficiency of 78% (states 4 to 5). The CO_2 is then condensed at constant pressure, 50 kPa above the saturation pressure, to 25°C (states 5 to 7). We used the regression equations from our prior work and assumed an ambient temperature of 15°C to calculate the parasitic loss fractions, which were used to calculate the parasitic power required to run the cooling and condensing tower fans [18]. After condensing, the CO_2 is pressurized and re-injected into the subsurface (states 7 to 2). We assumed the re-injection pump has an isentropic efficiency of 90%. Unlike the brine power cycle, the produced CO_2 is re-injected into the subsurface reservoir whenever the powerplant is dispatching electricity. Further, new CO_2 that is captured from a large point source (state 8) is also injected into the subsurface when the facility is dispatching electricity. We assumed that this CO_2 arrives at the facility at 25°C and 7.5 MPa (state 8).

We simulated the CRP-BES facility storing energy with the direct CO_2 power cycle by only operating the CO_2 injection pump (states 8 to 2). As before, we assumed this pump has an isentropic efficiency of 90%.

We modeled nine CO_2 production wells and nine CO_2 injection wells to maintain the per well CO_2 flowrate below 120 kgCO$_2$/s [54].

3.2.2 Investigation of Fluids for Thermal Energy Storage

We used the well model (Section 3.2.1.1) and the isentropic efficiency equation for a pump or compressor (Eq. 10) to calculate the power that is necessary to compress and inject CO_2 and brine at varying temperatures (Section 3.2.2.1),

$$Pumping\ Power = \dot{m}\left(\frac{h_{2s}-h_1}{\eta}\right) \tag{10}$$

where $\dot{m}$ is the mass flowrate of the fluid flowing through the pump, h_{2s} is the enthalpy of the fluid after an isentropic pump, and h_1 is the enthalpy of the fluid before the pump, and η is the isentropic efficiency of the pump.

We used the downhole temperature from this analysis in subsequent NUFT simulations to investigate the effect that the heated fluids could have on the downhole temperature in the reservoir and the total energy stored in the subsurface (Section 3.2.2.2).

3.2.2.1 Power Required to Compress and Inject Pre-Heated Fluids

We did not include a heat exchanger after the pump and instead we varied the temperature of the fluid prior to the pump from 50°C to 200°C in increments of 25°C and assumed that the downhole pressure increased at a rate of 10.5 MPa/km. With this temperature and the downhole pressure, we iterated with the well model and isentropic pump efficiency equation to find the downhole temperature that resulted in the brine pump operating with a 91% isentropic pump efficiency and the CO_2 pump operating with a 90% pump efficiency [18]. We assumed that the system that provided the brine and CO_2 was operated such that the brine entered the pump as a liquid and the CO_2 entered the pump as a supercritical fluid. As a result, the pressure before the pump was the lowest pressure required for the brine to be a liquid and for the CO_2 to be supercritical.

3.2.2.2 NUFT Reservoir Simulations

Since the purpose of these simulations was to compare the efficacy of different fluids as thermal energy storage media, we conducted simulations for generic operating conditions instead of a specific case study (e.g., the Minnelusa Aquifer). We simulated the injection of the fluids into a 4 km deep and 150 m thick reservoir, with a permeability of $5x10^{-14}$ m^2, a porosity of 12%, a specific heat of 2.8 kJ/kg*K, a density of 920 kg/m^3, and a thermal conductivity of 2 W/m*K. Fluid was injected at 60 kg/s for 6-month periods in a single well with a diameter of 0.41 m that was located in the center of the reservoir that extended throughout the entire thickness of the reservoir. Fluid was produced through the same well (i.e., a "huff-puff" well) at 60 kg/s for 6 months immediately following the 6-month injection periods. For each fluid, this 6-month injection, 6-month production cycle was repeated for ten years for two geothermal temperature gradients: 20 ^oC/km and 50 ^oC/km. By simulating these two temperature gradients, and a pre-heated fluid temperature of 150^oC, we conducted simulations in which the injected fluid was hotter and was colder than the initial temperature of the sedimentary basin geothermal reservoir.

For each scenario, we used the NUFT output to determine the downhole temperature. We used the CoolProp thermophysical fluid property library, the temperature and pressure output from the NUFT simulations, and Equation 11 to calculate the total energy in the reservoir,

$$Q_{res} = \sum_i [\upsilon_i \cdot ((1 - \emptyset_r) \cdot \rho_r \cdot c_{p,r} + \emptyset_r \cdot \rho_{f_i} \cdot c_{p,f_i})] \tag{11}$$

where i is each individual simulated mesh element within a 1 km radius of the huff-puff well; υ is the volume of the mesh element; $\emptyset_r$ is the porosity of the reservoir; ρ_r is the density of the reservoir; $c_{p,r}$ is the specific heat of the rock in the mesh element; ρ_f is the density of the fluid in the mesh element; and $c_{p,f}$ is the specific heat of the fluid in the mesh element. In the CO_2 simulations, a weighted average density and specific heat were used to estimate the density and specific heat of the fluid in the mesh element using the mass fractions of brine and CO_2 as the weighting factors.

3.3 Results

3.3.1 Capacities for Power Output and Pressure Energy Storage with the Integrated Model of CRP-BES

For all but one of the durations that we investigated, the capacities of the CRP-BES design in the Minnelusa Aquifer are up to ~130 MWe for dispatch and ~55 MWe for storage (Table 9). In these cycles, the dispatch capacity is greater than the storage capacity because the background geothermal heat flux adds energy to the injected fluids, which store pressure energy, while the fluids are in the reservoir. The storage capacity of the system decreases slowly with time because the geothermal heat is depleted at a faster rate than it can be recharged by the background geothermal heat flux, but the capacities were quite similar across the storage cycle durations for a snapshot in time.

In each storage-discharge duration scenario, the dispatch capacity due to the CO_2 cycle was approximately 8 MWe and injecting extra CO_2 required approximately 0.8 MWe (Table 21 in Appendix B). The remaining dispatch capacity and storage capacity of the facility was provided by the indirect brine cycle and injecting brine from the holding pond.

Table 9: Snapshots of Dispatch Capacity and Storage Capacity for the CRP-BES Design. See Table 21 in Appendix B for more information.

	Storage Cycle Duration				
	2 x 12 Hours	**2 x 24 Hours**	**2 x 3 Days**	**2 x 1 Week**	**2 x 1 Month**
Year	Dispatch Capacity [MWe]				
2	130.40	130.37	130.26	129.92	N/A
4	129.65	129.63	129.51	129.30	N/A
6	129.03	128.97	128.84	128.76	N/A
8	128.57	128.50	128.55	128.50	N/A
10	128.08	128.05	128.23	128.11	N/A
12	127.35	127.32	127.83	127.18	N/A
14	125.91	125.81	125.77	125.96	N/A
Year	Storage Capacity [MWe]				
2	-52.04	-52.04	-52.05	-52.02	N/A
4	-54.20	-54.24	-52.05	-55.56	N/A
6	-56.51	-56.84	-56.50	-53.01	N/A
8	-57.92	-58.37	-56.66	-52.57	N/A
10	-59.23	-59.45	-53.76	-53.16	N/A
12	-57.59	-57.70	-53.85	-52.63	N/A
14	-56.74	-58.66	-54.53	-52.38	N/A

Although CO_2 is more efficient at extracting geothermal heat than brine [16–18], the CO_2 cycle can generate less electricity than the brine cycle, in part because the brine flowrate is larger than the CO_2 flowrate. In addition, the dispatch capacity with CO_2 is reduced by the additional power requirements to compress and inject the CO_2 into the subsurface. This disadvantage in dispatch capacity relative to brine persists even when the power output is normalized by the fluid flowrate (Table 21 in Appendix B).

In our results, the storage capacity generally decreases as the duration of the storage cycle increases because the overpressure decreases (Figure 42 in Appendix B). Since the overpressure decreases, the amount of energy that is required to compress and inject fluids into the subsurface also decreases.

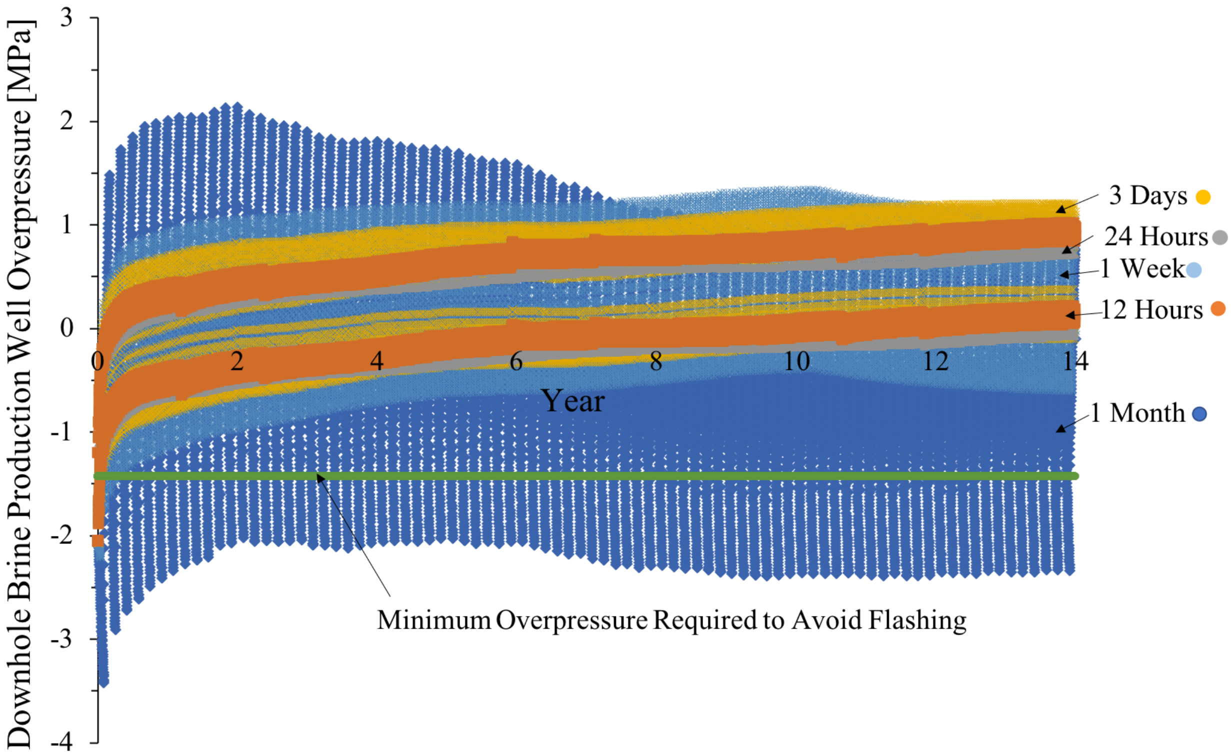

Figure 8: All Downhole Brine Production Well Overpressure Output NUFT Data. The durations that are shorter than 1 week appear to be split into two sets of data only because the time step taken in the NUFT model was short. (See Figure 43 in Appendix B for the sampled downhole brine production well overpressure data.)

In Table 9, the cycle with 1-month durations of storage and discharge does not have a dispatch capacity or a storage capacity because downhole brine production overpressure drops below -1.44 MPa, which causes the brine to flash in the production well (Figure 8). Over the course of a given cycle, the overpressure decreases when the facility dispatches electricity, because a substantial amount of brine is produced from the reservoir, and the overpressure increases when storing energy because this brine is reinjected (Figure 5). If the duration is too long, the overpressure will: (a) decrease during dispatch to the point where brine could flash in the production well; and (b) increase during storage to the point where a portion of the produced brine must be permanently removed (i.e., not re-injected) to limit the downhole overpressure to

10 MPa. The downhole production well pressure in the 1-month durations begins to decrease at year two, and at year ten in the 1-week durations, because less brine is re-injected than had been produced.

Before brine is removed from the system, the injection well overpressure increases with time across all scenarios because new CO_2 is continuously injected into the subsurface. Figure 8 shows that there are data points at the beginning of the 1-week duration in which the overpressure is low enough that the produced brine would flash. As a result, it is likely that a facility that uses the CRP-BES design would not operate with 1-week storage and dispatch durations at the beginning of operation. Instead, a shorter cycle would be used until the overpressure increased such that 1-week durations were feasible. Further, there is a ~1 to ~1.5 MPa "buffer" between the overpressure at the end of the dispatch periods in the 1-week cycle and the overpressure that causes flashing (Figure 8). As a result, it is likely that the CRP-BES design could be used for durations that are longer than 1-week. For example, assuming a linear interpolation between the results for the 1-week durations and the 1-month durations in Figure 8, it is possible that durations of ~two weeks could be feasible without the brine flashing for the flowrates that we used in our simulations.

3.3.2 Comparison of Thermal Energy Storage Using CO_2 or Brine

3.3.2.1 Pumping Power

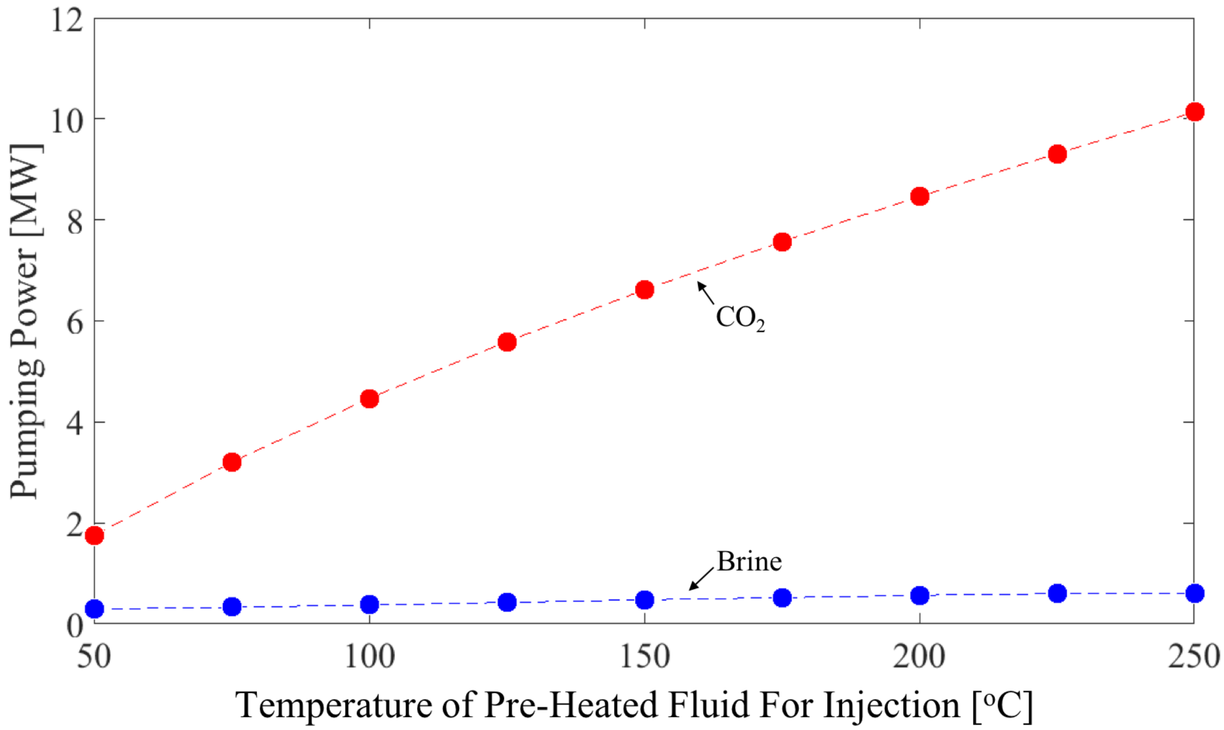

Figure 9: Power Required to Compress and Inject CO_2 and Brine Into a 4 km Deep Reservoir at Hydrostatic Pressure Calculated with Equation 10.

The pumping power that is needed to inject fluids into a reservoir that is 4 km below the surface increases with the temperature of the pre-heated fluid, and this increase is larger for CO_2 than for brine (Figure 9). For example, if the fluids are pre-heated to 50°C, CO_2 injection requires about 6x as much energy as brine injection; if the fluids are pre-heated to 250°C, CO_2 requires about 13x as much energy. These differences in the necessary pumping power are due to CO_2 having a higher compressibility than brine and because the density of CO_2 is more sensitive to temperature than is the density of brine (Figure 44 in Appendix B). That is, as the fluid heats up, the density of CO_2 decreases at a faster rate than does the density of brine.

3.3.2.2 Reservoir Temperature

The flat horizonal portions of the data in Figure 10 indicate the six months of injection of the pre-heated (and further compression heated) fluids. Even though the fluids are preheated to 150°C before being injected, the heat of compression increases the temperature of the fluids before they enter the sedimentary basin geothermal reservoir. In particular, the brine enters the geothermal reservoir at 153°C, which is about 55°C warmer than the initial temperature at the bottom of the reservoir with the 20°C/km geothermal temperature gradient and about 70°C colder than the initial temperature with the 50°C/km geothermal temperature gradient. In contrast, the higher compressibility of CO_2 results in an injection at 197°C into the geothermal reservoirs, which is about 100°C above, and 25°C below, the initial temperatures for the 20 °C/km and 50 °C/km reservoirs, respectively.

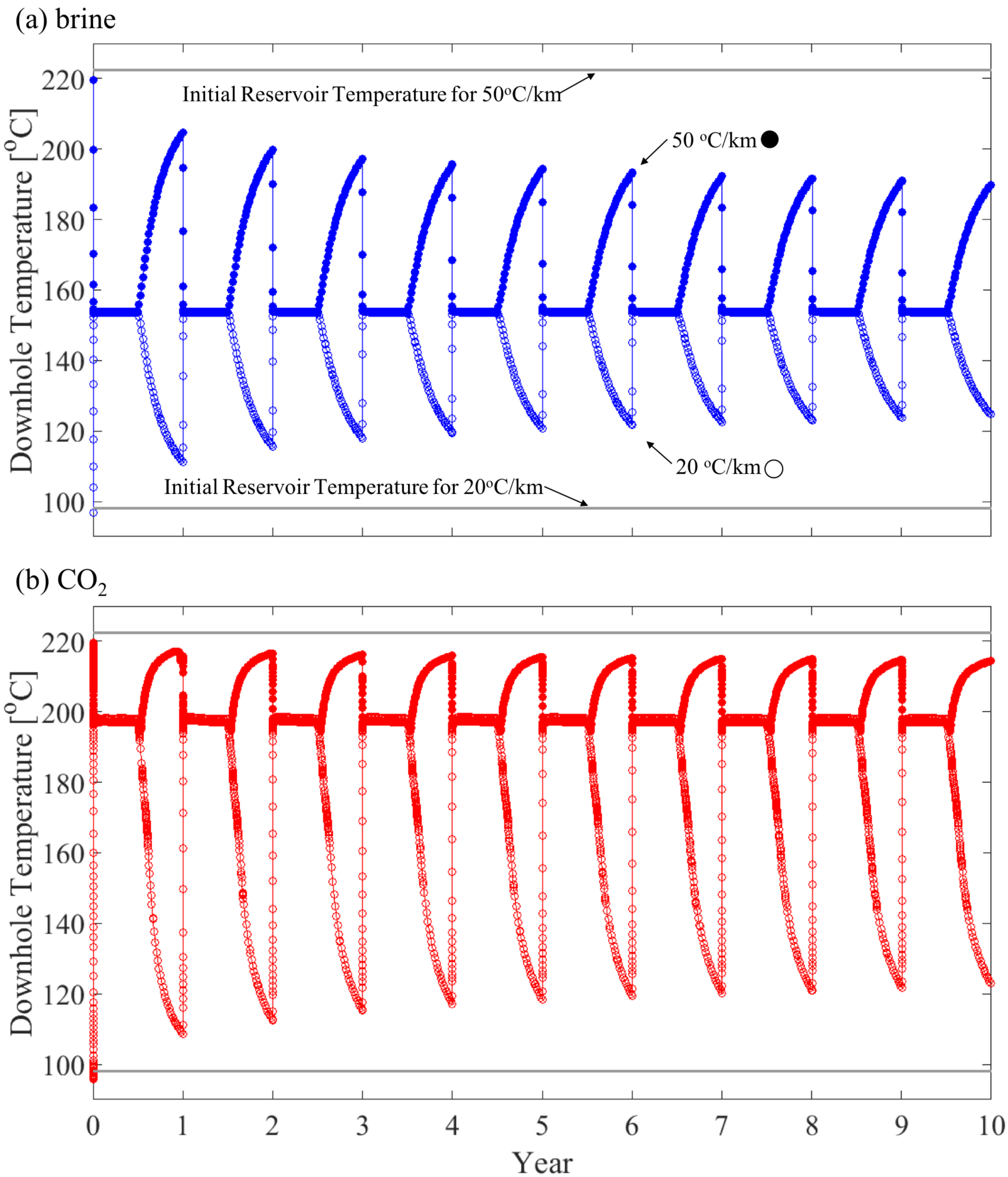

Figure 10: Downhole Temperature at the Bottom of the Reservoir for Ten Cycles of Six Months of Fluid Injection Followed by Six Months of Fluid Production with the Same Well for (a) Brine and (b) CO_2.

For the cooler reservoir, with the 20°C/km geothermal temperature gradient, the temperatures of the injected fluids are hotter than the initial reservoir temperature and thus the reservoirs heat up over time. This gradual deposition of heat in the reservoir is indicated in Figure 10 by the increase in the minimum downhole temperature after each six-month production period. With the injection of pre-heated CO_2, the downhole temperature after the first cycle of six months of fluid injection and six months of fluid production is 109°C and the reservoir heats up over time such that the downhole temperature is 123°C after the tenth cycle. With the injection of pre-heated brine, for the same cycles the reservoir warms from 111°C to 125°C after ten years of the injection and brine production.

In contrast, when the fluids are injected into the warmer reservoir, with the 50°C/km geothermal temperature gradient, the injected fluids are colder than the initial reservoir temperature. The injected fluids heat up while in the reservoir, but the reservoir cools. This cooling is more pronounced with the injection of the pre-heated brine. After the six-month production phase of the cycle, the produced fluid when pre-heated CO_2 was injected is 217°C at the end of the first cycle and 214°C at the end of the tenth cycle. The reservoir cools much more with the brine injection, and the maximum temperature of the produced fluid decreases from 205°C after the first cycle to 190°C after the tenth cycle.

Even though the CO_2 is injected into the 20°C/km reservoir at a higher temperature than the injected brine, the downhole temperature during the production phase of the cycle is slightly lower when CO_2 was injected than when the cooler brine was injected. This disparity between the injection temperatures and the production temperatures occurs because the buoyancy of CO_2 causes it to rise to the top of the reservoir. As a result, even though CO_2 was injected, most of the fluid that is produced over time is brine that was already in the subsurface and was heated, mostly by convection, within the reservoir.

Table 10: Absolute Difference Between the Initial Reservoir Temperature and the Downhole Well Temperature at the End of Each Cycle.

	20°C/km Gradient		**50°C/km Gradient**	
Cycle	Brine	CO_2	Brine	CO_2
1	13.2	10.6	17.8	5.4
2	17.6	14.6	22.6	5.9
3	20.0	17.4	25.2	6.3
4	21.5	19.1	26.9	6.6
5	22.7	20.4	28.2	6.9
6	23.6	21.4	29.2	7.2
7	24.4	22.2	30.1	7.4
8	25.1	22.9	30.9	7.6
9	25.7	23.6	31.5	7.8
10	26.7	24.9	32.6	8.1

Over time, the downhole well temperature approaches the temperature of the injected fluid (Table 10). In the cooler reservoir (20°C/km), the temperature of the produced fluid is closer to the initial temperature when pre-heated brine is injected than when pre-heated CO_2 is injected—even though with brine there is almost a 100°C difference between the injection temperature and the initial reservoir temperature. As a result, the injection of pre-heated fluids could be used to thermally prime the reservoir (in a manner that is similar to the priming of pressure in the CRP-BES design) where pre-heated fluids could be injected for some time before operation in order to increase the temperature of the reservoir and thus the fluids that would be produced from it.

Since brine has a greater specific heat than CO_2, pre-heated brine should increase the downhole temperature in colder reservoirs more than pre-heated CO_2. While the results in Table 10 support this expectation, the difference between using pre-heated CO_2 and using pre-heated brine is small in the cooler reservoir (at most 3°C). This similarity in the downhole temperatures is largely because CO_2 heats up more than brine when being compressed and injected down the well. Holding everything else constant, a greater temperature difference will result in more heat transfer. There may thus be situations (e.g., colder, deeper reservoir) where the higher heat of compression of CO_2 may compensate for the lower specific heat, and thus pre-heated CO_2 could be the preferred option for thermally priming a reservoir.

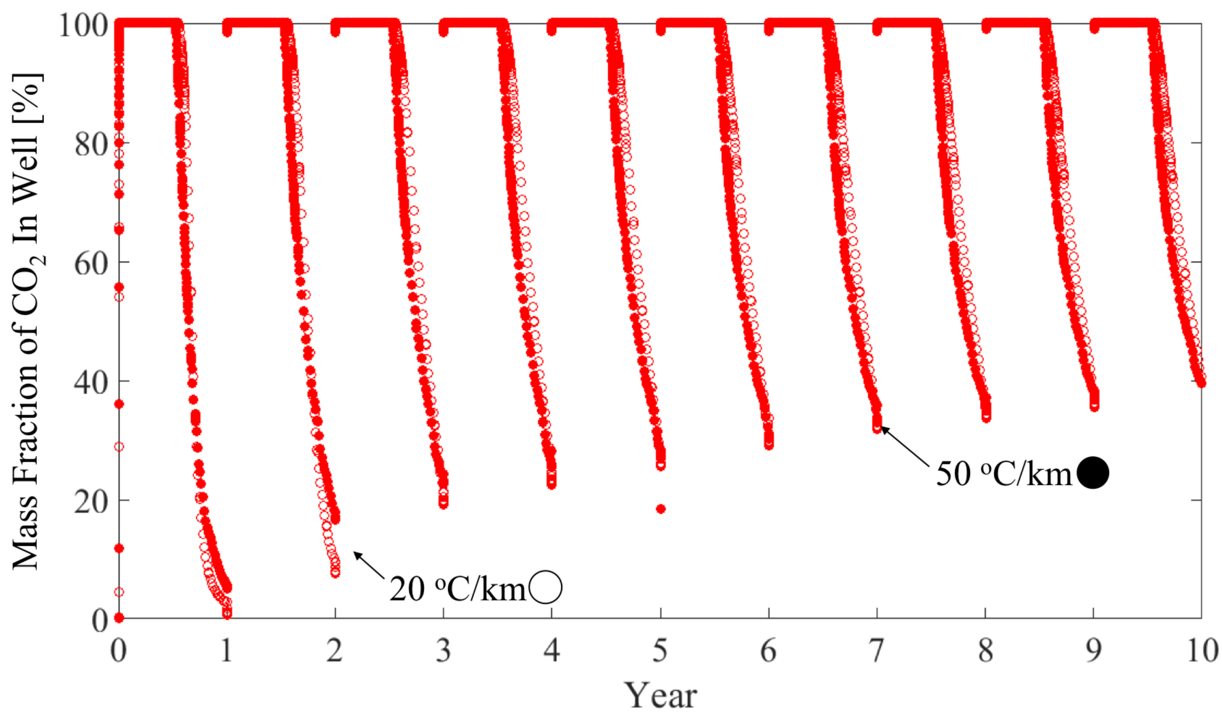

Figure 11: Mass Fraction of CO_2 Entering the Reservoir for the First Half of Each Year and Exiting the Reservoir for the Second Half of Each Year.

Figure 11 shows that the CO_2 mass fraction of the produced fluid decreases over the course of the six months of fluid production. In early cycles, almost none of the produced fluid contains CO_2 at the end of the six months of fluid production, but by the end of the tenth cycle (Year 10) the CO_2 mass fraction decreases to only 40%. As more CO_2 is injected into the reservoir over time, there is less brine available to be displaced and produced. For the hotter reservoir (50°C/km), the CO_2 mass fraction of the produced fluid decreases to a lesser extent than with the cooler reservoir (20°C/km). For example, after the second cycle (end of Year 2), ~8% of the produced fluid in the cooler reservoir was CO_2 whereas ~15% of the produced fluid was CO_2 in the warmer reservoir.

3.3.2.3 Total Energy in Reservoir

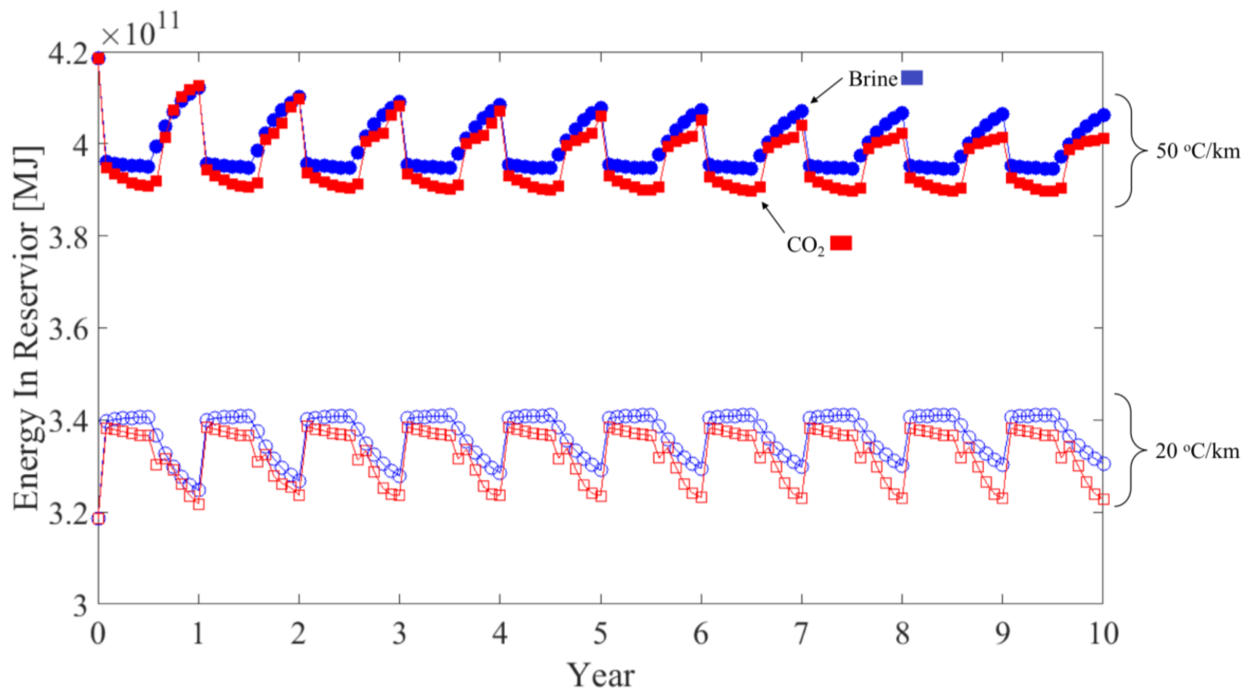

Figure 12: Total Energy in the Reservoir within a Radius of 1 km from the Huff-and-Puff Thermal Energy Injection/Production Well.

During the six-month injection phase, the total energy in the reservoir (Figure 12) decreases for three of the four thermal energy storage scenarios that we investigated. When fluids are injected into the warmer reservoir (50°C/km), the amount of energy in the reservoir decreases because the injected fluids are colder than the reservoir. The total energy in the reservoir decreases more with CO_2 injection than with brine injection because CO_2 has a lower heat capacity. This property of CO_2 also causes the total energy in the cooler reservoir (20ºC/km) to decrease when CO_2 is being injected, even though it is much hotter than the reservoir. When brine is injected into this cooler reservoir, the total energy in the reservoir increases, but the CO_2 injection displaces the native brine in the upper portion of the reservoir (due to buoyancy) and thus the total energy in the reservoir decreases.

During the six-month production phase, the total energy in the reservoir increases in the warmer reservoir, due to the removal of cooler fluids, and decreases in the cooler reservoir, due to the removal of fluids that are hotter than the reservoir. In early cycles, the total energy in the reservoir after an injection-production cycle is roughly the same if pre-heated CO_2 was injected or if pre-heated brine was injected—especially in the warmer reservoir wherein the trajectories of total energy in the reservoir during the production of fluids are the same. Over time, the differences between the use of brine and the use of CO_2 become apparent, with the reservoir into which pre-heated brine was injected retaining more energy than the reservoir into which pre-heated CO_2 was injected. For example, in the warmer reservoir, the total energy in the reservoir after pre-heated brine was injected was 1% greater after ten years than the total energy in the reservoir when pre-heated CO_2 was injected. In the cooler reservoir, this difference was 2%.

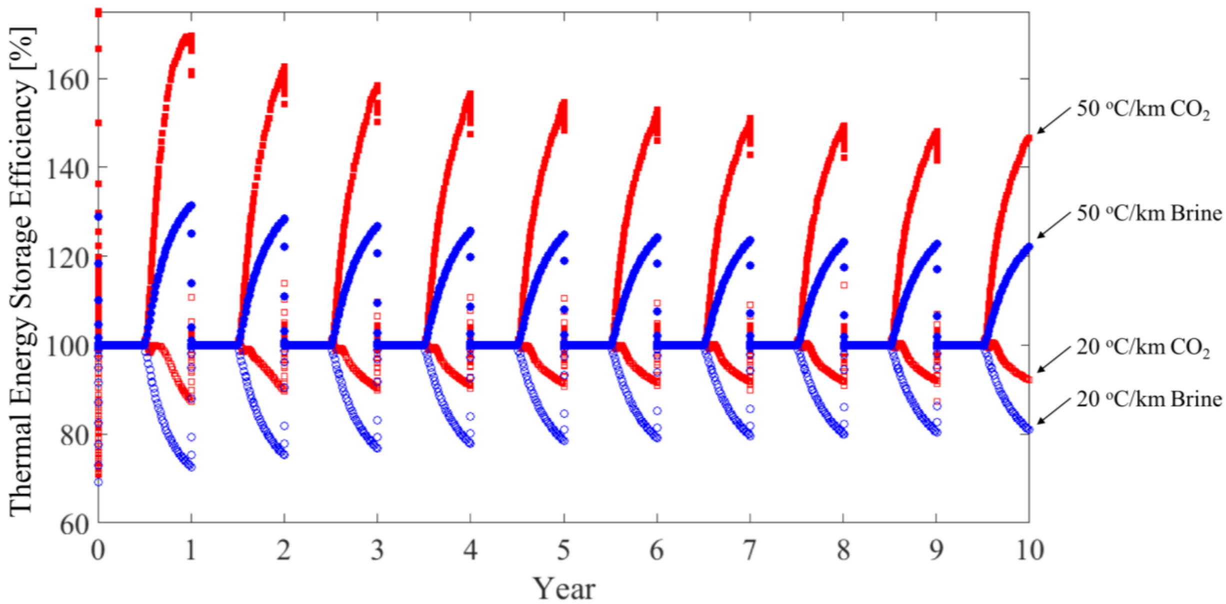

Figure 13: Thermal Energy Exiting the Reservoir Divided by the Thermal Energy Entering the Reservoir.

More energy can be produced from the warmer reservoir because the injected fluids heat up while in the reservoir. As a result, the thermal energy storage efficiency can be greater than 100% because the temperature of the produced fluid was greater than the temperature of the injected fluid (Figure 13). This thermal efficiency decreases over time (131% and 169% to 122% and 146% for brine and CO_2, respectively) because the reservoir is being cooled by the injection of fluids that are colder than the reservoir. The thermal efficiency was higher when pre-heated CO_2 was injected because the produced fluid was composed mostly of brine that has a higher heat capacity than CO_2, especially in the early cycles. In the cooler reservoir, the thermal energy storage efficiency was less than 100% and the produced fluids are cooler than what was injected. Here too, the thermal energy storage efficiency was greater for CO_2 than for brine (72% and 88% for brine and CO_2 respectively after one cycle; 81% and 92% after ten cycles). The increase in thermal energy storage efficiency over time results from warming the reservoir with pre-heated fluids that are hotter than the reservoir.

3.4 Discussion and Conclusions

In this work, we investigated two mechanisms for seasonal energy storage (SES)—by pressure and by heat—for different cycles that contain equal durations of energy storage and energy discharge. We built and implemented a new integrated model to investigate the feasibility of energy storage using a concentric-ring pressure-based bulk energy storage (i.e., CRP-BES) design for cycles that are longer than a day. For SES using thermal energy storage, we compared and contrasted the subsurface injection of pre-heated CO_2 and pre-heated brine as the media for energy storage. For the simulations with the injection of pre-heated CO_2 and of pre-heated brine, the combinations of geothermal temperature gradient, depth, and temperature of the injected fluids were chosen so that there would be a case where the injected fluids would be warmer than the initial reservoir temperature and there would be a case where the injected fluids would be cooler than the initial reservoir temperature. As such, the results provide insight into how the reservoir and produced fluids may heat up or cool down over time with cycled thermal energy storage.

1. *Geologically stored CO_2 can be used for long duration (>24 hours) storage of energy in the subsurface, but the design of the system must be tailored to site-specific conditions.* The CRP-BES design that we investigated was successful with cycles that stored energy for a week and then dispatched energy for a week continuously over the course of fourteen years (i.e., 364 cycles). While the design of the CRP-BES system that we implemented was not optimized for the reservoir parameters that we used based on the Minnelusa aquifer (Wyoming, USA), we have evidence that this design could successfully operate with longer durations—on the order of up to a couple weeks. From a technical standpoint, reducing the production flowrate could increase the viable durations of storage and dispatch beyond a couple of weeks to enable SES with a CRP-BES design, but the size of the brine holding pond may render the approach infeasible (Table 11), and would likely result in less capacity for energy storage and energy dispatch. It is thus likely that for seasonal

energy storage, the holding ponds would be replaced by natural underground reservoirs that are located at shallower depths than the main, deep reservoirs [154].

Table 11: Volume of Brine Holding Pond Required for Different Discharge Durations and Production Flowrates [million United States liquid gallons].

	Brine Production Flowrate [kg/s]			
Discharge Duration	**5,000**	**4,000**	**3,000**	**2,000**
12 Hours	57.23	45.78	34.34	22.90
24 Hours	114.46	91.57	68.68	45.79
3 Days	343.39	274.71	206.03	137.36
1 Week	801.25	641.00	480.75	320.50
1 Month	3,481.63	2,785.31	2,088.98	1,392.65

Another option for increasing the durations of energy storage and energy dispatch for seasonal applications could be to changing the spacing between the concentric rings of wells to better optimize the design of the CRP-BES system for the site-specific application.

2. *The CRP-BES design that we investigated has dispatch capacities that are greater than the storage capacities because of the geothermal heat input.* In our results, the CRP-BES design could dispatch up to ~130 MWe and store up to ~55 MWe. These capacities were remarkably consistent across the energy storage durations that we investigated and over their timeframes, with at most a 0.4% difference in dispatch capacities and a 10% difference in storage capacities. Most of the capacities are from the indirect brine power cycle, because the production flowrate was five times larger than in the direct CO_2 power cycle in our CRP-BES design without depleting geothermal heat. Further,

the brine power cycle generates more electricity per kg/s of produced fluid than the CO_2 power cycle, in part because the reinjection of brine uses electricity to store energy.

3. *The thermal energy efficiency of subsurface energy storage can be higher with the use of pre-heated CO_2 than with the use of pre-heated brine.* While the use of pre-heated brine will likely result in the storage and production of more thermal energy than the use of pre-heated CO_2, the use of pre-heated CO_2 could have advantages over the use of brine, especially in reservoirs with low geothermal temperature gradients. For example, in the reservoir that was cooler than the temperature of the injected fluids (20°C/km geothermal temperature gradient), the thermal energy storage efficiency was ≥11% more when pre-heated CO_2 was used than when pre-heated brine was used. The advantage with pre-heated CO_2 occurred in part because brine that was already in the reservoir was heated by the injected CO_2 and subsequently produced. Since SES will be more cost-effective with higher efficiencies, the higher thermal energy storage efficiency with the use of pre-heated CO_2, potentially with the subsequent production of heated brine, may enable a cost-competitive SES approach despite the smaller magnitude of thermal energy storage capacity, especially when multi-month timescales of storage and production are considered.

4. *Absent other considerations (e.g., CO_2 price, higher thermal energy storage efficiency) storing thermal energy in the subsurface for SES would likely use pre-heated brine as the energy storage medium, but CO_2 could have other important uses in an SES system.* While the design of such a thermal energy storage system will depend on the characteristics of the subsurface, the source of thermal energy, and other systems-level factors (e.g., the capacity of variable renewable energy technologies), brine is likely to be favorable over CO_2 for storing thermal energy because (a) the pumping power that is required to inject brine does not vary as substantially with temperature as for injecting CO_2 (CO_2 is much more compressible), and (b) more heat can be stored per unit of fluid with brine because the specific heat of brine is larger than that of CO_2. While CO_2 may not be

a favorable media for thermal energy storage on its own, it could be used in other ways as part of a subsurface thermal energy storage system that operates over seasonal timeframes: (1) to thermally prime cold, deep reservoirs; (2) to be produced after being geothermally heated and used to generate electricity [17,18]; (3) for pressure support to direct the migration of hot brine [164–166] or in situations where brine would otherwise flash.

Our reservoir simulations demonstrate the important role that the subsurface could play in seasonal energy storage (SES). The ability to contain pressure by controlling fluid production and injection, and the associated mass flowrates, through strategic placement of wells (concentric rings, in our case) facilitates the storage of energy as pressure in the subsurface. Proper design of the system that is tailored to the site-specific conditions has the possibility of enabling SES with pressure energy storage using a combination of CO_2 and of brine, although we have also suggested subsurface bulk energy storage (BES) systems that only use CO_2 to efficiently store energy at least over days and likely also over weeks, months, and seasons (Fleming et al., 2018).

For thermal energy storage, the use of pre-heated CO_2 requires more nuanced justifications than the use of pre-heated brine—in part due to differences in compressibility, specific heat, and density. Yet geologic CO_2 storage approaches are often included in least-cost, decarbonized, electricity systems [149] and the approaches that we considered here combine geologic CO_2 storage with renewable energy generation that does not emit CO_2. It is thus possible for a subsurface thermal SES system that uses pre-heated CO_2 to provide more systems-level benefits to decarbonizing the electricity system than a brine-based system, despite the thermophysical advantages of brine for thermal energy storage.

Chapter Four: Operational Characteristics of a Geologic CO_2 Storage Bulk Energy Storage Technology

4.1 Introduction

Carbon dioxide (CO_2) bulk energy storage (CO_2-BES) facilities use CO_2 in sedimentary basin geothermal resources to provide bulk energy storage (BES) services for the electricity system [54]. During an initial 3- to 5-year priming period, new CO_2 is injected into a deep saline aquifer to build overpressure. While CO_2-BES is scalable, the amount of CO_2 that is needed requires that it be captured from large point sources (e.g., coal-fired power plant). Since this CO_2 is permanently isolated from the atmosphere, CO_2-BES is a CO_2 capture, utilization, and storage (CCUS) technology.

To control the migration of the CO_2 plume and manage the overpressure, brine is produced from the reservoir to the surface and re-injected as needed. During operation, a CO_2-BES facility can dispatch electricity by producing geothermally-heated CO_2 and brine to the surface, and using the heat in these fluids to generate electricity in a direct CO_2 power cycle and indirect brine power cycle. The produced CO_2 is re-injected into the subsurface and the produced brine is stored in holding ponds at the surface. When the supply of electricity exceeds demand, energy can be stored by re-injecting the brine and additional new CO_2. As such, the performance of a CO_2-BES facilities relies on geothermal heat extraction and the overpressure in the subsurface.

In addition to permanently isolating large amounts of CO_2 from the atmosphere, CO_2-BES has several advantages over other BES approaches like Pumped Hydro Energy Storage (PHES) and Compressed Air Energy Storage (CAES). For example, the length of time that a PHES or CAES facility can generate electricity at capacity (the hours of storage) is limited by the amount of energy that was previously stored. In contrast, because CO_2-BES operation relies on the overpressure from the priming period and geothermal heat, the hours of storage of a CO_2-BES facility is an operational decision. For example, at any given time, there is flexibility for a CO_2-BES operator to dispatch electricity at capacity for 1 hour, or over 12 hours, independent of how much electricity was previously stored in the cycle. Despite this advantage, over the lifetime of the facility, the operational decisions regarding how many hours to discharge electricity and store energy could affect how a CO_2-BES facility operates, because the charge/discharge cycles change the overpressure and the rate at which geothermal heat is extracted. In this way, the durations of charging and discharging may affect the power output capacity (the maximum amount of power than can be generated at any one time) and the power storage capacity (the maximum amount of power that can be stored at any one time) of a CO_2-BES facility.

In this conference paper, we investigated how charge and discharge cycles less than 24 hours affect the power output capacity and power storage capacity of a CO_2-BES facility. Because a CO_2-BES facility will operate as a component of the electricity system, decisions regarding when and how long to charge or discharge will likely be influenced by external factors that are independent from the overpressure and geothermal heat resource. For example, charging may be needed from the standpoint of depleted overpressure, but discharging may be needed from the standpoint of the electricity system. As a result, knowledge of how the charging and discharging cycle affects the power storage and power output capacities of a CO_2-BES facility is necessary to determine how to simultaneously optimally operate CO_2-BES from a process-level and a systems-level perspective.

4.2 Methods

We used the integrated model of the CRP-BES design (Section 3.2.1) to simulate the operation over a range of (a) short (i.e., < 24 hour) charge and discharge cycles of equal charge and discharge durations, (b) charge and discharge cycles of unequal durations, and (c) charge and discharge cycles that include idle periods (Table 12). All cycles were simulated for fourteen years. For example, in Cycle 6 listed in Table 12, the CO_2-BES facility continuously operated to discharge electricity for 4 hours, then idle for 8 hours, then charge for 4 hours, then idle for 8 hours.

Table 12: Cycles of CO_2-BES Operation that Were Simulated - numbered entries refer to the order in the cycle.

	Discharge Duration (Hours)					Charge Duration (Hours)				Idle Duration (Hours)	
Cycle	**4**	**8**	**12**	**16**	**24**	**4**	**8**	**12**	**24**	**8**	**16**
1	1					2					
2		1					2				
3			1					2			
4					1				2		
5	1					2					3
6	1					3				2, 4	
7				1			2				

4.2.1 CO_2-BES Process-Level System Modeling

Following Chapter Three, we assumed that the CO_2-BES facility using the CRP-BES design was operating in the Minnelusa Aquifer in eastern Wyoming and as a result, we used the same subsurface parameters in the NUFT model as in Chapter Three (Section 3.2.1). Further, we also used the same injection and production flowrates, the same initial conditions from the priming period and also diverted produced brine as needed to maintain the overpressure at 10 MPa as new CO_2 was injected. Lastly, the same data sampling procedure was used in Chapter Three to obtain representative "snapshots" of the performance of the CO_2-BES facility over a multi-year period.

4.3 Results

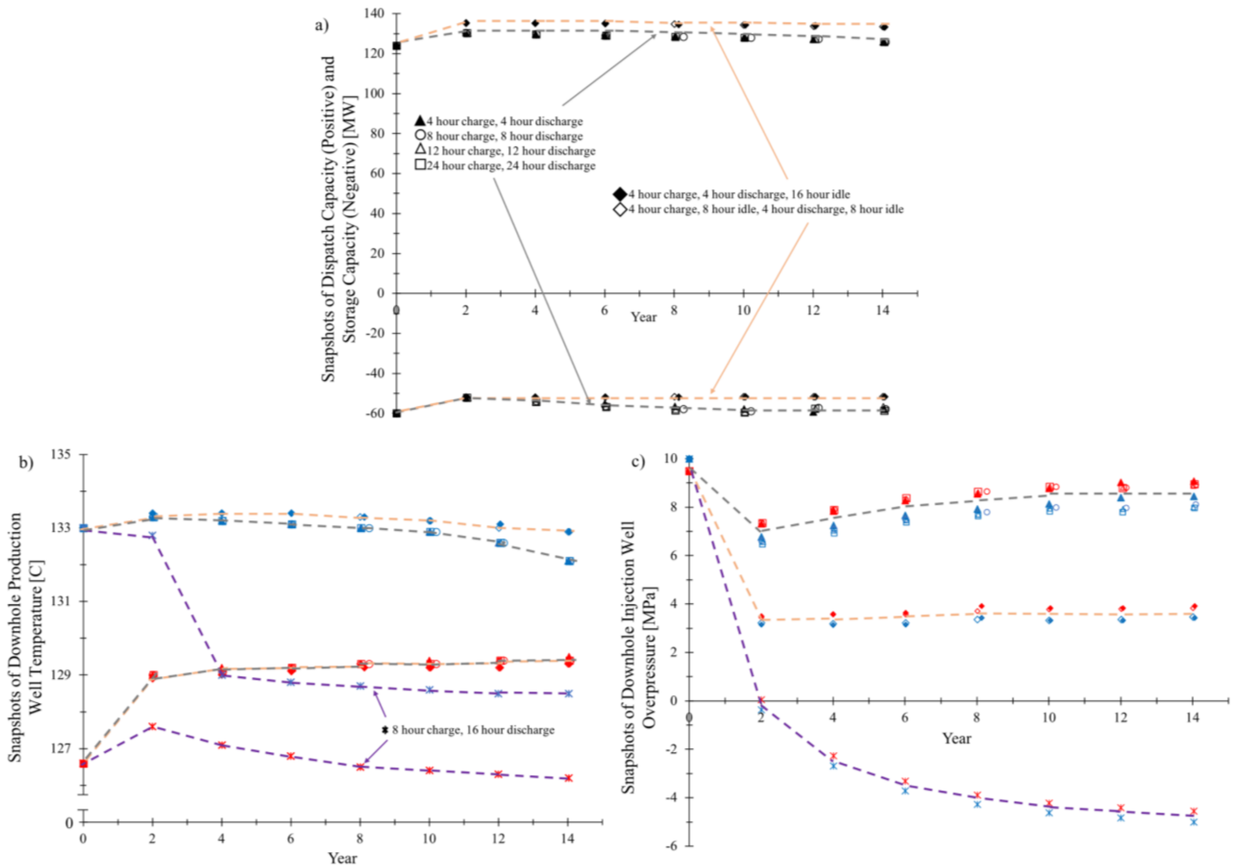

Figure 14: Snapshots of Power System Capabilities and Subsurface Conditions of CO_2-BES Operation Under Different Charging and Discharging Cycles. The grey, orange, and purple dashed lines were included to distinguish results across different grouping of charge and discharge cycles and are not intended to convey information between data points. In (b) and (c), the red markers indicate CO_2 and the blue markers indicate brine.

All but one of cycles that we investigated have the ability to store and produce power; in Cycle 7 (8-hour charge, 16-hour discharge), the overpressure decreased to the point that fluids in the production wells started to flash (i.e., change from liquid to gas). The power storage capacities and power output capacities are not sensitive to the durations of the charge and discharge cycles if the facility is continuously alternating between the two modes (Figure 14a): all of the cycles that are grouped with a grey dashed line generate approximately 130 MW and store approximately 55 MW. Similarly, the cycles that contain idle periods have relatively similar power storage capacities and generated approximately 133 MW and stored approximately 51 MW.

The inclusion of an idle period results in a decrease in overpressure that increases power output capacity and decreases power storage capacity (Figure 14c). The reduction in power storage capacity occurs because less energy is required to inject fluids. The power output capacity increases because some CO_2 migrates away from the production well when there is less overpressure to constrain it, and thus the fraction of CO_2 in the produced fluid decreases (Figure 15). Since brine has a higher heat capacity than CO_2, the amount of power that can be generated increases. Further, the indirect brine cycle also generates electricity without the parasitic losses associated with brine re-injection when CO_2-BES dispatches electricity. In contrast, the power output of the indirect CO_2 cycle is reduced by the pumping load for re-injecting CO_2 and for injecting new CO_2 when CO_2-BES dispatches electricity.

There was little effect on the depletion of geothermal heat. In fact, the downhole temperature of the production wells remained relatively constant across all of the cycles that we simulated (Figure 14b), with a decrease of at most of 4ºC over fourteen years in the cycles that we simulated.

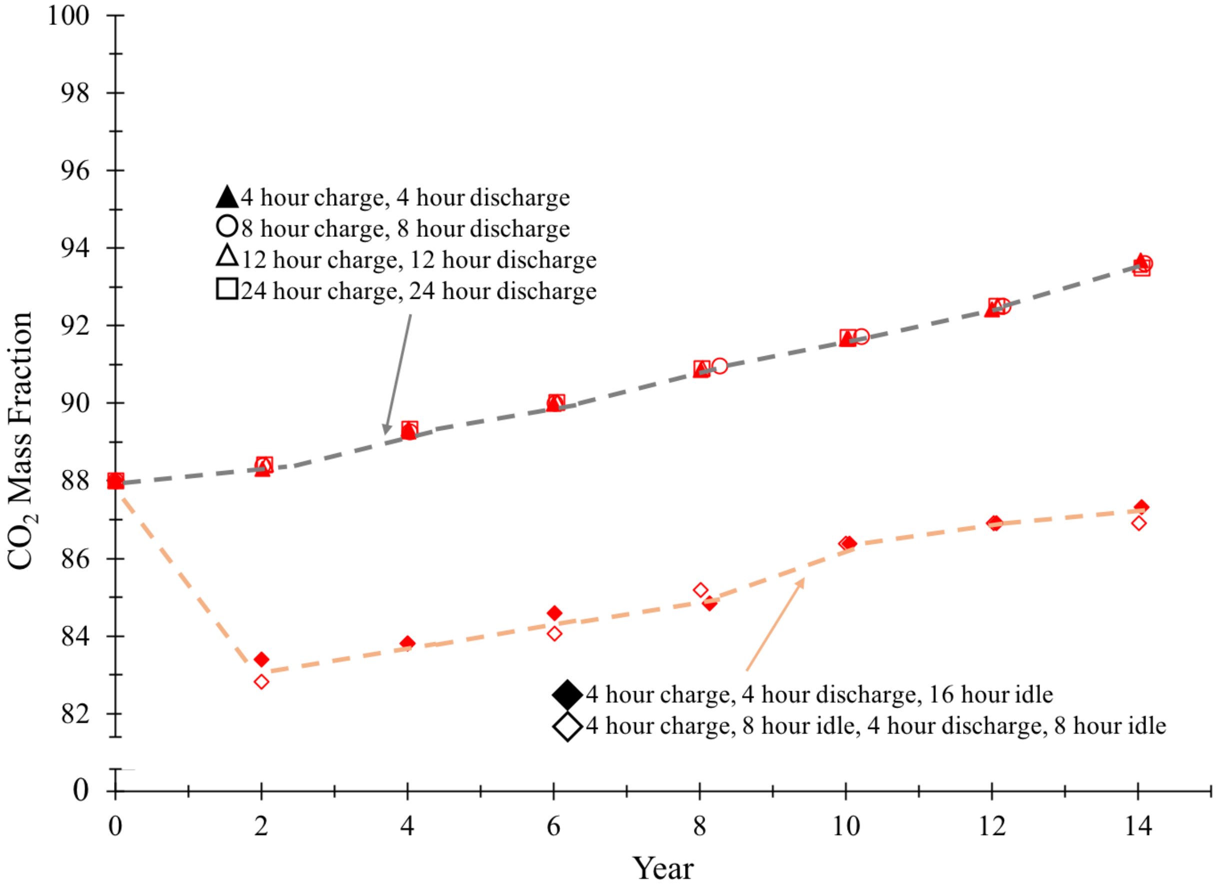

Figure 15: Snapshot of Percent of Fluid Produced from CO_2 Production Wells that is CO_2. Because the fluid being produced from the production wells is either brine or CO_2, a decrease in CO_2 production also indicates an increase in brine production.

4.4 Conclusions

We previously developed CO_2-BES, a technology that uses geothermal heat and the increase in reservoir overpressure from geologic CO_2 storage in sedimentary basin geothermal resources, to store and dispatch electricity [54]. Here, we simulated fourteen years of CO_2-BES operation across seven charge and discharge cycles to understand the effect that the durations of charging and discharging has on the power storage capacity and power output capacity of the CO_2-BES facility. Our results suggest that:

1. *The charge (storage) and discharge (generation) cycle influences the power output capacity and power storage capacity of a CO_2-BES facility through the effect on reservoir overpressure.* The power storage capacity of the CO_2-BES facility depends on the energy required to inject fluids into the subsurface, and therefore increases with increasing overpressure. But increasing overpressure also increases the amount of CO_2 in the production well, which reduces the power output capacity because less brine is produced. The power output capacity and power storage capacity depend on the subsurface temperature as well, but the storage and discharge cycle of a CO_2-BES does not substantially affect the rate at which the geothermal heat resource, and thus subsurface temperature, is depleted.
2. *Dispatching electricity for a duration of time that is longer than the duration of storage can create situations in which a CO_2-BES facility can no longer operate.* The overpressure decreases for a couple years following the transition from the initial priming period to bulk energy storage operation. If the duration of the charging period is longer than the duration of the discharging period, the overpressure will continuously decrease and be reduced below hydrostatic pressure, which can cause flashing in the production well and ultimately stall or end the operational life of a CO_2-BES facility.
3. *Including an idle period in the cycle increases the power output capacity and decreases the power storage capacity compared to a cycle of continuous charging and discharging.* The overpressure decreases more in cycles that have idle periods than in cycles with continuous charge and discharge. As a result, the power storage capacity is smaller and the power output capacity is larger in cycles with idle periods.
4. *If the total time spent charging, discharging, or idling is equal over a multi-year period, the duration of an individual cycle does not substantially affect the power storage capacity and power output capacity.* The power storage capacity and power output capacity of all of the cycles that we simulated did not change substantially across different cycle durations. As a

consequence, as long as CO_2-BES operators maintain equivalent charging and discharging durations, they may be able to make decisions based solely on systems-level factors (e.g. as the CO_2 price or diurnal variations in electricity prices), with less concern for heat or pressure depletion.

These results are contingent on the total production flowrates and total injection flowrates that were set in Chapter Three (Section 3.2.1); future work may investigate how the power output and power storage capacities are influenced by both the charging and discharging cycle and these flowrates. Changing the total production and injection flowrates will both directly and indirectly impact the power output and power storage capacities by (a) changing the amount of fluid flowing through the pumps and turbines and (b) altering the extent to which injecting and producing fluid effects subsurface overpressure.

Chapter Five: The Value of CO_2-Bulk Energy Storage with Wind in Transmission Constrained Electric Power Systems

5.1 Introduction

Human activities that emit greenhouse gases like carbon dioxide (CO_2) have already caused approximately 1°C of global warming and emissions reductions are needed across the entire economy to mitigate future warming [2]. For example, the electricity sector (35%), industrial processes (15%), residential and commercial processes (10%), and other processes like land-use change (7%) all emitted CO_2 into the atmosphere in the United States in 2015 [5]. Because the electricity sector is one of the single largest sources of CO_2 emissions and technologies currently exist that can generate electricity without emitting CO_2, stabilizing the atmospheric concentration of CO_2 emissions to address climate change will likely require substantially reducing, if not completely eliminating, CO_2 emissions from the electricity sector by 2050 [2,7,142,145].

Wind turbines and solar photovoltaics are well-known examples of electricity generating technologies that do not emit CO_2, but utilizing large penetrations of these variable renewable energy technologies is costly in part because wind and solar energy resources may not be located in the same geographic regions that electricity is demanded. For example, much of the high quality wind resource in the United States is far away from major load centers [64]. As a consequence, in addition to the increased investment in wind turbines and solar photovoltaics, integrating and using high penetrations of these variable renewable energy technologies will likely also require substantial investment in expensive high voltage direct current (HVDC) transmission lines to transfer the electricity generated by renewable energy technologies to more densely populated locations where the majority of electricity is consumed [147,167,168].

Sizing the capacity of the HVDC transmission line that connects a wind farm or solar photovoltaic field to a distant load center is challenging because (a) of the variability of wind and solar energy, which will also change as the climate changes [169], and (b) the cost of HVDC transmission infrastructure and the revenue from electricity sales both increase with the capacity of the HVDC transmission line. For example, maximum revenue from electricity sales is realized if the HVDC transmission capacity is equal to the capacity of the variable renewable energy technology because all electricity generated can be sold to the load center. But in this situation, the cost of the transmission infrastructure is also a maximum and the utilization of the transmission line is likely to be low because it is limited to the capacity factor of the renewable energy technology. For reference, the capacity factor for wind power and solar photovoltaic power across the United States in 2016 was only 34.7% and 27.2%, respectively [170]. As a consequence, it is difficult to financially justify investing in transmission capacity equal to the capacity of the variable renewable energy technology. Decreasing the HVDC transmission capacity decreases costs and increases the utilization of the transmission infrastructure, but it also decreases revenue from electricity sales (and ultimately the amount of electricity consumed that was generated by the variable renewable energy technology) because any electricity generation in excess of the transmission capacity is curtailed. As a result of these revenue and cost tradeoffs, an optimal HVDC transmission capacity that maximizes profit can be determined in these situations.

Energy storage approaches that can time-shift electricity generation can provide value in transmission-constrained electricity systems in the form of increased profits [136,171]. For example, energy storage could store a portion of the electricity generated by a wind farm during a windy time (e.g., when electricity generation exceeded the HDVC transmission capacity) and dispatch the stored electricity later when the wind farm was generating less electricity (e.g., when electricity generation was less than the HVDC transmission capacity). Operating as a transmission asset in this way, energy storage can increase revenue by increasing the utilization of the variable renewable energy technology and the utilization of the HVDC transmission infrastructure. If revenue increases enough, energy storage could also increase the profit-maximizing HVDC transmission capacity, and ultimately, the total profit from electricity sales. In this situation, the increase in transmission capacity enabled by energy storage will also indirectly reduce CO_2 emissions if the increase in electricity dispatched to the load center decreases the amount of electricity generated by a convention power plant that emits CO_2.

Compared to conventional approaches to energy storage like Pumped Hydro Energy Storage (PHES), Compressed Air Energy Storage (CAES), or batteries, it is likely that CO_2-Bulk Energy Storage (CO_2-BES) would be used in these situations if reducing CO_2 emissions is the primary motivation behind investing in the HVDC transmission infrastructure because CO_2-BES can indirectly *and* directly reduce CO_2 emissions. CO_2-BES has been recently proposed [54], and is an approach to energy storage based on CO_2 Plume Geothermal technology where CO_2 captured from a large point source (e.g., fossil-fuel power plant, cement manufacturer) is injected into deep (>800 m) naturally porous and permeable sedimentary basin geothermal resources and intentionally produced back to the surface to extract geothermal heat for the purpose of generating electricity [16–18,83].

In addition to being be a component of the CO_2 Capture and Storage (CCS) process, CO_2-BES is further unique compared to PHES, CAES, or batteries because it is capable of transitioning between operating as an energy storage approach (i.e., time-shifting electricity generation) and operating as a geothermal power plant (i.e., extracting geothermal heat and dispatching it as electricity). The CO_2-BES system that we consider in this study uses two geothermal power cycles to generate electricity: an indirect brine Organic Rankine Cycle (ORC) and a direct CO_2 cycle [54]. Externally captured CO_2 is injected into the sedimentary basin to store pressure and permanently isolate the CO_2 from the atmosphere over an initial 3 to 5 year "priming" period. During this period, in-situ brine is also produced to the surface and then re-injected to control the migration of the CO_2 plume and manage the overpressure (i.e., the pressure above the hydrostatic pressure) in the subsurface. Once operational, CO_2-BES operators can generate electricity when demanded using geothermal energy directly by simultaneously (a) producing geothermally-heated CO_2 and brine to the surface, (b) using the heat in these fluids to generate electricity in their respective power cycles, and (c) re-injecting the fluids into the subsurface. Alternatively, a CO_2-BES facility can also be operated as an energy storage facility by time-shifting when the produced brine is re-injected. In this mode of operation, the produced brine is held in ponds at the surface after electricity is generated and when needed, electricity is later stored as pressure energy in the subsurface by using electricity to power a pump to re-inject the brine. Further, electricity is also stored as pressure throughout the lifetime of a CO_2-BES facility because new CO_2 is constantly injected into the sedimentary basin, independent of how the facility is operated. If the CO_2-BES facility is operated as a geothermal power plant, the load from this injection of new CO_2 decreases the net power output from the facility.

In this study, we investigate the degree to which CO_2-BES use could result in an increase in the profit-maximizing HVDC transmission capacity that connects a wind farm in Eastern Wyoming to the electricity system managed by the California Independent System Operator (CAISO). Because CO_2-BES has been recently proposed, its optimal dispatch when coupled with a variable renewable energy technology to sell electricity to a distant load center, and its application to HVDC transmission issues, have yet to be investigated. Overall, there are many ways in which CO_2-BES could be used to address climate change within the United States because (a) there are many applications for energy storage in addition to increasing a profit-maximizing HVDC transmission capacity and (b) sedimentary basin underlie approximately half of North America [44,49,65]. But the potential of any component of the electricity system, including CO_2-BES, to address climate change will be limited by its profitability. As a consequence, the current potential for energy storage in the United States to address climate change is constrained because most electricity system market rules do not compensate energy storage operators for the services they could provide, and as a result, one of the largest markets for energy storage is applications with transmission infrastructure [66,67]. In other words, this study is also the first to determine the profitability of a CO_2-BES facility when being used in one of the most valuable applications for energy storage.

5.2 Methods

We developed and implemented a framework to determine the profit-maximizing HVDC transmission capacity with and without CO_2-BES (Figure 16). The framework includes a mixed linear integer optimization model to optimize how CO_2-BES is dispatched with a variable renewable electricity technology to maximize the revenue from selling electricity to a distant load center over a year. We simulated 30 years of CO_2-BES operation using an integrated process-level model that we previously developed (Chapter Three) and used the process-level results from the first year of CO_2-BES operation to constrain the CO_2-BES system within the optimization model. These process-level results were also used in a CO_2-BES cost model that we developed for this study to estimate the annualized cost of the CO_2-BES facility.

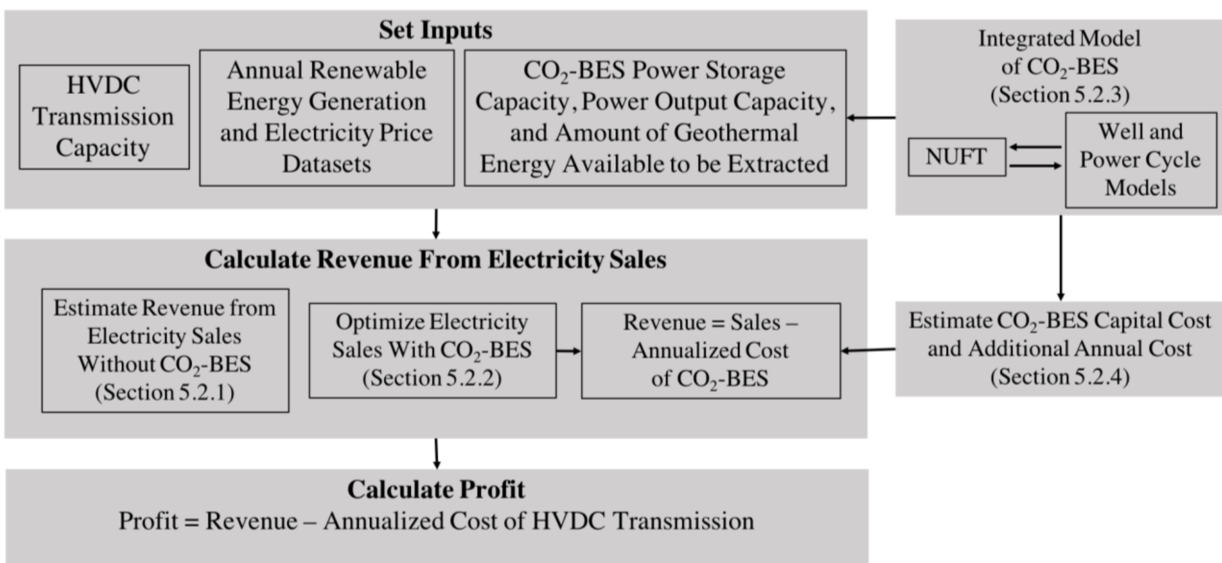

Figure 16. Framework for Estimating the Profit-Maximizing HVDC Transmission Capacity with and without CO_2-BES.

The optimal HVDC transmission capacity is the capacity that results in the maximum annualized profit. This profit is defined as the sum of the revenue from electricity sales less the annualized cost of HVDC transmission infrastructure (Figure 16). We used Equation 12 to annualize capital costs and assumed a capital recovery factor (CRF) of 11% [136].

$$\text{Annualized Cost} = \text{Capital Cost} * \text{CRF} \tag{12}$$

The optimal HVDC transmission capacity is a function of the wind conditions and electricity prices throughout the year. As a sensitivity analysis, we executed the study framework over every combination of wind conditions and electricity price datasets from three different years (i.e., baseline electricity price, high electricity price, future electricity price). For each combination, we also determined the rate at which CO_2-BES operators would need to be compensated for storing CO_2 for the profit with CO_2-BES to be equal to the profit without CO_2-BES (i.e., the breakeven CO_2 price) using Equation 13.

$$\text{Breakeven } \mathrm{CO_2} \text{ Price} = \frac{\text{Revenue}_{\text{without } \mathrm{CO_2}-\text{BES}} - \text{Revenue}_{\text{with } \mathrm{CO_2}-\text{BES}}}{\text{CRF} * \mathrm{tCO_2}_{\text{priming}} + \mathrm{tCO_2}_{\text{operating}}} \tag{13}$$

where $\mathrm{tCO_2}_{\text{priming}}$ is the volume of CO_2 permanently stored during the priming period, and $\mathrm{tCO_2}_{\text{operating}}$ is the volume of CO_2 permanently stored during each year of CO_2-BES operation.

In addition to electricity prices and wind conditions, the optimal HVDC transmission capacity is also a function of the geothermal heat depletion because CO_2-BES operation extracts geothermal heat at a faster rate than the geothermal heat flux recharges the geothermal resource (Chapter Three). As a result, revenue from electricity sales may decrease over the lifetime of the CO_2-BES facility because the power output capacity and the amount of geothermal energy that is available to be extracted decrease as the geothermal heat is depleted. Because our financing assumptions assume constant revenue from sales over the annualized facility lifetime, as part of our sensitivity analysis, we also implemented the study framework for an additional case of maximum heat depletion by using the power storage capacity, power output capacity, and amount of geothermal energy available to be extracted from the final (i.e., 30th) year of process-level results in the optimization model.

5.2.1 Wind Farm Revenue Model

The annual revenue of the wind farm operating without CO_2-BES can be calculated by multiplying the amount of electricity delivered to the load center by the sum of the wholesale energy price, as shown in Equation 14 [136].

$$\text{Annual Wind Farm Revenue} = \sum_{t=1}^{T}[(1-\gamma)p_t\sigma_t] \quad (14)$$

where γ is the transmission losses, p_t is the wholesale price of electricity [$/MWh], and σ_t is the amount of electricity sold [MWh].

This calculation assumes that the output from the wind farm is not sufficiently large to impact the wholesale price of electricity. Further, because CO_2-BES is not available, any electricity that is generated by the wind farm must be either sold or curtailed. We assumed that curtailment only occurs if selling electricity would yield negative revenue [136]. Therefore, unless the price of electricity is negative, the amount of electricity sold, σ_t, is equal to the amount of electricity generated by the wind farm.

5.2.2 Wind Farm with CO_2-Bulk Energy Storage Mixed Integer Linear Optimization Model

We adapted a CAES revenue optimization model from prior work so that it could be used for CO_2-BES [136]. Here we provide a brief description of the model and the constraints, and the full model is provided in Section of 1 Appendix C. The model maximizes the electricity sales revenue from the wind farm operating with CO_2-BES to sell electricity to a distant load center, given the CO_2-BES process level parameters (e.g., power output capacity) and assumes perfect foresight of wind availability and wholesale electricity prices over the year. We also assumed that the CO_2-BES facility is fully charged at the start of the year. The objection function is Equation 15,

$$\max \sum_{t=1}^{T}[(1-\gamma)p_t\sigma_t - (1+\gamma)p_t\theta_t] \quad (15)$$

where γ is the transmission losses, p_t is the wholesale price of electricity over time period t [$/MWh], σ_t is the amount of electricity sold over time period t [MWh], and θ_t is the amount of electricity purchased over time period t [MWh].

5.2.3 Integrated Model of CO_2-Bulk Energy Storage Operation

In Chapter Three, we simulated CO_2-BES operation using a variety of operational cycles of equal charge and discharge, ranging from of 2 x 12 hours (i.e., charging for 12 hours and then dispatching for 12 hours) to 2 x 1 month. While this prior work suggested that the CO_2-BES design that we considered here could successfully time-shift electricity for up to a couple weeks (i.e., 2 x ~2 weeks), we used the 2 x 12 hour cycle in this study because the size of the brine holding ponds required to store multiple weeks of fluid may not be practical to implement.

Following our prior work, we simulated a three year priming period where CO_2 was constantly injected and produced at a total flowrate of 2,000 kg/s. Further, during the subsequent 30 years of 2 x 12 hours cycling, we assuming that brine was produced and reinjected at a total flowrate of 5,000 kg/s and CO_2 was produced and reinjected at a total flowrate of 1,000 kg/s when the CO_2-BES facility was generating electricity. We also simulated a constant injection of new CO_2 at a rate of 120 kg/s (3.78 Mt/yr), independent of the charge and discharge cycle, which increased the overpressure in the subsurface. Despite this constant injection, we constrained the overpressure to 10 MPa by reducing the amount of brine that was re-injected during charging periods.

5.2.4 CO_2-Bulk Energy Storage Capital Cost and Additional Annual Cost Estimations

In prior work we estimated costs of the CO_2-BES facility using the Geothermal Electricity Technology Evaluation Model (GETEM) [54]. Here, we estimated the capital cost and additional annual cost of the CO_2-BES facility in more detail by starting with GETEM [175,176], and augmenting those cost estimates by appropriate CO_2 storage cost estimates from the United States Environmental Protection Agency [177], and other cost estimates (e.g., grid integration costs) from prior work [178–181].

The capital cost of the CO_2-BES facility was the sum of capital cost of the direct CO_2 cycle and the capital cost of the indirect brine ORC. The capital cost of each of these individual geothermal power cycles was the sum of the cost to drill and equip the wells, the cost of the pipeline from production wells to the power plant and the pipeline from the power plant to injection wells, the cost of the power plant (e.g., turbine-generator, cooling tower, pumps), the cost to construct the plant, indirect costs (e.g., project management, office work), and contingency costs. The direct CO_2 cycle capital cost estimate also accounts for CO_2 storage development costs. The grid integration cost was accounted for once for the entire CO_2-BES facility instead of once for each power cycle. (Section 2 of Appendix C contains more information on how we estimated the capital cost of the CO_2-BES facility.)

The annual cost of the CO_2-BES system was estimated as the sum of the annual cost of the indirect brine ORC and the annual cost of the direct CO_2 cycle. The indirect brine ORC annual cost estimates include insurance costs, field related operating costs, and non-field operating costs and the direct CO_2 cycle cost estimate includes costs for annual CO_2 storage in addition to these costs. (Section 3 of Appendix C contains more information on how we estimated the annual cost of the CO_2-BES facility.)

5.2.5 Case Study: Generating and Storing Electricity in Eastern Wyoming to Sell in Los Angeles

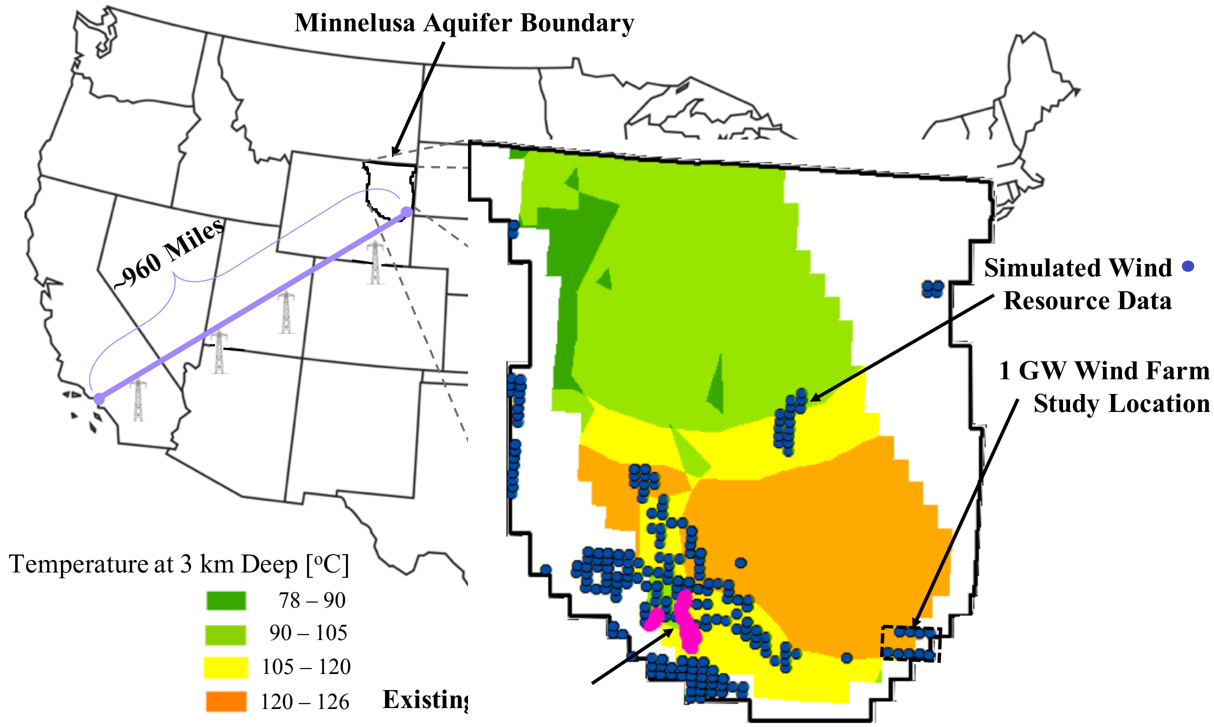

Figure 17. High Voltage Direct Current Transmission Line Connecting the Wind Farm and CO_2-Bulk Energy Storage Facility in Eastern Wyoming to Los Angeles, California. The simulated wind resource data shown in blue is from the National Renewable Energy Laboratory [182]; the location of existing wind turbines shown in pink is from the United States Geological Survey [183]; and the subsurface temperature at 3 km deep is from a combination of North American sedimentary basin, geothermal heat flux, and CO_2 storage datasets [49,157–163].

We chose the state of Wyoming as a case study because it has a relatively small population density and substantial wind resources that are currently undeveloped (Figure 17). Within the state of Wyoming, we chose to use the Minnelusa Aquifer in the Power River Basin as the sedimentary basin case study because the subsurface parameters (e.g., depth, thickness, permeability, temperature) are favorable for CO_2-BES operation and the mean technically accessible CO_2 storage capacity (5,100 $MtCO_2$ [162]) far exceeds the needed capacity for a single CO_2-BES facility (~220 $MtCO_2$). We used Los Angeles, California as the major load center case study because (1) it is densely populated, (2) California has progressive renewable energy generation targets, and (3) an HVDC transmission line would be used to electrically connect it to Eastern Wyoming because the two locations are ~960 miles apart.

5.2.6 Data

5.2.6.1 Wind Farm Electricity Generation Data and Electricity Price Data

We selected an area, above a portion of the Minnelusa Aquifer that has a high geothermal temperature gradient, for a hypothetical but realistic 1GW wind farm (Figure 17). We used simulated 2012 power generation of a wind farm in this area as the baseline annual generation because that was the most recent year of data available from the Wind Integration National Dataset [184]. As a result, we also used 2012 wholesale electricity prices (from the Vincent_2_N101 node within the system managed by the CAISO) as baseline electricity prices.

To investigate the impact that high electricity prices may have on our results we also used a 2005 price dataset from the LA1 congestion zone within the Los Angeles Water and Power system as part of our sensitivity analysis because the prices of electricity were higher on average in 2005 than in 2012 as a result of higher natural gas prices. For consistency, we also included simulated 2005 wind generation data using the Western Wind Dataset in our sensitivity analysis [182].

Lastly, we also included projected future electricity prices in California (2024 prices from the Southern California Edison region of the electricity system managed by the CAISO) in our sensitivity analysis that were created in prior work [185]. In this prior study, 2024 prices were projected under a variety of scenarios. A primary purpose of the study was to evaluate the change in electricity production costs as a result of the 1,325 MW energy storage mandate in California. As a result, one factor that was varied in the scenarios was the inclusion of this energy storage capacity. Second, the renewable energy penetration was set to 33% or 40% because the renewable portfolio standard in California is 50% by 2030 and it is expected that 33% to 40% renewable energy penetration should exist by 2024. Lastly, the wholesale electricity bid floor was set to \$0/MWh, -\$150/MWh, and -\$300/MWh because the CAISO avoids overgeneration via negative prices. We used the price datasets resulting from all twelve combination of these factors within our sensitivity analysis. Because simulated 2024 wind data is unavailable, we followed prior work and approximated 2024 wind data by adjusting the 2005 wind data so the days of the week matched that of the 2024 year [186]. As a result, our 2024 wind dataset is the same as the 2005 wind generation data, except shifted by two days so the 2005 weekends and weekdays align with the corresponding days of the week in 2024.

The wind generation data from the Western Wind Dataset and the Wind Integration National Dataset and are publicly available in 10-minute and 5-minute resolution, respectively, and we used the average of the data points in each hour as the hourly generation from the wind farm. Of the three wind condition datasets that we used in this study, the 1 GW generated the most electricity on average in 2012.

Section 4 of Appendix C shows the distributions of all electricity price and wind condition datasets that we used in this study and Table 13 shows the summaries of these datasets.

Table 13: Summaries of Wind Condition and Electricity Price Datasets.

	Year	Mean	Standard Deviation
Wind Conditions [MWh]	**2005**	326.19	329.82
	2012	423.86	337.73
	2024	325.35	329.59
Electricity Prices [$/MWh]	**2005**	55.90	29.46
	2012	29.72	11.59
	2024[a]: 33%, $0/MWh	43.77	52.65
	2024[a]: 33%, -$150/MWh	40.98	47.24
	2024[a]: 33%, -$300/MWh	38.64	58.70
	2024[a]: 33%, 0/MWh, NS	44.56	75.18
	2024[a]: 33%, -$150/MWh, NS	41.09	74.01
	2024[a]: 33%, -$300/MWh, NS	37.74	85.56
	2024[a]: 40%, $0/MWh	39.75	63.16
	2024[a]: 40%, -$150/MWh	23.35	82.80
	2024[a]: 40%, -$300/MWh	7.36	121.10
	2024[a]: 40%, $0/MWh, NS	41.34	95.16
	2024[a]: 40%, -$150/MWh, NS	22.21	112.97
	2024[a]: 40%, -$300/MWh, NS	3.15	144.23

[a]the penetration of variable renewable energy technologies, the bid floor, and NS is no energy storage mandate

5.2.6.2 Minnelusa Aquifer Data

The most likely subsurface parameters of the Minnelusa Aquifer are a permeability of 10^{-13} m^2, porosity of 16%, thickness of 120 m, and a depth of 2.74 km [162]. As a result, we assumed the CO_2-BES facility was operating within a homogeneous sedimentary basin geothermal resource with those characteristics. We assumed the geothermal temperature gradient was 42 ^{o}C/km, which we based off a combination of North American sedimentary basin, geothermal heat flux, and CO_2 storage datasets [49,157–163].

5.2.6.3 High Voltage Direct Current Transmission Data

We investigated HVDC transmission capacities scenarios from 100 MW (10% of wind farm capacity) to 1,000 MW (100% of wind farm capacity) in increments of 100 MW and assumed the HVDC transmission losses from Eastern Wyoming to Los Angeles were 6% [136]. We obtained HVDC transmission infrastructure cost estimates from prior work [167] and adjusted this cost to 2012 dollars by multiplying by the appropriate producer price index adjustment factor for Electric Bulk Power Transmission and Control Industry (Bureau of Labor Statistics Series ID PCU221121221121) [175].

5.3 Results

The degree to which CO_2-BES can result in an increase in the optimal HDVC transmission capacity depends on the effect that CO_2-BES has on the utilization of wind generation and on the utilization of the HVDC transmission capacity. Since these effects are contingent on how the CO_2-BES facility is operated, which is in turn influenced by the physical and economic performance of the CO_2-BES facility, we first present the estimated costs of the CO_2-BES facility (Section 5.3.1), the results of the performance of the CO_2-BES facility (Section 5.3.2), and the optimal modes of operation of the CO_2-BES facility (Section 5.3.3). Then we present the effect that CO_2-BES had on the utilization of wind generation and HVDC utilization (Section 5.3.4) and the sources of energy that contribute to the electricity sales (Section 5.3.5) before presenting the effect that CO_2-BES has on the optimal HVDC transmission capacity (Section 5.3.6) and the break-even CO_2 prices (Section 5.3.7). The effect of geothermal heat depletion is presented throughout these subsections.

5.3.1 Estimated Costs of the CO_2-BES Facility

The capital cost to construct the CO_2-BES facility was estimated to be $1.12B with an additional annual operating and maintenance cost of $53.4M (both estimated costs are in 2012 U.S. dollars). With the 11% CRF over the simulated 30-year lifetime of the facility, the total annualized cost was $176M/yr.

The three largest components of the capital costs were: (a) the construction of the power plants, (b) the drilling and equipping the wells, and (c) the construction of the pipelines that are required to transport the brine and the CO_2 between the wellheads and the power plants. These components accounted for 82% of the total capital cost (see Figure 51 of Appendix C for more details on the estimated costs). The components of the indirect brine power cycle were about 1.8x more costly than the components of the direct CO_2 cycle ($696M vs. $387M) because the costs scale with the electricity-generation capacity (Figure 18).

5.3.2 Performance of the CO_2-BES Facility

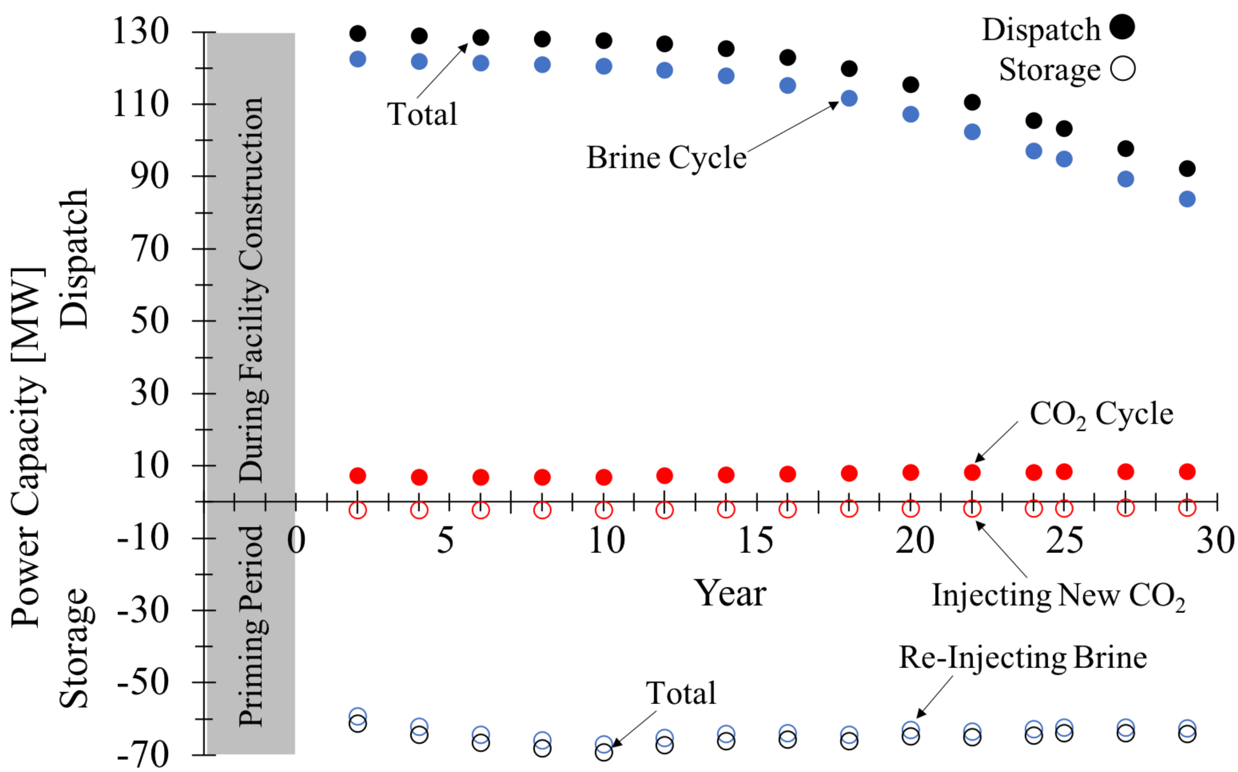

Figure 18: Performance of the CO_2-BES Facility in Our Case Study. The facility is operated with a 12-hour charge, 12-hour discharge cycle that is repeated continuously for a lifetime of 30 years.

Over the first ten years of operation, our results indicate that the design of the CO_2-BES facility that we implemented in the Minnelusa Aquifer could have a power storage capacity of ~60 MW to ~70 MW and a power dispatch capacity of up to ~130 MW (Figure 18). As such, the round-trip efficiency of the CO_2-BES facility was between 184% (in Year 10) and 212% (in Year 2) (127.7 MW/69.1 MW and 129.8 MW/61.2 MW, respectively). The round-trip efficiency was greater than 100% because the geothermal heat flux adds energy to the system, which can be extracted and dispatched as electricity. The round-trip efficiency decreased over the first decade of operation because of the increase power storage capacity due to the increase the overpressure in the subsurface that resulted from the injection of new CO_2. Over the remaining twenty years of the lifetime of the facility, the round-trip efficiency of the CO_2-BES facility decreased largely because the heat in the reservoir was depleted at a faster rate than it was replenished by the geothermal heat flux. This heat depletion decreased the power dispatch capacity, yet even after 30 years of operation more electricity can be generated than was stored: the round-trip efficiency was still ~144% (92.3 MW/64.1 MW).

5.3.3 Optimal Modes of CO_2-BES Operation

As Figure 19 shows, it was optimal to operate the CO_2-BES facility in five distinct combinations of energy storage and electricity generation, depending on the degree to which transmission was constrained:

1. Geothermal Power Plant – the facility was generating more electricity than the energy that it was simultaneously storing.
2. Net Energy Storage – the facility was storing more energy than it was simultaneously generating as electricity.
3. Energy Storage Only – the facility was only storing energy.
4. Electricity Generation Only –the facility was only generating and dispatching electricity.
5. Idle –the facility was neither storing energy nor generating electricity.

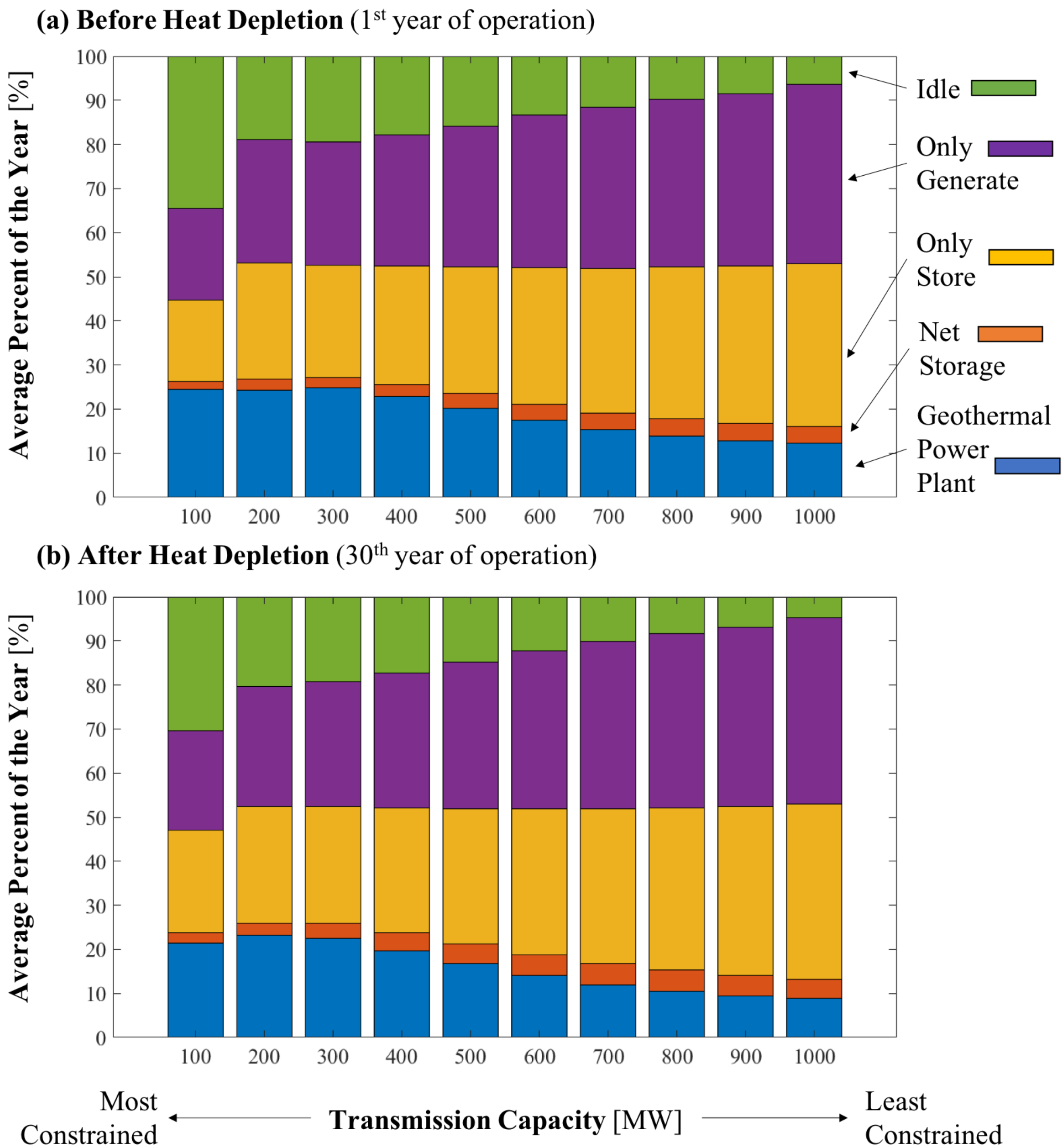

Figure 19: Optimal Modes of Operation of the CO_2-BES Facility (a) Before Geothermal Heat Depletion (b) After 30 Years of Geothermal Heat Depletion

Before the geothermal heat was depleted (Figure 19(a)), the CO_2-BES facility only stored energy 18.4% of the year and only generated electricity 20.8% of the year in the most transmission-constrained scenario. But in the least transmission-constrained scenario, the percent of time in these modes increased to 36.9% (only storage) and 40.6% (only generation). In contrast, the CO_2-BES facility was operated as a geothermal power plant 24.0% of the year when transmission was most constrained, and about half that amount (12.4% of the year) when transmission was least constrained.

After 30 years of heat depletion (Figure 19(b)), the concomitant decrease in the use of the CO_2-BES facility as a geothermal power plant (by 3% and by 4% of the year, in the most- and least-transmission constrained scenarios, respectively), was offset by an increase in the amount of the year spent as only an electricity generation facility and only as an energy storage facility. When transmission was most constrained, the CO_2-BES facility was only an electricity generating facility 22.5% of the year and was only an energy storage facility 23.4% of the year, which is respectively 2% more and 5% more of the year than before heat depletion. In contrast, in the scenario where transmission was least constrained, there was an increase by 2% of the year of operation as only an electricity generation facility (to 42.2% of the year) and by 3% of the year as only an energy storage facility (to 39.8% of the year).

The displacement of the amount of time spent as a geothermal power plant by the amount of time spent as an energy storage facility, in scenarios where transmission is progressively less constrained, occurred in part because the power output capacity of the CO_2-BES facility was approximately an order of magnitude lower than the electricity generation capacity of the wind farm (i.e., 1 GW vs. ~130 MW before heat depletion and ~90 MW after 30 years of heat depletion, see Figure 18). That is, the maximum amount of electricity that the CO_2-BES facility could generate as a geothermal power plant was a larger percentage of the transmission capacity in the most transmission-constrained scenario than it was in the least transmission-constrained scenario. As such, it was optimal to increase the amount of wind-generated electricity that was time shifted and decrease the amount of geothermal-generated electricity that was dispatched when transmission was least constrained.

Overall, the results in Figure 19 show that CO_2-BES has a capability that is unique to energy storage technologies, namely the capacity to extract geothermal heat and dispatch it as electricity. Operating the CO_2-BES facility as a geothermal power plant was optimal in non-trivial amounts of the year across all of the scenarios for transmission capacities that we investigated. As a consequence, the role that CO_2-BES can have in transmission-constrained systems partly reflects the flexibility of the technology to be used as a geothermal power plant or as an energy storage facility.

5.3.4 Effect of CO_2-BES on the Utilization of Wind Generation and HVDC Transmission Capacity

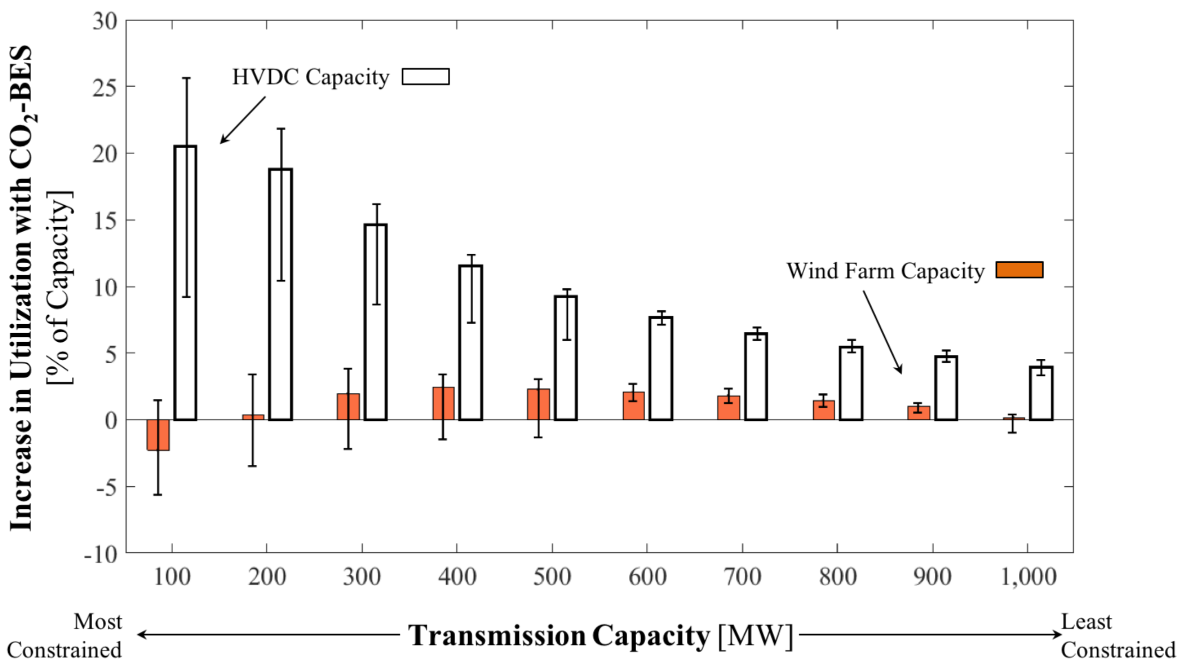

Figure 20: Average Increase in the Utilization of HVDC Transmission Capacity and in the Utilization of Wind Farm Capacity Due to the Use of CO_2-BES. The error bars show the maximum and minimum increase across all of the 42 combinations of electricity prices and wind conditions that we investigated.

Across all of the combinations of electricity prices and wind conditions that we investigated, the use of CO_2-BES in the Minnelusa Aquifer resulted in more of an increase in the utilization of the transmission capacity than in the increase in the utilization of the 1 GW wind farm capacity. Figure 20 shows that this result was consistent across all of the transmission capacities that we investigated. For example, in the most transmission-constrained scenario that we investigated (100 MW HVDC line), the utilization of the wind farm capacity decreased by an average of 2.3% and the utilization of the HVDC transmission capacity increased by 20.5% when CO_2-BES was implemented. As the transmission capacity constraint is relaxed, our results suggest that the effect that CO_2-BES has on the utilization of the HVDC transmission capacity decreases exponentially to 3.9% at the least constrained scenario we investigated (1,000 MW HVDC line), and the effect that CO_2-BES has on the utilization of wind capacity increases to 2.4% (400 MW HVDC line) before decreasing to 0.2% in the least constrained scenario. The reasons for these differing trends are twofold. First, even with transmission losses in the line over the ~960 miles between Eastern Wyoming and Los Angeles, it could be optimal to purchase electricity from Los Angeles when it was inexpensive, use the CO_2-BES facility to store that energy in the subsurface under Eastern Wyoming, and later dispatch electricity and sell it back to Los Angeles when the electricity price was high. This arbitrage of electricity prices resulted in an increase in the utilization of the transmission capacity but it did not directly affect the utilization of the wind farm capacity. Second, the geothermal heat flux provided energy that made it possible to directly dispatch electricity that was generated from the geothermal resource while simultaneously storing energy in the subsurface. The additional energy from the geothermal heat flux also resulted in an increase in the utilization of the transmission capacity. In fact, these two characteristics of CO_2-BES (price arbitrage and dispatching geothermal-generated electricity) could cannibalize the utilization of the wind farm capacity, especially when the transmission capacity was constrained. This displacement of wind-generated electricity with geothermal-generated electricity occurred because revenue could be realized from the sale of geothermal-generated electricity, regardless of whether or not the wind farm was generating electricity. As a result, when CO_2-BES was used in the most transmission-constrained scenario: (1) there was a decrease in the utilization of the wind farm capacity; and (2) the difference was greatest between the change in utilization of transmission capacity and the change in utilization of the wind farm.

5.3.5 Sources of Energy That Contribute to Electricity Sales

The average revenue from the 1 GW wind farm ranged from $26.7M (most-transmission constrained) to $121.2M (least transmission constrained). These amounts of revenue increased to $39.9M and $148.7M, respectively, when CO_2-BES was implemented, but the depletion of geothermal heat in the reservoir after 30 years of operation resulted in decreased revenue to $39.1M (most-transmission constrained, decrease of 0.97%) to $140.1M (least transmission constrained, decrease of 0.94%), depending on the degree to which the transmission capacity was constrained.

Wind-generated electricity accounted for the majority of the electricity sales across all of the transmission capacity scenarios that we investigated, with 69.3% to 89.6% of the total energy sold as electricity in the most- and least-transmission constrained scenarios, respectively, before geothermal heat depletion (Figure 21(a)), which increased to 83.9% to 94.6% of the energy sold in the most- and least-transmission constrained scenarios, respectively, after 30 years of geothermal heat depletion (Figure 21(b)). The dispatch of geothermal-generated electricity and energy that was previously stored for price arbitrage accounted for the rest of energy sold as electricity (at most 27.8% and 3.0%, respectively, in the most transmission-constrained scenario, before the geothermal heat was depleted).

The dominance of electricity sales by wind-generated electricity is also due to the small capacity of the CO_2-BES facility relative to the capacity of the wind farm. Since geothermal heat fluxes are constant, unlike wind resources, it is likely that a larger capacity design of the CO_2-BES facility, or multiple CO_2-BES facilities, would have had a greater percentage of the electricity sales from the dispatch of geothermal-generated electricity.

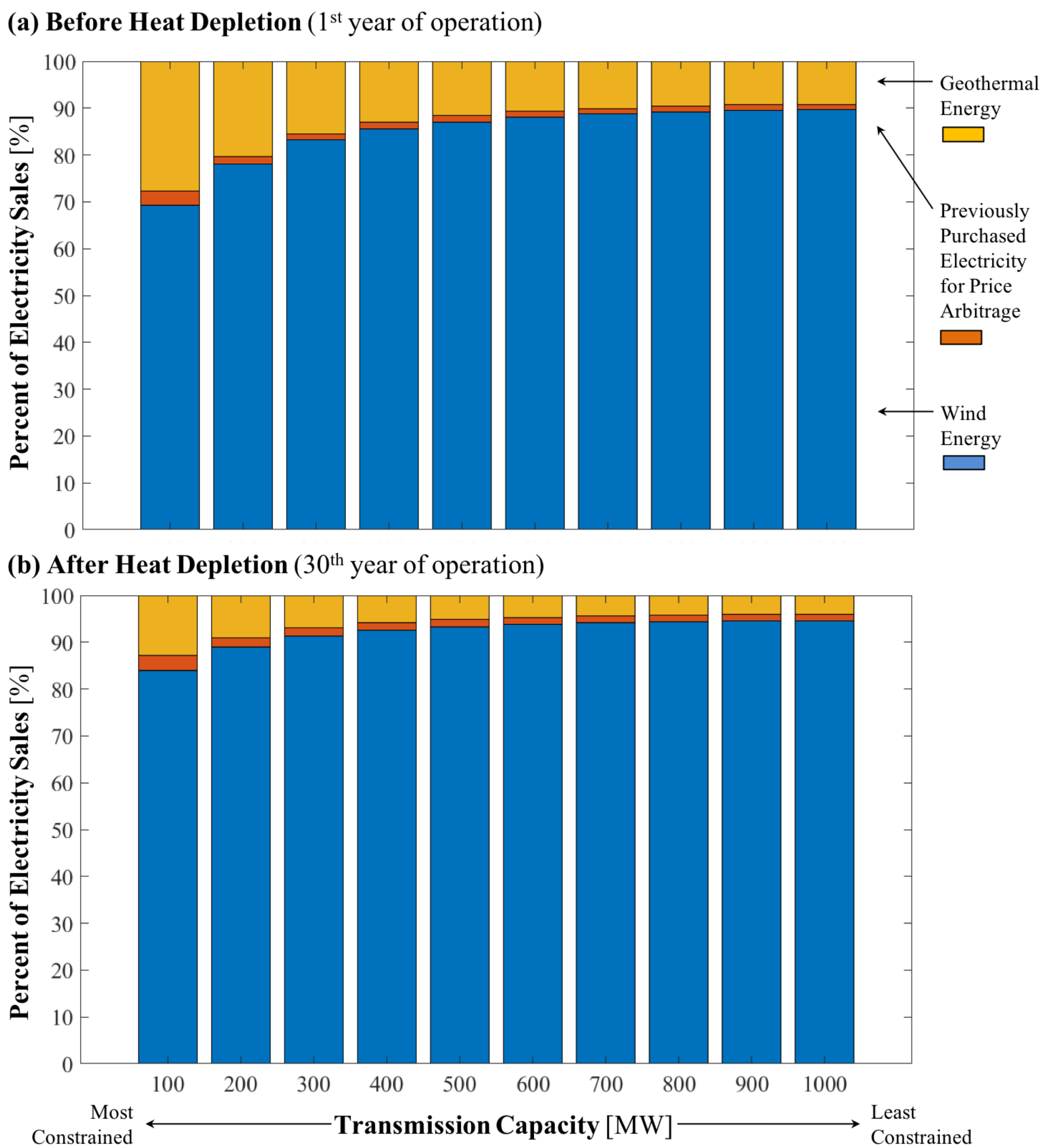

Figure 21: Sources of Energy Sales from the Combination of CO_2-BES and the Wind Farm (a) Before Geothermal Heat was Depleted and (b) After the Geothermal Heat Was Depleted.

5.3.6 Effect of CO_2-BES on the Optimal HVDC Transmission Capacity

Without CO_2-BES, the results in Table 14 show that the profit-maximizing capacity of the transmission line ranged from 300 MW to 800 MW, with 500 MW being the most frequent optimal capacity.[1] In addition, the optimal capacity of the transmission line without CO_2-BES was the same for a given wind condition across all of the variations in the parameters for the year 2024. That is, the uncertainty in major characteristics of the economics and regulation of the future of the electricity system that is managed by the CAISO had no effect on the optimal transmission capacity, holding wind conditions constant. With CO_2-BES, the range of optimal transmission capacities decreased to be between 400 MW and 800 MW, regardless of the degree of geothermal heat depletion. This smaller range of optimal transmission capacities occurred because it was never optimal to use a 300 MW transmission line with CO_2-BES. Further, in addition to being less spread out, the distribution of optimal transmission capacities with CO_2-BES became more bi-model, and was perfectly symmetric with equal density at 500 MW and 700 MW before the geothermal heat was depleted.

Table 14: Profit-Maximizing HVDC Transmission Capacity [MW]. The entries with CO_2-BES indicate the change from the optimal capacity without CO_2-BES.

Electricity Prices	**Wind Conditions** 2005			2012[a]			2024		
	w/o CO_2-BES	Δ w/ CO_2-BES Heat Depletion: None	Most	w/o CO_2-BES	Δ w/ CO_2-BES Heat Depletion: None	Most	w/o CO_2-BES	Δ w/ CO_2-BES Heat Depletion: None	Most
2005[b]	700	+0	+0	800	+0	+0	700	+0	+0
2012	300	+100	+100	500	+100	+0	300	+100	+100
2024[c]	500	+100	+0	700	+100	+0	500	+0	+0
2024[d]	500	+0	+0	700	+0	+0	500	+0	+0

[a]2012 had the windiest conditions, on average, of the three years that we considered.
[b]2005 had the highest electricity prices, on average, of the three years that we considered.
[c]33% renewable penetration; no energy storage mandate; $0/MWh bid floor.
[d]All of the eleven other combinations.

[1] Treating the variations in characteristics in 2024 that have different results as two separate conditions.

In five of the combinations of electricity prices and wind conditions, there was an increase in the optimal transmission capacity with CO_2-BES, which was more prevalent before the geothermal heat was depleted than after the geothermal heat was depleted. With CO_2-BES, it was never optimal to invest in more transmission capacity when the electricity prices were the highest (2005). But when electricity prices were lowest (2012), the only combination where CO_2-BES did not result in an increase in transmission capacity occurred after the geothermal heat was depleted with the windiest conditions (2012).

The uncertainty in the future of the electricity system managed by the CAISO had a minor effect on the optimal transmission capacity when CO_2-BES was implemented. That is, it was optimal to invest in more transmission capacity in only one of the twelve combinations of projected electricity price conditions for the year 2024—which was before the geothermal heat was depleted in two of the three wind conditions.

Holding everything else constant, revenue generally increased with higher electricity prices and with higher amounts of wind-generated electricity because more revenue can be obtained if prices are higher or if it is windy. For this reason, the optimal capacities of the transmission line were generally the largest in the windiest conditions (in 2012) and when the electricity prices were the highest (in 2005). As a result, if electricity prices are expected to be higher in the future, or conditions are expected to be consistently windier, larger capacity transmission lines should be installed.

5.3.7 Break-Even CO_2 Prices

Although the use of the CO_2-BES facility increased revenue, the CO_2-BES facility was costly and the total profit decreased when CO_2-BES was implemented—even with the additional revenue from the extra electricity sales that CO_2-BES enabled. As a result, the breakeven CO_2 prices that we calculated were all positive (Table 15).

Table 15: Break-Even CO_2 Prices to Equate Profit from the Wind Farm with Additional Revenue from Geologic CO_2 Storage using CO_2-BES [$/t$CO_2$].

	Only CO_2 Storage	**CO_2 Storage and Revenue from Electricity Sales**	
		Before Heat Depletion	After Heat Depletion
Break-Even CO_2 Price	$11.30		
Minimum		$8.35	$8.83
25th Percentile		$9.29	$9.77
Median		$9.75	$10.29
75th Percentile		$9.90	$10.41
Maximum		$10.43	$10.77

Table 15 shows that the breakeven CO_2 price for storing CO_2 with the CO_2-BES facility was $11.30/t$CO_2$, and that the distribution of revenue from the electricity sales reduced the breakeven CO_2 price to between $8.35/t$CO_2$ and $10.43/t$CO_2$—which depends on the wind conditions, the electricity prices, and the degree to which the geothermal heat was depleted in the reservoir—with a median of $9.75/t$CO_2$. After 30 years of geothermal heat depletion, the break-even price of CO_2 increased by about $0.50/t$CO_2$ throughout the distribution, such that the median break-even CO_2 price was $10.29/t$CO_2$ and the maximum break-even CO_2 price was $10.77/t$CO_2$. The entire distributions for the break-even CO_2 prices with the revenue from electricity sales and from geologic CO_2 storage were below the break-even CO_2 price for geologic CO_2 storage alone.

5.4 Discussion and Conclusions

Rapidly reducing CO_2 emissions to mitigate human-induced climate change is one of the most pressing challenges facing the electricity system. Technologies like CO_2-BES could play an essential role in that effort because CO_2-BES can indirectly reduce CO_2 emissions by addressing challenges that the variability of wind or solar energy resources pose to the electricity system *while* directly reducing CO_2 emissions by permanently storing them in sedimentary basin geothermal resources.

One of the challenges to using solar and wind energy technologies is that (a) wind and solar resources may not be located near major demand centers and (b) HVDC transmission infrastructure, which is used to transport electricity long distances, is expensive. Towards this end, in this study, we investigated the degree to which CO_2-BES use could result in an increase in the profit-maximizing HVDC transmission capacity that connected a wind farm in Eastern Wyoming to the electricity market in Los Angeles, California. To do this, we simulated a CO_2-BES facility continuously cycling between storing energy for 12 hours and dispatching electricity for 12 hours over 30 years using an integrated process-level model that we previously developed (Chapter Three). We used those process-level results to parameterize a mixed integer-linear optimization program that we used to maximize the revenue of the CO_2-BES facility operating with the wind farm. Using the optimization results we were able to determine the profit-maximizing HVDC transmission capacity. As a sensitivity analysis we executed our study framework over a range of past and projected future electricity prices, wind conditions, and geothermal heat depletion scenarios.

Our prior work shows that a CO_2-BES facility has flexibility in how it is operated as long as electricity is dispatched and stored for approximately equal durations of time [187] and the results from the mixed integer-linear optimization model generally suggest that storing and dispatching electricity for equal amounts of time over the year is optimal. Despite this coincidence, the simulated cycle of continuously alternating between storing electricity for 12 hours and dispatching electricity for 12 hours was not optimal in any combination of parameters we investigated and it is possible, although unlikely, that the optimal cycle could deplete reservoir overpressure, depending on the magnitude and timing of the optimal charging and discharging periods throughout the year. Because it was outside the scope of this study to iterate between the integral model of the CO_2-BES facility and the mixed integer-linear optimization model until both converged to the same operational cycle, the majority of our findings are contingent on the assumption that the optimal CO_2-BES operation cycle is feasible:

1. *While continuously storing CO_2 over its entire lifetime, a CO_2-BES facility will likely also be able to dispatch more electricity than was previously stored if it is operating within a sedimentary basin*

that is also a geothermal resource (e.g., the Minnelusa Aquifer). Over the 30 years that we simulated with the integrated process-level model, ~220 $MtCO_2$ were permanently sequestered in the subsurface and the round-trip efficiency of the CO_2-BES facility always remained above 100% (ranging from 212% initially to 144% after 30 years of operation) because of the geothermal energy that was input to the system. The round-trip efficiency decreased with time primarily because geothermal heat was extracted at a faster rate than it was recharged by the geothermal heat flux. Had we simulated the optimal operational cycle within the process-level model, the total amount of sequestered CO_2 would remain unchanged and it is possible that the round-trip efficiency would remain more constant because idle periods, which we did not simulate, could reduce the depletion of geothermal heat over a 30 year period.

2. *The optimal dispatch of CO_2-BES included operating as a geothermal power plant and as an energy storage facility at different times throughout the year.* Using a CO_2-BES facility to extract geothermal energy and dispatch it as electricity can be valuable because the revenue from selling geothermal energy can be realized regardless of whether or not the wind farm is generating electricity. As a consequence, across all HVDC transmission capacity scenarios that we investigated within the mixed-integer linear optimization model, the CO_2-BES facility was only operated as an energy storage facility 39.2% (most transmission-constrained scenario) to 77.5% (least transmission-constrained scenario) of the year on average and was operated as a geothermal power plant 12.4% (least transmission-constrained scenario) to 24% (most transmission-constrained scenario) of the year on average. Although selling electricity generated from geothermal energy can result in higher revenue compared to selling electricity generated from wind energy, the CO_2-BES facility was operated as a geothermal power plant for a smaller percentage of the year in the most transmission-constrained scenario than the least transmission-constrained scenario in part because the capacity of the CO_2-BES facility that we modeled was approximately an order of magnitude lower than the capacity of the wind farm. As a result, the maximum amount

of electricity that the CO_2-BES facility could generate as a geothermal power plant was a small percentage of the transmission capacity when the HVDC transmission was least constrained and it was optimal to time-shift wind instead.

3. *In part due to the unique ability to transition between operating as a geothermal power plant and as an energy storage facility, CO_2-BES could increase the profit-maximizing HVDC transmission capacity, even when operating in a heat depleted geothermal resource.* Across all electricity price datasets, wind conditions, and geothermal heat depletion scenarios that we investigated as our sensitivity analysis, CO_2-BES consistently increased revenue compared to the wind farm operating by itself. A combination of factors need to be considered for sizing transmission lines, and when operating in a geothermal resource with no heat depletion, the revenue increased enough in five of the electricity price and wind condition combinations that the profit-maximizing HVDC transmission capacity increased compared to the wind farm operating alone. When operating with maximum (i.e., 30 years) heat depletion, the CO_2-BES facility was generally operated as a geothermal power plant less often and as an energy storage facility more often, and there was less increase in revenue. Despite this result, CO_2-BES still increased the optimal HVDC transmission capacity in two of the electricity price and wind condition combinations that we investigated. While it was outside the scope of this study to investigate multiple locations, if the level of geothermal heat depletion is used as a proxy for temperature of geothermal resource, our results also suggest that a CO_2-BES facility could still increase the profit-maximizing HVDC transmission capacity when operating in colder geothermal resources than Eastern Wyoming.

Despite the potential advantages of adding a CO_2-BES facility to a wind farm, the total profit without CO_2-BES was greater than the total profit with CO_2-BES because the annualized cost of the CO_2-BES facility exceeded the additional revenue from electricity sales. As a result, for CO_2-BES to have value to transmission constrained electricity systems (i.e., increase profit), the design of the system itself must be modified and optimized, or operators could choose to operate CO_2-BES slightly differently to receive more revenue for providing additional services. For example, the direct CO_2 cycle contributed ~10% or less of the total power output capacity over the 30 years that we simulated, but accounted for ~30% of the total annualized system cost. As a result, profits may increase by not constructing the direct CO_2 cycle power plant and instead, (1) relying solely the indirect brine ORC power plant for generating electricity and (2) using the CO_2 injection to increase the pressure in the subsurface and the power storage capacity of the facility. At the same time, it may also be profitable to construct the direct CO_2 cycle and operate it separately from the indirect brine ORC cycle. In this study, we assumed both power cycles were operating simultaneously, but it is technically feasible to operate them isolated from one another as long as the overpressure in the subsurface does not exceed 10 MPa and also remains high enough to prevent the brine from flashing in the production well. It is likely possible, for example, to increase revenue by using the indirect brine ORC cycle to increase the profit-maximizing HVDC transmission capacity while using the direct CO_2 cycle to provide high-value ancillary services.

In addition to surface power cycle design modifications and electricity market participation decisions, there are also many aspects of the subsurface well design that could be optimized to maximize the value that CO_2-BES has to transmission constrained electricity systems, which would further increase the potential profitability of CO_2-BES. For example, the downhole CO_2 production wells could be moved from the bottom to the top of the sedimentary basin. This would (1) decrease the length of the priming period because CO_2 is buoyant so the mass fraction of CO_2 in the production well would reach 90% in less than three years, and (2) decrease the size of the CO_2 plume because less CO_2 would migrate beyond the hydraulic mound. As a result of the shorter priming period, revenue over the lifetime of the facility would increase because the power output capacity could be maintained at ~130 MW for a longer time. Further, the smaller CO_2 plume size would decrease the annual operating cost of the CO_2-BES facility by decreasing the Area of Review in the CO_2 storage monitoring process, which would in turn increase profit.

Because CO_2-BES can provide time-shifting energy storage services (i.e., as an energy storage facility), CO_2 storage services (as part of the CCS process), and dispatchable "baseload" power (i.e., as a geothermal power plant), it is likely that CO_2-BES could provide systems-level value to the overall effort to decarbonize the electricity system. In this sense, it is just as pressing for policy-makers to enable technologies like CO_2-BES through policy as it is for engineers to optimize the CO_2-BES system. For example, policies like a Renewable Energy Production Tax Credit, pricing Renewable Energy Certificates, instituting renewable energy portfolio standards, or a price on CO_2 could all increase revenue for CO_2-BES operators even if the system design was not optimized. Such policy would be beneficial to CO_2-BES operators because it would likely be more certain than the other variables that influence the value that CO_2-BES has in transmission constrained electricity systems (i.e., electricity prices, wind conditions, rate of geothermal heat depletion).

In this study, we focused on a potential policy that could price CO_2 and determined the minimum rate that operators would need to be compensated for storing CO_2 for CO_2-BES use to be as profitable as the wind farm operating alone (the breakeven CO_2 price). The breakeven CO_2 price for storing CO_2 was \$11.3/tCO_2 and, depending on the electricity prices and wind conditions, the breakeven CO_2 price for storing CO_2 and selling electricity decreased to between \$8.35/tCO_2 and \$10.43/tCO_2 (median of \$9.75/tCO_2). Even though these breakeven CO_2 prices represent the ceiling because the CO_2-BES system we modeled was not optimized, they are already much lower than estimates of the social cost of CO_2 that can range up to hundreds of dollars per ton of CO_2 [188]. Further, these prices are also comparable, if not below, current and historical CO_2 prices in the United States (ranging from ~\$12/tCO_2 to ~\$15/tCO_2 since 2013 in California [114] and from ~\$2/tCO_2 to ~\$6.50/tCO_2 since 2008 in the Regional Greenhouse Gas Initiative [189]), and well below the 45Q Federal tax incentive of \$50/tCO_2. As a result, if operators could receive revenue from storing CO_2, it would likely be at a higher rate than the breakeven CO_2 prices that we estimated and, in that situation, CO_2-BES operation would be profitable regardless if it increased the profit-maximizing HVDC transmission capacity.

Chapter 6. Conclusion

6.1 Introduction

The electricity system must quickly transition from being the one of the largest sources of carbon dioxide (CO_2) emissions in the United States to being a net negative source of CO_2 to meet climate change mitigation targets [5–7]. To successfully meet this challenge, multiple technologies and processes are required, one of which is geologic CO_2 storage.

Geologic CO_2 storage is part of a CO_2 capture and storage (CCS) process where CO_2 that would otherwise be emitted to the atmosphere is instead captured and injected underground into sedimentary basins [11]. Climate change mitigation pathways that achieve policy goals rely heavily on processes that include CCS because of the potential that they have to obtaining negative CO_2 emissions [2]. Despite this need, the economic viability of CCS may constrain its implementation and as a result, current work within the CCS field seeks to develop approaches that use captured CO_2 to provide a commodity or service in an effort to create a business case for CCS.

For example, much research has investigated using geologically stored CO_2 as a heat extraction fluid for geothermal power generation [16–19,45,46]. In this CO_2 capture, *utilization,* and storage (CCUS) process, a portion of the CO_2 that is injected underground is intentionally produced to the surface and the heat and pressure energy within the CO_2 is then used to generate electricity in a CO_2-geothermal power plant. This electricity could be sold, thus creating revenue and potentially profit.

In addition to increasing the economic viability of CCS, using geologically stored CO_2 as a heat extraction fluid has thermophysical advantages over conventional geothermal heat extraction fluids (i.e., brine) that enable more efficient heat extraction from geothermal resources. For example, CO_2 has a higher mobility (ratio of density to kinematic viscosity) than brine, which enables larger subsurface flowrates and thus more heat extraction. Further, the density of CO_2 is more sensitive to changes in temperature and pressure than brine, which reduces the pumping power required to circulate CO_2 compared to brine. As a result of these advantages, using CO_2 as a heat extraction fluid may expand the portion of the subsurface that can be used for geothermal power production to include sedimentary basins. These naturally porous and permeable formations underlie approximately half of North America, but have not conventionally been used for geothermal power production primarily because of their lower temperatures [43,44,50]. In contrast, the conventional geologic formation used for geothermal power production (i.e., naturally faulted and fractured formations that contain brine at high temperatures) are not ubiquitous and much of the known and economically-viable resources have already been developed [20].

Expanding the economically-viable geothermal resource base could have substantial ramifications to the overall effort to decarbonize the electricity system because geothermal heat is a renewable, but not variable, source of energy that can be used to generate electricity without emitting CO_2. As a result, geothermal power plants can be dispatched to generate electricity when demanded and are included in least-cost electricity systems that reduce CO_2 emissions despite having higher costs than variable renewable energy technologies (i.e., wind turbines, solar photovoltaics) [15]. Wind and solar energy technologies can also generate electricity without emitting CO_2 and are included in least-cost electricity systems that reduce CO_2 emissions, but relying on these technologies to meet most or all of electricity demand is challenging in part because the availability of wind and sunlight fluctuates on sub-hourly to seasonal timescales.

In addition to geothermal power plants and processes that include CCS, energy storage approaches can also be used to reduce CO_2 emission from the electricity system [96]. For example, energy storage can be used to address some of the challenges that the variability of wind and sunlight pose to the electricity system by time-shifting electricity generated by variable energy technologies to when it is demanded. Recent work has investigated approaches to energy storage that couple geologic CO_2 storage and sedimentary basin geothermal resources [54,154].

The research presented in this dissertation expanded upon this concept by (1) deepening the understanding of the physical and economic performance of a CO_2-BES facility using a pressure-based, concentric ring well bulk energy storage (CRP-BES) design, (2) valuing the use of the CRP-BES system in multiple electricity system applications, and (3) comparing and contrasting the use of CO_2 vs brine as a medium for thermal energy storage. Each chapter of this dissertation is a stand-alone paper with study-specific conclusions, and these study-specific conclusions can be used to draw more general, holistic conclusions. This conclusion chapter presents these holistic conclusions (Section 6.2) and also provides a few directions for future research that is related to this dissertation (Section 6.3).

6.2 Holistic Conclusions Drawn from Looking Across All Dissertation Chapters

1. *Energy storage approaches that use geologically stored CO_2 and geothermal resources can provide value to the electricity system in multiple ways, in part because these systems have unique operational capabilities.* For example, the CRP-BES design can provide a service to the electricity system (i.e., reducing operational CO_2 emissions and water requirements) that has a greater value than the cost to operate the facility (Chapter Two). The system can also be used to increase the profit-maximizing high voltage, direct current (HVDC) transmission capacity in a transmission constrained electric power system (Chapter Five). Both of these outcomes are results, in part, of the unique operational capabilities of the CRP-BES design when compared to other approaches to energy storage (e.g., Pumped Hydro Energy Storage (PHES), Compressed Air Energy Storage (CAES)). For example, because the geothermal heat flux adds energy to the system the round-trip efficiency of the energy storage process (i.e., electricity generated divided by electricity stored) can be greater than 100%. In the CRP-BES system specifically, the energy from geothermal heat flux and the over-pressurization that the concentric rings create provide operators with more control over the durations of charging and discharging (Chapter Four). Further, because the CRP-BES system is at a fundamental level, two geothermal power plants that operate in unison, the system can operate to provide a continuous supply of electricity by operating as a geothermal power plant

in addition to operating to time-shift electricity generation (Chapter Five). Sedimentary basins also have massive fluid capacities which, in part, enables the CRP-BES system to time-shift electricity for up to weeks at a time and ultimately uniquely positions these subsurface resources to be used for seasonal energy storage (Chapter Three).

2. *It is important to consider the systems-level effects that a component may have on the electricity system during the process of designing and developing that component.* A future, decarbonized, electricity system will likely be comprised of a portfolio of technologies (e.g., geothermal power plants, CCS, energy storage) that operate synergistically with variable renewable energy technologies to meet demand. As a result, it is possible for a component to be included in this portfolio because it provides a specific service, even if it has a disadvantage from a process-level perspective compared to alternative components. For example, the operating cost of the CRP-BES system exceeded the operating costs of other energy storage approaches, but the Environmental Return on Bulk Energy Storage for the CRP-BES system was more often greater than one than it was for PHES and CAES (Chapter Two). Insight like this cannot be gained without including a systems-level consideration. Further, because processes that include geologic CO_2 storage are included in least-cost, decarbonized, electricity systems [149] it is possible for a subsurface thermal seasonal energy storage approach that uses pre-heated CO_2 to provide more systems-level benefits to decarbonizing the electricity system than a brine-based system, despite the thermophysical advantages of brine for thermal energy storage (Chapter Three). Considering the systems-level ramifications of new electricity system components can also verify that there is not a discrepancy between what is needed by the system and what the component can feasibly provide. For example, the charge and the discharge cycle can affect the longevity of the CRP-BES system: dispatching electricity for a duration of time that is longer than the duration of storage can create situations in which a CRP-BES facility can no longer operate (Chapter Four). Considering a systems-level application of the CRP-BES facility confirmed that this type of operation was not optimal (Chapter

Five). Further, this systems-level consideration can also illuminate the need for new types of electricity system components that do not fall into conventional taxonomies. For example, it was optimal to alternate between operating a CRP-BES system as a geothermal power plant and as an energy storage facility (Chapter Five). As such, there is likely a need within the overall decarbonization effort for components that neither qualify as a conventional power plant or as an energy storage facility.

3. *In addition to designing and developing CO_2-based electricity system components, policy is also needed to support and potentially enable these components.* Due to the pressing need to reduce CO_2 emissions, CO_2-based electricity system components should be developed and implemented. Despite this need and the fact that systems like a CRP-BES facility could have value to multiple electricity system applications (Chapter Two, Chapter Five), it is unlikely that these CO_2-based components will be implemented if they are not profitable. As a consequence, in addition to further developing these systems through optimization and engineering, policy is likely also needed to enable these electricity system components. For example, it is possible that a non-optimized CRP-BES facility could be profitable, regardless of the effect that the system had to increasing the utilization of electricity generated by variable renewable energy technologies, if a policy existed that compensated operators for storing CO_2 (Chapter Five). In addition to market based approaches (e.g., a CO_2 price), however, there are other ways in which policy can impact the technologies and processes that comprise the electricity system. For example, energy storage mandates have been instituted in many states (e.g., California, Massachusetts, New York) that require utility companies to procure energy storage capacity. While these policies force utility companies and system operators to gain needed experience with integrating and using energy storage technologies, mandate policies may not result in a more environmentally benign electricity system long-term. For example, it is possible that the implementation of energy storage could lead to an increase in system-wide water requirements and in system-wide CO_2 emissions (Chapter Two). Further, the

system-wide impacts of one approach to energy storage may be substantially different than another approach (Chapter Two). As a result, policy-makers should construct policy as precisely as possible to avoid unintended consequences.

6.3 Potential Directions for Future Research Related to This Dissertation

There are multiple knowledge gaps related to the research presented in this dissertation that future work could address. This section discusses some of these gaps starting with potential directions for future research pertaining specifically to CO_2-based energy storage (Section 6.3.1) because CO_2-based energy storage was the primary focus of this dissertation. A broader knowledge gap related to seasonal energy storage is also presented (Section 6.3.2).

6.3.1 Knowledge Gaps Pertaining to CO_2-Based Energy Storage

6.3.1.1 Optimize the CRP-BES System Design for a Specific Application

There are many aspects of the CRP-BES design that could be optimized to maximize profit from a specific application (e.g., electricity price arbitrage). For example, the downhole CO_2 production wells could be moved from the bottom to the top of the sedimentary basin. This would (1) decrease the length of the priming period because CO_2 is buoyant so the mass fraction of CO_2 in the production well would reach 90% in less than three years, and (2) decrease the size of the CO_2 plume because less CO_2 would migrate beyond the hydraulic mound. As a result of the shorter priming period, it is likely that revenue would increase because less geothermal heat would be depleted at the start of operation. Further, the smaller CO_2 plume size would decrease the annual operating cost facility by decreasing the Area of Review (AOR) in the CO_2 storage monitoring process, which would in turn increase profit.

Another aspect of the design that could be modified is the radii of concentric rings, which would both directly and indirectly effect the profit of the facility. For example, profit would be directly affected because decreasing the radii would decrease the amount of pipeline needed to transport brine and CO_2 to and from the wells, thus decreasing costs. Further, this modification would also decrease the volume of CO_2 that could be stored, which could also reduce costs by reducing the AOR but would also reduce potential revenue from CO_2 storage. Profit could be indirectly affected if modifying the radii of the wells substantially impacted the performance of the facility. For example, holding everything else constant, decreasing the radii of the wells would likely increase the overpressure, which would decrease the net power output capacity when the facility operates as geothermal power plant, thus decreasing revenue.

Part of this system design optimization process could also include incorporating heterogeneity into reservoir simulation of the sedimentary basin. All the simulations presented in this dissertation assumed homogeneous vertical and horizontal permeability and porosity in the subsurface, and there are many potential ramifications of relaxing this assumption. For example, fluids flowing through a heterogeneous reservoir will likely follow circuitous paths of high permeability and porosity (a.k.a. channeling or fingering). As a result, heterogeneity could influence the heat extraction rate of the CO_2 and brine by effecting the residence time of the fluids in the subsurface. Depending on the effect that heterogeneity has on the performance of the system, it is possible that many aspects of the CRP-BES design would need to be optimized.

Lastly, the CPR-BES system design may also need to be modified or optimized if future work demonstrates that the optimal charge and discharge cycle for a given application (e.g., electricity price arbitrage) would be infeasible from a process-level standpoint. For example, the optimal charge and discharge cycle in Chapter Five did not match the simulated cycle of storing electricity for 12 hours followed by dispatching electricity for 12 hours. It is possible that the optimal cycle could deplete reservoir overpressure, depending on the magnitude and timing of the optimal charging and discharging cycle throughout the year.

6.3.1.2 Develop a CO_2-Seasonal Energy Storage System

Future work could build upon the results presented in Chapter Three and develop an energy storage approach that uses geologically stored CO_2 and sedimentary basin geothermal resources to time shift electricity generation over seasonal timescales. Such an approach would likely be coupled with a source of thermal energy because storing energy in the subsurface as pressure may limit the length of time that energy can be stored or discharged if the increase the overpressure exceeds the caprock fracture pressure. In such an approach, thermal energy could be stored by pre-heating fluids prior to injection, using the subsurface as a thermal insulator, and later producing the heated fluids to the surface and using the heat to generate electricity. For example, during seasons when energy needs to be stored, thermal energy from a nuclear powerplant could be transferred to a fluid, instead of being used to generate electricity, and the heated fluid could be stored underground [62,63].

6.3.1.3 Determine the Value of the CRP-BES System in the Decarbonization Transition

Capacity expansion models are used to determine the least-cost portfolio of electricity system components that can meet a given objective (e.g., reducing CO_2 emissions). As such, these models are used to provide guidance on pathways for optimal investment in infrastructure over multi-decade periods. Because the CRP-BES system is one component that can provide three distinct services to the electricity system (i.e., continuous power generation, time-shift electricity generation, CO_2 storage), it is likely that a CRP-BES system could provide substantial value in terms of cost savings in the transition to a decarbonized electricity system (i.e., a “3 for 1”). As a result, future work could test this hypothesis by including CPR-BES facilities as investment options within a capacity expansion model.

6.3.1.4 Expand Model Boundaries to Incorporate CO_2 Sources

The research in this dissertation was agnostic about the source of CO_2 and as such, future work could integrate the CO_2 capture and transportation processes into the model framework. The CRP-BES system, for example, continuously stores CO_2 over the lifetime of the facility, and so it is likely that a CO_2 pipeline would be used to transport this CO_2 from a large point source to the facility. This infrastructure would increase the cost of the CRP-BES facility and thus increase the revenue needed to be profitable. On the other hand, if the source of CO_2 was from a bio-energy power plant, the CRP-BES process could be a CO_2

negative technology, which would increase the systems-level benefits of the process. As a result, the increase in systems-level value of the process may exceed the increase in cost.

6.3.2 Knowledge Gap: The Need and Role of Seasonal Energy Storage

The need for seasonal energy storage and its role in a decarbonized electricity system is unknown. Most studies that suggest there is a need for seasonal energy storage do not use capacity expansion models, but instead use "energy balancing models" [10,56–61]. These models typically assume perfect transmission and 100% storage efficiency and either (a) exogenously set the penetration of wind and solar energy technologies, and then find the resulting energy storage capacity required to ensure demand is always met, or (b) exogenously set the capacity of energy storage and determine what impact that has on the use of wind and solar energy technologies. In other words, they balance a demand profile with wind and solar generation profiles and use energy storage to ensure supply equals demand without regard to costs or other low CO_2 emission technologies. While these studies have slightly different methods, and model different locations (e.g., Europe, United States, California, several towns in New Zealand), several general conclusions can be made from looking across them:

1. *The need for seasonal energy storage is highly system specific because it is driven by differences in (a) supply, which varies technology type, location, etc.; and (b) demand, which varies with weather, population, industry, etc*. For example, the capacity of energy storage will be minimized if supply and demand are highly correlated. In any given year, differences between supply and demand can occur over short periods (i.e., hours to weeks) and long periods (i.e., seasons). A given system will likely require a larger energy storage capacity (i.e., enough to time-shift over seasons) if imbalances between supply and demand occur over long periods, but if imbalances primarily exist only on shorter timescales, the capacity of storage needed will likely only be sufficient for short term (i.e., daily) time-shifting. For example, in locations close to the equator, the solar resource displays less seasonal fluctuations and little if any seasonal storage is likely needed there.

Overall, in most locations the penetration of variable renewable energy technologies must be substantial (>~80%) to cause mismatches between supply and demand over long enough periods that necessitate large enough energy storage capacities for seasonal time-shifting.

2. *The use of seasonal energy storage is also highly system specific because it would likely be dispatched to store electricity during periods of very low net demand and dispatched to discharge electricity during periods of very high net demand.* For example, in California, this would likely mean storing excess electricity in the spring to meet the loads during the winter when wind and solar generation are low. As a result, it is possible that the optimal dispatch of a seasonal energy storage may closely resemble a seasonal pattern (e.g., 3-month charge, 3-month discharge or 6-month charge, 6-month discharge), but it is also possible that the dispatch may not resemble any pattern if (a) demand or the variable energy resource itself (e.g., wind in some locations) is more sporadic or (b) the combination of wind and solar energy technologies being used does not display a strong seasonal availability pattern. Further, the optimal dispatch may include compensating for mismatches between supply and demand over shorter periods (e.g., days, weeks) in addition to seasons, which can also create more irregular use.
3. *Seasonal fluctuations in wind and solar energy availability drives the need for seasonal energy storage because substantially more energy storage capacity is needed to time-shift electricity over seasons, not because shorter-term duration storage is unnecessary.* It becomes increasingly difficult to match supply with demand during seasonal minima of wind or solar energy availability as the penetration of variable renewable energy technologies increases because there is very little supply during these times. Because these minima occur for weeks to months at a time (depending on temporal nature of the variable resource in a given location), a substantial amount of energy storage capacity is needed, ranging from several weeks to multiple months of average load. Within any given season, however, there will also likely be shorter periods (e.g., hours, weeks) where supply and demand are not matched and energy storage is also needed.

Overall, these conclusions present a possibility that seasonal energy storage approaches may not be needed, or that may cost more than the value they provide to any given electricity system. For example, because (1) such large energy storage capacities are needed to time shift electricity generation over seasonal timescales, and (2) this capacity is only required to meet the final 20% or less of electricity demand, it is likely that other low-CO_2 emission technologies (e.g., nuclear, geothermal, CCS, etc.) will reduce the need for energy storage in general and may even completely obviate the need for seasonal energy storage. Despite this possibility, there are no studies that use a capacity expansion model to determine the need and role of seasonal energy storage in a decarbonizing electricity system and how that need and role depend on the cost and availability of other technologies.

As a result, future work could explore the effect of seasonal energy storage in a decarbonized electricity system and determine the cost and performance parameters (e.g., round-trip efficiency) necessary for seasonal energy storage to play a role in decarbonizing the electricity system. This could be accomplished by using a capacity expansion model to determine the breakeven cost of seasonal energy storage and the round-trip efficiency required for seasonal energy storage to be deployed and then see how sensitive those metrics are to the cost of other low-carbon generation technologies.

References

[1] Cubasch U, Wuebbles D, Chen D, Facchini MC, Frame D, Mahowald N, et al. Introduction. In: Stocker TF, Qin D, Plattner G-K, Tignor M, Allen SK, Boschung J, et al., editors. Clim. Chang. 2013 Phys. Sci. Basis. Work. Gr. 1 Contrib. to Fifth Assess. Rep. IPCC, 2013.

[2] IPCC. Summary for Policymakers. In: Masson-Delmotte V, Zhai P, Portner HO, Roberts D, Skea J, Shukla P, et al., editors. Glob. Warm. 1.5C. An IPCC Spec. Rep. Impacts Glob. Warm. 1.5C Above Pre-Industrial Levels Relat. Glob. Greenh. Gas Emiss. Pathways, Context Strength. Glob. Response to Threat Clim. Chang. S, Geneva, Switzerland: World Meterogolical Organization; 2018.

[3] EPA. Greenhouse Gas Emissions 2018.

[4] Middleton RS, Clarens AF, Liu X, Bielicki M, Levine JS. CO_2 Deserts: Implications of Existing CO_2 Supply Limitations for Carbon Management. Environ Sci Technol 2014;48:11713–20. doi:10.1021/es5022685.

[5] EPA. Overview of Greenhouse Gases: Carbon Dioxide Emissions 2017. https://www.epa.gov/ghgemissions/overview-greenhouse-gases.

[6] IPCC. Climate Change 2014: Mitigation of Climate Change. Contribution of Working Group III to the Fifth Assessment Report of the Intergovernmental Panel on Climate Change. Cambridge University Press; 2014.

[7] Krey V, Luderer G, Clarke L, Kriegler E. Getting From Here to There – Energy Technology Transformation Pathways in the EMF27 Scenarios. Clim Change 2014:369–82. doi:10.1007/s10584-013-0947-5.

[8] Frew BA, Becker S, Dvorak MJ, Andresen GB, Jacobson MZ. Flexibility Mechanisms and Pathways to a Highly Renewable US Electricity Future. Energy 2016;101:65–78.

doi:10.1016/j.energy.2016.01.079.

[9] Denholm P, Hand M. Grid Flexibility and Storage Required to Achieve Very High Penetration of Variable Renewable Electricity. Energy Policy 2011;39:1817–30. doi:10.1016/j.enpol.2011.01.019.

[10] Shaner MR, Davis SJ, Lewis NS, Caldeira K. Geophysical Constraints on the Reliability of Solar and Wind Power in the United States. Energy Environ Sci 2018. doi:10.1039/C7EE03029K.

[11] IPCC. IPCC Special Report on Carbon Dioxide Capture and Storage. 2005.

[12] IPCC. Summary for Policymakers, In: Climate Change 2014, Mitigation of Climate Change. Contribution of Working Group III to the Fifth Assessment Report of the Intergovernmental Panel on Climate Change. 2014.

[13] Azar C, Lindgren K, Obersteiner M, Riahi K, Vuuren DP Van, Elzen KMGJ Den, et al. The Feasibility of Low CO2 Concentration Targets and the Role of Bio-Energy with Carbon Capture and Storage (BECCS) 2010:195–202. doi:10.1007/s10584-010-9832-7.

[14] Selosse S, Ricci O. Achieving Negative Emissions with BECCS (Bioenergy with Carbon Capture and Storage) in the Power Sector: New Insights from the TIAM-FR (TIMES Integrated Assessment Model France) Model. Energy 2014;76:967–75. doi:10.1016/j.energy.2014.09.014.

[15] Thomsen P. Geothermal Selection in California Resource Planning: Future Development and Analysis. GRC Trans 2018:2220–39.

[16] Randolph JB, Saar MO. Combining Geothermal Energy Capture With Geologic Carbon Dioxide Sequestration. Geophys Res Lett 2011;38:1–7. doi:10.1029/2011GL047265.

[17] Adams BM, Kuehn TH, Bielicki JM, Randolph JB, Saar MO. On the Importance of the Thermosiphon Effect in CPG (CO_2 Plume Geothermal) Power Systems. Energy 2014;69:409–18. doi:10.1016/j.energy.2014.03.032.

[18] Adams BM, Kuehn TH, Bielicki JM, Randolph JB, Saar MO. A Comparison of Electric Power Output of CO_2 Plume Geothermal (CPG) and Brine Geothermal Systems for Varying Reservoir

Conditions. Appl Energy 2015;140:365–77. doi:10.1016/j.apenergy.2014.11.043.

[19] Garapati N, Randolph JB, Saar MO. Brine Displacement by CO_2, Energy Extraction Rates, and Lifespan of a CO2 -Limited CO2-Plume Geothermal (CPG) System with a Horizontal Production Well. Geothermics 2015;55:182–94. doi:10.1016/j.geothermics.2015.02.005.

[20] Tester JW, Anderson BJ, Batchelor AS, Blackwell DD, DiPippo R, Drake EM, et al. Impact of Enhanced Geothermal Systems on US Energy Supply in the Twenty-First Century. Philos Trans A Math Phys Eng Sci 2007;365:1057–94. doi:10.1098/rsta.2006.1964.

[21] Mock JE, Tester JW, Wright PM. Geothermal Energy From the Earth: Its Potential Impact as an Environmentally Sustainable Resource. Annu Rev Energy Environ 1997;22:305–56. doi:10.1146/annurev.energy.22.1.305.

[22] Aldridge KD, Toole DG. Realizing the Potential of Base Load Electricity Generation from Geothermal Sources : the San Jacinto-Tizate Field. 2nd WSEAS/IASME Int. Conf. Renew. Energy Sources Corfu, Greece, Oct. 26-28, 2008, 2008, p. 240–5.

[23] Bromley CJ, Mongillo MA. Geothermal Energy from Fractured Reservoirs - Dealing with Induced Seismicity -. From IEA OPEN Energy Technol Bull 2008:1–7.

[24] Barbier E. Geothermal energy technology and current status: an overview. Renew Sustain Energy Rev 2002;6:3–65. doi:10.1016/S1364-0321(02)00002-3.

[25] Cengel YA, Boles MA. Thermodynamics: An Engineering Approach. Seventh. New York: The McGraw-Hill Companies, Inc; 2008.

[26] Goldstein B, Hiriart G, Bertani R, Bromley C, Gutierrez-Negrin L, Huenges E, et al. Geothermal Energy. IPCC Spec Rep Renew Energy Sources Clim Chang Mitig 2011:401–36.

[27] EIA. INTERNATIONAL ENERGY STATISTICS 2018. https://www.eia.gov/beta/international/data/browser/.

[28] Azim R, Amin S, Shoeb A. Prospect of enhanced geothermal system in baseload power generation. 2010 IEEE Int Conf Adv Manag Sci 2010;3:176–80.

[29] Goldstein B, Hiriart G, Tester J, Bertani B, Bromley, Gutierrez-Negrin L, et al. Great Expectations for Geothermal Energy To 2100. Thirty-Sixth Work. Geotherm. Reserv. Eng., 2011.

[30] U.S. DOE. EGS Basics 2012. http://www1.eere.energy.gov/geothermal/pdfs/egs_basics.pdf.

[31] U.S. DOE. Hydrothermal Resources Factsheet 2012. http://energy.gov/sites/prod/files/2014/02/f7/hydrothermal_factsheet.pdf.

[32] Dickson MH, Fanelli M. Geothermal Energy: Utilization and Technology. Routledge; 2013.

[33] Corp. C. U.S. EGS Projects Calpine Corp. and Santa Rosa Celebrate Completion of the World's Largest Wastewater-to-Energy Project. GRC Bull 2003:242.

[34] Arnorsson S, Thorhallsson S, Stefansson A. Utilization of Geothermal Resources. In: Sigurdsson H, Houghton B, McNutt S, Rymer H, Stix J, editors. Encycl. Volcanoes. 2nd ed., 2015, p. 1235–52. doi:10.1016/B978-0-12-385938-9.00071-7.

[35] Williams CF, Reed MJ, Mariner RH, DeAngelo J, Galanis P. U.S. Geological Survey Fact Sheet 2008-3082. 2008.

[36] Tester JW, Anderson BJ, Batchelor AS, Blackwell DD, DiPippo R, Drake EM. The Future of Geothermal Energy. vol. Im. 2006.

[37] Singhal BBS, Gupta RP. Applied Hydrogeology of Fractured Rocks. Second. Springer Science & Business Media; 2010.

[38] Duchane D, Brown D. Hot Dry Rock Geothermal Energy Development in the USA. Http://Www.Ees.Lanl.Gov/Ees11/Geophysics/Staff/Brown/HDRintheUS.Pdf: 2000.

[39] Horne RN, Tester JW. Geothermal Energy: An Emerging Option for Heat and Power. Spring Issue Bridg Emerg Issues Earth Resour Eng 2014;44:7–15.

[40] Giardini D. Geothermal quake risks must be faced. Nature 2009;462:848–9. doi:10.1038/462848a.

[41] Allen PA, Allen JR. Basin Analysis: Principles and Application to Petroleum Play Assessment. John Wiley & Sons; 2013.

[42] Einsele G. Sedimentary Basins: Evolution, Facies, and Sediment Budget. Springer Science &

Business Media; 2000.

[43] Runkel A, Miller J, McKay R, Palmer A, Taylor J. High-Resolution Sequence Stratigraphy of Lower Paleozoic Sheet Sandstones in Central North America: The Role of Special Conditions of Cratonic Interiors in Development of Stratal Architecture. Geol Soc Am Bull 2007;119:860–81.

[44] Coleman JL, Cahan SM. Preliminary Catalog of the Sedimentary Basins of the United States. US Geol Surv Open-File Rep 2012-111 2012. http://pubs.usgs.gov/of/2012/1111/.

[45] Brown D. A Hot Dry Rock Geothermal Energy Concept Utilizing Supercritical CO2 Instead of Water. Twenty-Fifth Work. Geotherm. Reserv. Eng., vol. 1995, 2000.

[46] Wang C, Cheng W, Nian Y, Yang L, Han B, Liu M. Simulation of Heat Extraction From CO_2-Based Enhanced Geothermal Systems Considering CO_2 Sequestration. Energy 2018;142:157–67. doi:10.1016/j.energy.2017.09.139.

[47] Pritchett JW. On the Relative Effectiveness of H20 and CO2 as Reservoir Working Fluids for EGS Heat Mining. GRC Trans 2009;33:235–40.

[48] Pruess K. Enhanced Geothermal Systems (EGS) Using CO2 as Working Fluid – A Novel Approach for Generating Renewable Energy with Simultaneous Sequestration of Carbon. 2006.

[49] NETL. Carbon Storage Atlas - Fifth Edition (Atlas V). 2015.

[50] Porro C, Esposito A, Augustine C, Roberts B. An Estimate of the Geothermal Energy Resource in the Major Sedimentary Basins in the United States. GRC Trans 2012;36:1359–70.

[51] Atrens AD, Gurgenci H, Rudolph V. Electricity generation using a carbon-dioxide thermosiphon. Geothermics 2010;39:161–9. doi:10.1016/j.geothermics.2010.03.001.

[52] Buscheck T, Chen M, Hao Y. Multi-Fluid Geothermal Energy Production and Storage in Stratigraphic Reservoirs. 2013 Geotherm. Resour. Counc. Annu. Meet., 2013, p. 1–15.

[53] Buscheck TA, Bielicki JM, Randolph JB, Chen M, Hao Y, Edmunds TA, et al. Multi-Fluid Geothermal Energy Systems in Stratigraphic Reservoirs: Using Brine , N2 , and CO2 for Dispatchable Renewable Power Generation and Bulk Energy Storage. 39th Work. Geotherm.

Reserv. Eng. Stanford Univ., 2014.

[54] Buscheck T, Bielicki J, Edmunds T, Hao Y, Sun Y, Randolph J, et al. Multi-Fluid Geo-Energy Systems: Using Geologic CO_2 Storage for Geothermal Energy Production and Grid-Scale Energy Storage in Sedimentary Basins. Geosphere 2016;12. doi:10.1130/GES01207.1.

[55] Masters G. The Electric Power Industry. Renew. Effic. Electr. power Syst., 2004, p. 107–63.

[56] Becker S, Frew BA, Andresen GB, Zeyer T, Schramm S, Greiner M, et al. Features of a Fully Renewable US Electricity System: Optimized Mixes of Wind and Solar PV and Transmission Grid Extensions. Energy 2014;72:443–58. doi:10.1016/j.energy.2014.05.067.

[57] Dujardin J, Kahl A, Kruyt B, Bartlett S, Lehning M. Interplay Between Photovoltaic, Wind Energy and Storage Hydropower in a Fully Renewable Switzerland 2017;135:513–25. doi:10.1016/j.energy.2017.06.092.

[58] Heide D, Bremen L Von, Greiner M, Hoffmann C, Speckmann M, Bo S. Seasonal Optimal Mix of Wind and Solar Power in a Future, Highly Renewable Europe 2010;35:2483–9. doi:10.1016/j.renene.2010.03.012.

[59] Rasmussen MG, Andresen GB, Greiner M. Storage and Balancing Synergies in a Fully or Highly Renewable Pan-European Power System. Energy Policy 2012;51:642–51. doi:10.1016/j.enpol.2012.09.009.

[60] Mason IG. Comparative Impacts of Wind and Photovoltaic Generation on Energy Storage for Small Islanded Electricity Systems. Renew Energy 2015;80:793–805. doi:10.1016/j.renene.2015.02.040.

[61] Tarroja B, Shaffer BP, Samuelsen S. Resource Portfolio Design Considerations for Materially-Efficient Planning of 100% Renewable Electricity Systems. Energy 2018;157:460–71. doi:10.1016/j.energy.2018.05.184.

[62] Denholm P, King JC, Kutcher CF, Wilson PPH. Decarbonizing the Electric Sector: Combining Renewable and Nuclear Energy Using Thermal Storage. Energy Policy 2012;44:301–11.

doi:10.1016/j.enpol.2012.01.055.

[63] Forsberg C, Brick S, Haratyk G. Coupling Heat Storage to Nuclear Reactors for Variable Electricity Output With Baseload Reactor Operation. Electr J 2018;31:23–31. doi:10.1016/j.tej.2018.03.008.

[64] U.S. DOE. 20% Wind Energy by 2030: Increasing Wind Energy's Contribution to U.S. Electricity Supply. 2008.

[65] Günter N, Marinopoulos A. Energy Storage for Grid Services and Applications: Classification, Market Review, Metrics, and Methodology for Evaluation of Deployment Cases. J Energy Storage 2016;8:226–34. doi:10.1016/j.est.2016.08.011.

[66] Sioshansi R, Denholm P, Jenkin T. Market and Policy Barriers to Deployment of Energy Storage. Econ Energy Environ Policy 2012;1:1–14. doi:10.5547/2160-5890.1.2.4.

[67] EPRI. Electricity Energy Storage Technology Options. 2010.

[68] IPCC. Summary for Policy Makers. In: Stocker TF, Qin G, Plattner G-K, Tignor M, Allen SK, Boschung J, et al., editors. Clim. Chang. 2013 Phys. Sci. Bases. Contrib. Work. Gr. 1 to Fifth Assess. Rep. Intergov. Panel Clim. Chang., New York: Cambridge University Press; 2013.

[69] EIA. Frequently Asked Questions: How Much of U.S. Carbon Dioxide Emissions Are Associated with Electricity Generation? 2017. https://www.eia.gov/tools/faqs/faq.php?id=77&t=11 (accessed July 14, 2017).

[70] EIA. Form EIA-923 Detailed Data 2017. https://www.eia.gov/electricity/data/eia923/.

[71] Maupin MA, Kenny JF, Hutson SS, Lovelace JK, Barber NL, Linsey KS. Estimated Use of Water in the United States in 2010 Circular 1405 2014. doi:10.3133/cir1405.

[72] Averyt K, Meldrum J, Caldwell P, Sun G, McNulty S, Huber-Lee A, et al. Sectoral Contributions to Surface Water Stress in the Coterminous United States. Environ Res Lett 2013;8. doi:10.1088/1748-9326/8/3/035046.

[73] Blanc E, Strzepek K, Schlosser A, Jacoby H, Gueneau A, Fant C, et al. Modeling U.S. Water

Resources Under Climate Change. Earth's Futur 2014;2:197–224. doi:10.1002/2013EF000214.

[74] Meldrum J, Nettles-Anderson S, Heath G, Macknick J. Life Cycle Water Use for Electricity Generation: A Review and Harmonization of Literature Estimates. Environ Res Lett 2013;8. doi:10.1088/1748-9326/8/1/015031.

[75] Fricko O, Parkinson SC, Johnson N, Strubegger M, van Vliet MTH, Riahi K. Energy Sector Water Use Implications of a 2°C Climate Policy. Environ Res Lett 2016;11:34011. doi:10.1088/1748-9326/11/3/034011.

[76] Leonard MD, Michaelides EE, Michaelides DN. Substitution of Coal Power Plants with Renewable Energy Sources of the Power Demand and Energy Storage. Energy Convers Manag 2018;164:27–35. doi:10.1016/j.enconman.2018.02.083.

[77] Shahmohammadi A, Sioshansi R, Conejo AJ, Afsharnia S. The Role of Energy Storage in Mitigating Ramping Inefficiencies Caused by Variable Renewable Generation. Energy Convers Manag 2018;162:307–20. doi:10.1016/j.enconman.2017.12.054.

[78] Castillo A, Gayme DF. Grid-Scale Energy Storage Applications in Renewable Energy Integration: A Survey. Energy Convers Manag 2014;87:885–94. doi:10.1016/j.enconman.2014.07.063.

[79] Deane JP, Gallachioir BP, McKeogh EJ. Techno-Economic Review of Existing and New Pumped Hydro Energy Storage Plant. Renew Sustain Energy Rev 2010;14:1293–302. doi:10.1016/j.rser.2009.11.015.

[80] Akhil AA, Huff G, Currier AB, Kaun BC, Rastler DM, Chen SB, et al. DOE/EPRI Electricity Storage Handbook in Collaboration with NRECA 2015. http://prod.sandia.gov/techlib/access-control.cgi/2015/151002.pdf.

[81] Lv S, He W, Zhang A, Li G, Luo B, Liu X. Modelling and Analysis of a Novel Compressed Air Energy Storage System for Trigeneration Based on Electrical Energy Peak Load Shifting. Energy Convers Manag 2017;135:394–401. doi:10.1016/j.enconman.2016.12.089.

[82] Mueller JM. Increasing Renewable Energy System Value Through Storage 2015.

https://dspace.mit.edu/handle/1721.1/98540.

[83] Saar MO, Randolph JB, Kuehn TH, the Regents of the University of Minnesota. Carbon dioxide-based geothermal energy generation systems and methods related thereto. U.S. Patent No. 8316955 (issued 2012); Canada Patent No. 2.753.393 (issued 2013); Europe Patent No. 2406562 (issued 2014); Australia Patent No. 2010223059 (issued 2015), n.d.

[84] EIA. About 60% of the U.S. Electric Power Supply is Managed by RTOs. Today In Energy 2011. https://www.eia.gov/todayinenergy/detail.php?id=790.

[85] Paine N, Homans FR, Pollak M, Bielicki JM, Wilson EJ. Why Market Rules Matter: Optimizing Pumped Hydroelectric Storage When Compensation Rules Differ. Energy Econ 2014;46:10–9. doi:10.1016/j.eneco.2014.08.017.

[86] EIA. Electric Generator Dispatch Depends on System Demand and the Relative Cost of Operation. Today In Energy 2012. http://www.eia.gov/todayinenergy/detail.cfm?id=7590.

[87] Hittinger ES, Azevedo IML. Bulk Energy Storage Increases United States Electricity System Emissions. Environ Sci Technol 2015;49:3203–10. doi:10.1021/es505027p.

[88] Lueken R, Apt J. The Effects of Bulk Electricity Storage on the PJM Market. Energy Syst 2014;5:677–704. doi:10.1007/s12667-014-0123-7.

[89] Tuohy A, O'Malley M. Pumped Storage in Systems with Very High Wind Penetration. Energy Policy 2011;39:1965–74. doi:10.1016/j.enpol.2011.01.026.

[90] Craig M, Jaramillo P, Hodge B-M. Carbon Dioxide Emissions Effects of Grid-Scale Electricity Storage in a Decarbonizing Power System. Environ Res Lett 2018;13. doi:https://doi.org/10.1088/1748-9326/aa9a78.

[91] McMahon JE, Price SK. Water and Energy Interactions. Annu Rev Environ Resour 2011;36:163–91. doi:10.1146/annurev-environ-061110-103827.

[92] Goteti NS, Hittinger E, Williams E. How Much Wind and Solar are Needed to Realize Emissions Benefits from Storage? Energy Syst 2017. doi:10.1007/s12667-017-0266-4.

[93] Mileva A, Johnston J, Nelson JH, Kammen DM. Power System Balancing for Deep Decarbonization of the Electricity Sector. Appl Energy 2016;162:1001–9. doi:10.1016/j.apenergy.2015.10.180.

[94] Denholm P, Kulcinski GL. Life Cycle Energy Requirements and Greenhouse Gas Emissions from Large Scale Energy Storage Systems. Energy Convers Manag 2004;45:2153–72. doi:10.1016/j.enconman.2003.10.014.

[95] Bouman EA, Øberg MM, Hertwich EG. Environmental Impacts of Balancing Offshore Wind Power with Compressed Air Energy Storage (CAES). Energy 2016;95:91–8. doi:10.1016/j.energy.2015.11.041.

[96] de Sisternes FJ, Jenkins JD, Botterud A. The Value of Energy Storage in Decarbonizing the Electricity Sector. Appl Energy 2016;175:368–79. doi:10.1016/j.apenergy.2016.05.014.

[97] Safaei H, Keith DW. How Much Bulk Energy Storage is Needed to Decarbonize Electricity? Energy Environ Sci 2015. doi:10.1039/C5EE01452B.

[98] Sioshansi R, Denholm P, Jenkin T, Weiss J. Estimating the Value of Electricity Storage in PJM: Arbitrage and Some Welfare Effects. Energy Econ 2009;31:269–77. doi:10.1016/j.eneco.2008.10.005.

[99] Bradbury K, Pratson L, Patiño-Echeverri D. Economic Viability of Energy Storage Systems Based on Price Arbitrage Potential in Real-Time U.S. Electricity Markets. Appl Energy 2014;114:512–9. doi:10.1016/j.apenergy.2013.10.010.

[100] ERCOT. Quick Facts 2016. http://www.ercot.com/content/wcm/lists/89475/ERCOT_Quick_Facts_9916.pdf.

[101] ERCOT. ERCOT 2005. http://www.ercot.com/content/.

[102] ERCOT. About ERCOT 2005. http://www.ercot.com/about (accessed January 14, 2016).

[103] Lopez A, Roberts B, Heimiller D, Blair N, Porro G. U.S. Renewable Energy Technical Potentials: A GIS-Based Analysis. NREL Tech Rep 2012. http://www.nrel.gov/docs/fy12osti/51946.pdf.

[104] Hartmann J, Moosdorf N. The New Global Lithological Map Database GLiM: A Representation of Rock Properties at the Earth Surface. Geochemistry, Geophys Geosystems 2012;13:1–37. doi:10.1029/2012GC004370.

[105] AWEA. Texas Wind Energy 2016. http://awea.files.cms-plus.com/FileDownloads/pdfs/Texas.pdf.

[106] The Texas Office Of Public Utility Council. Map of Electricity System Area that is Managed by ERCOT n.d. http://www.opuc.texas.gov/images/ERCOT_Region_map.jpg.

[107] ERCOT. 60-Day SCED Disclosure Report 2015. http://mis.ercot.com/misapp/GetReports.do?reportTypeId=13052&reportTitle=60-Day SCED Disclosure&showHTMLView=&mimicKey (accessed December 12, 2015).

[108] EIA. Form EIA-860 detailed data 2017. http://www.eia.gov/electricity/data/eia860/.

[109] Macknick J, Newmark R, Heath G, Hallett KC. Operational Water Consumption and Withdrawal Factors for Electricity Generating Technologies: A Review of Existing Literature. Environ Res Lett 2012;7:045802. doi:10.1088/1748-9326/7/4/045802.

[110] NRC US. Operating Nuclear Power Reactors (by Location or Name) 2017. https://www.nrc.gov/info-finder/reactors/.

[111] ERCOT. Generation 2015. http://www.ercot.com/gridinfo/generation.

[112] Fertig E, Apt J. Economics of Compressed Air Energy Storage to Integrate Wind Power: A Case Study in ERCOT. Energy Policy 2011;39:2330–42. doi:10.1016/j.enpol.2011.01.049.

[113] Middleton RS, Levine JS, Bielicki JM, Viswanathan HS, Carey JW, Stauffer PH. Jumpstarting Commercial-Scale CO_2 Capture and Storage With Ethylene Production and Enhanced Oil Recovery in the US Gulf. Greenh Gases Sci Technol 2015:241–53. doi:10.1002/ghg.

[114] Climate Policy Initiation. California Carbon Dashboard 2017. calcarbondash.org (accessed May 3, 2017).

[115] RGGI. RGGI Auction Results 2017. https://www.rggi.org/market/co2_auctions/results (accessed May 3, 2017).

[116] Sanders KT, Blackhurst MF, King CW, Webber ME. The Impact of Water Use Fees on Water Used for Cooling Thermoelectric Power Generators. Environ Sci Technol 2014;48:7128–34. doi:dx.doi.org/10.1021/es500469q.

[117] Sahin O, Siems RS, Stewart RA, Porter MG. Paradigm Shift to Enhanced Water Supply Planning Through Augmented Grids, Scarcity Pricing and Adaptive Factory Water: A System Dynamics Approach. Environ Model Softw 2016;75:348–61. doi:10.1016/j.envsoft.2014.05.018.

[118] Lazard. Levelized Cost of Energy Analysis - Version 3.0. 2009.

[119] Lazard. Levelized Cost of Energy Analysis - Version 4.0. 2010.

[120] Lazard. Levelized Cost of Energy Analysis - Version 5.0. 2011.

[121] Lazard. Levelized Cost of Energy Analysis - Version 6.0. 2012.

[122] Lazard. Levelized Cost of Energy Analysis - Version 7.0. 2013.

[123] Lazard. Levelized Cost of Energy Analysis - Version 8.0. 2014.

[124] Lazard. Levelized Cost of Energy Analysis - Version 9.0. 2015.

[125] Lazard. Levelized Cost of Energy Analysis - Version 10.0. 2016.

[126] EIA. Coal Data Browser 2017. https://www.eia.gov/beta/coal/data/browser/#/topic/45?agg=1,0&geo=0000000002&rank=g&linechart=COAL.SHIP_PLANT_PRICE.TX-TOT.Q&freq=Q&start=200801&end=201602&ctype=linechart&ltype=pin&rtype=s&pin=COAL.SHIP_PLANT_PRICE.TX-TOT.Q&rse=0&maptype=0.

[127] EIA. Texas Natural Gas Price Sold to Electric Power Consumers 2016. http://www.eia.gov/dnav/ng/hist/n3045tx3m.htm.

[128] EIA. Frequently Asked Questions: How Much Carbon Dioxide is Produced per Kilowatthour When Generating Electricity With Fossil Fuels? 2016. https://www.eia.gov/tools/faqs/faq.php?id=74&t=11.

[129] Black & Vetch Holding Company. Cost and Performance Data for Power Generation

Technologies. Natl Renew Energiy Lab 2012. http://bv.com/docs/reports-studies/nrel-cost-report.pdf.

[130] Cochran J, Lew D, Kumar N. Flexible Coal: Evolution from Baseload to Peaking Plant 2013. doi:10.2172/1110465.

[131] Grigg C, Wong P, Albrecht P, Allan R, Bhavaraju M, Billinton R, et al. The IEEE Reliability Test System. IEE Trans Power Syst 1999;14. doi:10.1109/59.780914.

[132] Schroder A, Kunz F, Meiss J, Mendelevitch R, von Hirschhausen C. Current and Prospective Costs of Electricity Generation until 2050 2013. https://www.diw.de/documents/publikationen/73/diw_01.c.424566.de/diw_datadoc_2013-068.pdf.

[133] Drury E, Denholm P, Sioshansi R. The Value of Compressed Air Energy Storage in Energy and Reserve Markets. Energy 2011;36:4959–73. doi:10.1016/j.energy.2011.05.041.

[134] Lazard. Lazard's Levelized Cost of Storage Analysis - Version 1.0 2015. https://www.lazard.com/media/2391/lazards-levelized-cost-of-storage-analysis-10.pdf.

[135] Lazard. Levelized Cost of Storage - Verson 2.0 2016. doi:10.1080/14693062.2006.9685626.

[136] Denholm P, Sioshansi R. The Value of Compressed Air Energy Storage with Wind in Transmission-Constrained Electric Power Systems. Energy Policy 2009;37:3149–58. doi:10.1016/j.enpol.2009.04.002.

[137] Cooley H, Fulton J, Gleick PH. Water for Energy: Future Water Needs for Electricity in the Intermountain West. Pacific Inst 2011:1–64. http://pacinst.org/wp-content/uploads/2013/02/water_for_energy3.pdf.

[138] Augustine C, Bain R, Chapman J, Denholm P, Drury E, Hall DG, et al. Volume 2: Renewable Electricity Generation and Storage Technologies 2012;2:185–8. http://www.nrel.gov/docs/fy12osti/52409-2.pdf.

[139] Geissmann T, Ponta O. A Probabilistic Approach to the Computation of the Levelized Cost of Electricity. Energy 2017;124:372–81. doi:10.1016/j.energy.2017.02.078.

[140] Cohen J, Schweizer T, Laxson A, Butterfield S, Schreck S, Fingerish L, et al. Technology Improvement Opportunities for Low Wind Speed Turbines and Implications for Cost of Energy Reduction 2008.

[141] Hussey K, Pittock J. The Energy-Water Nexus: Managing the Links between Energy and Water for a Sustainable Future. Ecol Soc 2012;17.

[142] IPCC. Summary for Policymakers. Clim Chang 2014 Mitig Clim Chang Contrib Work Gr III to Fifth Assess Rep Intergov Panel Clim Chang 2014.

[143] Morrison GM, Yeh S, Eggert AR, Yang C, Nelson JH, Greenblatt JB, et al. Comparison of Low-Carbon Pathways for California. Clim Change 2015:545–57. doi:10.1007/s10584-015-1403-5.

[144] Elliston B, Macgill I, Diesendorf M. Comparing Least Cost Scenarios for 100% Renewable Electricity with Low Emission Fossil Fuel Scenarios in the Australian National Electricity Market. Renew Energy 2014;66:196–204. doi:10.1016/j.renene.2013.12.010.

[145] Kriegler E, Weyant JP, Blanford GJ, Krey V, Clarke L, Edmonds J, et al. The Role of Technology for Achieving Climate Policy Objectives: Overview of the EMF 27 Study on Global Technology and Climate Policy Strategies. Clim Change 2014:353–67. doi:10.1007/s10584-013-0953-7.

[146] Riesz J, Elliston B. Research and Deployment Priorities for Renewable Rechnologies: Quantifying the Importance of Various Renewable Technologies for Low Cost, High Renewable Electricity Systems in an Australian Case Study. Energy Policy 2016;98:298–308. doi:10.1016/j.enpol.2016.08.034.

[147] Pleßmann G, Blechinger P. How to Meet EU GHG Emission Reduction Targets? A Model Based Decarbonization Pathway for Europe’s Electricity Supply System Until 2050. Energy Strateg Rev 2017;15:19–32. doi:10.1016/j.esr.2016.11.003.

[148] Williams JH, Debenedictis A, Ghanadan R, Mahone A, Moore J, Iii WRM, et al. The Technology Path to Deep Greenhouse Gas Emissions Cuts by 2050: The Pivotal Role of Electricity. Science (80-) 2012;335. doi:10.1126/science.1208365.

[149] Yang C, Yeh S, Zakerinia S, Ramea K, Mccollum D. Achieving California's 80% Greenhouse Gas Reduction Target in 2050: Technology, Policy and Scenario Analysis Using CA-TIMES Energy Economic Systems Model. Energy Policy 2015;77:118–30. doi:10.1016/j.enpol.2014.12.006.

[150] O'Dwyer C, Flynn D. Using Energy Storage to Manage High Net Load Variability at Sub-Hourly Time-Scales. IEEE Trans Power Syst 2015;30:2139–48. doi:10.1109/TPWRS.2014.2356232.

[151] Luo X, Wang J, Dooner M, Clarke J. Overview of Current Development in Electrical Energy Storage Technologies and the Application Potential in Power System Operation. Appl Energy 2015;137:511–36. doi:10.1016/j.apenergy.2014.09.081.

[152] Götz M, Lefebvre J, Mörs F, McDaniel Koch A, Graf F, Bajohr S, et al. Renewable Power-to-Gas: A Technological and Economic Review. Renew Energy 2016;85:1371–90. doi:10.1016/j.renene.2015.07.066.

[153] McKain K, Down A, Raciti SM, Budney J, Hutyra LR, Floerchinger C, et al. Methane Emissions from Natural Gas Infrastructure and Use in the Urban Region of Boston, Massachusetts. Proc Natl Acad Sci 2015;112:1941–6. doi:10.1073/pnas.1416261112.

[154] Fleming MR, Adams BM, Randolph JB, Ogland-Hand JD, Kuehn TH, Buscheck TA, et al. High Efficiency and Large-Scale Subsurface Energy Storage with CO_2. Proc 43rd Work Geotherm Reserv Eng Stanford Univ Stanford, CA 2018:1–12.

[155] Hao Y, Sun Y, Nitao JJ. Overview of NUFT: Versatile Numerical Model for Simulating Flow and Reactive Transport in Porous Media. In: Zhang F, Yeh G-T, Parker J, editors. Groundw. React. Transp. Model., Bentham Books; 2012, p. 212–39.

[156] Bell IH, Wronski J, Quoilin S, Lemort V. Pure and Pseudo-pure Fluid Thermophysical Property Evaluation and the Open-Source Thermophysical Property Library CoolProp. Ind Eng Chem Res 2014;53:2498–508. doi:10.1021/ie4033999.

[157] Frezon S, Finn T, Lister J. Total Thickness of Sedimentary Rocks in the Conterminous United States. 1983.

[158] Fuis G, Ryberg T, Godfrey N, Okaya D, Murphy J. Crustal Structure and Tectonics from the Los Angeles Basin to the Mojave Desert, Southern California. Geology 2001;29.

[159] Jachens R, Griscom A, Roberts C. Maps of the Thickness of Cenozoic Deposits and the Isostatic Residual Gravity over Basement for Nevada. 1996.

[160] Langenheim V, Jachens R. Gravity Data Collected Along the Los Angeles Regional Seismic Experiment (LARSE) and Preliminary Model of Regional Density Variations in Basement Rocks, Southern California. 1996.

[161] Mooney WD, Kaban MK. The North American Upper Mantle: Density, Composition, and Evolution. J Geophys Res Solid Earth 2010;115:1–24. doi:10.1029/2010JB000866.

[162] USGS. National Assessment of Geologic Carbon Dioxide Storage Resources - Results: U.S. Geological Survey Circular 1386. 2013.

[163] Jachens RC, Griscom A, Roberts CW. Regional Extent of Great Valley Basement West of the Great Valley, California: Implications for Extensive Tectonic Wedging in the California Coast Ranges. J Geophys Res 1995;100:12769. doi:10.1029/95JB00718.

[164] Buscheck T, Bielicki J, White J, Sun Y, Hao Y, Bourcier WL, et al. Pre-injection Brine Production in CO2 Storage Reservoirs: An Approach to Augment the Development, Operation, and Performance of CCS While Generating Water. Int J Greenh Gas Control 2016. doi:10.1016/j.ijggc.2016.04.018.

[165] Buscheck TA, White JA, Chen M, Sun Y, Hao Y, Aines RD, et al. Pre-Injection Brine Production for Managing Pressure in Compartmentalized CO2 Storage Reservoirs. GHGT-12 Conf. Proc., 2014, p. 1–8.

[166] Buscheck TA, Bielicki JM, White JA, Sun Y, Hao Y, Bourcier WL, et al. Managing Geologic CO2 Storage With Pre-Injection Brine Production in Tandem Reservoirs. Energy Procedia 2017;114:4757–64. doi:10.1016/j.egypro.2017.03.1826.

[167] MacDonald AE, Clack CTM, Alexander A, Dunbar A, Wilczak J, Xie Y. Future Cost-Competitive

Electricity Systems and Their Impact on US CO2 Emissions. Nat Clim Chang 2016;6. doi:10.1038/NCLIMATE2921.

[168] Mai T, Mulcahy D, Hand MM, Baldwin SF. Envisioning a Renewable Electricity Future for the United States. Energy 2014;65:374–86. doi:10.1016/j.energy.2013.11.029.

[169] Craig MT, Cohen S, Macknick J, Draxl C, Guerra OJ, Sengupta M, et al. A Review of the Potential Impacts of Climate Change on Bulk Power System Planning and Operations in the United States. Renew Sustain Energy Rev 2018;98:255–67. doi:10.1016/j.rser.2018.09.022.

[170] EIA. Electric Power Monthly 2017. https://www.eia.gov/electricity/monthly/epm_table_grapher.php?t=epmt_6_07_b (accessed October 13, 2017).

[171] Go RS, Munoz FD, Watson JP. Assessing the Economic Value of Co-Optimized Grid-Scale Energy Storage Investments in Supporting High Renewable Portfolio Standards. Appl Energy 2016;183:902–13. doi:10.1016/j.apenergy.2016.08.134.

[172] Deng H, Bielicki JM, Oppenheimer M, Fitts JP, Peters CA. Leakage risks of Geologic CO2 Storage and the Impacts on the Global Energy System and Climate Change Mitigation. Clim Change 2017;144:151–63. doi:10.1007/s10584-017-2035-8.

[173] Bielicki M, Pollak MF, Deng H, Wilson EJ, Fitts P, Peters CA. The Leakage Risk Monetization Model for Geologic CO2 Storage. Environ Sci Technol 2016;50:4923–31. doi:10.1021/acs.est.5b05329.

[174] Buscheck TA, Sun Y, Hao Y, Wolery TJ, Bourcier WL, Tompson AFB, et al. Combining Brine Extraction, Desalination, and Residual-Brine Reinjection with CO_2 Storage in Saline Formations: Implications for Pressure Management, Capacity, and Risk Mitigation. Energy Procedia 2011;4:4283–90. doi:10.1016/j.egypro.2011.02.378.

[175] Mines GL. GETEM User Manual 2016.

[176] U.S. DOE. GETEM: Geothermal Energy Technology Evaluation Model 2012.

[177] EPA. Geologic CO_2 Sequestration Technology and Cost Analysis 2010.

[178] Moisseytsev A, Sienicki JJ. Investigation of a Dry Air Cooling Option for an SCO2 cycle. 4th Int Symp - Supercrit CO2 Power Cycles 2014;1:1–21.

[179] Pidaparti SR, Moisseytsev A, Sienicki JJ, Ranjan D. Counter Flow Induced Draft Cooling Tower Option for Supercritical Carbon Dioxide Brayton Cycle. Nucl Eng Des 2015;295:549–58. doi:10.1016/j.nucengdes.2015.09.026.

[180] Short W, Sullivan P, Mai T, Mowers M, Uriarte C, Blair N, et al. Regional Energy Deployment System (ReEDS) 2011. doi:NREL/TP-6A20-46534.

[181] NETL. Cost Estimation Methodology for NETL Assessments of Power Plant Performance. Quality Guidelines for Energy System Studies 2011.

[182] NREL. Development of Regional Wind Resource and Wind Plant Output Datasets: Final Subcontract Report 15 October 2007 - 15 March 2009. 2010.

[183] USGS. Energy News and Current Publications 2013. https://energy.usgs.gov/GeneralInfo/EnergyNewsroomAll/TabId/770/ArtMID/3941/ArticleID/1056/USGS-Releases-First-Ever-National-Wind-Turbine-Map-Database.aspx.

[184] Draxl C, Clifton A, Hodge BM, McCaa J. The Wind Integration National Dataset (WIND) Toolkit. Appl Energy 2015;151:355–66. doi:10.1016/j.apenergy.2015.03.121.

[185] Eichman J, Denholm P, Jorgenson J. Operational Benefits of Meeting California's Energy Storage Targets 2015.

[186] CAISO. Integration of Renewable Resources: Technical Appendices for California ISO Renewable Integration Studies. Version 1, First Draft for External Review 2010.

[187] Ogland-Hand JD, Miranda MW, Bielicki JM, Adams BM, Buscheck TA, Saar MO. Operational Characteristics of a Geologic CO2 Storage Bulk Energy Storage Technology. Energy Procedia 2018.

[188] EPA. The Social Cost of Carbon 2017. https://www.epa.gov/climatechange/social-cost-carbon

(accessed April 20, 2017).

[189] EIA. Regional Greenhouse Gas Initiative Auction Prices are the Lowest Since 2014. Today In Energy 2017. https://www.eia.gov/todayinenergy/detail.php?id=31432.

Appendix A: Supplemental Information for Chapter 2

1 Full Specification of the Mixed Integer Linear Program

The problem is formulated as minimizing the operating cost of the electricity system to meet demand:

$$\sum_{t=0}^{T}\left(\frac{(1+\eta)}{\eta}Q_{B,t}O_B+Q_{B,t}\left(\alpha P_{CO_2}+\beta_B P_{H_2O}\right)+Q_{r,t}O_r+\sum_i\left[Q_{i,t}O_i\right]+\sum_j\left[Q_{j,t}O_j\right]+\sum_k\left[Q_{k,t}O_k\right]\right) \tag{16}$$

The subscripts in Equation 16 refer to the fuel type, where each technology that is dispatched is drawn from the following sets:

B: bulk energy storage component

r: variable renewable energy technology component

i: nuclear power plants

j: coal EGUs

k: natural gas EGUs

Operating Cost Equations:

$$O_w=O_w^{v+f} \tag{17}$$

$$O_i=O_i^{v+f}+\beta_i*P_{H_2O} \tag{18}$$

$$O_j=O_j^{f}+H_j*\left(P_{coal}+R_{coal}*P_{CO_2}\right)+\beta_j*P_{H_2O} \tag{19}$$

$$O_k=O_k^{f}+H_k*\left(P_{ng}+R_{ng}*P_{CO_2}\right)+\beta_k*P_{H_2O} \tag{20}$$

BES component constraints:

$$E_t=E_{t-1}+\sum_i\left[Q_{i,t}\right]+\sum_j\left[Q_{j,t}\right]+\sum_k\left[Q_{k,t}\right]+Q_{w,t}-D_t \tag{21}$$

$$E_t\leq\overline{Q_B} \tag{22}$$

$$Q_{B,t} \leq \eta * E_{t-1} \tag{23}$$

Variable renewable energy technology component constraints:

$$0 \leq Q_{r,t} \leq \overline{Q}_{r_t} \tag{24}$$

Nuclear power plant constraints:

$$Q_{i,t} = U_i * \overline{Q_i} \tag{25}$$

$$Q_{i,t} = Q_{i,t-1} \tag{26}$$

Coal EGU constraints:

$$U_{j,t} * \underline{\theta}_j * \overline{Q_j} \leq Q_{j,t} \tag{27}$$

$$Q_{j,t} \leq U_{j,t} * \overline{Q_j} \tag{28}$$

$$Q_{j,t} \geq Q_{j,t-1} - \dot{\theta}_j * \overline{Q_j} \tag{29}$$

$$Q_{j,t} \leq Q_{j,t-1} + \dot{\theta}_j * \overline{Q_j} \tag{30}$$

$$U_{j,t} - U_{j,t-1} \leq U_{j,t+\mu_j} \tag{31}$$

$$U_{j,t-1} - U_{j,t} \leq 1 - U_{j,t+\delta_j} \tag{32}$$

Natural gas EGU constraints:

$$U_{k,t} * \underline{\theta}_k * \overline{Q_k} \leq Q_{k,t} \tag{33}$$

$$Q_{k,t} \leq U_{k,t} * \overline{Q_k} \tag{34}$$

$$Q_{k,t} \geq Q_{k,t-1} - \dot{\theta}_k * \overline{Q_k} \tag{35}$$

$$Q_{k,t} \leq Q_{k,t-1} + \dot{\theta}_k * \overline{Q_k} \tag{36}$$

$$U_{k,t} - U_{k,t-1} \leq U_{k,t+\mu_k} \tag{37}$$

$$U_{k,t-1} - U_{k,t} \leq 1 - U_{k,t+\delta_k} \tag{38}$$

Meet electricity demand constraint:

$$D_t \leq \sum_i \left[Q_{i,t}\right] + \sum_j \left[Q_{j,t}\right] + \sum_k \left[Q_{k,t}\right] + Q_{B,t} + Q_{r,t} \quad (39)$$

Decision variables:

- Q - the amount of electricity that is dispatched from the power plant, unit, or component in time period *t* (MWh);
- E_t - the cumulative amount of energy stored in time period *t* (MWh);
- $\overline{Q_B}$ - the BES component energy storage capacity (MWh),
- U - an integer variable that represents if a unit is dispatched (1 = dispatched, 0 = not dispatched);

Inputs:

- O^f - the fixed operating cost of the generation unit (\$/MWh);
- O^{v+f} - the sum of the variable and fixed operating cost of the power plant or component (\$/MWh);
- P_{coal}, P_{ng}, P_{CO2}, and P_{H2O} - the price of coal (\$/MMBtu), the price of natural gas (\$/MMBtu), the price of CO_2 (\$/tCO_2), and the price of water (\$/gal), respectively;
- R_{coal} and R_{ng} - the CO_2 emission rates of each fossil fuel (tCO_2/MMBtu);
- α - the CO_2 emission rate of BES (tCO_2/MWh);
- β - the water withdrawal rate of the power plant, generation unit, or component (gal/MWh);
- $\overline{Q}$ - the maximum amount of energy that can be dispatched by a power plant, generation unit, or component in any time period (MWh);
- $\dot{\theta}$ - the maximum rate at which a generation unit can increase or decrease the amount of electricity dispatched, in terms of the percent of $\bar{Q}$ (%/hour);
- $\underline{\theta}$ - the lower limit of the amount of electricity that must be generated by a power plant that is dispatched, in terms of the percent of $\bar{Q}$ (%);
- $\overline{Q}_{r_t}$ - the amount of electricity generated by the variable renewable energy component that is available for dispatch in a given time period (MWh);

- H - heat rate of the generation unit (MMBtu/MWh);
- D - the system-wide demand for electricity (MWh);
- η - the roundtrip efficiency of the BES technology;
- μ - minimum number of hours that a unit must remain dispatched once it is dispatched;
- δ - the minimum number of hours that a unit must remain not dispatched once it is not dispatched.

The costs of emitting CO_2 and of using water for the BES component are included in the objective function because the operating cost for the BES component accounts for charging and discharging energy (as described in Section 1.1 of Appendix A). If the CO_2 price and the water price were included in the operating costs, the cost to emit CO_2 or use water would be double-counted.

1.1 Representation of Bulk Energy Storage Operating Costs

We account for the operating cost of BES using the operating cost of discharge, O_B, and the BES round-trip efficiency, η. Figure 22 and Equations 40 to 48 justify the appropriateness of this simplification.

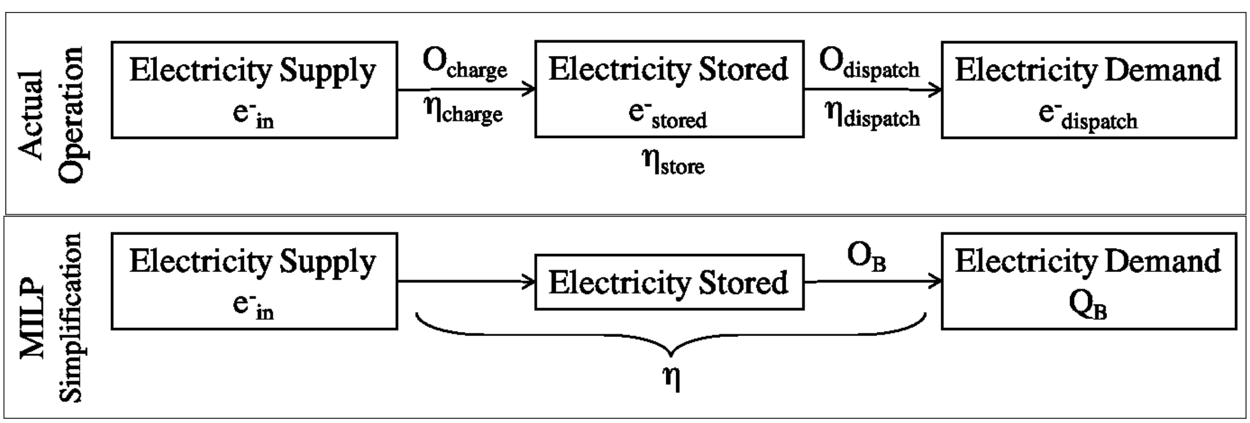

Figure 22: Actual BES Operation Compared to the Simplifications Made in the Mixed Integer Linear Program (MILP).

The actual amount of electricity dispatched by the BES component, $e^{-}_{dispatch}$, is the product of the amount of electricity stored, e^{-}_{in} and the charge, store, and dispatch efficiencies:

$$e^{-}_{dispatch}= e^{-}_{stored}*\eta_{dispatch} \quad (40)$$

$$e^{-}_{stored}= e^{-}_{in}*\eta_{charge}*\eta_{store} \quad (41)$$

$$e^{-}_{dispatch}= e^{-}_{in}*\eta_{charge}*\eta_{store}*\eta_{dispatch} \quad (42)$$

As suggested in Figure 22, we defined the BES round trip efficiency η, as the product of η_{charge}, η_{store}, and $\eta_{dispatch}$ and assign the variable Q_B to $e^{-}_{dispatch}$ in the MILP. As such, Equation 42 can be re-written:

$$Q_B=e^{-}_{in}*\eta \quad (43)$$

The total operating cost of BES operating is the cost of storing and dispatching electricity:

$$\text{Total operating cost}=e^{-}_{in}*O_{charge}+ e^{-}_{dispatch}*O_{dispatch} \quad (44)$$

The operating cost of storing electricity is largely a function of the price of electricity that is being stored. Endogenously determining the price of electricity within our MILP was outside the scope of this study; we assumed that O_{charge} was equal to $O_{dispatch}$ and assigned the variable O_B to this cost. Equation 44 can be further simplified using this information and Equations 42 and 43:

$$\text{Total operating cost}=e^{-}_{in}*O_{charge}+e^{-}_{in}*\eta_{charge}*\eta_{store}*\eta_{dispatch} *O_{dispatch} \quad (45)$$

$$\text{Total operating cost}=e^{-}_{in}*O_{charge}+e^{-}_{in}*\eta *O_{dispatch} \quad (46)$$

$$\text{Total operating cost}=e^{-}_{in}*O_B*(1+\eta) \quad (47)$$

The total operating cost can be defined in terms of Q_B and η by using Equation 48:

$$\text{Total operating cost}=\frac{(1+\eta)}{\eta}Q_B*O_B \quad (48)$$

2 ERCOT Data Processing

2.1 60-Day SCED Disclosure Report Data

60-Day Security Constrained Economic Dispatch (SCED) Disclosure Reports from ERCOT provide, among other information, the amount of electricity generated by each electric generation unit (EGU) in 15-

minute time intervals and the fuel type (e.g., coal, combined cycle, wind) for EGU in ERCOT [107]. Specifically, the SCED_Gen_Resource_Data files and the SMNE_GEN_RES_Data files for 2014 were used from the SCED Disclosure Reports. SCED_Gen_Resource_Data files list the name of every EGU and the fuel type and SMNE_GEN_RES_Data files list the name of every EGU and the amount of electricity that each EGU generated every 15 minutes. These two files were combined to determine how much electricity was generated by each fuel type in 2014. For example, SCED_Gen_Resource_Data file lists the power plant BBSES_UNIT1 as CLLIG (which is the abbreviation for a coal, lignite power plant) and every EGU named BBSES_UNIT1 in the SMNE_GEN_RES_Data files were classified as CLLIG. Some of the EGUs were named more specifically in one data set compared to the other (i.e., CVC_CC1_1 vs. CVC_CC1), so we only used the first five characters in each EGU for this matching process (i.e., CVC_C instead of CVC_CC1_1). EGUs listed in the SMNE_GEN_RES files that did not exist in the SCED_Gen_Resource_Data files were classified as "other" fuel type. Table 16 shows the percent of electricity generated by each fuel type.

Table 16: Percent of Electricity Generated by ERCOT EGUs by Fuel Type in 2014

Type of Generator as Defined in the 60-Day SCED Disclosure Report	Annual Electricity Generation (MWh)	Percent of Total Generation	Fuel Type
Combined Cycle (capacity greater than 90MW)	28,198,892	33.3%	Natural Gas
Combined Cycle (capacity less than or equal to 90MW)	1,284,035	1.5%	Natural Gas
Coal, Lignite	27,004,676	31.9%	Coal
Dynamically Scheduled Generation	0.00	0.00%	Natural Gas
Gas Steam Non-Reheat Boiler	109,642	0.1%	Natural Gas
Gas Steam Reheat Boiler	4,147,798	4.9%	Natural Gas
Gas Steam Super Critical Boiler	398,093	0.5%	Natural Gas
Hydro	44,705	0.1%	Hydro
Nuclear	9,822,119	11.6%	Nuclear
Other renewable	98,946	0.1%	Renewable
Simple Cycle (capacity greater than 90MW)	2,731,757	3.2%	Natural Gas
Simple Cycle (capacity less than or equal to 90MW)	1,660,496	2.0%	Natural Gas
Wind	9,028,334	10.7%	Wind
Other	208,865	0.3%	Other

2.2 Nuclear, Coal, and Natural Gas EGU Data

Table 17: EIA Plant ID Number, Capacity, Water Withdrawal Rate, and Heat Rate for Each EGU Included in the MILP. Natural gas combined cycle and natural gas steam cycle are abbreviated with NGCC and NGST, respectively.

EIA Plant ID	Capacity (MW)	Water Withdrawal Rate (gal/MWh)	Heat Rate (MMBtu/MWh)	EGU Type
56611	1,008	351	9.208	**Coal**
7097	878	40,602	9.487	**Coal**
6178	622	28,715	9.774	**Coal**
7097	566	45,605	9.904	**Coal**
6180	1,796	397,431	10.079	**Coal**
6136	454	44,404	10.086	**Coal**

6181	486	42,591	10.184	**Coal**
6181	446	36,562	10.270	**Coal**
298	957	462	10.351	**Coal**
298	893	512	10.447	**Coal**
6179	615	33,377	10.664	**Coal**
6648	591	31,961	10.788	**Coal**
6179	615	36,122	10.828	**Coal**
52071	662	784	10.880	**Coal**
6179	460	39,767	10.934	**Coal**
6146	2,379	46,789	11.230	**Coal**
3497	1,186	24,136	11.244	**Coal**
6147	1,979	287,485	11.640	**Coal**
6183	410	551	11.797	**Coal**
55137	940	409	4.557	**NGCC**
55123	801	750	4.843	**NGCC**
55172	807	493	4.847	**NGCC**
55320	746	362	4.941	**NGCC**
55664	570	700	5.079	**NGCC**
55215	1,152	498	5.096	**NGCC**
55097	1,108	5012	5.155	**NGCC**
55501	1,370	178	5.511	**NGCC**
55062	939	372	5.607	**NGCC**
56350	580	5012	5.629	**NGCC**
55132	939	265	5.646	**NGCC**
55480	1,852	270	5.653	**NGCC**
55153	1,088	232	5.848	**NGCC**
56349	574	5,012	6.054	**NGCC**
55230	1,280	322	7.18	**NGCC**
58001	803	322	7.186	**NGCC**
7512	550	91,974	7.206	**NGCC**
55223	418	406	7.21	**NGCC**
55226	1,038	311	7.227	**NGCC**
55154	596	34,158	7.251	**NGCC**
7900	388	660	7.299	**NGCC**
55098	529	365	7.411	**NGCC**
55545	552	906	7.443	**NGCC**

55144	990	205*	7.679	**NGCC**
56806	537	4,645,628	7.836	**NGCC**
55091	1,734	2*	7.846	**NGCC**
55139	789	444	9.101	**NGCC**
3469	664	5,012	9.729	**NGCC**
3441	731	9,257,099	68.422	**NGCC**
4939	1,083	1,176,944	9.372	**NGST**
3628	100	108,488	11.004	**NGST**
3612	417	44,203	11.445	**NGST**
3601	144	88,355	11.69	**NGST**
3460	1,530	1,176,944	12.146	**NGST**
3601	144	77,242	12.38	**NGST**
3611	446	168,316	12.578	**NGST**
56708	155	302	12.879	**NGST**
56708	155	267	13.161	**NGST**
3548	321	653,679	13.197	**NGST**
3628	200	254,423	13.482	**NGST**
3548	405	390,498	13.507	**NGST**
3452	928	626,144	13.67	**NGST**
3612	252	24,026	13.887	**NGST**
3490	635	2,470,513	14.036	**NGST**
3628	66	318,704	14.26	**NGST**
3576	345	1,176,944	14.563	**NGST**
6243	105	212,126	14.777	**NGST**
3494	651	49,544	14.834	**NGST**
3508	1,176	49,544	14.834	**NGST**
3611	446	121,435	14.868	**NGST**
3507	239	3,334,496	15.024	**NGST**
3612	225	37,357	15.777	**NGST**
3504	704	2,020,760	15.868	**NGST**
3491	1,315	566,097	16.174	**NGST**
4266	126	49,544	17.22	**NGST**
3464	446	447	21.691	**NGST**
3468	826	1,176,944	48.621	**NGST**
3453	853	6,116,801	242.99	**NGST**

3601	351	415,839	417.031	NGST
***water withdrawal rates that were not gap filled (Plant 55144: natural gas combined cycle with recirculating cooling; Plant 55091: natural gas combined cycle with dry cooling).**				

Table 18: The Water Withdrawal Rate and the Nameplate Capacity of Both Nuclear Power Plants in the ERCOT System.

Power Plant Name	EIA Plant ID	Withdrawal Rate (gal/min)	Nameplate capacity (MW)	Water Withdrawal Rate (gal/MWh)
South Texas Project	6251	850,360	2,820	20,311
Comanche Peak	6145	1,918,000	2,350	54,976

Both of these nuclear power plants had a capacity factor of 0.90 in 2014, which was used to calculate the water withdrawal rate in the final column of Table 18.

3 CO_2-BES Coupled Power Cycle and Well Model Description and Results

We based the coupled power cycle and well model assumptions (e.g., turbine and pump efficiencies, pinch-point temperatures) off prior work [18].

3.1 Well Model

The pressure and temperature of the fluids throughout the injection and production wells is calculated numerically with 100 m long axial elements. The first law of thermodynamics, patched Bernoulli, and the conservation of mass equations are used to determine the state of fluid at each subsequent element (i+1), knowing the fluid properties at the current element (i) [18]:

$$h_i+gz_i= h_{i+1}+gz_{i+1} \tag{49}$$

$$P_i+\frac{\rho_i V_i^2}{2}+\rho_i gz_i= P_{i+1}+\frac{\rho_i V_{i+1}^2}{2}+\rho_{i+1} gz_{i+1}-\Delta P_{loss} \tag{50}$$

$$\Delta P_{loss}=f*\frac{L_{pipe}}{D^5}*\frac{8*\dot{m}^2}{\rho*\pi^2} \tag{51}$$

$$\dot{m}=\rho_i A V_i=\rho_{i+1} A V_{i+1} \tag{52}$$

Where the friction factor, f, was assumed to be 0.02 and the well diameter is 0.40 m. The downhole fluid state, obtained from the NUFT simulation results, were used as the starting element (i) for the CO_2 and brine wells (with the exception of the downhole injection temperatures, as described in power cycle model sections 3.2 and of 3.3 Appendix A), and we used this well model to determine the state of the fluid at throughout the production and injection wells.

3.2 Direct CO_2 Power Cycle Model

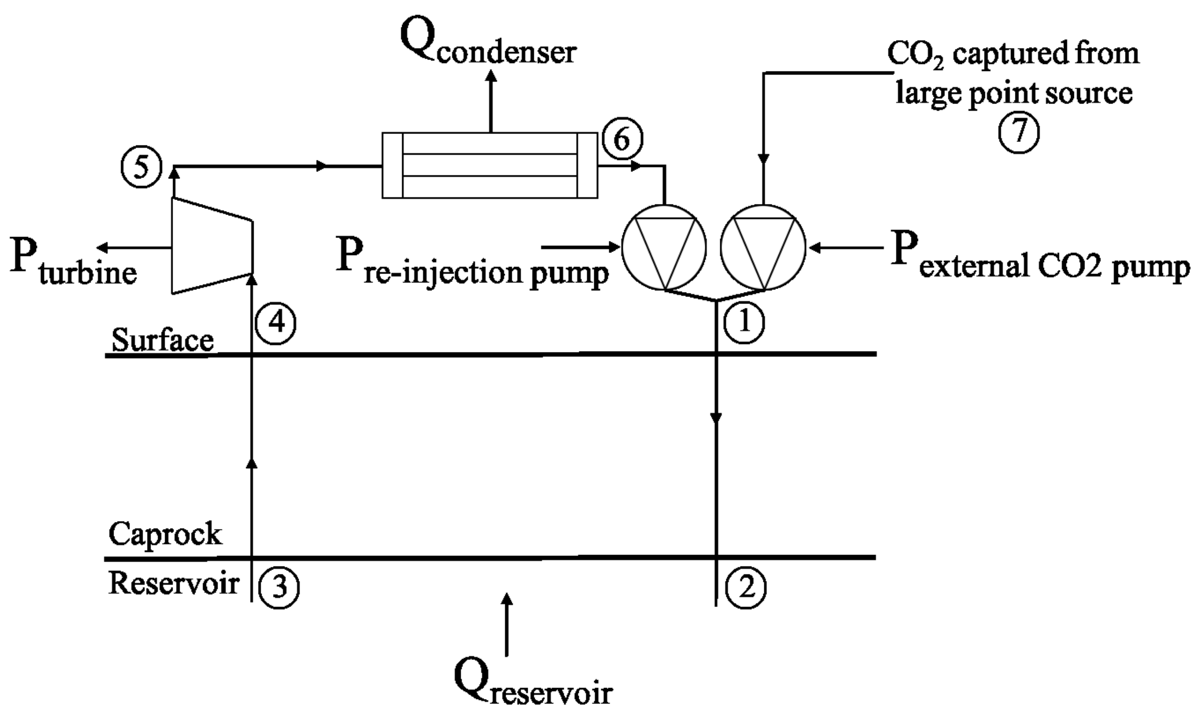

Figure 23: Direct CO_2 Power Cycle Component Diagram

CO_2 captured from large point sources is constantly injected (state 7) at a flowrate of 240 kg/s and we assume this captured CO_2 arrives at the CO_2-BES facility at 25 °C and 7.5 MPa. When the demand for electricity is greater than the supply, electricity can be generated by producing CO_2 at artesian flowrates (states 3 to 4) and expanding the hot CO_2 through a two-phase turbine with isentropic efficiency of 78% to generate electricity (states 4 to 5). The CO_2 is condensed at constant pressure to 25 °C (states 5 to 6). We assumed that this constant pressure was 50 kPa above the saturation pressure of CO_2 at 25 °C (P=6.48 MPa) to keep the fluid in liquid state. We used the regression equations from prior work [18] and assumed an ambient temperature of 15 °C to calculate parasitic loss fraction ($\lambda_{condenser}$), which was used to calculate the parasitic power required to run the condensing tower fan. After being condensed, the CO_2 is pressurized and re-injected into the reservoir (states 6 to 2), which is added to the fixed CO_2 injection flowrate of 240 kg/s. We assumed the re-injection pump has an isentropic efficiency of 90%.

When the demand for electricity is less than the supply, electricity can be stored from the grid by stopping the direct CO_2 power cycle and only operating the external CO_2 injection pump. We also assumed this pump has an isentropic efficiency of 90%.

We assumed that there are 10 CO_2 production and 10 CO_2 injection wells.

CO_2 entered the reservoir at a downhole temperature of 25 °C in the NUFT reservoir simulation [54]. We assumed that the temperature of CO_2 at state 6 and 7 is 25 °C, which results in a downhole temperature (state 2) greater than 25 °C because the temperature of CO_2 increases as it is compressed through the pump and down the well. Thus, compared to the NUFT simulations, this model extracts less thermal energy from the reservoir for the same flowrate and production temperature. So using the NUFT simulations in conjunction with our well and surface model provides a lower bound of power production. We also assume the increase in injection temperature in our power cycle model compared to the NUFT reservoir model does not substantially impact the pressure profile of the reservoir. However, the pressure differential from states 2 to 3 is dependent on the CO_2 temperature and will likely decrease as temperature decreases. Thus, we over-estimate reservoir pressure difference which results in under-estimated mass flowrate and our results provide a lower estimate of power production.

3.3 Indirect Brine Power Cycle Model

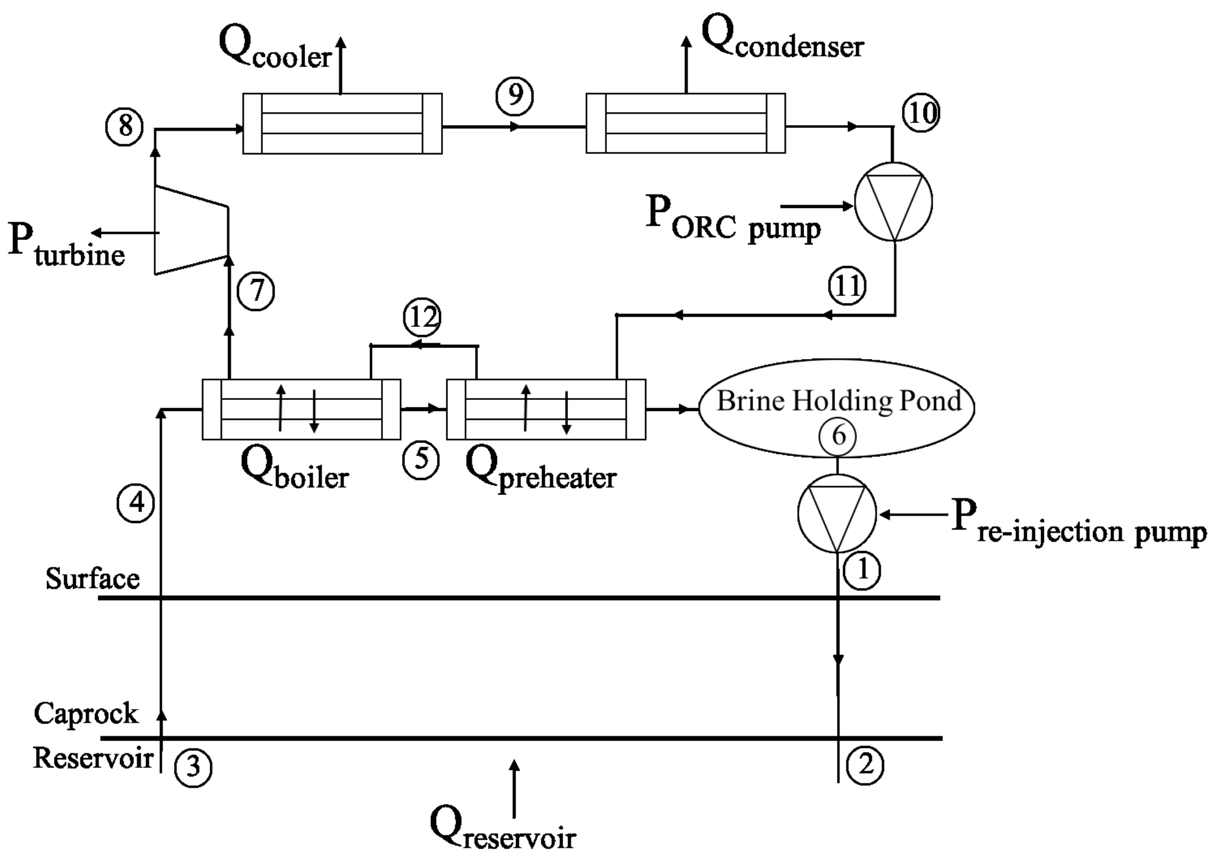

Figure 24: Indirect Brine Power Cycle Component Diagram.

When the demand for electricity is greater than supply, electricity can be generated with the indirect brine cycle by producing brine at artesian flowrates (state 3 to 4). The 10 MPa over-pressure of the reservoir induces a flow to the surface brine holding pond (state 6) at atmospheric pressure. Heat is isobarically transferred (states 4 to 6) from the brine to a secondary working fluid, which we assumed to be R245fa, and then the brine is held at the surface until the demand for electricity is less than the supply (state 6).

Within the secondary cycle, the heated R245fa is expanded through a turbine with an isentropic efficiency of 80% (states 7 and 8), cooled at constant pressure to a saturated vapor at a temperature of 7 ºC above ambient (states 8 to 9), condensed at constant pressure and temperature to a saturated liquid (states 9 to 10), and then pumped by a secondary ORC pump with an isentropic efficiency of 90% (states 10 to 11). The heat exchanger parasitic loss fractions ($\lambda_{condenser}$ and $\lambda_{condenser}$) used to calculate the parasitic power cooling and condensing fan requirements were calculated using the regression equations provided in prior work [18] and assuming an ambient temperature of 15 ºC.

We assumed that there are 19 brine production and 19 brine injection wells.

When the demand for electricity is less than the supply, electricity can be stored from the grid by stopping brine production and re-injecting the brine in the holding pond (states 6 to 1). We assumed the brine re-injection pump has an isentropic efficiency of 91% and that the fluid properties of the brine remain constant over time in the holding pond. Initially, all produced brine will be reinjected. However, once the desired reservoir overpressure of 10 MPa is reached, 6.6% of the produced brine is not re-injected and is permanently removed from the system to maintain the desired overpressure [54].

Our coupled power cycle and well model provided a brine downhole injection temperature of 61 ºC, due to the constraints of the power cycle (i.e., maintaining an isentropic re-injection pump efficiency of 91%). This downhole temperature is slightly less than the brine injection temperature in the NUFT simulations (65ºC), but because water is an incompressible fluid, and this is only a 4ºC difference, we do not believe the discrepancy will have substantial ramifications on the pressure differential from states 2 to 3 or the rate of geothermal heat depletion.

3.4 CO_2-BES Round Trip Efficiency Calculation

The round-trip efficiency of a bulk energy storage (BES) facility is typically defined as the electricity dispatched divided by the electricity stored:

$$\eta=\frac{\text{Electricity Dispatched}}{\text{Electricity Stored}}=\frac{D}{S} \tag{53}$$

Table 19 describes how each power cycle component operates when the CO_2-BES facility is storing and dispatching electricity, and equations 54 and 55 mathematically define the amount of electricity dispatched to the grid, D, and stored from the grid, S, respectively, in terms of the power required to run the cycle components.

Table 19: Power Cycle Component Operation During Storing (i.e., Charging) and Dispatching (i.e., Discharging) of CO_2-BES

	Indirect Brine Cycle	**Direct CO_2 Cycle**
Storing electricity	Prod. Well Flowrate: 0 kg/s Inj. Well Flowrate: X* Re-injection Pump: On Boiler + Preheater: Off Turbine: Off Cooler + Condenser: Off ORC Pump: Off	Prod. Well Flowrate: 0 kg/s Inj. Well Flowrate: 240 kg/s External CO_2 Pump: On Re-injection pump: Off Turbine: Off Condenser: Off
Dispatching electricity	Prod. Well Flowrate: artesian rate, X Inj. Well Flowrate: 0 kg/s Re-injection Pump: Off Boiler + Preheater: On Turbine: On Cooler + Condenser: On ORC Pump: On	Prod. Well Flowrate: thermosiphon rate, Y Inj. Well Flowrate: 240 kg/s + Y External CO_2 Pump: On Re-injection pump: On Turbine: On Condenser: On

***After the desired overpressure of 10 MPa is reached, this value becomes 0.934X because 6.6% of the produced brine is permanently removed from the system to maintain the overpressure.**

$$D=P_{\text{brine turbine}}-P_{\text{brine cool+condensing fans}}-P_{\text{ORCpump}}+P_{\text{CO2 turbine}}-P_{\text{CO2 condensing fan}}-P_{\text{external CO2 pump}}-P_{\text{CO2 re-inj pump}} \tag{54}$$

$$S = P_{\text{brine re-injection pump}} + P_{\text{external CO2 pump}} \quad (55)$$

Figure 25 shows the round-trip efficiency of the CO_2-BES facility over the lifetime of the facility (i.e., Equation 54 divided by Equation 55).

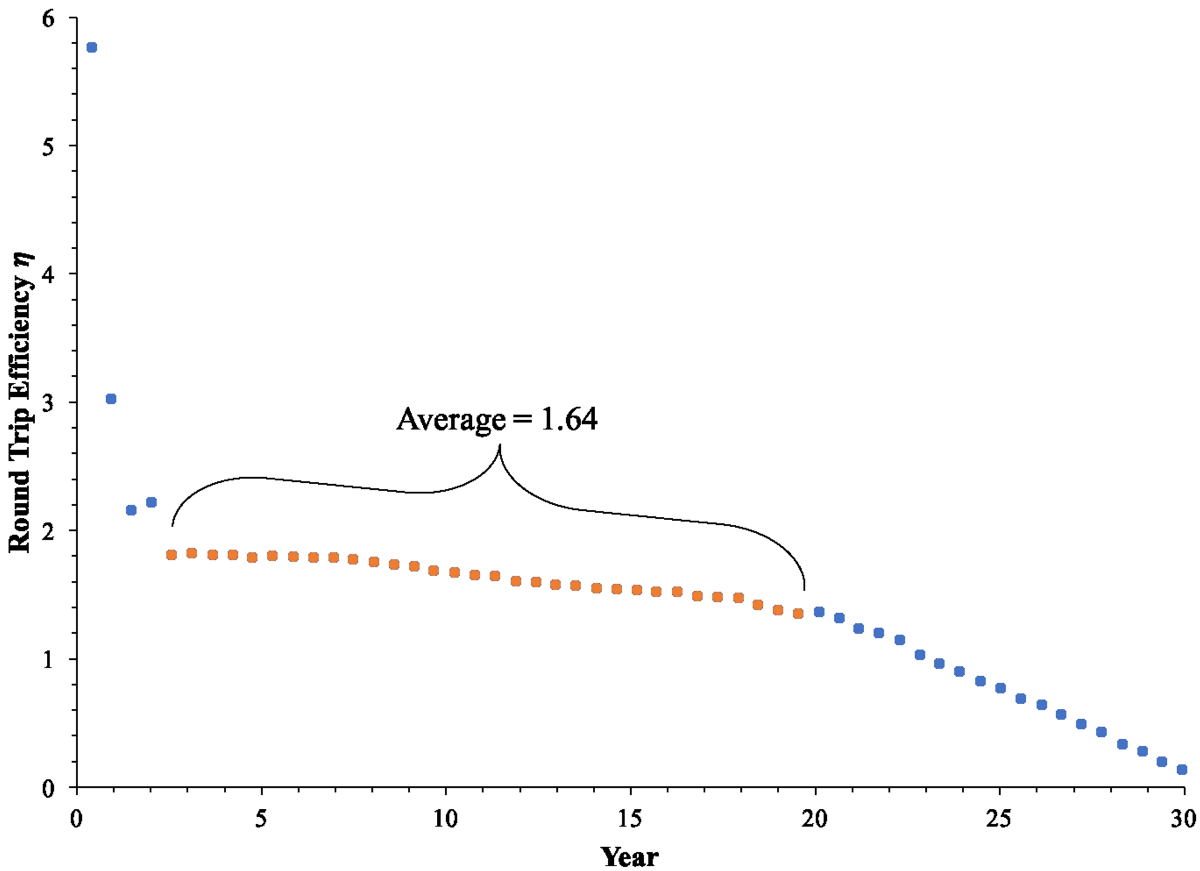

Figure 25: The Round-Trip Efficiency of the CO_2-BES Facility Over the Lifetime Of the Facility, Assuming Continuous Operation

The round-trip efficiency decreases throughout the lifetime of the facility due to the temperature drawdown of the geothermal reservoir. In the MILP, we used a round-trip efficiency of 1.64, which is the average round-trip efficiency from after the CO_2-BES facility was "primed" up to 20 years, which is highlighted in orange in Figure 25.

The CO_2-BES round-trip efficiency is likely greater than what is shown in Figure 25 because the NUFT simulations do not model CO_2-BES operation perfectly and the CO_2 and brine production flowrates were not optimized to maximize performance. For both the CO_2 and brine systems, an increase in power could be achieved by reducing the system mass flowrate. However, we did not re-run the NUFT simulation nor optimize the production flowrates because it was beyond the scope of this study.

Also, in the NUFT simulation, CO_2 and brine are continuously produced, CO_2 is constantly re-injected, and the produced brine remains in the holding pond for 12 hours before being re-injected [54]. During CO_2-BES operation, the timing of the charging and discharging cycles would be dependent on the price signals from the Independent System Operator (ISO); CO_2 and brine would not be constantly produced. It is unlikely that electricity would be constantly produced and as a consequence, the temperature drawdown of the reservoir would likely occur at a slower pace than the NUFT simulation results suggest. Thus, the round-trip efficiency is likely much higher than 1.67. Further, it may also be possible to reconfigure the well-design to increase the power output, which would also increase the round-trip efficiency compared to what is shown in Figure 25, but this was also outside the scope of this study.

3.5 CO_2-BES Water Intensity Calculation

In a CO_2-BES facility, water evaporates in the cooling and condensing towers as it cools the working fluid. The wet cooling tower makeup water rate can be estimated as the mass rate required if all the rejected heat were to vaporize water. Thus, we used equation 56 to estimate the amount of water required for cooling a CO_2-BES facility, where W is the power transferred from the working fluid and λ_v is the latent heat of vaporization of water at atmospheric pressure (2,257.92 kJ/kg).

$$\dot{m}_{\text{cooling water}}=\frac{W}{\lambda_v} \tag{56}$$

The total amount of water required for cooling is the sum of the cooling water from the CO_2 cycle condensing tower, brine cycle cooling tower, and brine cycle condensing tower. The water intensity, shown in Figure 26, was determined by dividing this sum by the amount of electricity dispatched by the CO_2-BES facility.

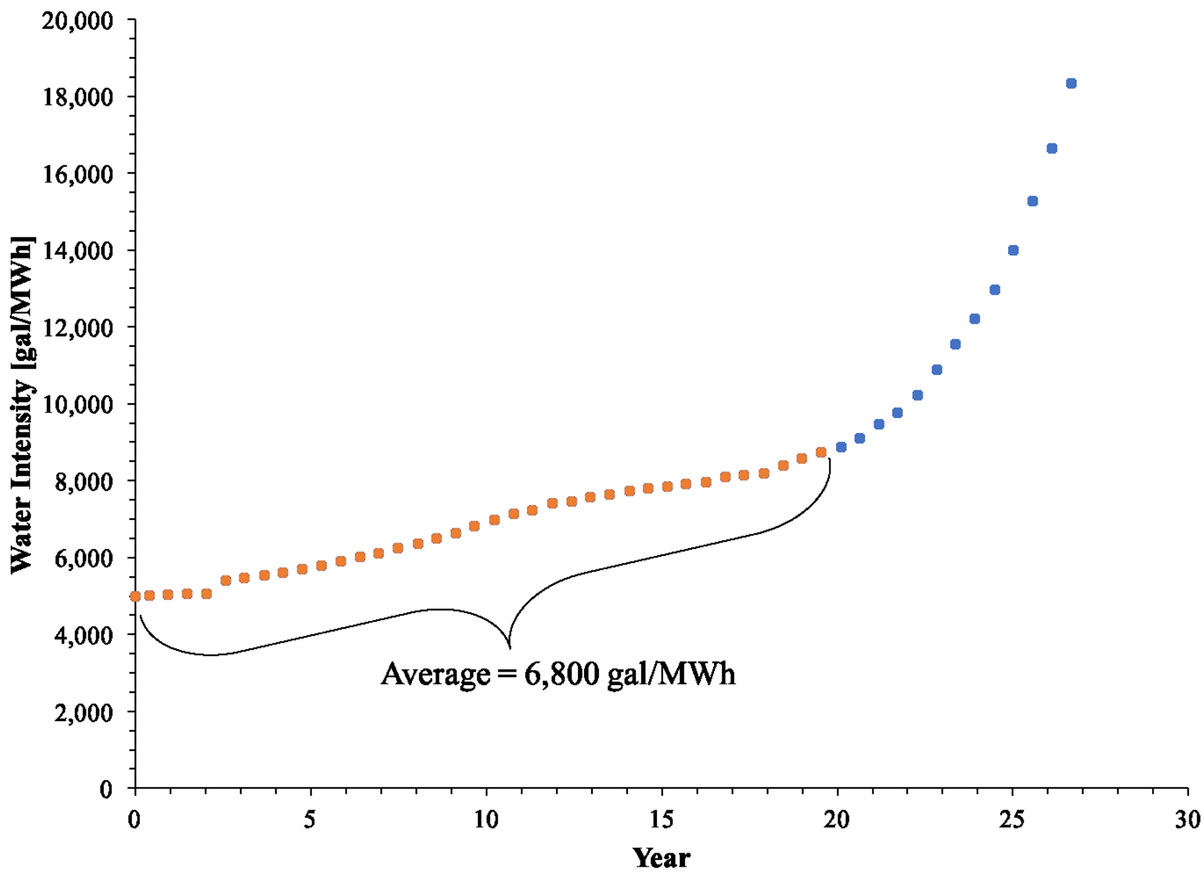

Figure 26: Water Intensity of the CO_2-BES Facility when Operating to Dispatch Electricity

The water intensity increases throughout the lifetime of the facility largely because the amount of electricity dispatched by the CO_2-BES facility (the denominator) decreases with time while the heat rejection remains roughly constant. We used a value of 6,800 gal/MWh in this study, which is the rounded average of the first 20 years of data, highlighted in orange in Figure 26. We neglected the water losses due to drift (entrainment of water into the air in the towers) and blowdown (water in the towers that is used for cleaning, not cooling) in our approximation.

4 Initial Bounding Analysis

The four results most pertinent to this study are how (1) the deployment of BES decreases the system-wide CO_2 emissions, (2) how it decreases the amount of water required by the system, (3) the value that BES has to reducing CO_2 emissions, and (4) the value it has for reducing water requirements. Each of these results varied based on the CO_2 price, water price, and minimum and maximum uncertain parameter, and the twelve days we chose were the days that the mean, median, and standard deviation were close to the mean, median, and standard deviation of results when all days of the year were included. For example, the distribution of decreases in water requirements facilitated by BES availability for Jan. 4th was very similar to the distribution of decreases in water requirements when all days of the year were included (Table 20). We reduced the bounds of the distributions that included the results over the year to [-5,5] for the change in water requirements and the change in CO_2 emissions, [-500,500] for the value of reducing CO_2, and [-2000,15000] for the value of reducing water requirements because extreme values were influencing the mean, mean, and standard deviations.

Table 20: The Mean, Median, and Standard Deviation of Each Selected Day Compared to the Entire Year.

			$0/tCO$_2$				$100/tCO$_2$		
Result	**P_{H2O} ($/gal)**		**Mean**	**Median**	**Std.**		**Mean**	**Median**	**Std.**
Decrease [Mgal/MWh]	**0**	Year	0.070	0.000	0.515	Year	0.175	0.016	0.753
		Jan. 4	0.072	0.000	0.506	Mar. 10	0.162	0.000	0.816
Value [$/MWh]	**0**	Year	0.000	0.000	0.000	Year	0.000	0.000	0.000
Decrease [tCO$_2$/MWh]	**0**	Year	-0.06	0.000	0.620	Year	0.440	0.510	0.66
		Mar. 12	-0.052	0.000	0.504	May 10	0.493	0.485	0.509
Value [$/MWh]	**0**	Year	0.00	0.00	0.00	Year	43.7	50.7	65.97
						July 19	50.0	51.2	47.440
Decrease [Mgal/MWh]	**0.10**	Year	0.038	0.024	0.068	Year	0.039	0.024	0.068
		Feb. 4	0.024	0.024	0.001	Aug. 17	0.025	0.025	0.018
Value [$/MWh]	**0.10**	Year	2634	2382	2673	Year	2616	2371	2670.9
		May 13	2873	2924	2649	May 24	2360	2310	92.896
Decrease [tCO$_2$/MWh]	**0.10**	Year	0.270	0.283	0.609	Year	0.205	0.205	0.598
		Aug. 14	0.280	0.286	0.075	July 12	0.210	0.207	0.049
Value [$/MWh]	**0.10**	Year	0.000	0.000	0.000	Year	20.5	20.5	59.82
						Dec. 19	20.7	21.2	4.606

5 Fossil-Fuel Price Distribution Used in the Monte Carlo Approach

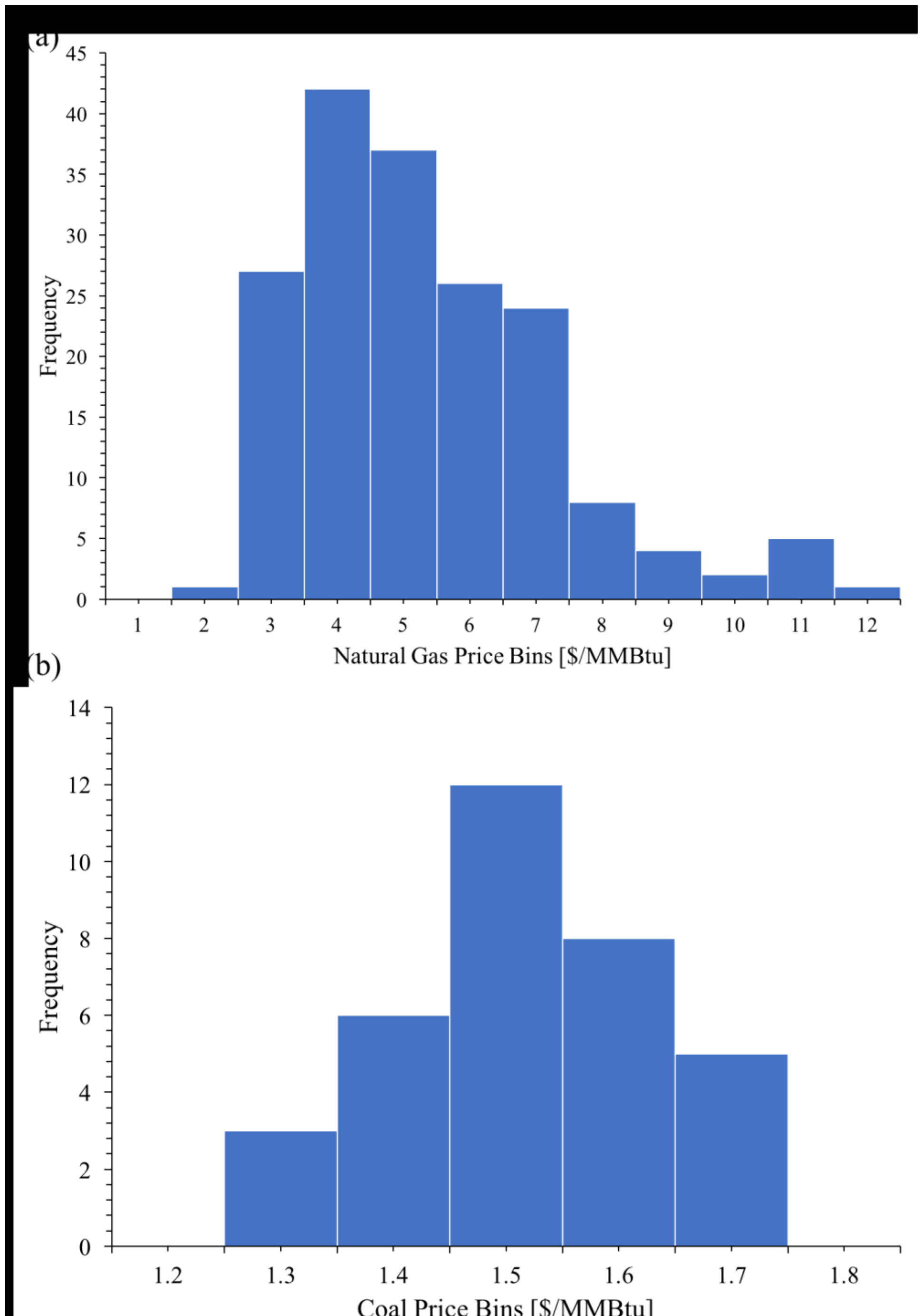

Figure 27: Distributions of (a) Natural Gas Prices [127] **and (b) Coal Fuel Prices** [126] **That Were Sampled in the Monte Carlo Analysis.**

6 Results

6.1 Change in System-Wide CO_2 Emissions and System-Wide Water Requirements as a Result of BES Deployment

6.1.1 Increased Utilization of Natural Gas Power Capacity

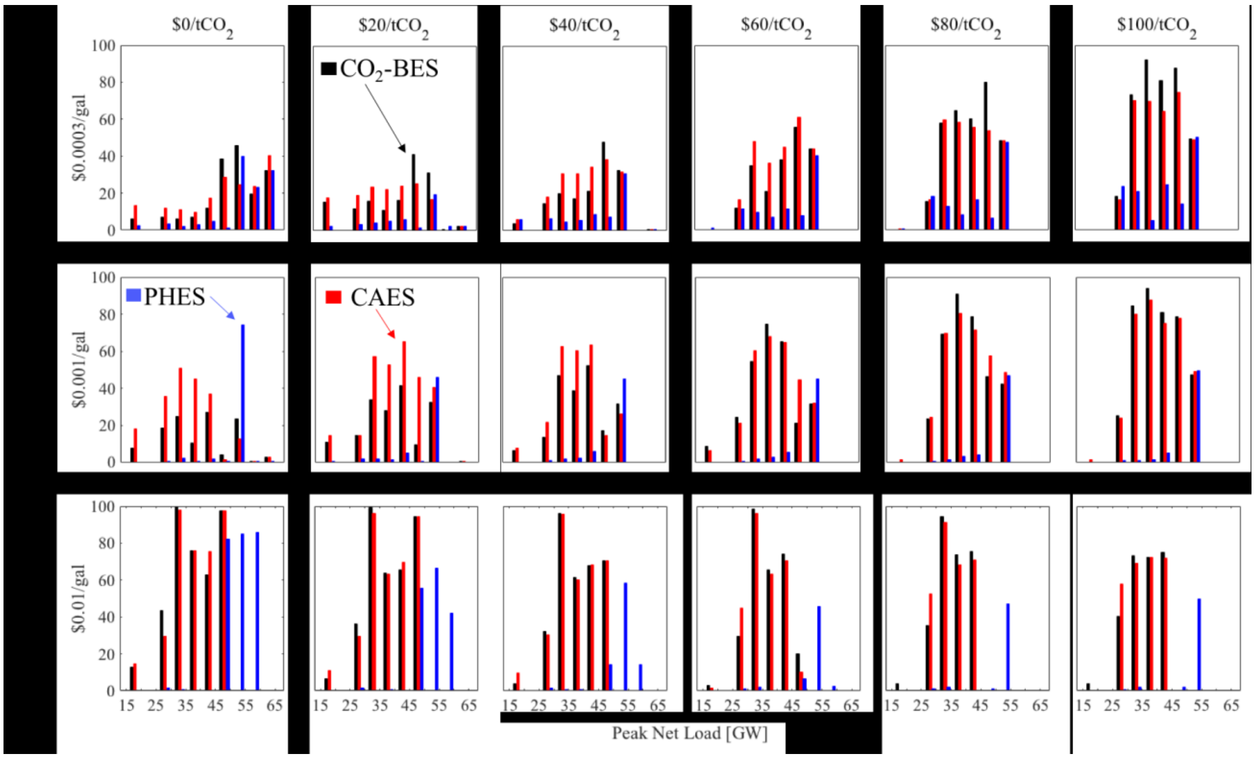

Figure 28: Percentage of Combinations in Which the Deployment of BES Resulted in an Increase in Natural Gas Capacity Utilization. There were no combinations of days and wind generation scenarios that resulted in a peak net load between 20 and 25 GW.

As shown in Figure 28, the increased utilization of natural gas power capacity occurred most often when the peak net load was between 25 and 45 GW, where coal EGUs would be dispatched if BES was not used. For example, coal power capacity was displaced ~94% of the time when the utilization of natural gas power capacity increased due to the dispatch of CO_2-BES or of CAES. As a result, the system-wide CO_2

emissions tended to decrease because the natural-gas EGUs in this portion of the dispatch order have lower CO_2 intensities than the coal EGUs that were displaced.

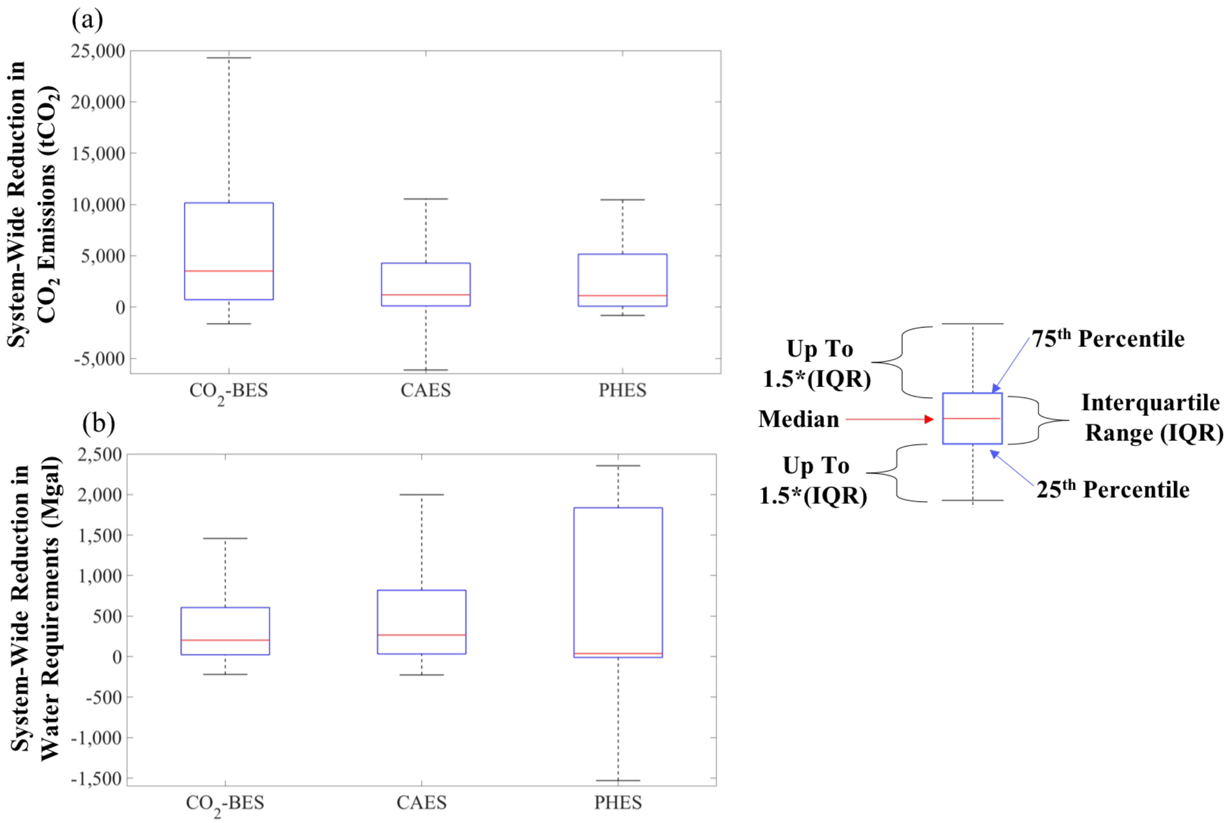

Figure 29: BES Dispatch that Increased the Utilization of Coal Power Capacity. The box and whisker plots represent the distribution of results across all critical parameters and representative days that we optimized. For ease of presentation, extreme results (those outside of 1.5·IQR + 75th percentile or 25th percentile - 1.5·IQR) are not shown.

As Figure 29(a) shows, CO_2-BES engendered the highest median decrease in system-wide CO_2 emissions (3,524 tCO_2, compared to 1,197 tCO_2 when CAES was dispatched and 1,121 tCO_2 when PHES was dispatched) and the largest range of the reductions in CO_2 emissions across all of the combinations:

the interquartile range (IQR) was between 773 and 10,153 tCO_2 with CO_2-BES, between 118 and 4,286 tCO_2 with CAES, and between 91 and 5,159 tCO_2 with PHES.

System-wide water requirements also tended to decrease because the natural gas EGUs that were dispatched require less water than the coal EGUs that would have been dispatched. Figure 29(b) shows that the median decrease in system-wide water requirements with CAES dispatch (267 Mgal) was higher than with CO_2-BES dispatch (203 Mgal) or with PHES dispatch (38 Mgal) because CAES has a lower water intensity than CO_2-BES or PHES. But PHES consistently enabled larger reductions in system-wide water requirements with less sensitivity to the critical parameters; the IQR for PHES was between -9.9 and 1,836 Mgal, whereas the IQR for CO_2-BES was between 23 and 606 Mgal and between 33 and 819 Mgal for CAES.

6.1.2 Increased Utilization of Coal Power Capacity

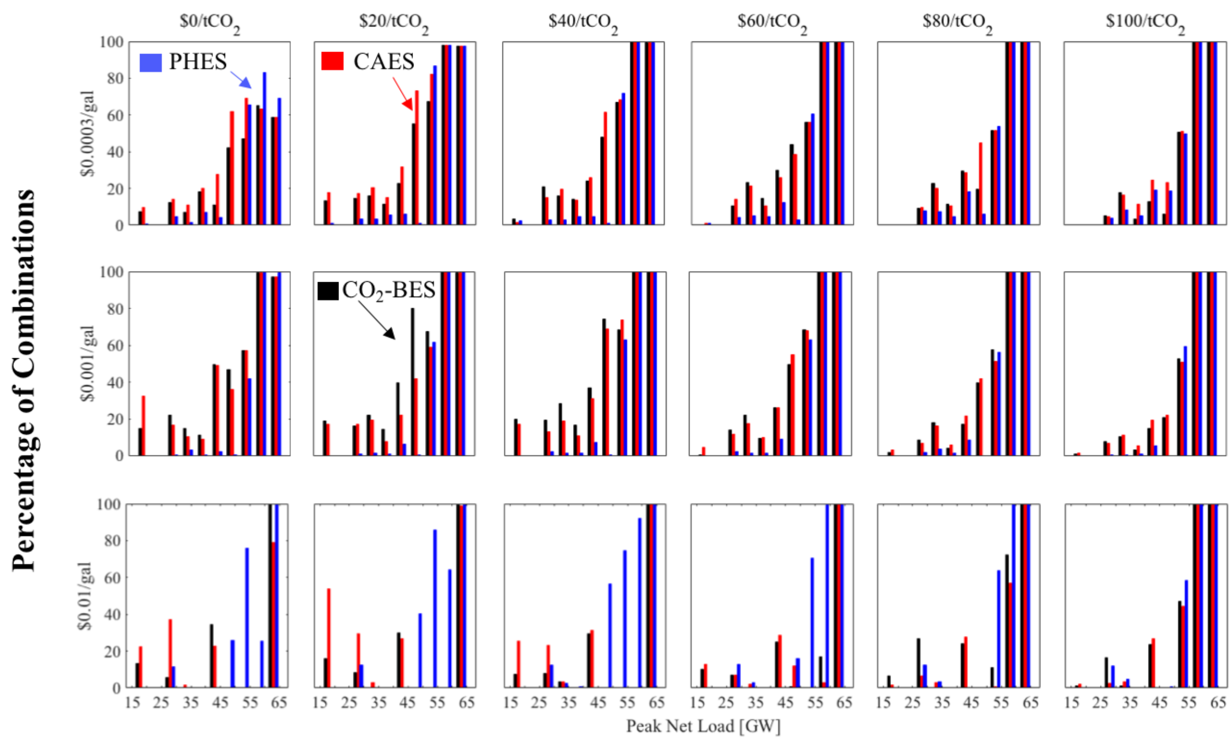

Figure 30: Percent of Combinations in Which the Deployment of BES Results in an Increase in the Utilization of Coal Power Capacity. There were no combinations of days and wind generation scenarios that resulted in a peak net load between 20 and 25 GW.

As shown in Figure 30, the utilization of coal power capacity increased if (a) the peak net load was less than 50 GW and coal EGUs have lower operating costs than natural gas EGUs, or (b) the peak net load was greater than 50 GW, where peaking natural gas EGUs with high heat rates (thus CO_2 intensities) and high water intensities would otherwise have been dispatched. System-wide CO_2 emissions increased when the peak net load was below 50 GW because the natural gas EGUs that were displaced have lower CO_2 intensities than the coal EGUs that were dispatched. In contrast, when the peak net load was above 50 GW, system-wide CO_2 emissions tended to decrease because the peaking natural gas EGUs that were displaced had higher CO_2 intensities than the coal EGUs that displaced them.

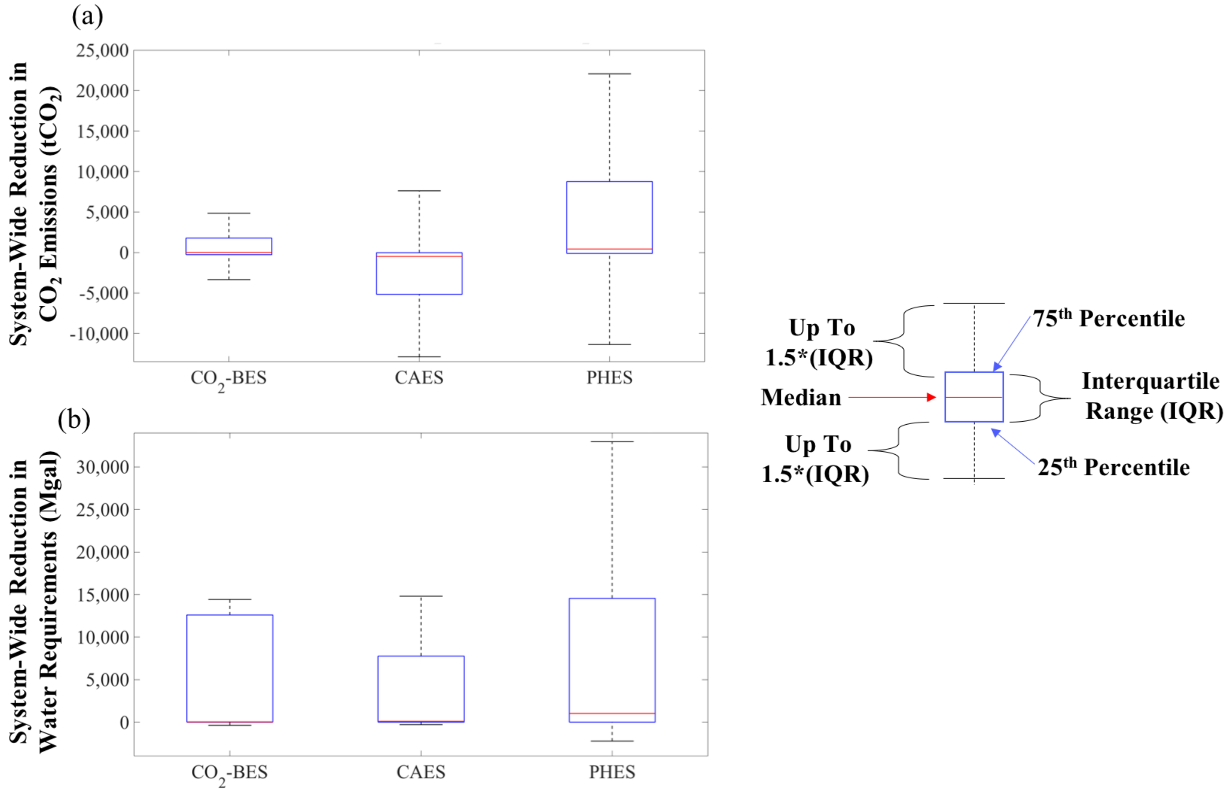

Figure 31: BES Dispatch that Increased the Utilization of Coal Power Capacity. The box and whisker plots represent the distribution of results across all critical parameters and representative days that we optimized. For ease of presentation, extreme results (those outside of 1.5·IQR + 75th percentile or 25th percentile - 1.5·IQR) are not shown.

Figure 31(a) shows that system-wide CO_2 emissions were likely to increase with the dispatch of CAES, in part because the technology emits CO_2; the IQR is between -5,170 and -25 tCO_2, with a median of -494 tCO_2. In contrast, there is likely to be a large decrease in system-wide CO_2 emissions when PHES was dispatched—the median decrease is 429 tCO_2, with an IQR between -118 and 8,759 tCO_2—because PHES is dispatched less often than CO_2-BES and CAES when the peak net load is less than 50 GW.

As shown in Figure 30, the increase in the utilization of coal power capacity occurred more often when the peak net load was above 50 MW than when the peak net load was below 50 MW. As a result, as shown

Figure 31(b), system-wide water requirements tended to decrease because the water-intense peaking natural gas EGUs were displaced by less water-intense coal EGUs. The reductions in system-wide water requirements could be large; with CO_2-BES the median reduction was 37 Mgal (IQR between -0.2 and 12,597 Mgal) and with CAES the median reduction was 105 Mgal (IQR between 1.5 and 7,762 Mgal). The largest reduction in system-wide water requirements occurred when PHES was used, where the median decrease was 1,029 Mgal amidst an IQR that was between 3.7 and 14,549 Mgal. The large reduction in system-wide water requirements when PHES was dispatched occurred because nuclear power plants were displaced when the peak net load was between 50 and 60 MW and the water price was high ($0.001/gal). In contrast, CAES and CO_2-BES are located in a different part of the dispatch order than PHES and therefor nuclear power capacity was not displaced.

6.1.3 Increased Utilization of Wind Power Capacity

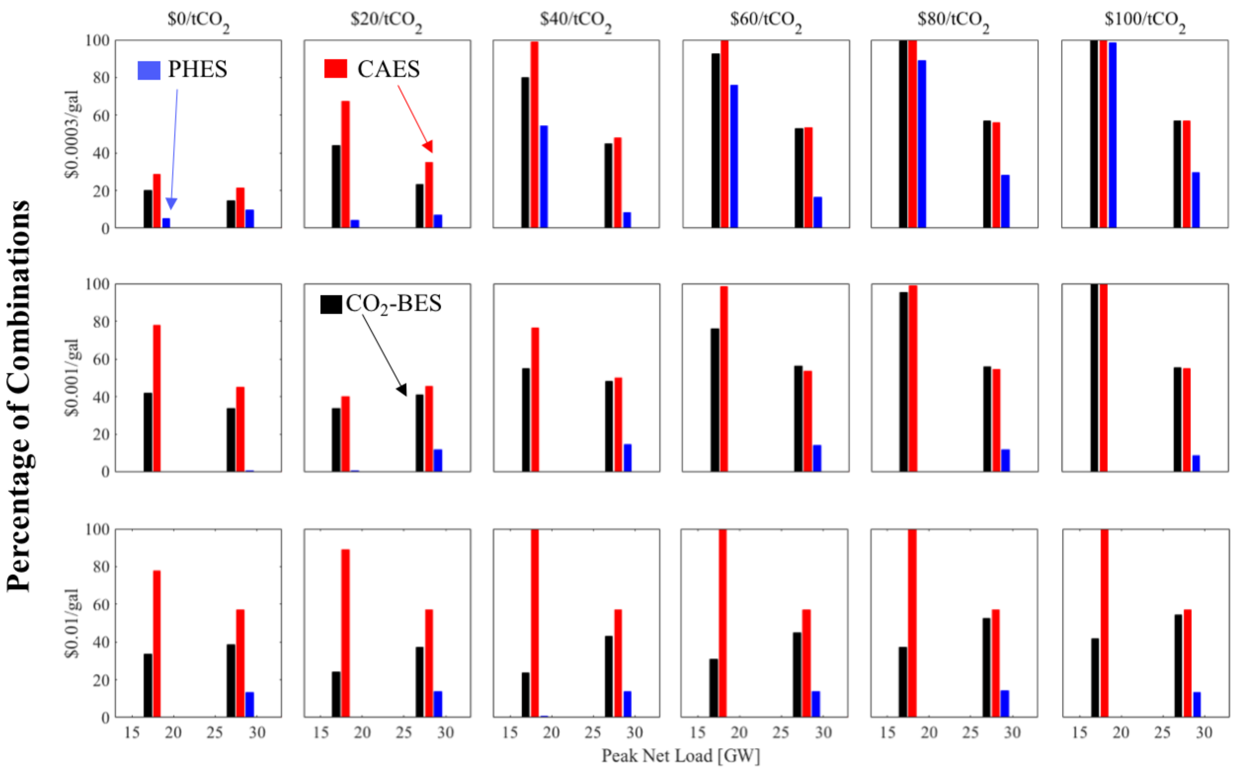

Figure 32: Percent of Combinations in Which BES Results in an Increase in the Utilization of Wind Power Capacity. For ease of presentation, the x-axis upper limit is 30 GW. There were no combinations of days and wind generation scenarios that resulted in a peak net load between 20 and 25 GW.

As shown in Figure 32, in the 44% wind generation scenario, BES time-shifted some of the wind-generated electricity on windy days with little demand (i.e. the net load was negative), and dispatched it later when the net load was positive. This time-shifting occurred more often at higher CO_2 prices. Since coal EGUs and natural gas EGUs that emit CO_2 were often displaced, system-wide CO_2 emissions typically decreased.

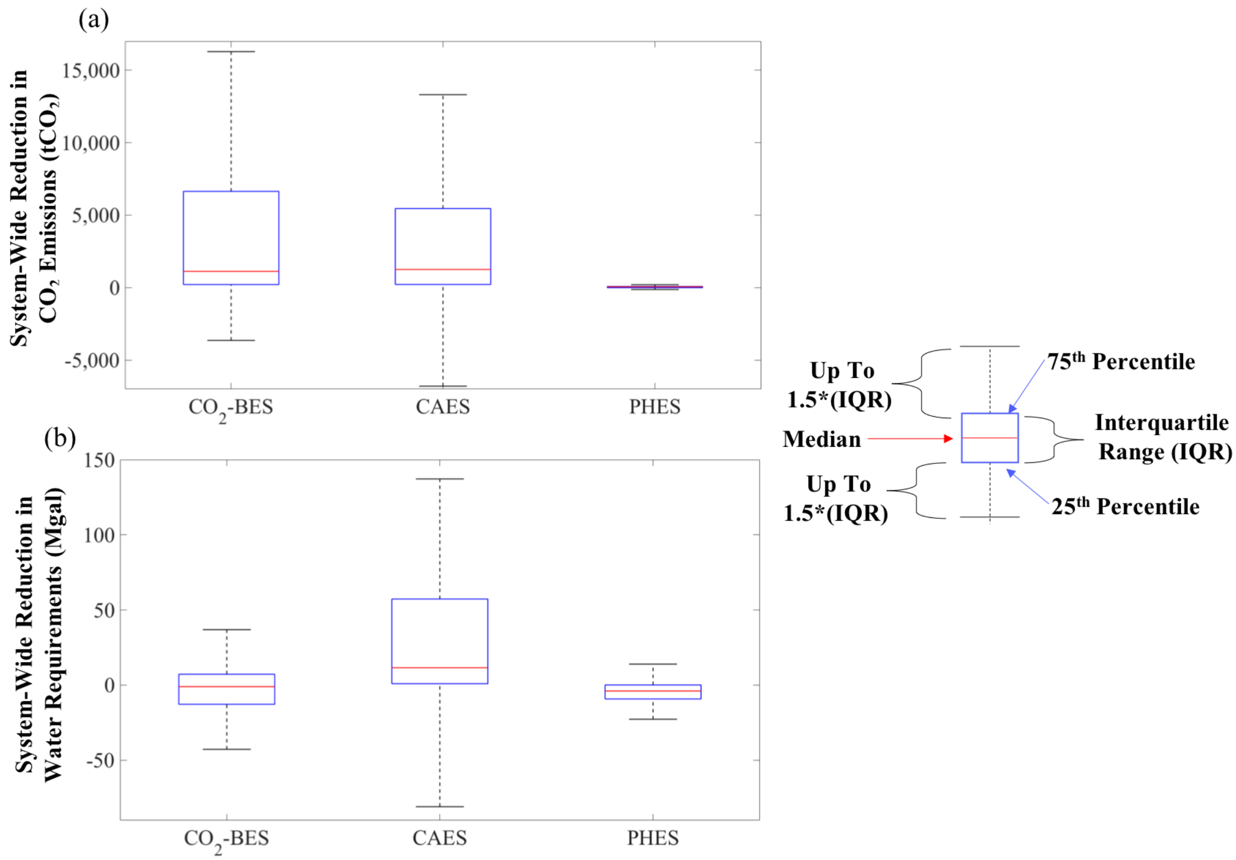

Figure 33: BES Deployment that Increased the Utilization of Wind Power Capacity. The box and whisker plots represent the distribution of results across all critical parameters and representative days that we optimized. For ease of presentation, extreme results (those outside of 1.5·IQR + 75th percentile or 25th percentile - 1.5·IQR) are not shown.

Figure 33(a) shows that the median decrease in CO_2 emissions was essentially the same for CO_2-BES (1,125 tCO_2) and CAES (1,157 tCO_2), amidst a similar range of uncertainty (the IQR was between 211 and 6,643 tCO_2 for CO_2-BES and between 219 and 5,458 tCO_2 for CAES). The median decrease in system-wide CO_2 emissions was smaller when PHES was dispatched (60.4 tCO_2), because PHES requires a lot of water and was thus expensive to operate. As a consequence, PHES tended to be dispatched more often at levels below 1 MWh than above 1 MWh, which can be seen in Table 5 of Chapter Two, and thus the time-shifting of wind-generated electricity by PHES did not reduce system-wide CO_2 emissions as much as with the other BES technologies.

As shown in Figure 32, the utilization of wind power capacity increased more often at high water prices because the coal EGUs and the natural gas EGUs became more expensive to operate. Even though wind-generated electricity requires little water, the water requirements of CO_2-BES or PHES offset the decrease in water requirements from the water-intensive coal EGUs and natural gas EGUs that were displaced. The IQR for the system-wide reduction in water requirements was between -12.6 and 7.2 Mgal for CO_2-BES (median, -1.0 Mgal), and -9.2 and 0.1 Mgal for PHES (median, -3.9 Mgal). Since these BES technologies were dispatched less often than CAES, they were less likley to reduce system-wide water requirements. In addition, CAES technology requires less water than CO_2-BES or PHES, and was thus the only BES technology that reliably engendered a decrease in system-wide water requirements: median was 11.5 Mgal, IQR is 0.9 and 57.3 Mgal.

6.1.4 Decreased Utilization of Nuclear Power Capacity

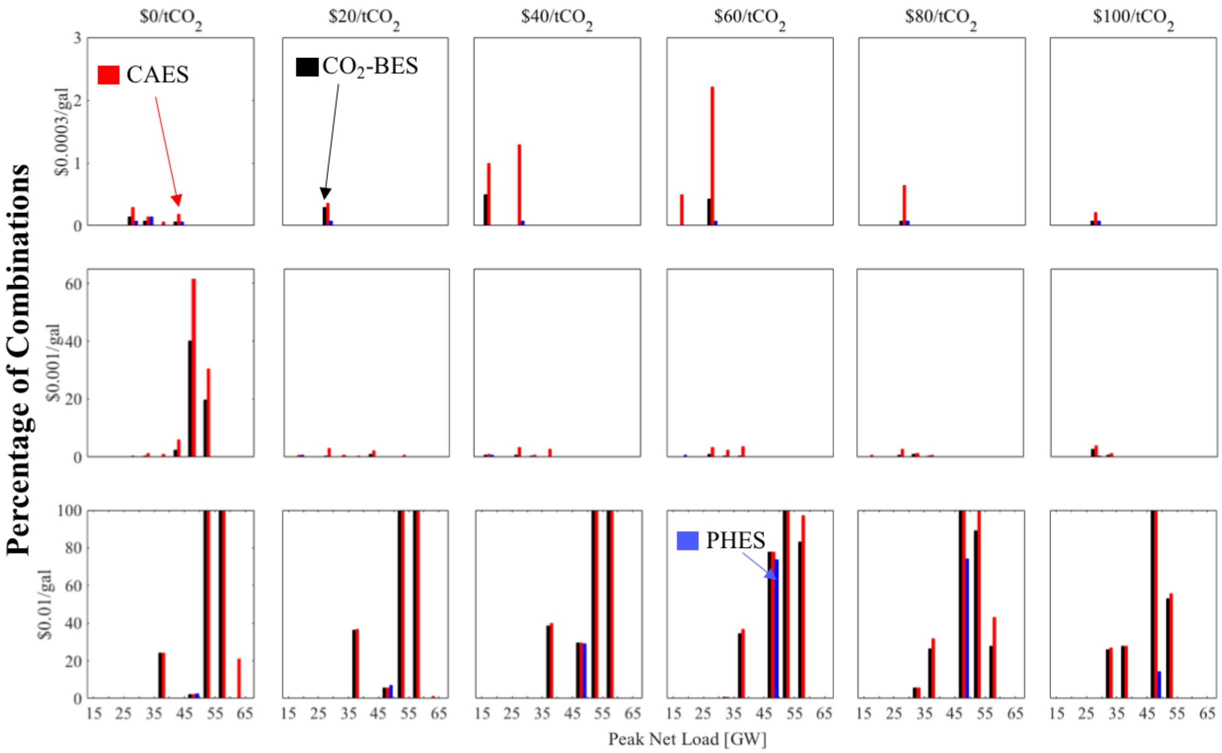

Figure 34: Percentage of Combinations in Which BES Results in a Displacement of Nuclear Power. The upper limit of the y-axis change based on water price to improve resolution. There were no combinations of days and wind generation scenarios that resulted in a peak net load between 20 and 25 GW.

When the peak net load was high (>50 GW), nuclear capacity was often dispatched to meet demand because it was cost-effective. But when the CO_2 price was low, BES dispatch enabled the displacement of nuclear power capacity by coal EGUs and natural gas EGUs. Less often, as shown in Figure 34, nuclear power capacity was also displaced when the peak net load was less than 50 GW and when the CO_2 price was high.

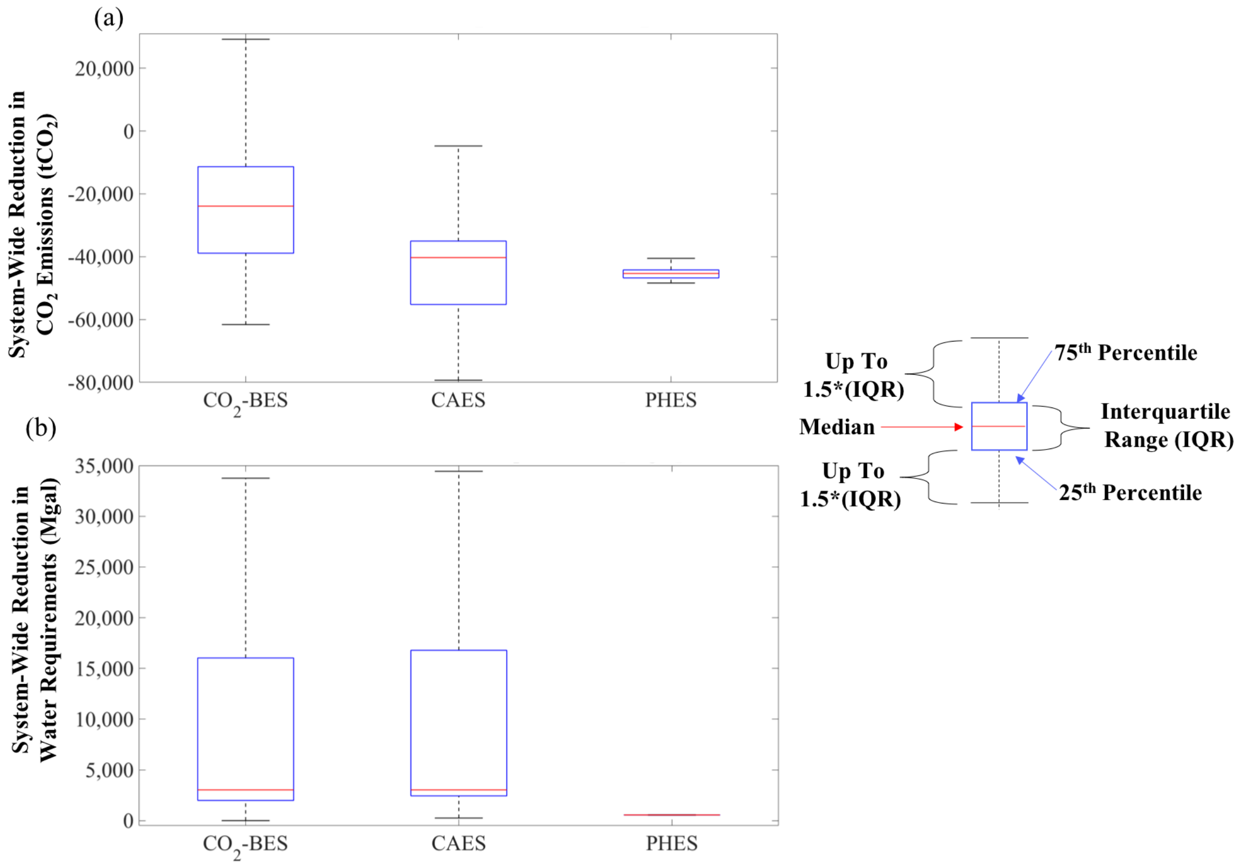

Figure 35: BES Dispatch that Decreased the Utilization of Nuclear Power Capacity. The box and whisker plots represent the distribution of results across all critical parameters and representative days that we optimized. For ease of presentation, extreme results (those outside of 1.5·IQR + 75th percentile or 25th percentile - 1.5·IQR) are not shown.

Overall, system-wide CO_2 emissions increased the least with CO_2-BES (median 23,897 tCO_2; IQR between 11,350 and 38,882 tCO_2), in part because CO_2-BES does not emit CO_2. The dispatch of PHES had the highest median increase in system-wide CO_2 emissions, but the smallest IQR (between 44,221 and 46,749 tCO_2) because it was only dispatched when the peak net load was less than 50 GW.

The decrease in the utilization of nuclear power capacity by the increased utilization of coal and natural gas capacity also occurred when the water price was high. As a result, system-wide water requirements decreased because the coal EGUs and the natural gas EGUs have lower water intensities than the nuclear power plants. The decrease with CO_2-BES was roughly the same as with CAES, mostly because the nuclear power plants must be dispatched at full capacity; as shown in Figure 35(b), the median was 3,026 Mgal for CO_2-BES and 3,029 Mgal for CAES, with IQRs between of 1,984 and 16,028 Mgal (CO_2-BES) and 2,432 and 16,785 (CAES).

6.2 Summary of Changes in System-Wide CO_2 Emissions and Water Requirements for Each BES Technology

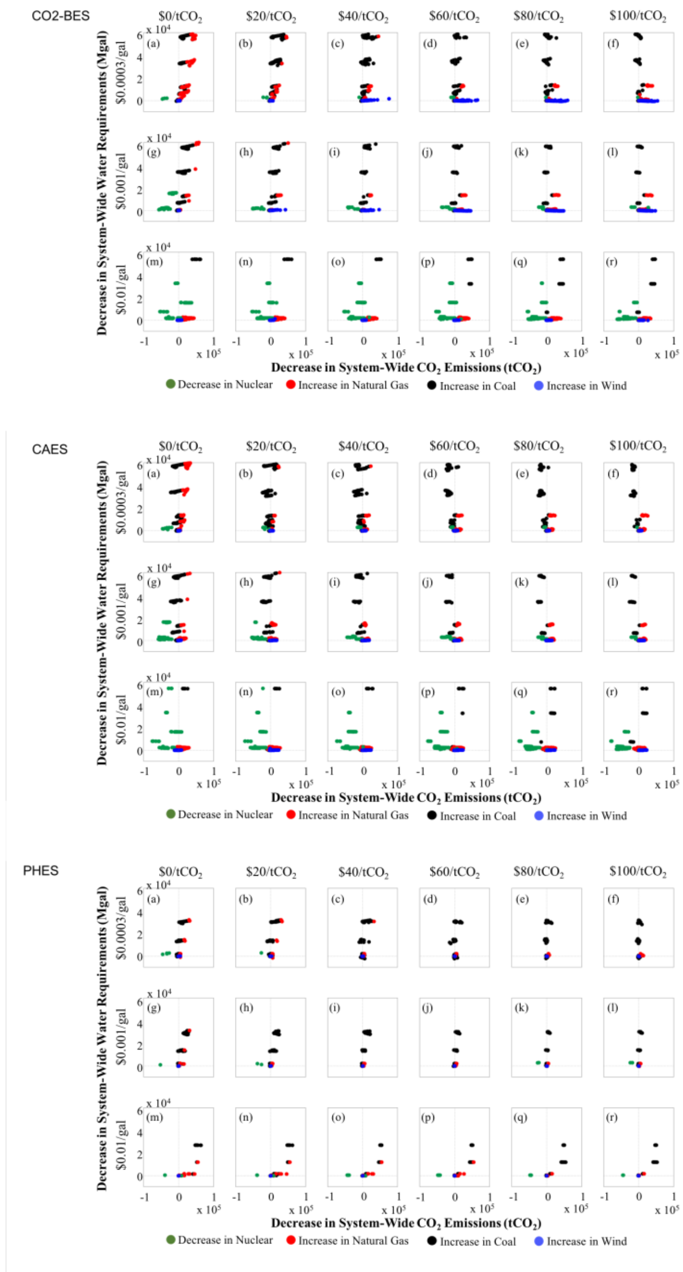

Figure 36: Effect of the Dispatch of BES on System-Wide CO_2 Emissions and System-Wide Water Requirements.

6.3 Summary of Changes in System-Wide CO_2 Emissions and Water Requirements as a Function of Wind Generation Scenario

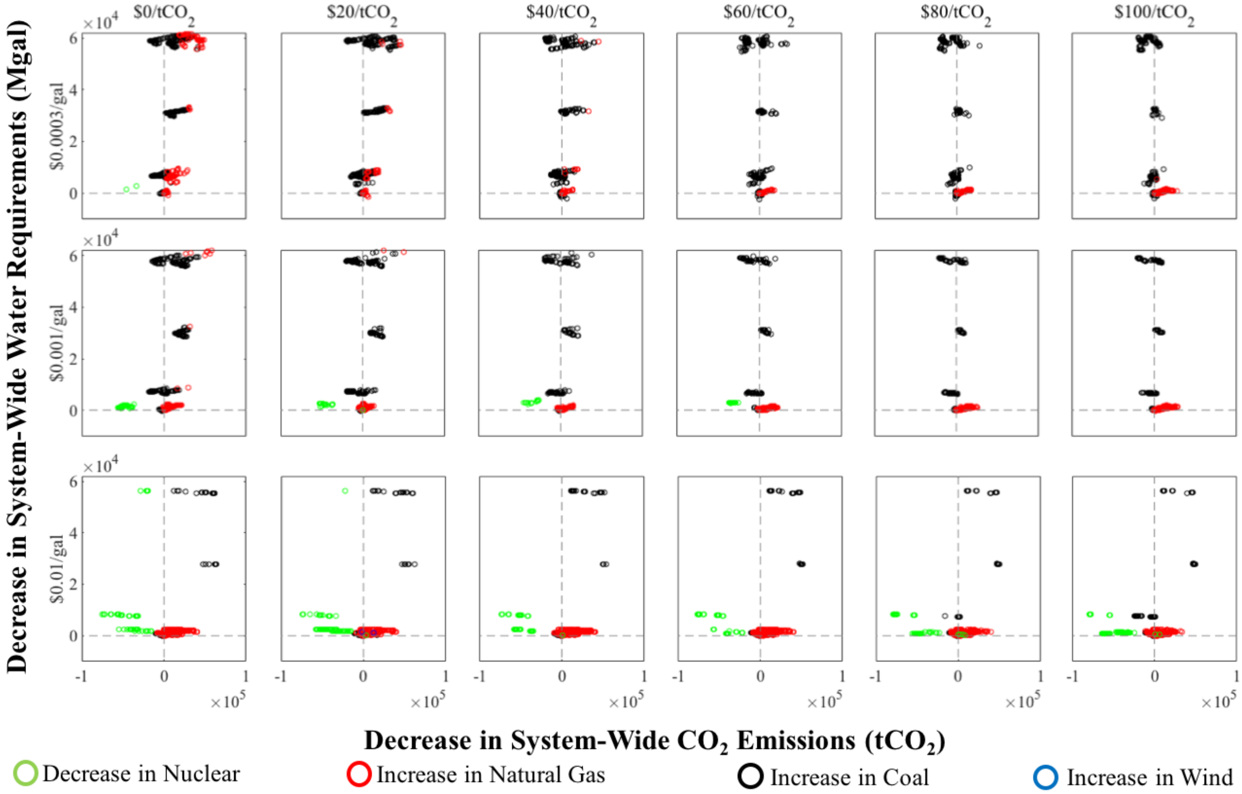

Figure 37: Effect of the Deployment of BES Due to Changes in the Dispatch Order When Wind Generation is Sufficient to Meet 11% of Total Demand. Markers to the right of the vertical line indicate a decrease in system-wide CO_2 emissions. Markers above the horizontal line indicate a decrease in system-wide water requirements.

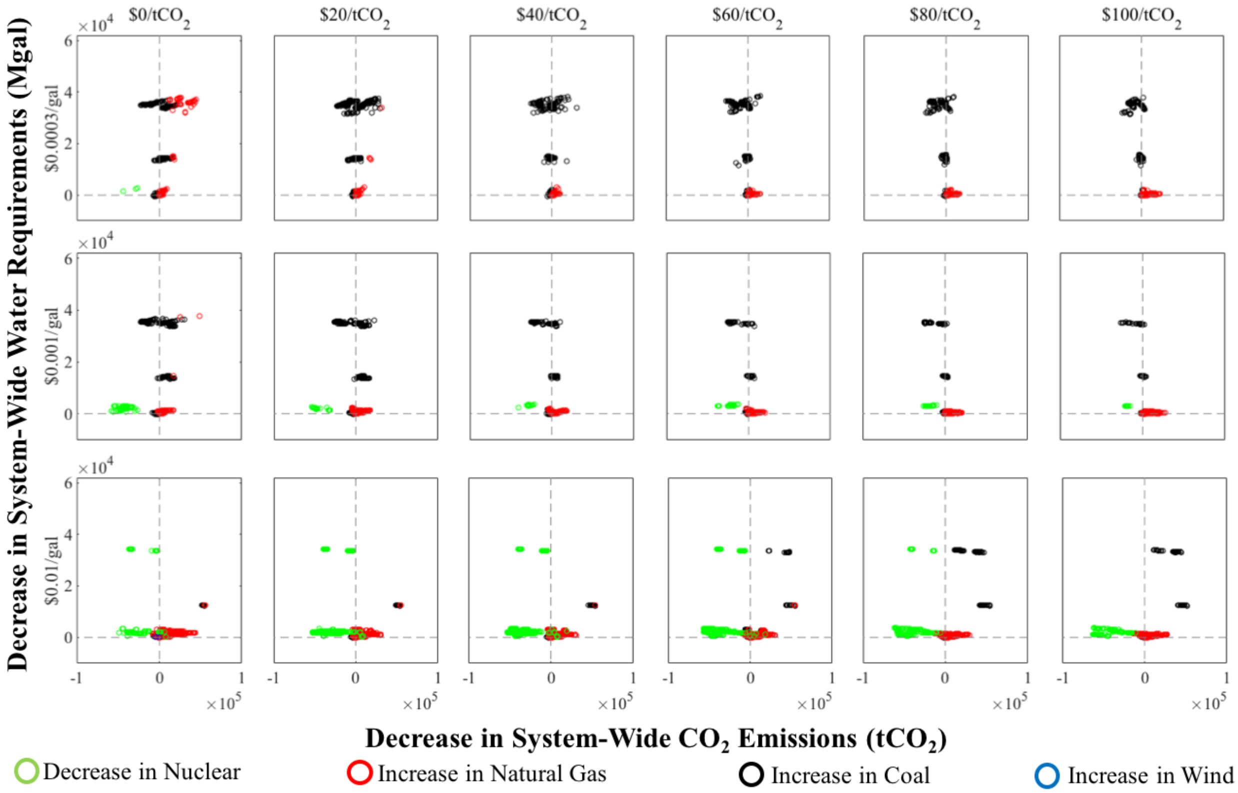

Figure 38: Effect of the Deployment of BES Due to Changes in the Dispatch Order When Wind Generation is Sufficient to Meet 22% of Total Demand. Markers to the right of the vertical line indicate a decrease in system-wide CO_2 emissions. Markers above the horizontal line indicate a decrease in system-wide water requirements.

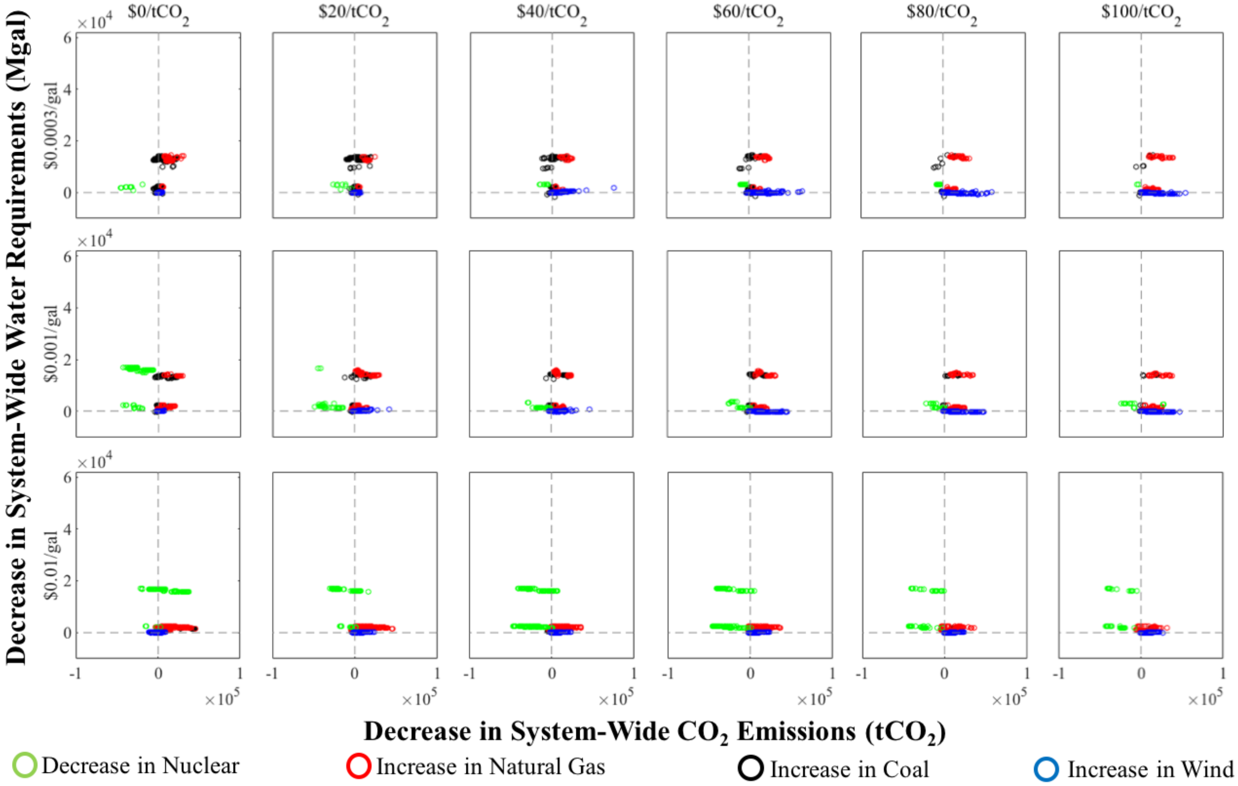

Figure 39: Effect of the Deployment of BES Due to Changes in the Dispatch Order When Wind Generation is Sufficient to Meet 44% of Total Demand. Markers to the right of the vertical line indicate a decrease in system-wide CO_2 emissions. Markers above the horizontal line indicate a decrease in system-wide water requirements.

6.4 The Value of BES for Reducing System-Wide CO_2 Emissions and System-Wide Water Requirements

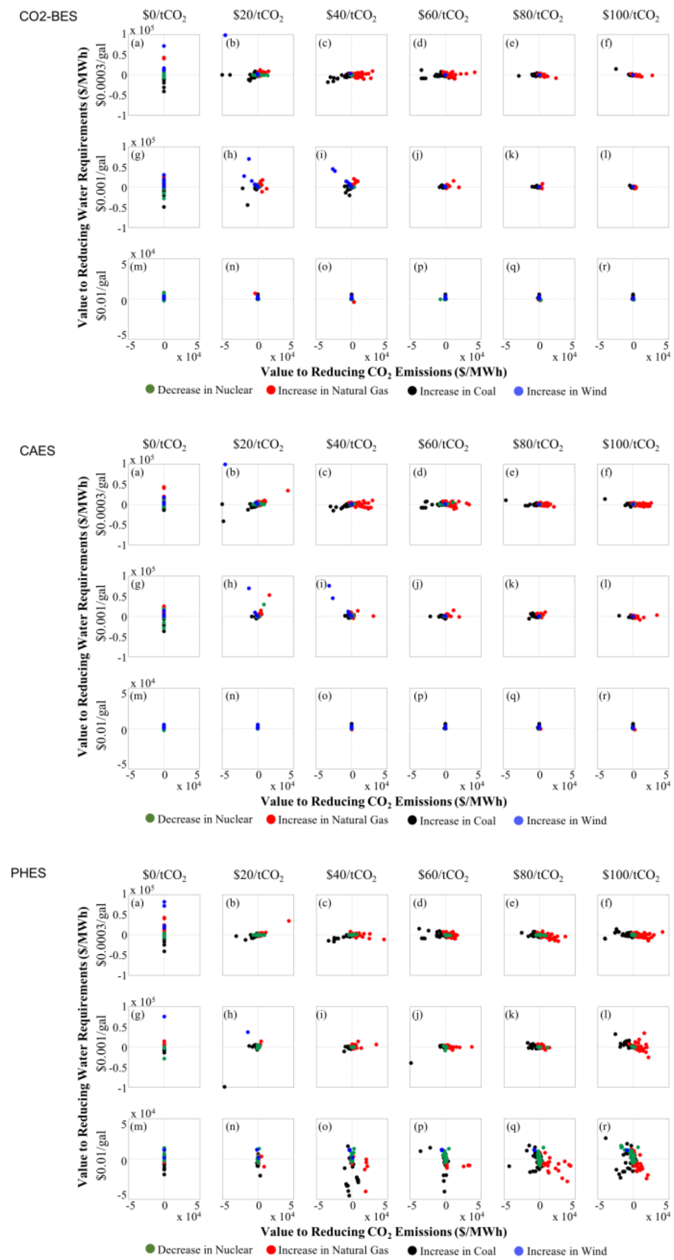

Figure 40: Effect of the Dispatch of BES on the Value of Reducing System-Wide CO_2 Emissions and the Value of Reducing System-Wide Water Requirements.

Appendix B: Supplemental Information for Chapter 3

1 Optimal Flowrate for BES Operation

We simulated the CRP-BES facility operating as a power plant over a range of combinations of mass flowrates: 3,000 kg/s, 4,000 kg/s, 4,500 kg/s, and 5,000 kg/s for brine; 500 kg/s, 1,000 kg/s, and 2,000 kg/s for CO_2. The corresponding power output capacities after ten years of operation is shown in Figure 41.

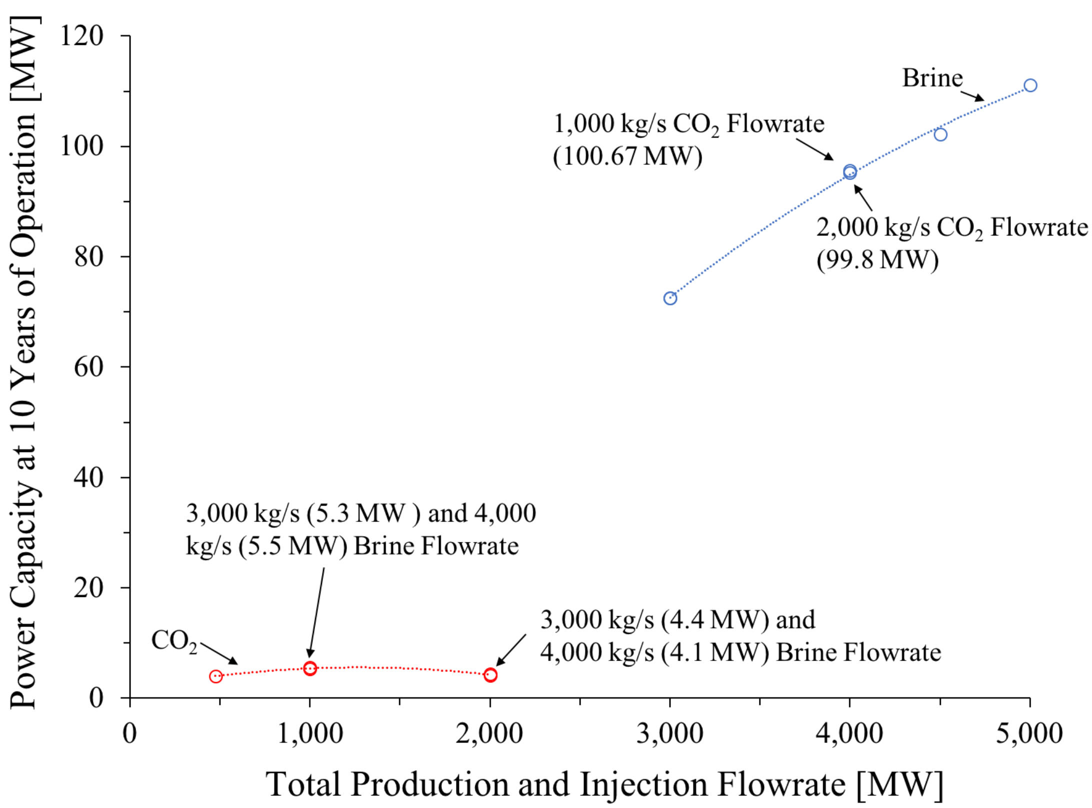

Figure 41: Power Output Capacity of the Direct CO_2 Cycle and the Indirect Brine Cycle for the CRP-BES Facility.

The power capacity of each cycle after ten years depends on the mass flowrate. For the CO_2 cycle, the maximum power output capacity occurs at a mass flowrate between the 1,000 kgCO_2/s and 2,000 kgCO_2/s. Since the power output capacity at the CO_2 mass flowrates is only slightly influenced by the brine mass flowrates that we investigated, and geothermal heat can be depleted if the CO_2 mass flow rate is too high, we chose to use a CO_2 mass flowrate of 1,000 kgCO_2/s. In contrast, the power output capacity of the brine power cycle continues to increase with the mass flowrate for over the range of flowrates that we used in the simulations. we chose to implement a 5,000 kg_{brine}/s total flowrate. It may be possible to increase the performance of the brine power cycle by increasing the brine flowrate without substantially increasing the geothermal heat depletion, but the pressure in the downhole production well decreases as a result. Such a decrease could cause the brine to flash in the production wellbore.

2 Results

2.1 Integrated Model of the CRP-BES Facility

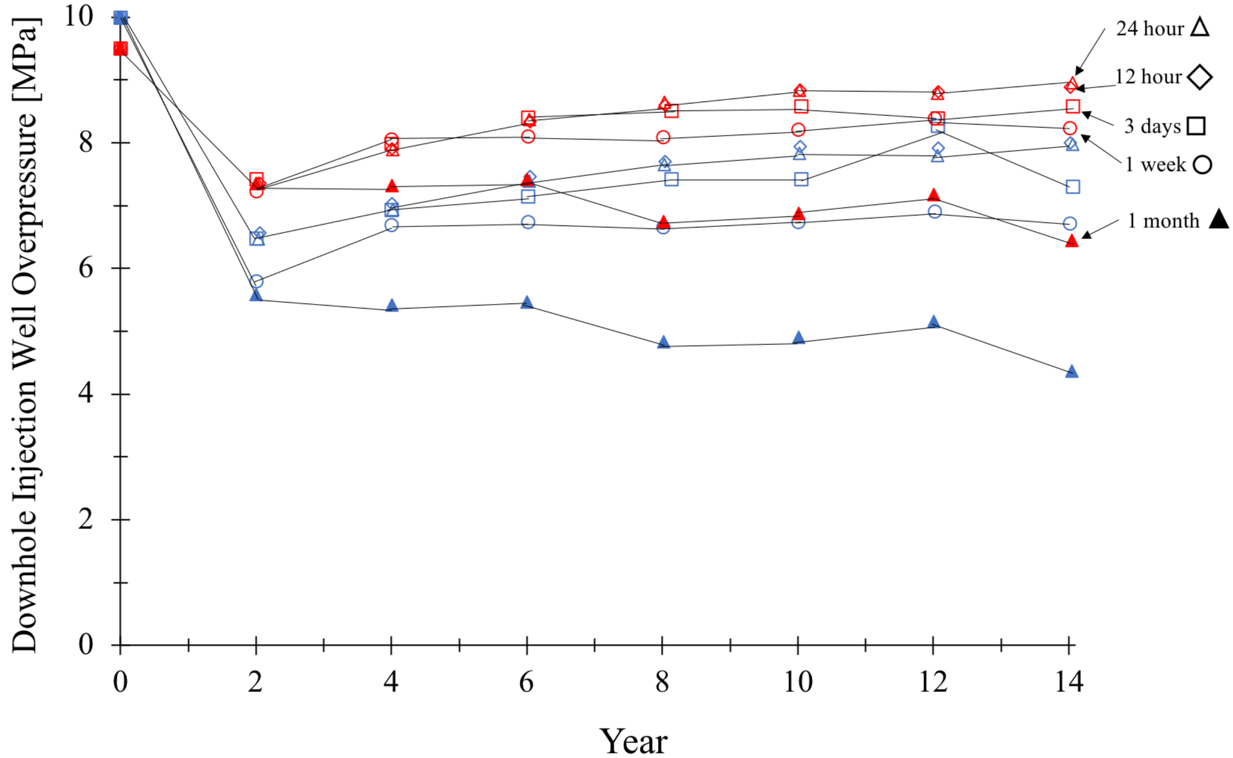

Figure 42: Downhole Injection Well Overpressure Sampled for Use in Power Cycle Models. The blue markers indicate brine and the red markers indicate CO_2.

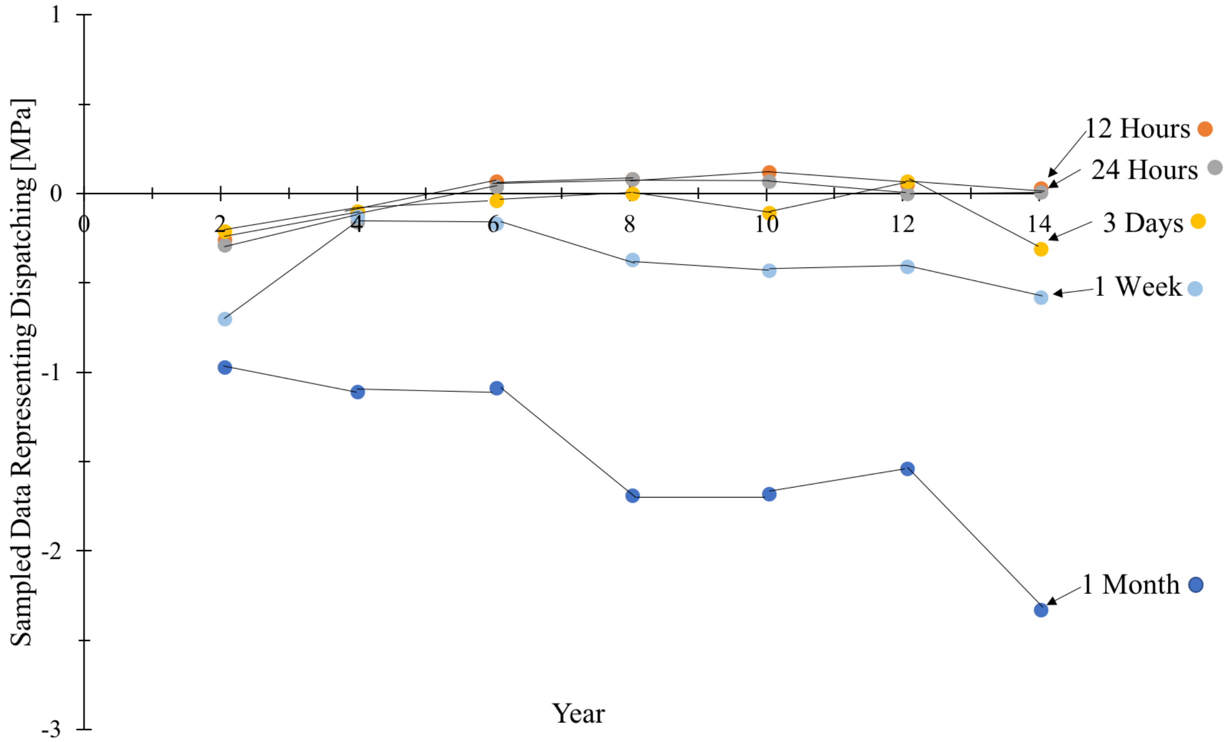

Figure 43: Downhole Brine Production Well Overpressure Sampled for Use in Power Cycle Model.

Table 21: Power Cycle Output Results for Each Cycle Simulated

Year	Brine Cycle Storage [MWe]	Brine Cycle Dispatch [MWe]	CO_2 Cycle Storage [MWe]	CO_2 Cycle Dispatch [MWe]	Brine Cycle Output/Flowrate Ratio [MWe/kg/s]	CO_2 Cycle Output/Flowrate Ratio [MWe/kg/s]
	Cycle: 12 Hours					
2	51.32	122.23	0.72	8.17	0.024	0.009
4	53.39	121.73	0.81	7.91	0.024	0.009
6	55.65	121.29	0.86	7.74	0.024	0.009
8	57.02	120.80	0.90	7.76	0.024	0.009
10	58.30	120.35	0.93	7.74	0.024	0.008
12	56.66	119.33	0.93	8.02	0.024	0.009
14	55.80	117.72	0.94	8.19	0.023	0.009
	Cycle: 24 Hours					
2	51.32	122.23	0.72	8.13	0.024	0.009

4	53.45	121.73	0.80	7.90	0.024	0.009
6	55.99	121.29	0.86	7.68	0.024	0.009
8	57.48	120.80	0.90	7.69	0.024	0.008
10	58.52	120.34	0.93	7.71	0.024	0.008
12	56.77	119.33	0.92	7.99	0.024	0.009
14	57.71	117.74	0.94	8.07	0.023	0.009
	Cycle: 3 Days					
2	51.34	122.28	0.71	7.97	0.024	0.009
4	51.25	121.77	0.80	7.74	0.024	0.009
6	55.65	121.29	0.86	7.54	0.024	0.008
8	55.80	120.83	0.86	7.73	0.024	0.009
10	52.90	120.36	0.86	7.88	0.024	0.009
12	52.99	119.37	0.86	8.47	0.024	0.009
14	53.66	117.55	0.87	8.22	0.023	0.009
	Cycle: 1 Week					
2	51.32	121.85	0.70	8.07	0.024	0.009
4	54.77	121.77	0.79	7.53	0.024	0.008
6	52.22	121.04	0.79	7.72	0.024	0.009
8	51.78	120.53	0.79	7.97	0.024	0.009
10	52.35	120.09	0.81	8.02	0.024	0.009
12	51.80	119.12	0.83	8.06	0.023	0.009
14	51.56	117.60	0.82	8.36	0.023	0.009
	Cycle: 1 Month					
2	49.24	121.84	0.65	7.87	0.024	0.009
4	48.15	115.67	0.66	8.13	0.023	0.009
6	46.57	120.08	0.66	8.22	0.024	0.009
8						
10						
12						
14						

2.2 Pumping Power

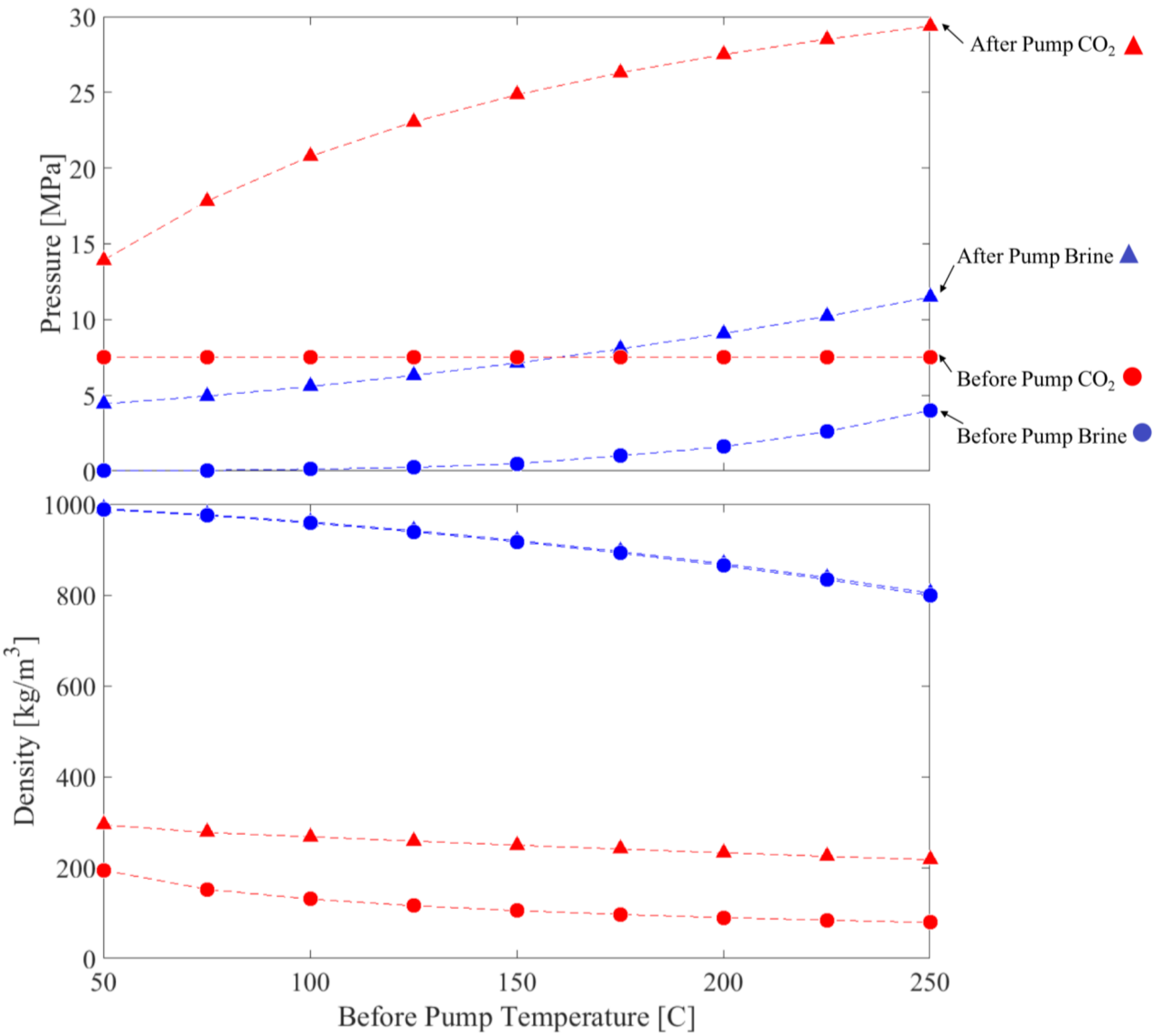

Figure 44: Before and After Pumping Pressure and Density For Injecting CO_2 and Brine into a 4 km Deep Reservoir at Hydrostatic Pressure.

Appendix C: Supplemental Information for Chapter 5

1 Full Specification of the Mixed Integer Linear Optimization Model

The problem is formulated as maximizing the revenue from electricity sales:

$$max\ \sum_{t=1}^{T}[(1-\gamma)p_t\sigma_t-(1+\gamma)p_t\theta_t] \tag{57}$$

Constraint equations:

- storage level

$$l_t = l_{t-1}+\frac{\kappa_d}{\kappa_s}s_t-d_t \qquad \forall t=1,\ldots,T \tag{58}$$

- ability to charge

$$A_t = A_{t-1}+\frac{\kappa_s}{\kappa_d}d_t-s_t \qquad \forall t=1,\ldots,T \tag{59}$$

- Geothermal Energy Extraction

$$G_t = G_{t-1}-\frac{G_0}{\kappa_d*H*365}d_t \qquad \forall t=1,\ldots,T \tag{60}$$

- electrical energy balance

$$\sigma_t-\theta_t+s_t+x-d_t=w_t \qquad \forall t=1,\ldots,T \tag{61}$$

- electricity storage constraint

$$s_t \le A_{t-1} \qquad \forall t=1,\ldots,T \tag{62}$$

- wind availability

$$0 \le w_t \le \overline{w_t} \qquad \forall t=1,\ldots,T \tag{63}$$

- CO_2-BES facility power output capacity

$$0 \le d_t \le \kappa_d \qquad \forall t=1,\ldots,T \tag{64}$$

- CO_2-BES facility energy storage capacity

$$0 \le l_t \le H\kappa_d \qquad \forall t=1,\ldots,T \tag{65}$$

- CO_2-BES facility power storage capacity

$$0 \leq s_t \leq \kappa_s \qquad \forall t = 1, \ldots, T \tag{66}$$

- transmission capacity

$$\theta_t \leq \beta_1 \tau \qquad \forall t = 1, \ldots, T \tag{67}$$

$$\sigma_t \leq \beta_2 \tau \qquad \forall t = 1, \ldots, T \tag{68}$$

$$\beta_1 + \beta_2 \leq 1 \qquad \forall t = 1, \ldots, T \tag{69}$$

- non-negativity

$$\sigma_t, \theta_t, G_t \geq 0 \qquad \forall t = 1, \ldots, T \tag{70}$$

Decision Variables:

σ_t – the amount of electricity sold over time period t [MWh], t = 1,…,T

θ_t – the amount of electricity purchased over time period t [MWh], t = 1,…,T

l_t – the cumulative amount of electricity stored by the CO_2-BES facility over time period t [MWh], t = 1,…,T

s_t – the amount of electricity stored by CO_2-BES facility over time period t [MWh], t = 1,…,T

d_t – the amount of electricity dispatched by CO_2-BES facility over time period t [MWh], t = 1,…,T

G_t – the amount of energy remaining to be extracted from the geothermal resource [MWh], t = 1,…,T

A_t – the amount of electricity that could be stored over time period t [MWh]. This variable represents the amount of brine in the surface holding pond that is available to be re-injected (which stores electricity), t = 1,…,T

w_t – the amount of electricity generated by the wind farm that is not curtailed over time period t [MWh], t = 1,…,T

β_1 – binary variable that is 1 if the CO_2-BES and wind farm hybrid facility are purchasing electricity

β_2 – binary variable that is 1 if the CO_2-BES and wind farm hybrid facility are selling electricity

Inputs:

T – the number of hours in the planning horizon

γ – transmission losses across the HVDC transmission line [%]

p_t – the price of electricity over time period t [$/MWh], t=1,…,T

κ_s – the maximum amount of electricity that could be stored by the CO_2-BES facility over time period t [MWh]

κ_d – the maximum amount of electricity that could be generated by the CO_2-BES facility over time period t [MWh]

H – the maximum length of time that a CO_2-BES facility can dispatch electricity at capacity [hours]

x – the amount of electricity that is required to constantly inject external CO_2 over time period t [MWh], t = 1,…,T

G_0 – the maximum amount of energy that could be extracted from the geothermal resource over the planning horizon [MWh], t = 1,…,T

τ – the maximum amount of electricity that the HVDC transmission line can transmit over time period t [MWh]

$\overline{w_t}$ – the amount of electricity generated by the wind farm that is available to be used over time period t [MWh], t = 1,…,T

1.1 Optimization Model Inputs that Are Influenced by the Integrated Model of CO_2-BES

We set the maximum length of time that a CO_2-BES facility can dispatch electricity at capacity (i.e., H) to 12 hours because we simulated CO_2-BES operation using a 2 x 12 hour cycle in the integrated model of CO_2-BES.

Although we did not simulate idle periods (i.e., periods where electricity was neither stored nor dispatched) in the integrated model of CO_2-BES, it is possible that the optimal operation of CO_2-BES, as determined with the optimization model, includes idle periods throughout the year. To ensure the electricity required to constantly inject CO_2 (i.e, x) was accounted for during idle periods, we separated it out in the electrical energy balance (Eq. 61). As a consequence, we increased the electricity dispatch capacity (K_d)

and decreased the electricity storage capacity (K_s) by the value of x so that the net dispatch or net storage from the CO_2-BES facility was appropriately represented. For example, if the CO_2-BES facility could dispatch a maximum of 130 MWh or store a maximum of 60 MWh, and 2 MWh were required to constantly inject CO_2, then x was set to 2, K_s was set to 58, and K_d was set to 132. As a result of this separation in Equation 61, the values of x, Ks, and Kd are all required to define energy storage capacity and energy output capacity within the optimization model for a given heat depletion scenarios; we used the values listed in Table 22 for each heat depletion scenario that we optimized for this study.

Table 22: Optimization Model Inputs that Vary Based on Level of Geothermal Heat Depletion

Geothermal Heat Depletion Scenario (Year)	Electricity Storage Capacity (K_s) [MWh]	Electricity Dispatch Capacity (K_d) [MWh]	Electricity Needed Inject External CO_2 (x) [MWh]	Geothermal Energy Available to be Extracted (G_0) [MWh]
No Heat Depletion (1)	59.1	131.89	2.10	8,454,383.74
Heat Depletion (30)	62.5	93.85	1.55	5,207,435.52

We determined the amount of geothermal energy available to be extracted in a given year by using the NUFT reservoir simulation results to calculate the energy in the sedimentary basin over time and converted the units from MJ to MWh to align with the units used in the optimization model. For example, the amount of energy available to be extracted in year one (i.e., 8,454,383.74 MWh) is the difference between the total amount of energy in the reservoir after year one and year zero.

2 CO_2-Bulk Energy Storage System Capital Cost Estimation

We adjusted the capital cost estimates to 2012 by multiplying by the appropriate Producer Price Index (PPI) adjustment factor because that is the method used to adjust costs to different years within GETEM [175]. We chose 2012 as the reference year for this study because our baseline electricity price dataset and wind farm generation dataset was from 2012. We used the same or similar Bureau of Labor Statistic Series categories as was used in GETEM and used a general Engineering Services to adjust the costs related to CO_2 storage development because a majority of these costs involve engineering (Table 23). GETEM uses an average PPI adjustment factor across a range of Bureau of Labor Statistic Series categories to adjust the cooling tower cost and condensing tower cost estimates (Table 24) [175]. The Bureau of Labor Statistics supplies monthly PPI data and we used the January value as the PPI for each year.

Table 23: Producer Price Index Categories Used to Adjust Costs and Reference Cost Year

Cost	Bureau of Labor Statistics Series ID	Reference Year
Drilling and Equipping Brine Wells	PCU213111213111P Drilling Oil and Gas Wells: Primary Services	2012
Drilling and Equipping CO_2 Wells	PCU213111213111P Drilling Oil and Gas Wells: Primary Services	2010
Brine Pipeline and CO_2 Pipeline	WPU101706 Steel Pipe and Tube	2010
CO_2 Storage Development	PCU5413354133 Engineering Services	2010
Brine Cycle Heat Exchanger	WPU1075 Heat Exchangers and Steam Condensers	2015
Turbine-Generator	WPU1197 Turbines and Turbine Generator Sets	2002
Condensing and Cooling Towers	Average of PPIs in Table 24	
Brine Pump	PCU3339113339111Z4 Pump and Pumping Equipment	2002
CO_2 Pump	PCU3339113339111Z4 Pump and Pumping Equipment	2013
Grid Integration	PCU221121221121 Electric Bulk Power Transmission and Control	2009

Table 24: Bureau of Labor Statistics Series IDs Used to Adjust the 2013 Condensing and Cooling Tower Costs.

Bureau of Labor Statistics Series ID
PCU334513334513 Industrial Process Variable Instruments Manufacturing
PCU332911332911 Industrial Valve Manufacturing
WPU1061 Steam and How Water Equipment
WPU114902 Metal Valves

2.1 Cost of Drilling and Equipping the Wells

We used drilling cost estimates from GETEM to estimate the drilling costs of the brine wells. For the CO_2 wells, we augmented these costs by relevant estimated costs for CO_2 injection wells [176,177]. Within GETEM, the estimated well costs have step functions that increase with well diameter and well depth (Figure 45). We linearly interpolated between the red highlighted costs in Figure 45 to estimate the well costs for our case study (2.74 km deep).

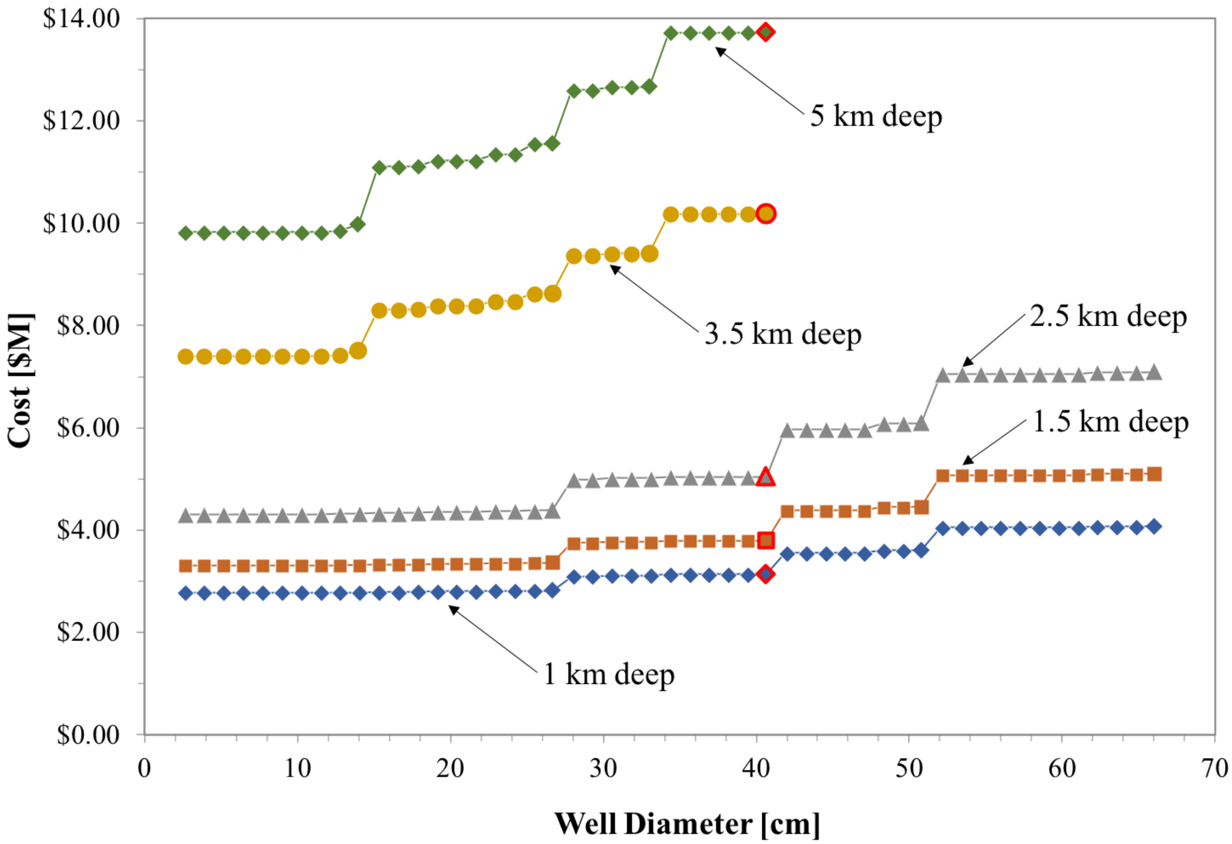

Figure 45: Well Drilling and Equipping Costs from GETEM [176]**.** These cost estimates include the Bit Cost, Mud Cost, Casing Cost, Cement Cost, Rig Cost, Logging Cost, Well Head Cost, Directional Drilling Cost, Site Prep Cost, Mobilization and Demobilization Cost, Rental Cost, and Contingency Cost.

For the CO_2 wells, we augmented the per well cost using Equation 71.

$$CO_2\ Well\ Cost\ \left[\frac{\$}{Well}\right] = GETEM\ Cost + 432.10 * Depth + 4.9 * Depth * Well\ Diameter \qquad (71)$$

Where 432.10 is the sum of the costs listed in Table 25 and 4.9 is the sum of the costs listed in Table 26.

Table 25: Additional Costs Associated with Drilling CO_2 Wells [177].

Description	Cost [$/ft/injection well]**
Downhole safety shut-off valve	$1.05
Obtain geomechanical information on fractures, stress, rock strength, in situ fluid pressures (new cores and tests)	$78.00
List names and depth of all potentially affected USDWs	$1.05
Standard monitoring well stopping above the injection zone (used lookup table). Standard monitoring wells for ER projects stop below the injection zone.*	$176.00
Standard monitoring well drilled into the injection zone (used lookup table); applies to RA 3-4 only)*	$176.00
Total	**$432.10**
*The EPA listed these costs in the units of $/ft/monitoring well and we assumed they were in the units of $/ft/injection well; **We applied these costs to both CO_2 injection wells and CO_2 production wells	

Table 26: Additional Costs Associated with Casing CO_2 Wells [177].

Description	Cost [$/ft/in/well]
Corrosion resistant tubing	$1.15
Corrosion resistant casing	$2.25
Cement well from surface through base of lowermost USDW and throughout injection zone.	$1.20
Use CO_2-resistant cement	$0.30
Total	**$4.90**

2.2 Cost of Brine Pipeline and CO_2 Pipeline

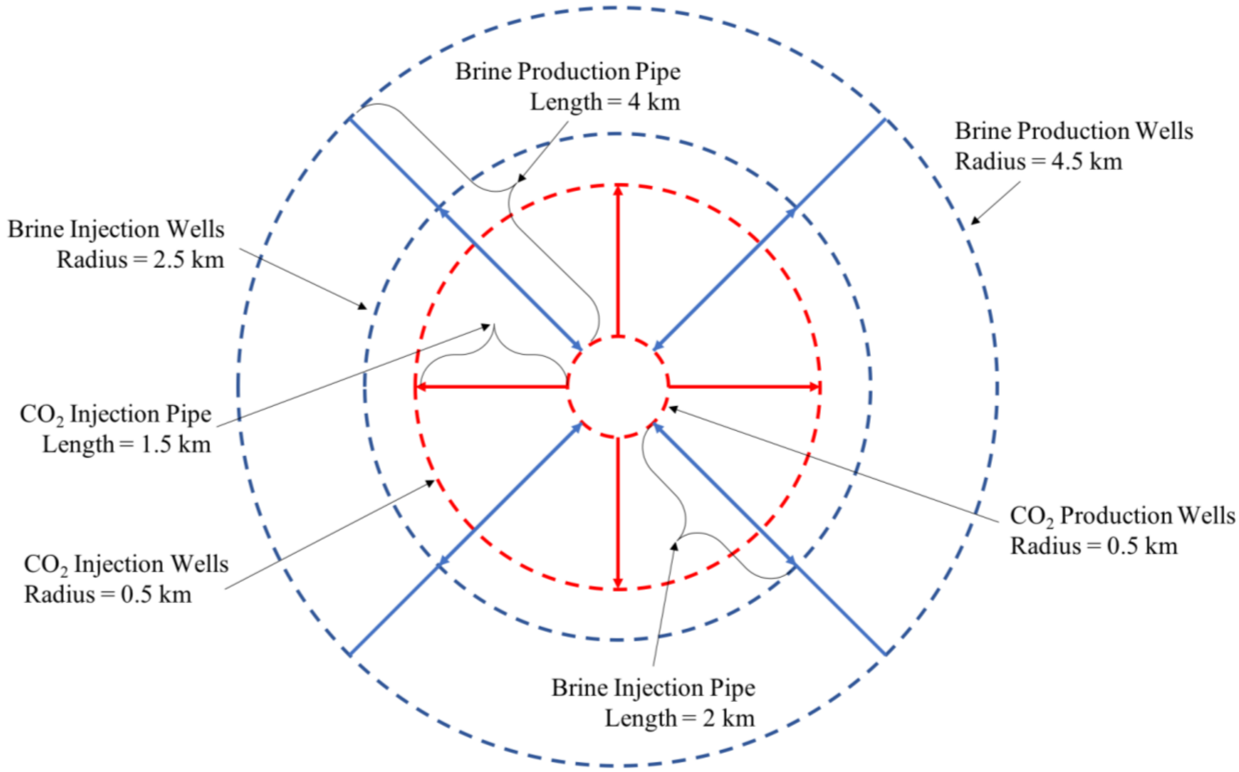

Figure 46: Pipeline Configuration for a CO_2-BES Facility with Four Brine Production Wells, Four CO_2 Production Wells, Four Brine Injection Wells, and Four CO_2 Injection Wells. The blue arrows represent the brine pipeline and the red arrows represent the CO_2 pipeline.

We assumed that the CO_2-BES surface facility and brine holding pond were located within the area enclosed by the CO_2 production ring well radius and that the required pipeline within this area (and thus pressure losses over this distance) were negligible. Following the pipeline lengths shown in Figure 46, the total length of pipeline used in a CO_2-BES facility was determined with Equation 72.

$$Total\ Pipeline\ [km] = 4P_B + 2I_B + 1.5I_C \qquad (72)$$

Where P_B is the number of brine production wells, I_B is the number of brine injection wells, and I_C is the number of CO_2 injection wells. For the case study used in this study, the total pipeline needed was 139.5 km. Following our prior work, we assumed 21 brine production wells, 21 brine injection wells, 9 CO_2 production wells, and 9 CO_2 injection wells (Chapter Three). We determined the pressure loss over the length of the pipeline using Bernoulli's Equation and assumed the density of the fluid was constant throughout the pipeline.

We assumed the cost of pipeline was \$83,000/in-mi for both the Indirect Brine Cycle and Direct CO_2 Cycle [177]. Because this cost estimate is representative of CO_2 pipeline it likely overestimates the cost of brine pipeline. We estimated the cost of the pipeline required for a CO_2-BES system by multiplying by the total length of pipeline needed to transport fluid from production wells to the power plant and from the power plant to injection wells (determined with Eq. S16).

We used a pipeline diameter of 22 inches because it resulted in the largest CO_2-BES power output per total capital cost (Figure 47). Pipeline diameters less than 22 inches are not feasible for the pipeline configuration used in this study because the pressure losses become large enough that power cannot be generated. It may be possible to decrease capital costs with a smaller pipeline by co-optimizing the CO_2 flowrate and the brine flowrates to reduce costs while maximizing performance but that was outside the scope of this study.

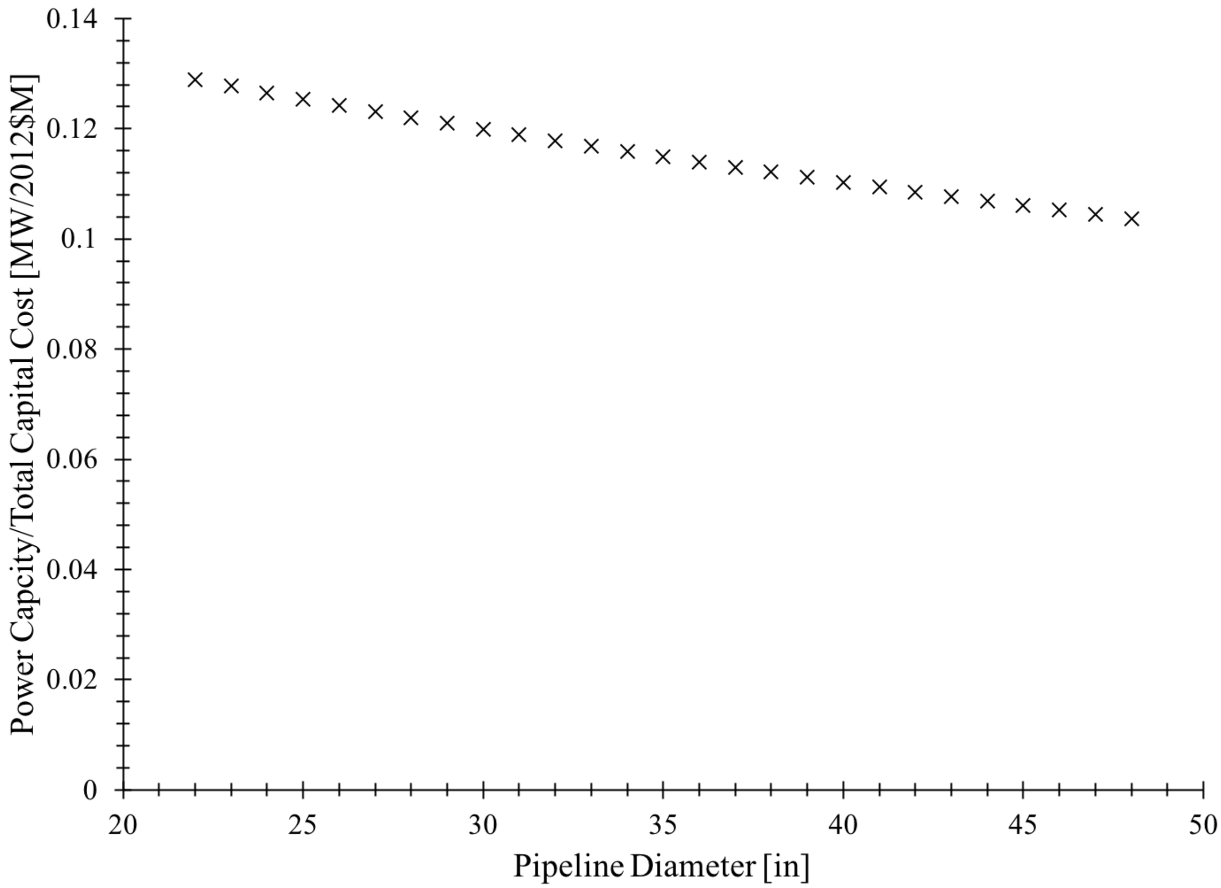

Figure 47: Ratio of Power Output Capacity of CO_2-BES to Total Capital Cost as a Function of Pipeline Diameter.

2.3 CO_2 Storage Development Cost

The CO_2 storage development costs were estimated as the sum of the CO_2 plume related costs (Section 2.3.1), injection well related costs (Section 2.3.2), injection and production well related costs (Section 2.3.3), control equipment costs (Section 2.3.4), and monitoring site costs (Section 2.3.5). We accounted for all CO_2 storage development costs within the capital costs for the Direct CO_2 Cycle.

2.3.1 CO_2 Plume Related Costs

The CO_2 plume related cost was calculated with Equation 73.

$$Plume\ Cost\ [\$] = \frac{\$512{,}505}{site} + \frac{\$202{,}000}{mi^2} * Plume\ Area + \frac{\$0.086}{tCO_2} * CO_2\ Stored \quad (73)$$

Where the \$512,505/site cost is the sum of the costs listed in Table 27, the \$202,000/mi^2 cost is the sum of the costs listed in Table 28, the Plume Area was assumed to be the area of a circle with a radius of 7 km (Figure 48), the \$0.086/tCO_2 cost is the sum of costs listed in Table 29, and the mass of CO_2 stored in the initial three-year charging phase was determined with the output of the NUFT simulations.

Table 27: Components of CO_2 Storage Development Costs Associated With Site Costs [177]

Description	Cost [$/site]
Develop maps and cross sections of local geologic structure	$6,434
Obtain and analyze seismic (earthquake) history	$6,434
Remote (aerial) survey of land, land uses, structures etc. Should assume survey is twice the project's actual CO_2 footprint due to uncertainty during site characterization phase of exact location of facilities and plume	$3,100
Obtain data on areal extent, thickness, capacity, porosity and permeability of receiving formations and confining systems	$2,574
Obtain geomechanical information on fractures, stress, rock strength, in situ fluid pressures (from existing data and literature)	$12,868
List names and depth of all potentially affected USDWs	$2,574
Provide geochemical information and maps/cross section on subsurface aquifers	$6,434
Provide information on water-rock-CO_2 geochemistry and mineral reactions	$36,035
Prepare geologic characterization report demonstrating: suitability of receiving zone, storage capacity and injectivity, trapping mechanism free of nonsealing faults, competent confining system, etc.	$25,735
Conduct front-end engineering and design (monitoring wells above injection zone)	$20,700
Develop plan and implement Eddy Covariance air monitoring	$4,289
Develop plan and implement soil zone monitoring	$4,289
Develop plan and implement vadose zone monitoring wells to sample gas above water table	$4,289
Develop plan and implement monitoring wells for samples from water table	$4,289
Conduct front-end engineering and design (general and injection wells), pre-op logging, sampling, and testing	$207,000
Land use, air emissions, water discharge permits	$103,400
UIC permit filing, including preparation of attachments	$10,400
Simple fluid flow calculations to predict CO_2 fluid flow.	$3,982

Complex modeling of CO_2 fluid flows and migration (reservoir simulations) over 100 years	$19,912
Complex modeling of CO_2 fluid flows and migration (reservoir simulations) over 10,000 years	$19,912
Areal search for old wells (artificial penetrations)	$5,200
Develop a corrosion monitoring and prevention program	$2,655
Total	**$512,505**

Table 28: Components of CO_2 Storage Development Cost Associated With CO_2 Plume Area [177].

Description	Cost [$/mi^2]
Conduct 3D seismic survey to identify faults and fractures in primary and secondary containment units	$104,000
Remote (aerial) survey of land, land uses, structures etc. Should assume survey is twice the project's actual CO_2 footprint due to uncertainty during site characterization phase of exact location of facilities and plume.	$930
Develop list of water wells within AoR	$3,860
Develop plan and implement Digital Color Infrared Orthoimagery (CIR) or Hyperspectral Imaging to detect changes to vegetation	$10,000
Develop plan and implement LIDAR airborne survey to detect surface leaks. Works best where vegetation is sparse	$10,000
Lease rights for subsurface (pore space) use	$33,280
Land use, air emissions, water discharge permits	$20,700
UIC permit filing, including preparation of attachments	$6,000
Areal search for old wells (artificial penetrations)	$13,230
Total	**$202,000**

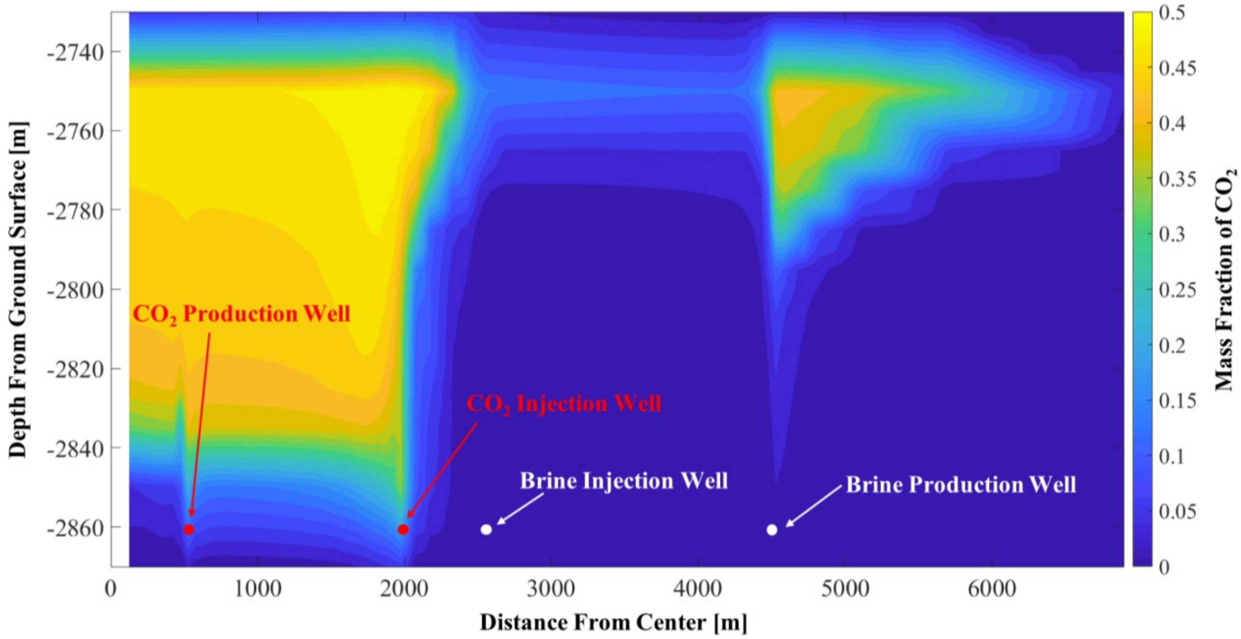

Figure 48: Mass Fraction of CO_2 in the Sedimentary Basin Geothermal Resource After 30 Years of Continuous Cycling Between Storing Electricity for 12 Hours and Dispatching Electricity for 12 Hours.

Table 29: Components CO_2 Storage Development Costs Associated with Injecting CO_2 [177]**.**

Description	**Cost [$/tCO$_2$]**
Pore space use costs	$0.036
Tracers in injected fluid	$0.05
Total	**$0.086**

2.3.2 Injection Well Related Costs

The injection well related costs were determined by multiplying the sum of the costs listed in Table 30 by the number of CO_2 injection wells.

Table 30: Components of CO_2 Storage Development Costs Associated with Injection Wells [177]**.**

Description	Cost [$/injection well]
Obtain geomechanical information on fractures, stress, rock strength, in situ fluid pressures (new cores and tests)	$3,100
List names and depth of all potentially affected USDWs	$15,500
Provide geochemical information and maps/cross section on subsurface aquifers	$500
Develop geochemical baseline for injection zones and confining zone	$828
Simple fluid flow calculations to predict CO_2 fluid flow	$1,327
Complex modeling of CO_2 fluid flows and migration (reservoir simulations) over 100 years	$2,655
Complex modeling of CO_2 fluid flows and migration (reservoir simulations) over 10,000 years	$3,982
Conduct front-end engineering and design (monitoring wells above injection zone)*	$5,200
Conduct front-end engineering and design (monitoring wells into injection zone)*	$5,200
Pressure, temperature, and resistivity gauges and related equipment for monitoring wells ABOVE injection zone*	$10,400
Pressure, temperature, and resistivity gauges and related equipment for monitoring wells INTO injection zone*	$10,400
Salinity, CO_2, tracer, etc. monitoring equipment for wells ABOVE injection zone (portion of equipment may be at surface such as for in situ sampling using U-tubes)*	$10,400
Salinity, CO_2, tracer, etc. monitoring equipment for wells INTO injection zone (portion of equipment may be at surface such as for in situ sampling using U-tubes)*	$10,400
Conduct periodic monitoring of groundwater quality and geochemistry. (146.90(d) of GS Rule).*	$800
Total	**$80,692**

*These costs were listed by the EPA in the units of $/monitoring well and we assumed they were $/injection well

2.3.3 Injection Well and Production Well Related Costs

The injection well and production well related costs were determined by multiplying the sum of the costs listed in Table 31 by the sum of the CO_2 injection wells and CO_2 production wells.

Table 31: Components of CO_2 Storage Development Costs Associated with Production and Injection Wells [177]**.**

Description	**Cost [$/well]***
Downhole safety shut-off valve	$15,500
Downhole check valve	$500
Conduct front-end engineering and design (general and injection wells), pre-op logging, sampling, and testing	$41,400
Obtain rights-of-way for surface uses. (equipment, injection wells)	$20,700
Well stimulation	$112,500
Continuous measurement / monitoring equipment: injected volumes, pressure, flow rates and annulus pressure	$15,500
Equipment to add tracers	$10,400
Total	**$216,500**
*These costs were listed by the EPA in the units of $/injection well and we applied them to both injection and production wells.	

2.3.4 Control Equipment Costs

The control equipment cost was estimated with Equation 74 [177].

$$Control\ Equipment\ Cost\ [\$] = 520 * \left(\frac{CO_2\ Stored}{365}\right)^{0.6} \qquad (74)$$

Where the mass of CO_2 stored was determined with the output of the NUFT simulations and 365 is the number of days in a year.

2.3.5 Monitoring Site Costs

The injection well related costs were determined by multiplying the sum of the costs listed in Table 32 by the number of CO_2 injection wells.

Table 32: Components of CO_2 Storage Development Costs Associated with Monitoring Site [177].

Description	Cost [$/injection well]*
Develop baseline of surface air CO_2 flux for Eddy Covariance leakage monitoring	$36,200
Obtain rights-of-way for surface uses. (monitoring wells above injection zone)	$10,400
Obtain rights-of-way for surface uses. (monitoring wells into injection zone)	$10,400
Obtain rights-of-way for surface uses. (monitoring sites)	$5,200
Develop plan and implement Eddy Covariance air monitoring	$75,000
Develop plan and implement soil zone monitoring	$6,000
Develop plan and implement vadose zone monitoring wells to sample gas above water table	$8,000
Develop plan and implement monitoring wells for samples from water table	$80,000
Surface microseismic detection equipment	$52,000
Total	**$283,200**
*These costs were listed by the EPA in the units of $/monitoring site and we scaled it to the size of a CO_2-BES facility by assuming they were in the units of $/injection well.	

2.4 Power Plant Costs

The total cost of the power plant is comprised of the cost of individual power cycle components (e.g., pumps, turbine-generator, cooling tower), the cost to construct the power plant, indirect costs (e.g., office work, project management), and contingency. The cost to construct the power plant was estimated with Equation 75 [175].

$$Construction\ Cost\ [\$] = Cost\ of\ Components * (1 + x_{MCC} + x_{LCC} + x_{CMC} + x_{ST} + x_F) \quad (75)$$

Where the Cost of Components is the sum of all power cycle components (e.g., turbine-generator) and the $x_{(\cdot)}$ variables are defined in Table 33.

Table 33: Additional Cost Multipliers for Construction Costs [175]**.**

Variable	Value	Description
x_{MCC}	0.70	Material Capital Costs (physical structure, electrical, etc)
x_{LCC}	0.39	Labor Costs (0.25 plus 45% for fringe)
x_{CMC}	0.25	Construction Material Costs (rentals, equipment)
x_{ST}	0.05	Sales Tax
x_F	0.05	Freight

Indirect costs are assumed to be 12% [175]. As a result, we used Equation 76 to estimate the total cost of Engineering, Procurement, and Construction.

$$C_{EPCC}\ [\$] = 1.12 * Construction\ Cost \quad (76)$$

We included both the cost process contingency and project contingency to account for power and operational shortfalls for untested processes and unexpected expenses due to incomplete project definition, respectively [181] using Equations 77 and 78.

$$C_{Process\ Contigency}\ [\$] = 0.10 * C_{EPCC} \quad (77)$$

$$C_{Project\ Contigency}\ [\$] = 0.15 * (C_{EPCC} + C_{Process\ Contigency}) \quad (78)$$

We did not include the cost of the electricity required to injection CO_2 and circulate brine during the initial 3-year priming period because we assumed the CO_2-BES facility could supply this electricity. We also did not include any revenue that would be received over this 3-year period from selling electricity generation that is in excess of the power required to inject CO_2 and circulate brine. Had we included this additional income, the capital cost estimates for the CO_2-BES facility would have been substantially lower.

2.4.1 Indirect Brine Cycle: Heat Exchanger Cost

We assumed the per kW_{th} cost of a heat exchanger was that of a Heatric CO_2-Water plate heat exchanger [178,179]. As a result, we likely overestimated this cost because the heat exchanger used in the CO_2-BES system would likely be that of a standard ORC system. Prior work suggests that a single Heatric CO_2-Water plate heat exchanger costs $62,800, assuming that (1) 63% of the total volume (0.34 m^3) is Stainless Steel (density 7,800 kg/m^3) which costs $8.48/kg, and (2) a manufacturing cost of $48,480. Further, a single Heatric CO_2-Water plate heat exchanger has a Log Mean Temperature Difference (LMTC) of 16.3 C for a heat transfer of 1,980 kW_{th}, which equates to a UA of 120 kW_{th}/C. Additionally, the cost of flash condenser heat exchangers decrease by a power of 0.85 within GETEM [175]. As a result, we estimated the cost of a heat exchanger with Eq. 79.

$$C_{HX}\,[2015\$] = \$62800 \cdot \left(\frac{Q}{LMTD*120}\right)^{0.85} \tag{79}$$

Where Q is heat transfer in kW_{th}, and the LMTD for any heat exchanger is defined with Eq. 80.

$$LMTD = \frac{\Delta T_A - \Delta T_B}{ln\left(\frac{\Delta T_A}{\Delta T_B}\right)} \tag{80}$$

Where ΔT_A is the temperature difference between the two fluids at one end of the heat exchanger and ΔT_B is the temperature difference between the two fluids at the other end.

2.4.2 Indirect Brine Cycle: Turbine-Generator Cost

The total cost of the turbine-generator is the sum of the turbine cost (Equation 81) and the generator cost (Equation 82) [175].

$$Turbine\ Cost\,[2002\$] = 7400 * (P_{kWe,turbine})^{0.6} \tag{81}$$

$$Generator\ Cost\,[2002\$] = 1800 * (P_{kWe,turbine})^{0.67} \tag{82}$$

Where $P_{kWe,turbine}$ was assumed to be the maximum power generated by the turbine over the 30-year lifetime of the CO_2-BES facility in kW.

2.4.3 Indirect Brine Cycle: Cooling Tower and Condensing Tower Costs

We used equations 83 to 85 to estimate the cost of the cooling tower and condensing tower, respectively.

$$C_{BAC,cooling\ tower}\left[\frac{\$}{kW_{th}}\right] = (0.0168 * T_{amb} - 0.914) * T_{range} + (1740 - 39.8 * T_{amb}) * \left(\frac{1}{T_{app}}\right) \tag{83}$$

$$C_{BAC,condensing\ tower}\left[\frac{\$}{kW_{th}}\right] = (1010 - 18.5 * T_{amb}) * \frac{1}{T_{app}} \tag{84}$$

$$C_{Tower,i}[2013\$] = C_{BAC,i} * \left(\frac{Q}{Q_{base}}\right)^{0.8} \tag{85}$$

Where T_{amb} is the ambient temperature used in the power cycle model, T_{range} is the difference between the entrance and exit temperature of the cooled fluid, T_{app} is the degrees above ambient temperature that the fluid to which the fluid is cooled in the power cycle model (the "approach" temperature), Q_{base} is 1,000 kW_{th}, and Q is the heat transfer kW_{th}.

We derived Equations 83 and 84 using 2013 data from Boston AirCoil for model PC2-509-1218-30 (509 nominal ton, R22 evaporative condensing tower), and models FXV-0812B-12D-J and FXV-1212C-16Q-K (98 ton and 123 ton glycol closed-circuit cooling towers). As these relationships were for 1000 kW_{th} systems (Q_{base}), we scaled them using a power for 0.8, which is based off a similar relationship used within GETEM for a flash steam cooling tower.

2.4.4 Indirect Brine Cycle: Pump Cost

We used Equation 86 to estimate the cost of a brine pump [175].

$$Brine\ Pump\ Cost\ [2002\$] = 2.35 * 1185 * (P_{HP,Pump})^{0.767} \tag{86}$$

Where $P_{HP,Pump}$ was assumed to be the maximum pumping power required over the 30-year lifetime of the CO_2-BES facility in horsepower and the 2.35 increase accounts for stainless steel parts. We used Equation 86 to estimate the cost of the ORC pump and for the brine re-injection pump.

2.4.5 Direct CO_2 Cycle: Turbine-Generator Cost

We followed the same approach presented in Section 2.4.2 to estimate the cost of the turbine-generator for the Direct CO_2 Cycle and multiplied this cost by 1.2 based on recent conversations with CO_2 turbine manufacturers.

2.4.6 Direct CO_2 Cycle: Pump Cost

We estimated the cost of the CO_2 re-injection pump and external CO_2 pump using the same 0.767 power relationship from the GETEM brine pumps, but fitting the curve to align with a quote from Flowserve for an 8x15DMXD-A 3 stage pump (Eq. 87):

$$CO_2\ Pump\ Cost\ [2013\$] = 3604 * (P_{pump})^{0.767} \tag{87}$$

Where P_{pump} is the maximum power used by the pump over the 30-year lifetime of the CO_2-BES facility in kW.

2.4.7 Direct CO_2 Cycle: Cooling and Condensing Tower Costs

We used Equations 84 to 85 to estimate the costs of the cooling tower and condensing tower and multiplied both these costs by three to account for the difference in construction when using high-pressure CO_2 instead of R22 or glycol.

2.5 Grid Integration Costs

Grid integration costs for geothermal power plants are \$227/kW [180]. As a result, we estimated the grid integration costs by multiplying the maximum amount of electricity that the CO_2-BES facility generated over the 30-year operational lifetime by \$227/kW.

3 CO_2-Bulk Energy Storage Annual Cost Estimation

3.1 Indirect Brine Cycle

We followed the approach used within GETEM to calculate annual costs and also added 3% of the total capital costs to account for the annual cost of insurance [176]. The GETEM annual costs are the sum of the annual field cost (Section 3.1.1) and the annual plant cost (Section 3.1.2).

3.1.1 Annual Field Cost

The annual field cost is the sum of field labor cost (Eq. 88), non-well related O&M, and well related O&M. The non-well related O&M cost was assumed to be 1% of the well development cost, which was assumed to be \$200,000/well. Further, the well related O&M was assumed to the 1% of the total cost of drilling and equipping the injection wells and production wells (Section 2.1).

$$Field\ Labor\ Cost\ \left[\frac{\$}{yr}\right] = H_o * N_O * PR_O * LCM * 0.25 \quad (88)$$

Where the number of hours worked per year by an operator (H_o) was 8,760; the number of operators (N_O) was defined with Equation 89; the pay rate for operators (PR_O) was $22.92/hr; the Labor Cost Multiplier (LCM) was 2.5; and the 0.25 multiplier was the fraction of operators assigned to the field.

$$N_O = 0.25 * (Plant\ Size_{MW})^{0.525} \quad (89)$$

Where $Plant\ Size_{MW}$ was the net power that would be generated by the power cycle if it was not operating to time-shift electricity production in MW.

We assumed the operator PPI was the same as an engineer (Bureau of Labor Statistics Series PCU5413354133: Engineering Services) and we multiplied the $22.92/hr operator pay rate by the appropriate PPI adjustment factor to adjust the cost from 2012 dollars.

3.1.2 Annual Plant Cost

The annual plant cost is the sum of labor cost and non-labor costs. The labor cost is the difference between the total labor cost (Eq. 90) and the field labor cost (Eq. 88). The non-labor cost is assumed to be 2% of the cost of the turbine-generator.

$$Total\ Labor\ Cost\ \left[\frac{\$}{yr}\right] = LCM * [H_o * N_O * PR_O + H_M * N_M * (PR_E + PR_M + PR_G) + H_{of} * N_{Of} * (PR_P + PR_{OM} + PR_C)] \quad (90)$$

Where the number of hours worked per year by a maintenance employee (H_M) was 2,000; the number of maintenance employees (N_M) was defined with Equation 91; the pay rate for electricians (PR_E) and mechanics (PR_M) were both $27.50/hr; the pay rate for general maintenance employees (PR_G) was $20.05/hr; the number of hours worked per year by office employees (H_{Of}) was 2,000; the number of office employees (N_{Of}) was defined with Equation 92; the pay rate for plant engineers (PR_P) was $45.83/hr; the pay rate for operations managers (PR_{OM}) was $34.37/hr; and the pay rate for general clerical employees (PR_C) was $13.75/hr.

$$N_M = 0.15 * (Plant\ Size_{MW})^{0.65} \quad (91)$$

$$N_{Of} = 0.075 * (Plant\ Size_{MW})^{0.65} \quad (92)$$

We did not adjust any of these employee rates by PPI adjustment factors because they were already in 2012 dollars.

3.2 Direct CO_2 Cycle

The Annual Cost for the Direct CO_2 Cycle was estimated using the same approach as the Indirect Brine Cycle but adding other costs to account for storing CO_2. These additional CO_2 storage costs include annual monitoring costs (Section 3.2.1), annual site costs (Section 3.2.2), annual injection well related costs (Section 3.2.3), annual injection well and production well related costs (Section 3.2.4), and annual CO_2 plume related costs (Section 3.2.5). Following the same approach used for the capital cost adjustments, we multiplied these additional costs by the general engineering services PPI adjustment factor (PCU5413354133) to adjust from 2010 dollars to 2012 dollars.

3.2.1 Annual Monitoring Costs

We estimated the annual monitoring cost by multiplying the sum of costs listed in Table 34 by the total number of CO_2 injection wells.

Table 34: Components of Annual CO_2 Storage Costs Associated with Monitoring [177]**.**

Description	**Cost [$/injection well/yr]***
Annual cost of air and soil survey: Eddy Covariance	$10,000
Annual cost of digital color infrared orthoimagry	$5,000
Annual cost of LIDAR airborne survey to detect surface leaks	5,000
Annual cost of soil zone monitoring	$900
Annual cost of vandose zone monitoring	$900
Annual cost of monitoring wells for samples from water table	$1,800
Annual cost of passive seismic equipment	$10,500
Total	**$34,100**

*The EPA listed these costs in the units of $/monitoring well/year and we assumed they were $/injection well/year

3.2.2 Annual Site Costs

The annual site cost was estimated as the sum of the costs listed in Table 35.

Table 35: Components of Annual CO_2 Storage Costs Associated with the Site [177]**.**

Description	**Cost [$/yr]**
Complex modeling of fluid flows and migration (reservoir simulations) over 100 years (RA0-3) or 10,000 years (RA4)	$19,912
Annual reports to regulators and recordkeeping for all data gathering activities	$4,867
Semi-Annual (RA3) or quarterly (RA4) reports to regulators and record keeping for all data gathering activities and recordkeeping	$11,282
Monthly reports to regulators and recordkeeping for all data gathering activities and recordkeeping	$10,620
Total	**$46,681**

3.2.3 Annual Injection Well Related Costs

The annual injection well related cost was estimated with Equation 93.

$$Cost\left[\frac{\$}{yr}\right] = I_C * (57{,}723.83 + Depth * 6.20) \quad (93)$$

Where I_C is the number of CO_2 injection wells, 57,723.38 is the sum of costs listed in Table 36, and 6.20 is the sum of the costs listed in Table 37.

Table 36: Components of Annual CO_2 Storage Costs Associated with the Injection Wells [177].

Description	Cost [$/injection well/yr]
Complex modeling of fluid flows and migration (reservoir simulations) over 100 years (RA0-3) or 10,000 years (RA4)	$7,080.00
Conduct periodic monitoring of groundwater quality and geochemistry. (146.90(d) of GS Rule)	$643.38
Monitoring well O&M (ABOVE injection zone)	$25,000.00
Monitoring well O&M (INTO injection zone)	$25,000.00
Total	**$57,723.38**

Table 37: Components of Annual CO_2 Storage Costs Associated with the Monitoring Wells [177].

Description	Cost [$/ft/injection well/yr]*
Annual monitoring well O&M (ABOVE injection zone)	$3.10
Annual monitoring well O&M (INTO injection zone)	$3.10
Total	**$6.20**
*The EPA listed these costs in the units of $/ft/monitoring well/yr and we assumed they were $/ft/injection well/yr.	

3.2.4 Annual Injection Well and Production Well Related Cost

The annual injection well and production well related cost was estimated using Equation 94.

$$Cost\left[\frac{\$}{yr}\right] = (I_C + P_C) * (83{,}063 + Depth * 3.10) \quad (94)$$

Where 83,063 is the sum of costs listed in Table 38 and 3.10 is the annual cost of injection well O&M in the units of $/injection well/ft/yr, which we assumed to be $/well/ft/yr [177].

Table 38: Components of Annual CO_2 Storage Costs Associated with the All Wells [177]**.**

Description	Cost [$/well/yr]*
Annual corrosion monitoring and quarterly analysis of injectate stream and measurement of corrosion of well material coupons	$5,563
Annual injection well O&M	$77,500
Total	**$83,063**
*The EPA listed these costs with the units of $/injection well and we applied them to both injection wells and production wells	

3.2.5 Annual CO_2 Plume Related Cost

The annual cost related to the CO_2 plume was estimated by multiplying the area of the plume by the sum of the costs listed in Table 39.

Table 39: Components of Annual CO_2 Storage Costs Associated with the CO_2 Plume [177]**.**

Description	Cost [$/mi^2/yr]
Annual cost of air and soil surveys: Digital Color Infrared Orthoimagery (CIR) or Hyperspectral Imaging to detect changes to vegetation	$6,250
Annual cost of air and soil surveys: LIDAR airborne survey to detect surface leaks. Works best where vegetation is sparse	$6,250
Periodic seismic surveys: 3D	$104,000
Land use rent, rights-of-way	$3,328
Total	**$119,828**

4 Data

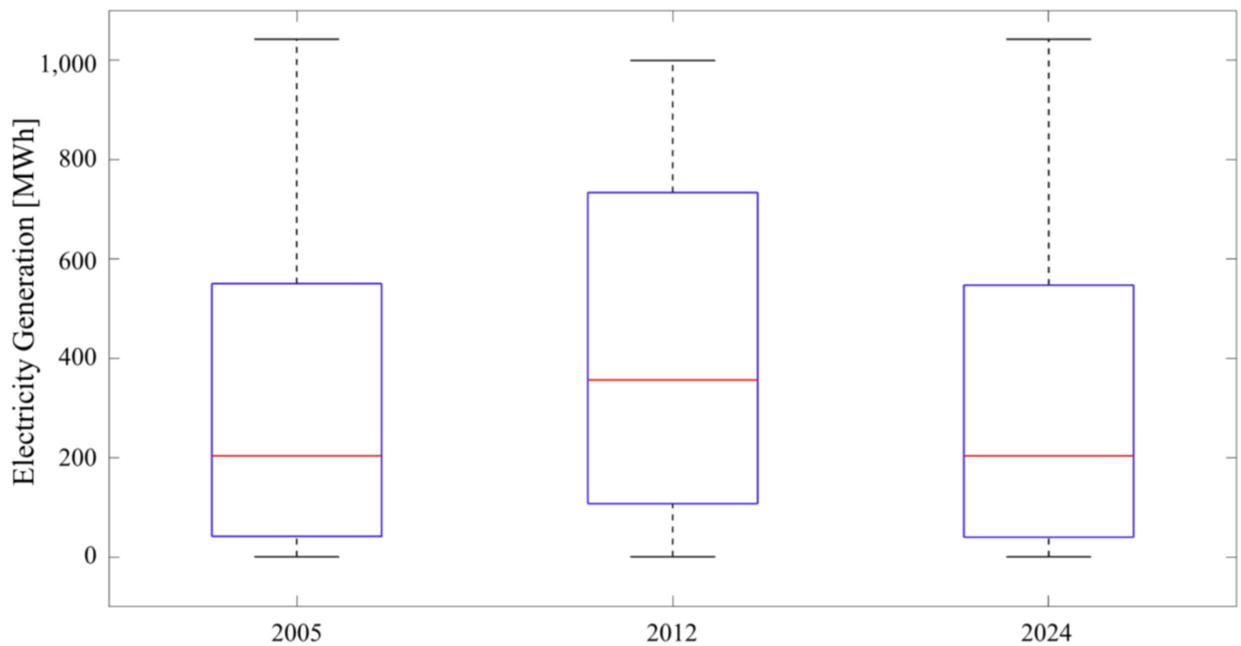

Figure 49: Wind Condition Datasets. The red line is the median, the upper and lower extremes of the blue box are the 25th and 75th percentiles, and the end of the whiskers are the maximum and minimum.

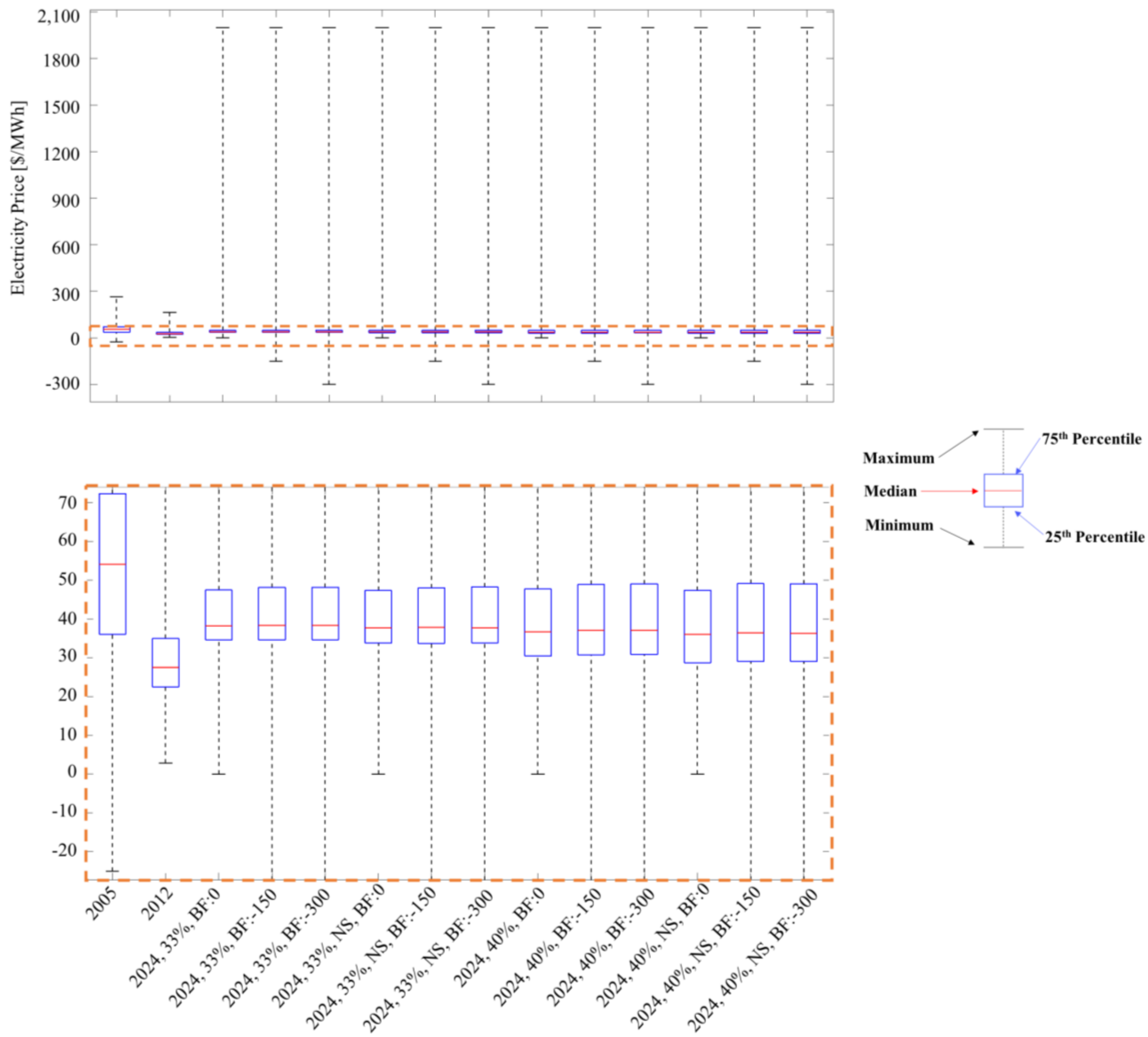

Figure 50: Distribution of Electricity Prices for Each Dataset Used in this Study. For the 2024 datasets, the percentage refers to the penetration of renewable energy technologies, the "NS" is an abbreviation for no storage, and the BF is an abbreviation for bid floor.

5 Results

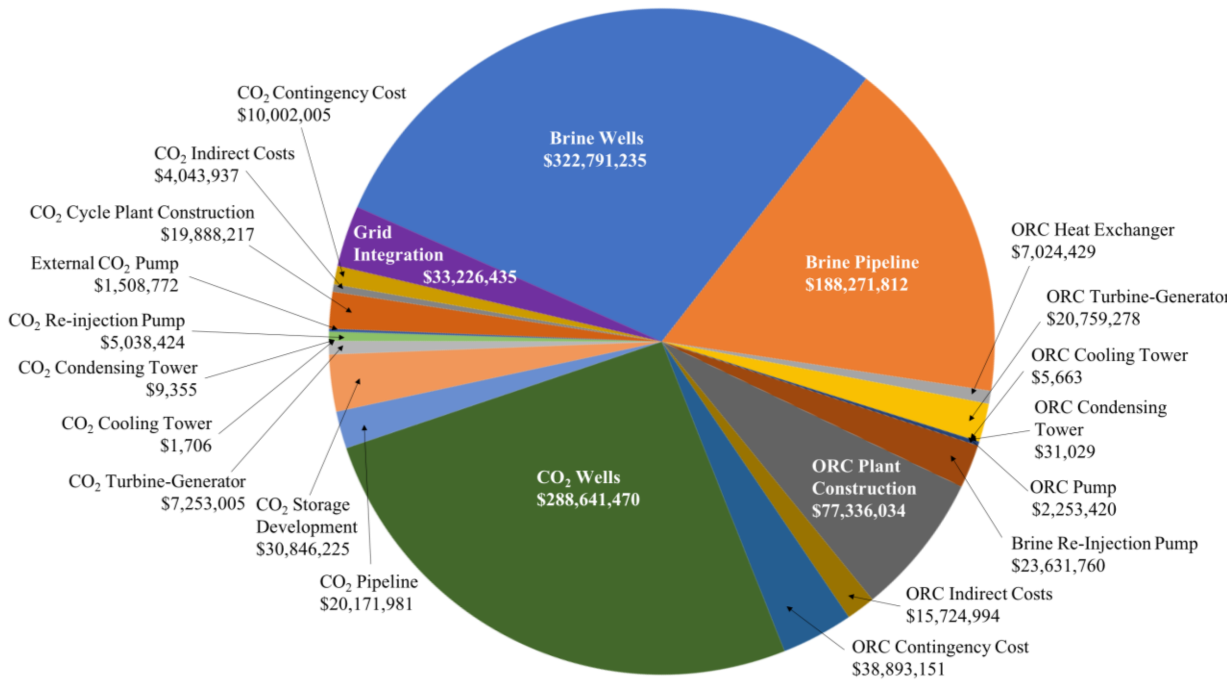

Figure 51: Components of Capital Costs for the CO_2-BES System [2012$]. These cost estimates assume a pipeline diameter of 22 inches (See Section 2.2 of this Appendix).